Kinetics and Mechanism of H/D Exchange Reactions and Racemisation in Aqueous Solutions: Configurational Stability of Ester and Amide Arylglycine Derivatives
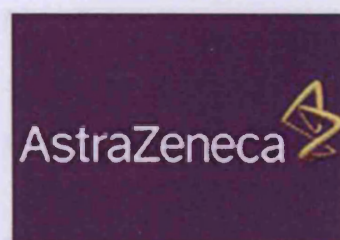
Andrew Ballard

A thesis submitted for the Degree of Doctor of Philosophy

School of Chemistry

Cardiff University

July 2011

UMI Number: U585519

UMI

Dissertation Publishing

ProQuest

Summary

The configurational stability of a range of stereogenic centres in aqueous media has been studied, with the goal of understanding the structural and environmental factors contributing to configurational instability. This information will be of use to the pharmaceutical industry, for which the chiral integrity of drug compounds is imperative. Chapter 1 outlines the background to this project, providing an overview of pharmacological racemisation including potential mechanisms, examples from literature, and the methodology used.

Chapter 2 focuses on database mining studies undertaken on AstraZeneca compound libraries, the results of which guided the structures investigated in the rest of the thesis. Most compounds in the libraries do not appear at risk of racemisation. Of those that do, stereogenic centres with proton, carbonyl, aromatic and nitrogen substituents appear most frequently.

Chapter 3 discusses experimental work determining rate constants of proton-deuterium exchange (as a model for racemisation) under physiological conditions, for a set of N-acetyl arylglycine methyl esters. These rate constants suggest that such compounds are susceptible to *in vivo* racemisation through an S_E1 mechanism.

Chapter 4 outlines experimental work determining rate constants of proton-deuterium exchange, for a set of N-substituted phenylglycine amides. These compounds undergo H/D exchange through an S_E1 mechanism, although the rate at which H/D exchange occurs suggests they would not be at risk of *in vivo* racemisation. These results show that an amide substituent is far weaker than a methyl ester in facilitating racemisation.

Chapter 5 reports the results of computational studies performed on the compounds investigated in Chapters 3 and 4. The energy gap between a molecule and its anion when deprotonated at the stereogenic centre was correlated with the experimentally determined data, suggesting that prediction of configurational instability for novel compounds may be possible. This correlation only holds when the PCM solvent model is used in calculations.

Acknowledgements

Table of Contents

1 Introduction

1.1 Project Background

Chirality is of major interest in the research and development of novel pharmacologically active molecules. In 2008, it was estimated that around 50 % of marketed drugs are chiral,[1] increased from 40 % in 1993.[2] In the past 30 years there has also been a drastic increase in the proportion of drugs solely administered as a single-enantiomer. In 2003 not a single new drug on the market was administered as a racemate,[3] and the three top-selling drugs of 2008[*] were all single-enantiomers.[4] Alongside this move away from developing new drugs as racemates is the strategy of many pharmaceutical companies known as a 'chiral switch', whereby drugs previous marketed as a racemate are re-marketed as a single-enantiomer.[5-7] The switch to homochirality can be therapeutically advantageous and can therefore enable the manufacturer to extend the duration of patent protection. It has also been shown that the presence of a chiral carbon within a molecule correlates with its successful transition from discovery to marketable drug.[8]

Because of the chiral environment found within the human body, opposing enantiomers for many chiral molecules can have drastically different physiological actions.[9, 10] Enantiomers of some compounds stimulate different smell and taste receptors to produce different odours and flavours.[11, 12] Of greater interest are the different pharmaceutical properties found in many drug molecules. Most pharmaceuticals dispensed as a racemate have one enantiomer ('eutomer') that is more bioactive than the other ('distomer').[13] For the class of compounds known as non-steroidal anti-inflammatory agents only one enantiomer is pharmaceutically active. An example of this is ibuprofen, shown in Scheme 1.1.[14]

(+)-(*S*)-Ibuprofen
anti-inflammatory

(-)-(*R*)-Ibuprofen
inactive
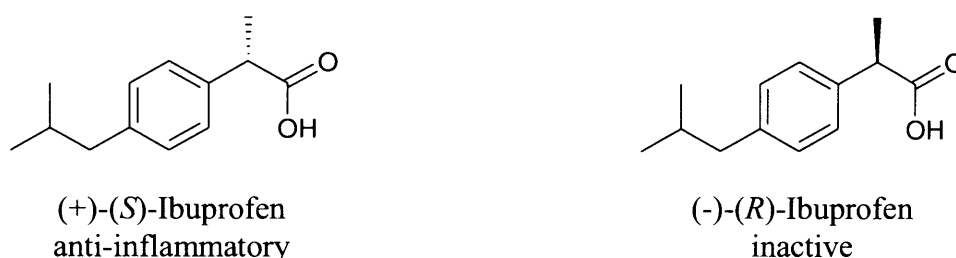
Scheme 1.1: Enantiomers of ibuprofen.

The administration as a racemate of drugs such as ibuprofen results in a reduction of the effective dose. The therapeutically non-active isomer of the drug can essentially be considered an impurity.[15] More significantly, in some cases the enantiomer of a pharmacologically active drug may be harmful to the patient. The molecule thalidomide (Scheme 1.2) is often cited as an example.

<div align="center">

(+)-(R)-Thalidomide
sedative

(-)-(S)-Thalidomide
teratogen

</div>
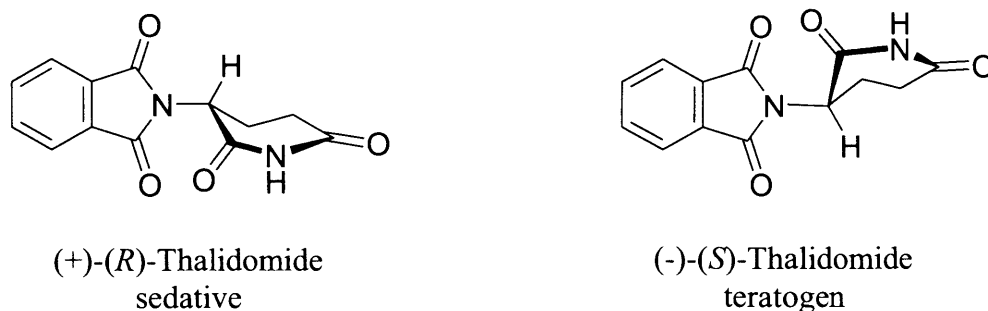
Scheme 1.2: Enantiomers of thalidomide.

Thalidomide was administered to pregnant women in the late 1950's to ease morning sickness pains. It was later discovered to be teratogenic, resulting in many recipients of the drug giving birth to babies with severe deformities. It has since been documented that the teratogenic activity is caused by the (S)-enantiomer only.[16-18] Other studies have suggested that both enantiomers can cause birth defects.[19, 20] Either way, one legacy of this tragedy was to increase awareness of the potential hazards of the presence of more than one enantiomer in a drug. It has been contended that administration of enantiopure (R)-thalidomide would have prevented the catastrophe.[21, 22] However, this would not solve the problem as thalidomide racemises under physiological conditions. *In vivo* experiments showed half-lives of chiral inversion of less than 6 hours in humans.[23, 24] As a result, the administration of only one enantiomer of thalidomide as a drug will not prevent the presence of both enantiomers within the body.

To minimise the possibility of an incident such as that involving thalidomide occurring again, confirmation that a potential drug molecule is configurationally stable under certain conditions must be obtained prior to its release.[25] The configurational stability at ambient temperature and humidity over a period of many months should be determined to ensure the shelf life of the drug is known. Of greater risk is that a drug may undergo racemisation in the blood stream, as in the case of thalidomide. Therefore the configurational stability of the molecule of interest should be known under aqueous conditions, at temperatures ~37 °C and at pH levels from neutral down to very acidic.

The susceptibility of a compound to racemise is evidently related to its molecular structure. The mechanism by which a molecule undergoes racemisation is largely dependent on the interaction between molecular structure and its environment. It is therefore of interest to the pharmaceutical industry and chemists in general to understand this interaction, to allow insight into which aspects of the molecular structure facilitate racemisation under physiological conditions.

Knowledge of the structural factors affecting racemisation could also be of use in areas other than the configurational stability of drugs. In dynamic kinetic resolutions (DKRs) for example, racemisation is harnessed in the production of enantiomerically pure compounds.[26-28] Kinetic resolution of a racemic material works on the basis that the two enantiomers are transformed to products at different rates (e.g. in an enzymatic transformation), with the desired enantiomer reacting faster. In a DKR, the start material is simultaneously racemised. This allows the transformation of all the racemic start material to the desired enantiopure product. Racemisation must occur faster than reaction of the undesired starting enantiomer in order for the DKR to be effective. As a result, understanding of the structural factors that facilitate or hinder racemisation could also be informative to chemists working on DKR procedures.

1.2 Definitions

It is important to define the concepts of racemisation and enantiomerisation.[29, 30] Racemisation (Scheme 1.3) is a statistical, macroscopic and irreversible process in which half of an enantiopure quantity of compound is transformed into the opposing enantiomer. It is complete when the enantiomeric excess (*ee*) of the sample under analysis is reduced to 0%. Accordingly, the half-life of racemisation is the length of time it takes for the *ee* of a sample to drop to half its original value. Distinct from this is enantiomerisation (Scheme 1.4), which refers to the microscopic, reversible conversion of one molecule of an enantiomer into the other.

$$(R) \quad (R) \quad (R) \qquad \xrightarrow{k_{rac}} \qquad (R) \quad (S) \quad (R) \qquad \xleftarrow{k_{rac}} \qquad (S) \quad (S) \quad (S)$$
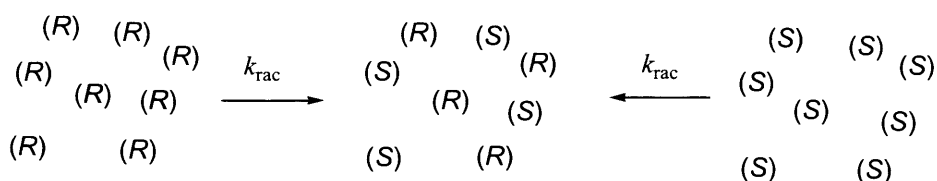
Scheme 1.3: Illustration of racemisation.

$$(R) \quad \xrightleftharpoons[k_{\text{enant}}]{k_{\text{enant}}} \quad (S)$$
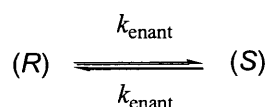
Scheme 1.4: Illustration of enantiomerisation.

Chiral inversion of one molecule to its enantiomer reduces the *ee* by two molecules. The rate constant of racemisation (k_{rac}) is therefore twice that of enantiomerisation (k_{enan}) (eqn 1.1).

$$k_{\text{rac}} = 2k_{\text{enan}} \qquad\qquad (1.1)$$

The rate of diastereoisomerisation (Scheme 1.5) is more complex than the rates of racemisation or enantiomerisation.

$$(R, R) \quad \xrightleftharpoons[k_{-1}]{k_1} \quad (S, R)$$
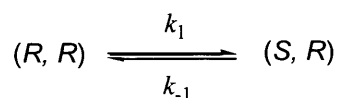
Scheme 1.5: Illustration of diastereoisomerisation.

As diastereoisomers have (by definition) inequivalent thermodynamic stabilities, the rate constant of conversion of one diastereomer into another will differ from that of the reverse reaction (eqn 1.2).

$$k_1 \neq k_{-1} \qquad\qquad (1.2)$$

The definition of epimers as 'diastereoisomers that differ in only one configuration of two or more elements of chirality'[29] means that the example displayed in Scheme 1.5 could also be referred to as epimerisation.

1.3 Mechanism

Although one can never be 100% certain of the mechanism by which organic molecules react,[31] information on the path a particular reaction (or series of reactions) take affords insight into the factors affecting the mechanism. In the context of this thesis, for example, awareness of the mechanism by which a racemisation reaction takes place could allow prediction of stereocentres that may be susceptible, or conditions under which certain stereocentres are at risk. For stereocentres of the type R''R'RC-H,[†] the rate constant of

---

[†] The notation R''R'RC-H used throughout this thesis refers to any stereogenic centre with one proton substituent and any three other non-identical substituents (not necessarily alkyl substituents).

4

exchange between the proton bound to the stereogenic centre with deuterium (or tritium) from the environment in which the reaction is being studied, can be compared with the rate constant of racemisation to provide insight into the mechanism of racemisation. There are four limiting ratios of k_{deut} (rate constant of deuteration) divided by k_{rac} (rate constant of racemisation):[32, 33]

1) if H/D exchange occurs with retention of stereochemistry, the ratio k_{deut} / k_{rac} tends to infinite (isoinversion)

2) if H/D exchange occurs with total racemisation, deuteration can occur on either face and the ratio k_{deut} / k_{rac} is equal to 1

3) if H/D exchange occurs with complete stereochemical inversion, then for each event the *ee* is reduced by two molecules and the ratio k_{deut} / k_{rac} is equal to 0.5

4) if racemisation occurs with no H/D exchange, the ratio k_{deut} / k_{rac} tends to 0.

H/D exchange with retention of stereochemistry has been observed in a handful of examples.[34-36] Dehydronation at the stereogenic centre by a base such as ammonia (k_1) can be followed by rehydronation on the same face by the same base molecule (k_{-1}'), if rotation of the base ion (k_2) is faster than ion pair dissociation (k_3) (Scheme 1.6).

R = CON(CH$_3$)$_2$

Racemic Product   Dissociated ions   Retained Configuration
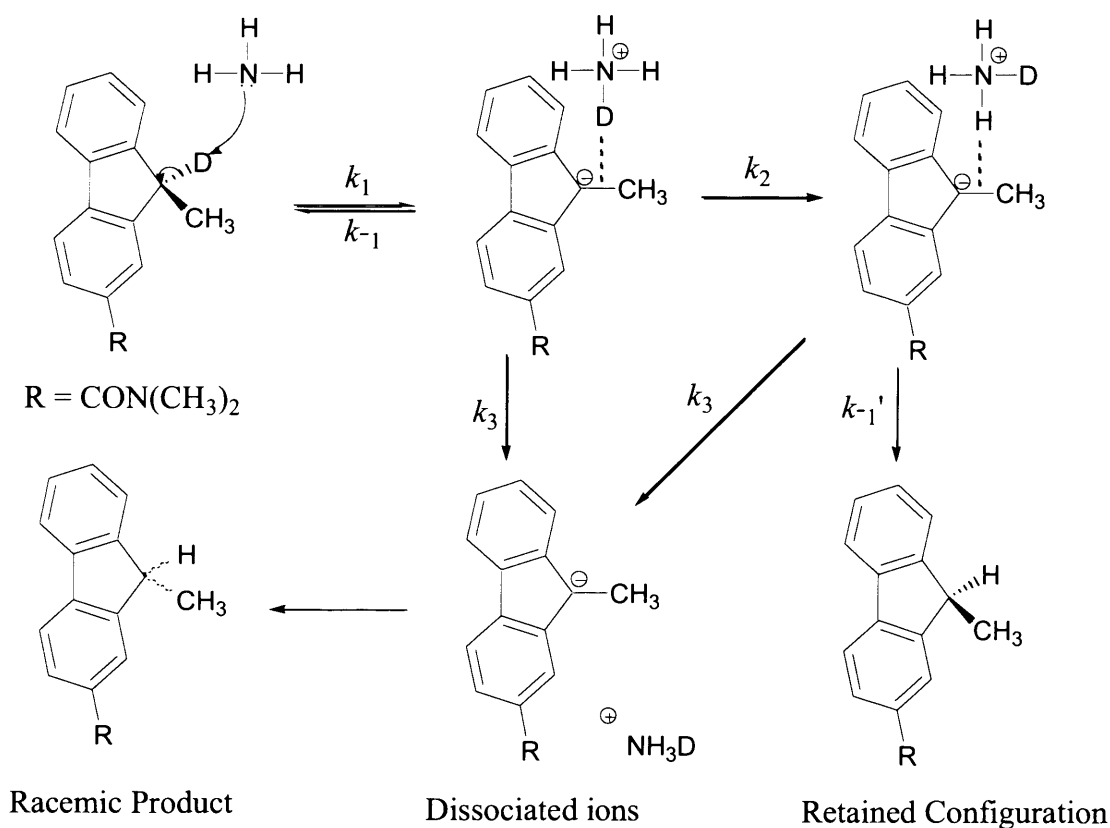
Scheme 1.6: Mechanism of H/D exchange with retention of configuration.[32]

The rate constants depicted in Scheme 1.6 are temperature and solvent dependent. The retention mechanism applies when k_2 and k_{-1} are greater than k_3. When this is the case, k_{deut} / $k_{rac} > 1$. At 145 °C in tetrahydrofuran with 0.3 M ammonia, k_{deut} / $k_{rac} = 148$ for the reaction depicted in Scheme 1.6.

An S_E1 mechanism will result in equal rates of H/D exchange and racemisation. The S_E1 mechanism entails the initial rate-determining loss of a proton to give a planar carbanion, which can then be deuterated on either face (Scheme 1.7).

$$k_{deut} = k_{rac} = 2k_{enant}$$
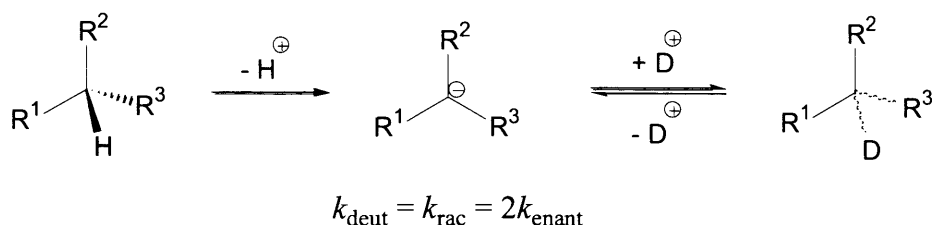
Scheme 1.7: S_E1 mechanism of racemisation.

If a negative charge can be delocalised onto adjacent functional groups, the carbanion intermediate will be stabilised (see Section 1.4). Equal rates of proton deuterium exchange and racemisation have been observed in several circumstances where a negative charge can be stabilised through delocalisation.[37-40]

If H/D exchange occurs with stereochemical inversion, k_{deut} / k_{rac} is equal to 0.5 and the S_E2 'push-pull' mechanism is presumed to be occurring. The S_E2 mechanism consists of simultaneous bond cleavage and bond formation with a hydron as both the incoming and leaving group, resulting in chiral inversion (Scheme 1.8).

$$k_{deut} = \tfrac{1}{2}\, k_{rac} = k_{enant}$$
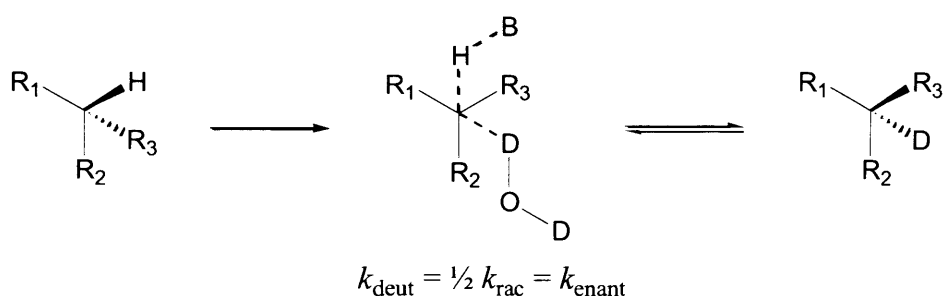
Scheme 1.8: S_E2 mechanism of racemisation.

Reist *et al.* proposed an S_E2 mechanism for the racemisation of 5-substituted hydantoins, based on an observed k_{deut} / k_{rac} ratio of 0.5.[33]

Adjacent groups that can stabilise a negative charge, and thus facilitate racemisation through the S_E1 mechanism, may also promote racemisation through an S_E2-like mechanism, although bond breaking and bond formation may not occur precisely simultaneously. If the bond with

the leaving proton is broken before the new bond with the incoming deuteron is formed, but there is insufficient time for the ion-pair intermediate to fully dissociate before the new bond is formed, then chiral inversion will still be seen and $k_{deut} = \frac{1}{2} k_{rac} = k_{enan}$. Negative charge will be built up though, and this can be stabilised by adjacent functional groups.

The continuum of mechanisms by which an electrophilic substitution of a proton by a deuteron takes place can be summarised by a More O'Ferrall-Jencks diagram (Scheme 1.9).[41] The x- and y-axes of the diagram correspond to the extent of C-D bond formation and the C-H bond being broken, respectively. Starting material is typically represented by the bottom-left-hand corner of the diagram and the product of the electrophilic substitution in the top-right-hand corner. The S_E1 mechanism goes via the top left hand corner, with the C-H bond being broken before the C-D bond is formed. The S_E2 mechanism, with simultaneous C-H bond breaking and C-D bond formation, is depicted by a diagonal line proceeding from the origin to the top right corner. An S_E2-like mechanism, with negative charge build up, but not enough time for the ion-pair intermediate to break apart, will proceed somewhere in-between the 'pure' S_E1 and S_E2 mechanisms.
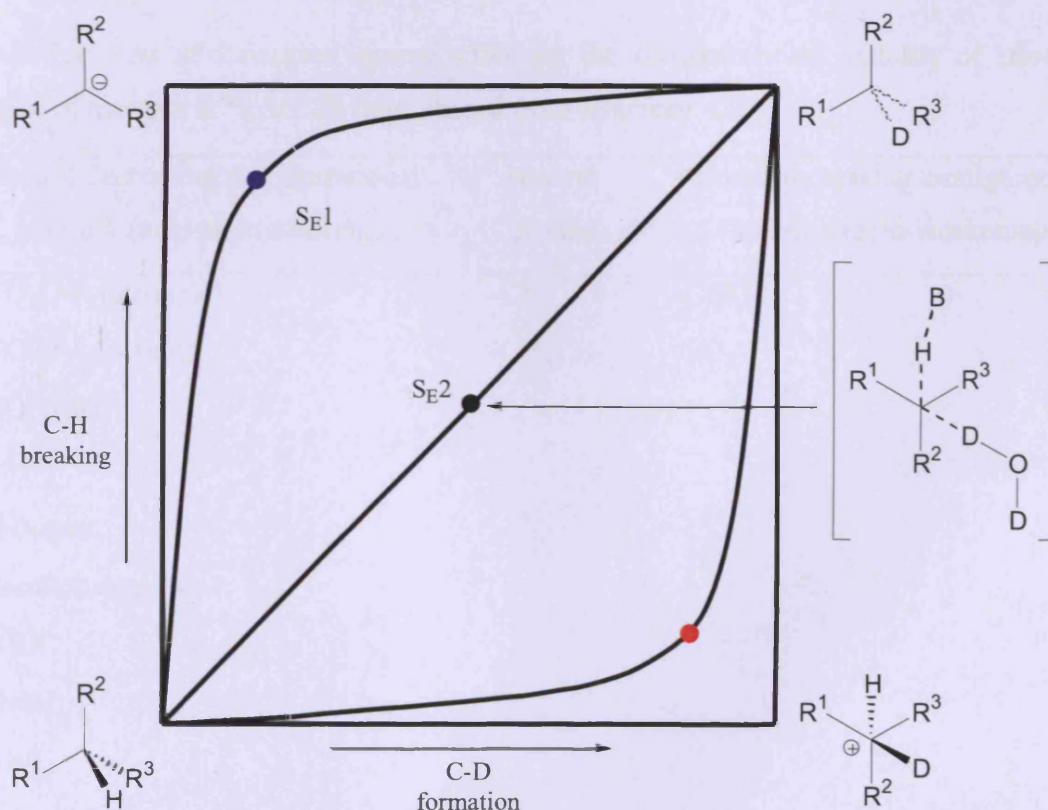
Scheme 1.9: More O'Ferrall-Jencks diagram for electrophilic substitution reactions.

7

Addition of the deuteron followed by loss of a proton (as depicted in the bottom-right-hand corner of Scheme 1.9) is unlikely for carbon-based chiral centres as it would involve the formation of a pentavalent carbocation intermediate.

There are many other routes through which drug-like molecules may undergo racemisation. These will be explored further in Section 1.5.2.

1.4 Substituent Effects

As discussed above, certain functional groups can stabilise a negative charge and as such can facilitate racemisation of stereogenic centres of the type R''R'RC-H. Similarly, there are certain functional groups that destabilise a negative charge and hence promote configurational stability. Testa *et al.* classified several functional groups as either increasing, decreasing or neutral to configurational stability (Table 1.1) and concluded that in order to be of pharmaceutical or pharmacological significance, there must be either three carbanion-stabilising groups present or two carbanion-stabilising groups (one of which must be strongly so) and one neutral group.[42, 43]

Table 1.1: List of functional groups affecting the configurational stability of stereogenic centres of the type R''R'RC-H (reproduced from reference 42).

Groups decreasing configurational stability (acid-strengthening)	Neutral groups	Groups increasing configurational stability (acid-weakening)
-CO-O-R (strong)	-CH$_3$	-COO$^-$
-CO-aryl (strong)	-CH$_2$CH$_3$	-SO$_3^-$
-CONRR'		
-OH		
-Halogens		
-Pseudohalogens		
-NRR'		
-N=R		
-Aryl		
-CH$_2$-aryl		
-CH$_2$OH		

The classifications in Table 1.1 as decreasing or increasing configurational stability can be seen as a direct consequence of the ability of the functional groups to stabilise or destabilise a negative charge, either through direct resonance delocalisation or inductive contributions. Groups such as a carbonyl, nitrile or aryl will be able to stabilise a carbanion through delocalisation (Scheme 1.10).
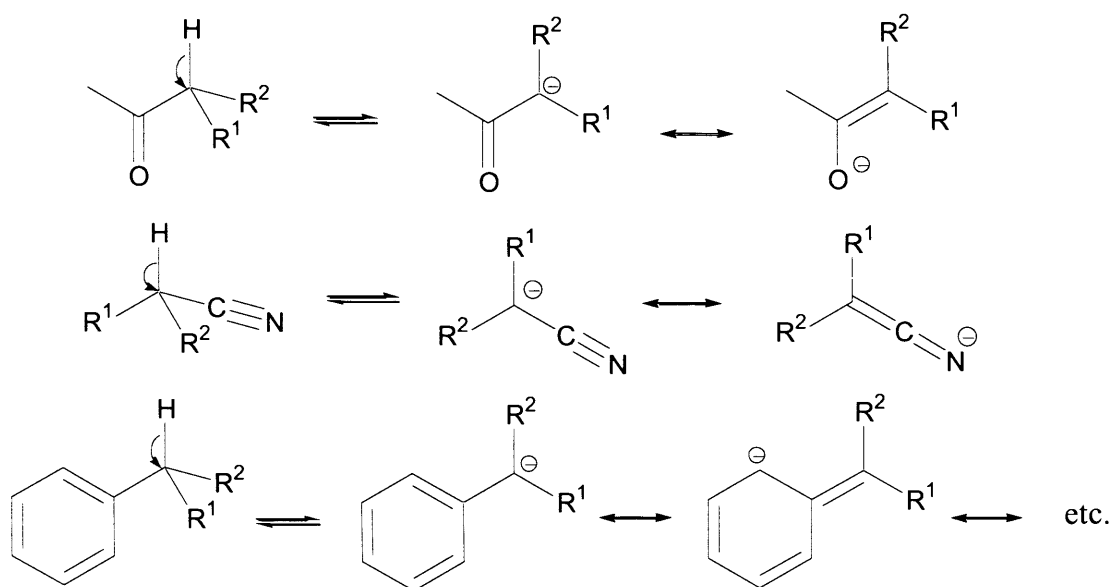
Scheme 1.10: Stabilisation of an anion by carbonyl, nitrile and aryl groups.

Table 1.1 also suggests that adjacent amide (orientated with nitrogen adjacent to the stereogenic centre) and amine groups will stabilise a negative charge and decrease configurational stability. In these two cases, direct delocalisation of charge cannot be depicted as in Scheme 1.10, although work by the Richard group supports the supposition that these groups, amongst others, stabilise a negative charge.[44, 45]

The Richard group has published substantial information on the stability of carbanions in water. [44-53] By determining equilibrium constants for formation of carbanions (i.e. pK_a's of carbon acids), structural effects on the stability of the carbanion can be quantified through the variation of these equilibrium constants. pK_a's were obtained from the ratio of the rate constants for the reversible proton transfer from the carbon acid to either the solvent or to a Brønsted base, together with the pK_a of the reacting base.[44] One method used for determination of these rate constants of deprotonation for carbon acids was through monitoring deuterium incorporation into the compound using D_2O as a solvent. Rate constants for protonation of the carbanion were estimated by using an encounter-controlled reaction as a 'clock' for proton-transfer. For reactions of carbanions, which exist in water only

9

for as long as solvent reorganisation can occur, the rate constant for the dielectric relaxation (reorganisation) of solvent water ($k_{reorg} \approx 10^{11}$ s^{-1}) can be used as such a 'clock'.[46, 48]

Richard *et al.*[44, 49] found that the addition of an adjacent –NH(Ac) group made a proton more acidic by more than 4 pK_a units (Scheme 1.11a). The authors attribute this to extra stabilisation of the intermediate carbanion by electrostatic interactions with a partial positive charge on the amide nitrogen (Scheme 1.11b).

a)

$pK_a = 18.7$ $pK_a = 14.5$

b)
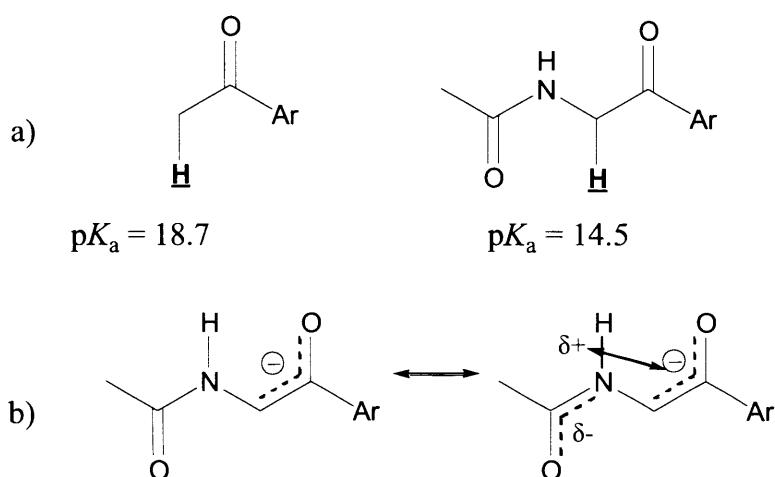
Scheme 1.11 a) Illustration of pK_a change upon addition of an acetyl amide group b) stabilising electrostatic interactions between an enolate anion and the partial positive charge on amide nitrogen.[44]

A protonated amine adjacent to a carbon acid will stabilise the conjugate base carbanion because of its positive charge (Scheme 1.12).

favourable
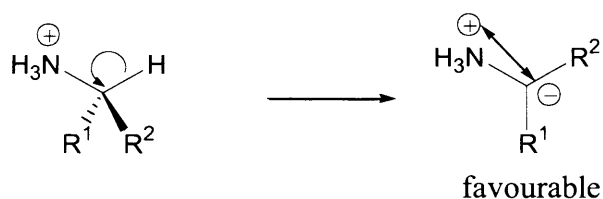
Scheme 1.12: Stabilisation of anion by protonated amine.

Rios and Richard[45] found that the rate constant for deuterium incorporation at α-carbon in D$_2$O was 3500 times greater for *N*-protonated glycine methyl ester than for ethyl acetate. The greater rate constant was attributed to the effect of the NH$_3$$^+$ group on enolate stability, resulting in a lower pK_a. The importance of this positive charge on the amine is further clear from the decrease in pK_a values for the proton at the α-carbon for the glycine anion upon protonation. The positive charge on the amine makes the proton at the α-carbon more acidic by 5 orders of magnitude (Scheme 1.13).[44, 50]

$pK_a = 34$ $pK_a = 29$
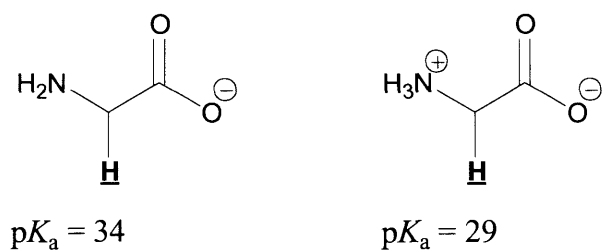
Scheme 1.13: Change in pK_a value upon protonation of adjacent amine.[44]

The classification in Table 1.1 of an imine as decreasing configurational stability is also supported by work of the Richard group. Addition of acetone to N-protonated glycine methyl ester to form the iminium adduct was shown to lower the pK_a of the adjacent proton by 7 (Scheme 1.14).[51]

Acetone

$pK_a = 21$ $pK_a = 14$
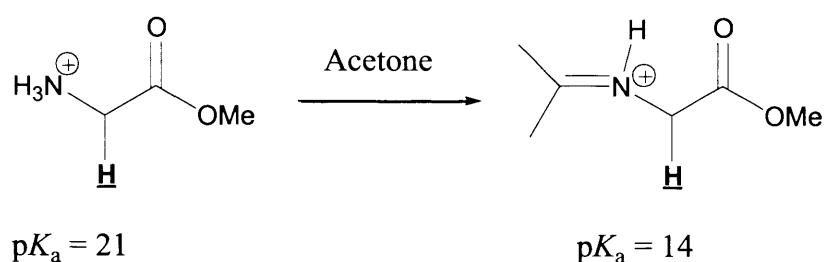
Scheme 1.14: Change in pK_a upon formation of an iminium ion from a protonated amine.

Richard *et al.*[49, 52] also summarised the effect of different carbonyl groups on carbon acidity (Table 1.2).

Table 1.2: Effect of carbonyl substituents on pK_a of α-carbon.

X	pK_a
H	16.7
Me	19.3
SEt	21.0
OMe	25.6
OH	26.6
NH_2	28.4
O^-	33.5
$C_6H_4CH_3$	18.7

The authors suggest two factors for the range of pK_a values seen in Table 1.2; 1) the polar effect of electron-withdrawing groups that stabilise negative charge at the enolate ion, and 2) the π-donor effect of interactions between any substituent lone-pair and the electron deficient π-orbital of the adjacent carbonyl carbon.

The pK_a values reported in Table 1.2 suggest that a methyl ester group is more carbanion stabilising than a primary amide group, by two orders of magnitude. This difference was attributed to the partial carbon-nitrogen double-bond character of amides, due to resonance delocalisation of the nitrogen lone pair onto the carbonyl oxygen. The presence of a negative charge on the carbonyl oxygen of a primary amide prevents delocalisation of any negative charge built up during enolisation.

In Table 1.1, Testa *et al.* defined both aryl ketone and ester groups as strongly configurationally destabilising. As shown in Table 1.2, Richard *et al.*[49, 52] found that the α-carbon of an aryl ketone has a far lower pK_a (7 pK_a units) than that of a methyl ester. This lower pK_a suggests that an aryl ketone substituent would be far more configurationally destabilising than a methyl ester substituent, if positioned adjacent to a stereogenic centre.

Although possessing a carbonyl, a carboxylate anion is said to increase configurational stability. This is because an adjacent anion will destabilise any negative charge built up during racemisation (Scheme 1.15).

unfavourable
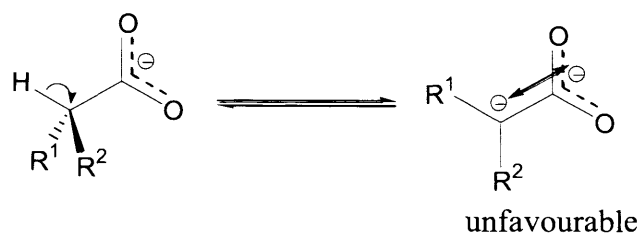
Scheme 1.15: Destabilisation of an anion by carboxylate group.

The pK_a of a carboxylic acid is obviously dependent on the structure of the rest of the molecule but is generally < 5.[54] Therefore we can assume that under physiological conditions the carboxylate will be deprotonated and hence an anion will be present. This effect on carbanion stability is also reflected in Table 1.2, where the pK_a of the carboxylate anion substituted ketone is 8 units lower than the equivalent methyl ester compound.

In conclusion, existing studies generally support the assignments in Table 1.1, although many of the listed functional groups appear untested. It is also important to acknowledge that configurational stability is a relative term and that nearly all stereogenic centres can be
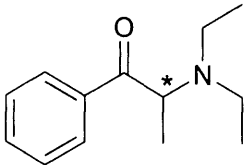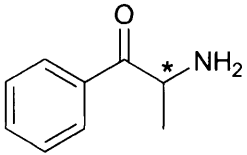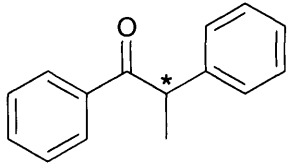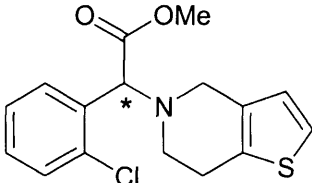
destabilised under certain conditions.[43] The assignments in Table 1.1 are made with regards to physiological conditions as set out in Section 1.1. Functional group dependence will be further discussed in the following section containing case studies of racemisation.
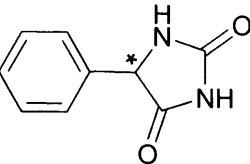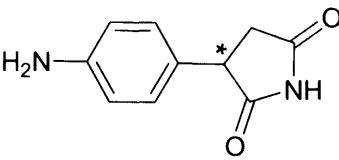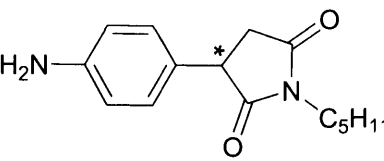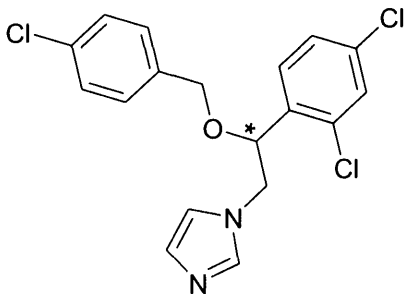
1.5 Racemisation Case Studies
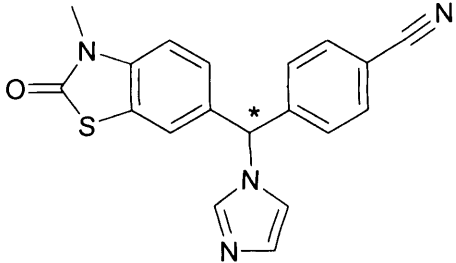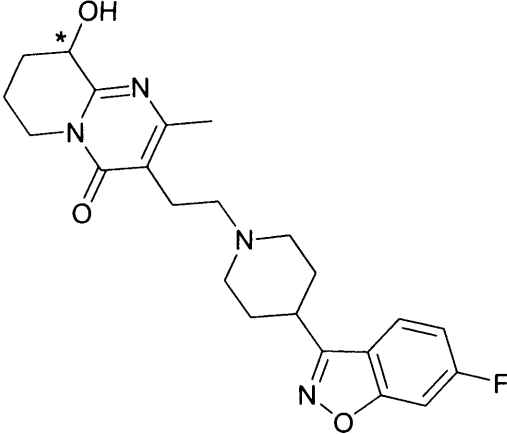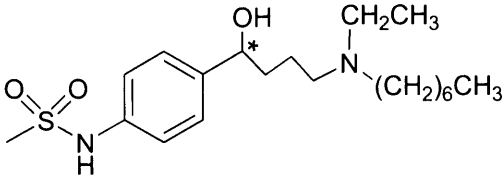
There are many examples of *in vitro* studies on the racemisation of drugs or drug-like molecules. A review article on the subject was written by Ali *et al.*[55] and a review on racemisation in general by Ebbers *et al.*[56] Rate constants, conditions and mechanisms of racemisation of some chiral compounds (including several drugs) are listed in Table 1.3.
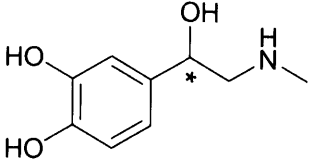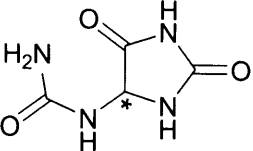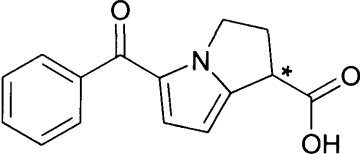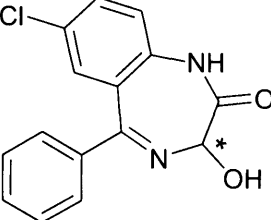
As noted, the rate constants in Table 1.3 were obtained under a variety of conditions. This means that direct comparisons between the compounds in Table 1.3 will be of little value, although approximate qualitative evaluations can be made.
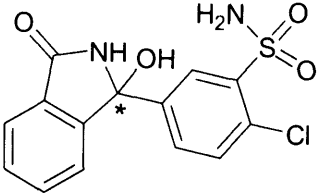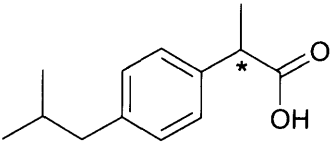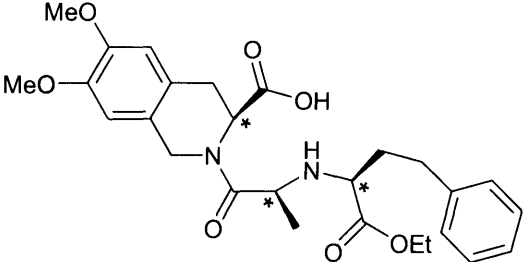
Table 1.3: Examples from the literature of rate constants of racemisation.

	Compound	Structure	k_{rac} / s^{-1}	Conditions	Details[a]
1.1[57]	Amfepranone		6.47×10^{-4}	D_2O, pD 7.4, 37 °C, 0.2 M phosphate	R''R'RC-H type, GBC, S_E1
1.2[57]	Cathinone		1.30×10^{-4}	D_2O, pD 7.4, 37 °C, 0.2 M phosphate	R''R'RC-H type, GBC, S_E1
1.3[58]	1,2-Diphenylpropanone		3.17×10^{-4}	EtOH, 25 °C, 8 mM NaOEt	R''R'RC-H type,
1.4[59]	Clopidogrel		5.79×10^{-7}	H_2O, pH 7.4, 37 °C, 0.1 M phosphate	R''R'RC-H type, GBC, Also see hydrolysis

14

1.5[33]	5-Phenylhydantoin	2.56×10^{-3}	1:1 H$_2$O:DMSO pH 7.4, 40 °C, 0.1 M phosphate	R''R'RC-H type, S$_E$2, BC
1.6[60]	3-(4-Aminophenyl) pyrrolidine-2,5-dione	4.81×10^{-5}	H$_2$O, pH 7.4, 37 °C, 0.01 M phosphate	R''R'RC-H type, BC
1.7[60]	1-Pentyl-3-(4-aminophenyl) pyrrolidine-2,5-dione	6.42×10^{-5}	H$_2$O, pH 7.4, 37 °C, 0.01 M phosphate	R''R'RC-H type, BC
1.8[60]	Econazole	7.29×10^{-5}	H$_2$O, pH 7.4, 37 °C, 0.01 M phosphate	R''R'RC-H type, BC

15

1.9[61]	3-Methyl-6-[1-(imidazo-1-yl)-1-(4-cyanophenyl) methyl benzothiazolinone		9.69×10^{-8}	9:1 H_2O:EtOH pH 7.4, 50 °C, 0.05 M phosphate	R''R'RC-H type, BC
1.10[62]	9-Hydroxyrisperidone		4.47×10^{-5}	H_2O, pH 2.5, 37 °C, 0.01 M phosphate	R''R'RC-H type, GAC, imine-enamine tautomerism
1.11[63, 64]	Ibutilide		N/A	H_2O, range of pH and temperatures	AC, via dehydration and intramolecular nucleophilic attack

16

1.12[65]	Adrenaline		6.83×10^{-6}	H_2O, 1.0M HCl, 30 °C	AC, via dehydration
1.13[66]	Allantoin		Not stated, $t_{1/2} > 10$ hr	H_2O, neutral pH, phosphate buffers	R''R'RC-H type, racemises through intramolecular nucleophilic attack and S_E1/S_E2 elimination
1.14[67]	Ketorolac		5.0×10^{-9}	H_2O, pH 7.2, 25 °C, 0.04 M phosphate	R''R'RC-H type, GBC and GAC
1.15[68]	Oxazepam		3.85×10^{-3}	H_2O, pH 7.5, 23 °C, 0.1M Tris-HCl buffer	Cyclic hemi-aminal opening, accelerated at high pH

1.16[69]	Chlorthalidone		4.24×10^{-4}	H_2O, pH 6.5, 22 °C, Briton-Robinson buffer	AC via dehydration, BC through ring-opening and –closing, rate slowed by liposomes
1.17[70]	Ibuprofen		N/A	No examples of *in vitro* racemisation at moderate pH and temperature	R''R'RC-H type, many examples of *in vivo* racemisation through thioester formation and enzyme catalysis
1.18[71]	RS-10085		N/A	H_2O, pH > 7, Range of temperatures	Three stereogenic centres of R''R'RC-H type, epimerisation seen at one, BC

[a] GBC – general-base catalysed, BC – base catalysed, GAC – general-acid catalysed, AC – acid catalysed

18

1.5.1 Base-Catalysed Racemisation of Stereocentres of the Type R''R'RC-H

Many of the entries in Table 1.3 are for racemisation of stereocentres of type R''R'RC-H, catalysed by base. Although a specific mechanism was not concluded for some of these entries, a rate-determining step involving proton abstraction by specific or general base is plausible in all. As such, the data can be used as a basis for comparison of the role adjacent functional groups play in facilitating racemisation of R''R'RC-H type stereocentres, seemingly through stabilisation of negative charge (Section 1.4).

The data in Table 1.3 loosely supports the assignments of functional groups by Testa *et al.* displayed in Table 1.1. The designation of C(O)-aryl as strongly destabilising is supported by data from compounds **1.1** and **1.2** (amfepramone and cathinone). It was determined that these compounds undergo racemisation through an S_E1 mechanism, with half lives of approximately 20 and 90 minutes respectively (in D_2O based 0.2 M phosphate buffers, at 37 °C).[57] By the assignments in Table 1.1, both compounds have one neutral substituent (methyl), one destabilising (amine groups, primary for **1.2**, tertiary for **1.1**) and one strongly destabilising ($C(O)C_6H_5$). In comparison, for **1.4** (clopidogrel) the rate constants are 2-3 orders of magnitude lower. Compound **1.4** has, by Testa's classifications, two destabilising groups (a tertiary amine and an aryl group) and one strongly destabilising group (methyl ester). This suggests that a methyl ester is (despite its classification in Table 1.1) less destabilising than an aryl ketone. This would also be consistent with the far lower pK_a value found for a ketone than a methyl ester by Richards *et al.* (Table 1.2). Compound **1.3** (1,2-Diphenylpropan-1-one) also contains an aryl ketone and racemises much faster than **1.4**, however, as the rate constants were determined in ethanol solution rather than water, direct comparison is inappropriate.

Reist *et al.*[57] attributed the difference in racemisation rates of **1.1** and **1.2** to the different pK_a values of the amines of 8.79 and 8.37, respectively. They conclude that the greater basicity of **1.1** means that a larger fraction of its molecules will be protonated (and hence more electron withdrawing and configurationally destabilising) than **1.2** at the pH at which the experiments were carried out. However, the rate constants were determined at pH 7.4. At this pH the vast majority of molecules of both **1.1** and **1.2** will be protonated, suggesting that the protonation state is unlikely to be responsible. pK_a values determined by Rios *et al.*[50] (Scheme 1.13) suggest that the α-proton of a positively charged amine is more acidic for more substituted amines (i.e. the pK_a for the α-proton is lower for a compound containing Me_3N^+ than for H_3N^+). This difference is attributed to two effects: (1) hydrogen bond formation between

H_3N^+ and solvent, which diffuses positive charge away from nitrogen and onto solvent molecules and decreases interaction between charges; (2) methyl groups of Me_3N^+ reduce the dielectric constant of the local medium through which the electrostatic interactions occur, giving greater stabilisation of the negative charge.[72, 73] It is also noted that a lower pK_a for a proton α to Me_3N^+ than for H_3N^+ is consistent with the σ_I (field effect) values of 0.92 and 0.60 respectively reported by Hine,[74] although other sources[75] record field effects to be nearly the same for both substituents.

Reist et al.[33] determined the rates of H/D exchange for a series of substituted hydantoins. By comparison with the rate of racemisation for some of the compounds, they concluded that hydantoins undergo racemisation through an S_E2 mechanism, whereby deuteration proceeds with chiral inversion (Section 1.3). To the best of our knowledge, this is the only reported example of an S_E2 mechanism of racemisation found in the literature, although recent results suggest the reaction may follow an S_E1 mechanism.[76] The rate constants of H/D exchange for the series of hydantoins can be used to analyse the effect of substituents on the lability of the proton bound to the stereogenic centre (Table 1.4).

Table 1.4: Rate constants of H/D exchange and racemisation of hydantoins, reproduced from reference 33.

R group	k_{deut}[a] h^{-1}	k_{rac}[b] h^{-1}
Ph	11.3	23.7
CH_2Ph	0.060	0.119
CH_2OH	0.280	-
$NHC(O)NH_2$	0.118	-
CH_3	0.033	-
CH_2COOH	0.017	-
$CH(CH_3)_2$	0.006	-
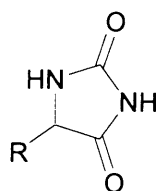
[a] determined in a mixture of D_2O phosphate buffer (pD 7.4, 0.1M, I = 0.22) and (d^6)DMSO in proportion 1:1 (v/v) at 50 °C. [b] determined in a mixture of phosphate buffer (pH 7.4, 0.1M, I = 0.22) and DMSO in proportion 1:1 (v/v) at 50 °C

The rate constant for H/D exchange determined for phenyl substituted hydantoin is far larger than any other. This is consistent with the designation of aryl groups as destabilising. Table 1.1 also suggests NRR' substituents are destabilising. However, the rate constant of the amido

substituent in Table 1.4 is two orders of magnitude smaller than that of the phenyl substituent. This suggests that the assignments made by Testa *et al.* are qualitative rather than quantitative, and there is much variation within the general classification as 'destabilising'. Comparison of the other rate constants provided in Table 1.3 with those in Table 1.4 is difficult. Compared with most of the other data sets the H/D exchange of hydantoins were studied at a higher temperature, and using DMSO as a co-solvent (for solubility) which will affect the observed rate constants.

Compounds **1.6** and **1.7** have similar structures to **1.5** (5-phenylhydantoin). Both are of the type R''R'RC-H and racemisation is base catalysed. The rate constants for racemisation, however, are around two orders of magnitude less than for **1.5**. This may be due to the different conditions or due to the differences in structure. For example, **1.6** and **1.7** do not have the adjacent carbonyl as found in **1.5**. Also of note is the amide substitution on the phenyl ring adjacent the stereogenic centre in **1.6** and **1.7**. The electron-donating nature of the amide group will destabilise any negative charge built up at the stereogenic centre during racemisation and hence reduce the rate.

Table 1.3 also provides evidence supporting the classification of a carboxylate group as configurationally stabilising. **1.4** contains a methyl ester and racemises. However, **1.4** also undergoes hydrolysis to the carboxylate after which no further racemisation is observed.[59] This is due to the negative charge already existing on the carboxylate.

It is interesting to consider ibuprofen (and indeed, all profens) at this point, as ibuprofen also has a carboxylate substituent on the stereogenic centre. Profens are known to undergo racemisation *in vivo* and a substantial literature exists documenting this.[77-81] However, profen racemisation occurs via an enzymatic conversion of the carboxylate to its acyl CoA thioesters which increases the lability of the proton bound to the stereogenic centre and chiral inversion occurs.[70, 82, 83] When the ester is hydrolysed, the starting material is recovered but any enantiopurity is lost. Similarly, in order to racemise naproxen (another profen), Noorduin *et al.*[84] first converted the carboxylate into methyl or ethyl esters.

Direct racemisation of ibuprofen without ester formation, required harsh conditions: high DMSO concentration, very high temperatures (100°C) and a very basic reaction medium (0.5 M NaOH).[85] The racemisation of free amino acids by Smith and Sivaua[40] also required temperatures in excess of 100°C. These results support the assignment of a carboxylate as configurationally stabilising under physiological conditions. However, the case of ibuprofen shows the importance of distinguishing between *in vivo* and *in vitro* testing.

21

Compound **1.18** (RS-10085) contains 3 stereogenic centres of type R''R'RC-H. Although epimerisation rates were not determined, Gu and Strickley[71] noted that only one of the three stereogenic centres showed any chiral instability. Comparison of the functional groups present on each stereogenic centre provides a rationale for this observation. The only stereogenic centre to show any chiral instability has amine (destabilising), alkyl (neutral) and ester (strongly destabilising) substituents. The other two stereocentres have an amine (destabilising), an amide (destabilising) and a methyl (neutral) substituent and an amine (destabilising), a methyl (neutral) and a carboxylate (stabilising) substituent. These observations provide general support for Testa's conclusion that either three destabilising substituents or two destabilising substituents (with one strongly so) and one neutral substituent must be present in order to see configurational instability in a stereogenic centre of type R''R'RC-H under physiological conditions.

1.5.2 Other Mechanisms of Racemisation

Stereogenic centres of the type R''R'RC-H with an adjacent carbonyl may also be susceptible to racemisation in acidic conditions. Protonation of the carbonyl followed by keto-enol tautomerism will result in loss of enantiopurity (Scheme 1.16).[86]
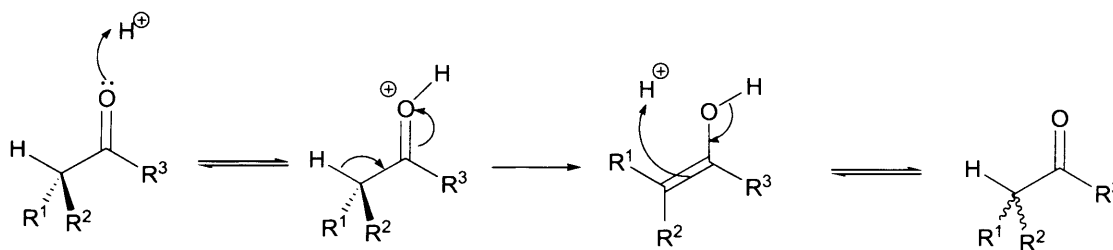
Scheme 1.16: Acid-catalysed racemisation of α-carbonyl stereocentres.

Similarly, acid-catalysed racemisation via imine-enamine tautomerism has been observed for **1.10** (9-hydroxyrisperidone) in aqueous conditions (Scheme 1.17).[62]

1.10

R = (CH₂)₂—N(piperidine)—(benzisoxazole)—F

$+/- H^{\oplus}$

$-H^{\oplus}$
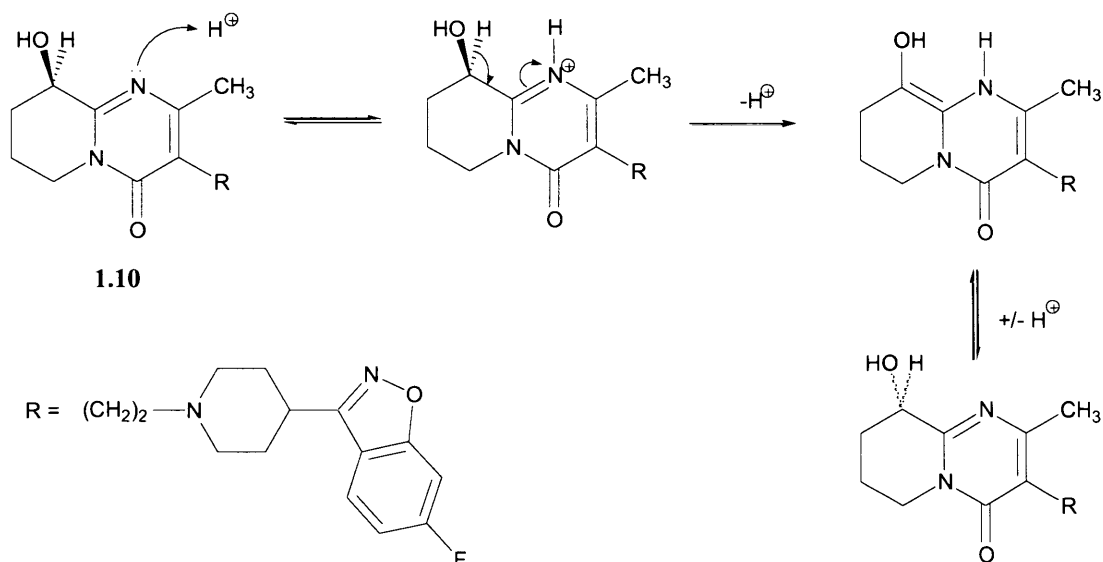
Scheme 1.17: Mechanism of racemisation of 9-hydroxyrisperidone (**1.10**).

General-acid catalysis by phosphate was observed for racemisation of **1.10**. The racemisation of this compound also showed some general-base catalysis, probably through proton abstraction, but this required severely basic conditions.

Compounds with a stereogenic centre of the form R''R'RC-OH have been shown to racemise through protonation of the alcohol followed by dehydration to give an achiral carbocation intermediate which can be hydroxylated on either face. Such a mechanism has been observed for catecholamines, such as **1.12** (adrenaline) (Scheme 1.18).[65]

1.12
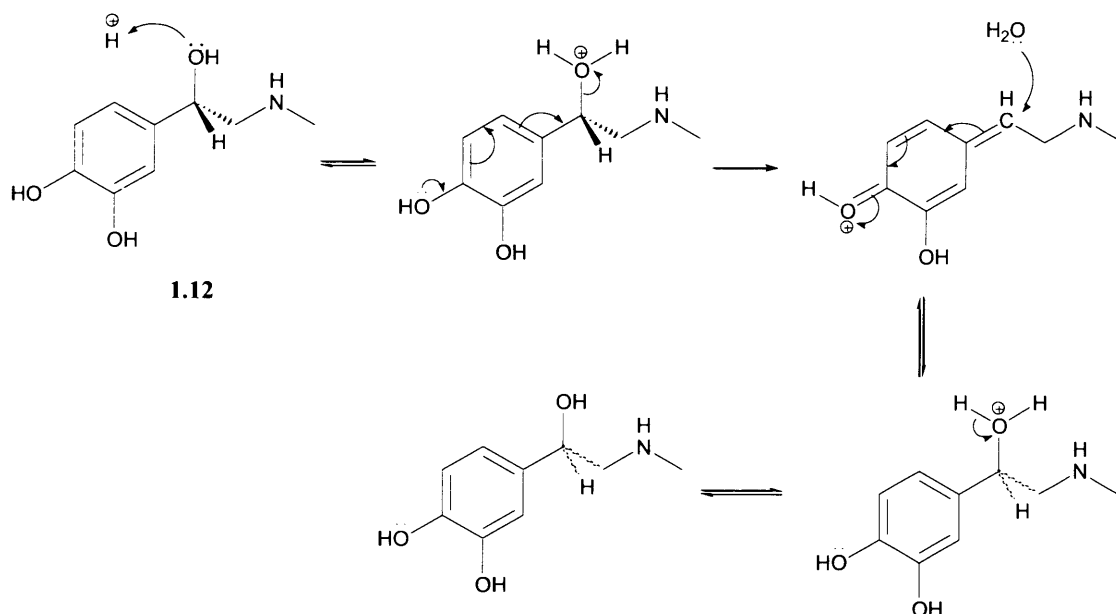
Scheme 1.18: Acid-catalysed racemisation mechanism of adrenaline (**1.12**).

For **1.12**, the electron-donating hydroxy substituent on the phenyl group adjacent to the stereogenic centre helps stabilise the positive charge build up during racemisation. Removal of the *p*-OH group results in a drop in the rate constant of racemisation by three orders of magnitude.

1.11 (ibutilide) and **1.16** (chlorthalidone) also contain stereogenic centres of the type R''R'RC-OH. They too show acid-catalysed racemisation as depicted in Scheme 1.18, with protonation of the alcohol followed by dehydration giving an achiral cationic intermediate which is hydroxylised on either face. **1.11** and **1.16** also undergo competing reactions that complicate the issue. For example, **1.11** also undergoes intramolecular nucleophilic attack by nitrogen at the stereogenic centre (Scheme 1.19).
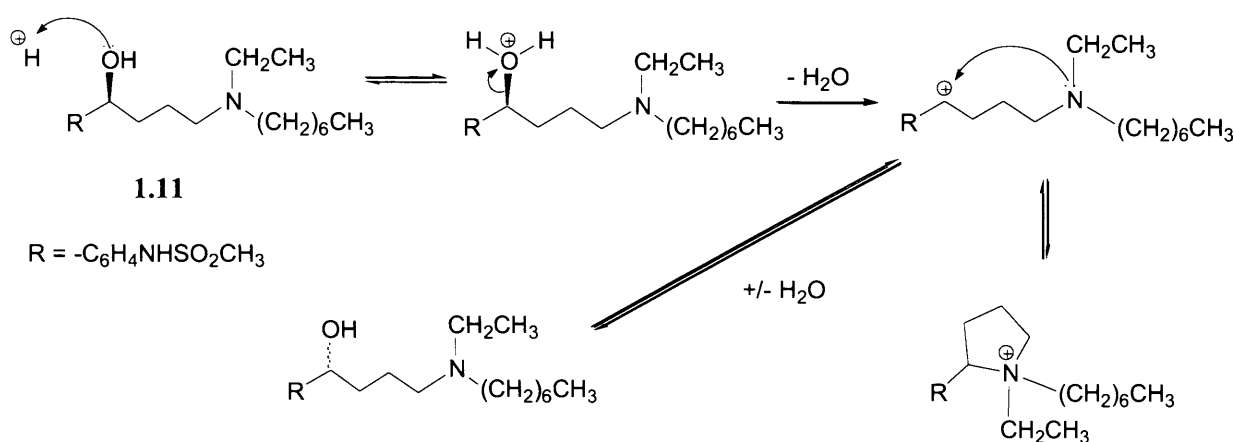
Scheme 1.19: Reactions of ibutilide (**1.11**).

Lambert *et al.*[64] concluded that some of the observed racemisation goes through the carbocation intermediate depicted in Scheme 1.19. This can be stabilised by electron donation from the *para* amine substituent on the adjacent aryl group (not depicted). However, there is also direct S_N2 racemisation through intramolecular nucleophilic attack by the amine with a hydroxyl leaving group.

Lamparter *et al.*[69] observed a U-shaped pH rate profile for the racemisation of **1.16** and observed both acid and base catalysis. Under acidic conditions protonation of the alcohol caused racemisation as depicted in Scheme 1.20a, but under basic conditions deprotonation of the alcohol group leads to ring opening to give an achiral intermediate (Scheme 1.20b).
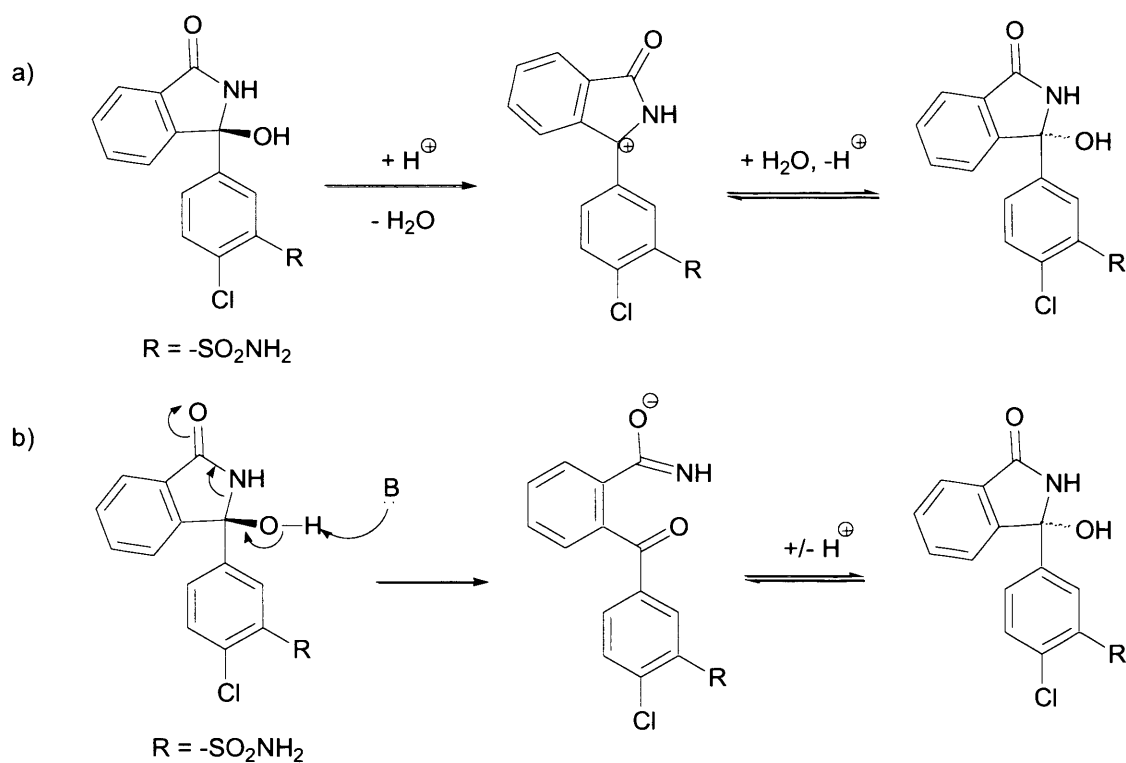
Scheme 1.20: Racemisation mechanisms of chlorthalidone (**1.16**) catalysed by a) acid, b) base.

The drug **1.15** (oxazepam) undergoes rapid racemisation with a half-life of around 3 minutes at ambient temperature in aqueous media.[68, 87, 88] As the rate of racemisation is fast in comparison to its pharmacologically active period, it has been suggested to regard **1.15** as 'a single compound existing in two very rapidly interconverting chiral states'.[89] **1.15** undergoes racemisation through the breaking and reforming of a bond adjacent the chiral centre. As the bond being broken is part of a seven membered ring, the reformation is not entropically demanding. This leads to a tautomeric equilibrium depicted in Scheme 1.21.
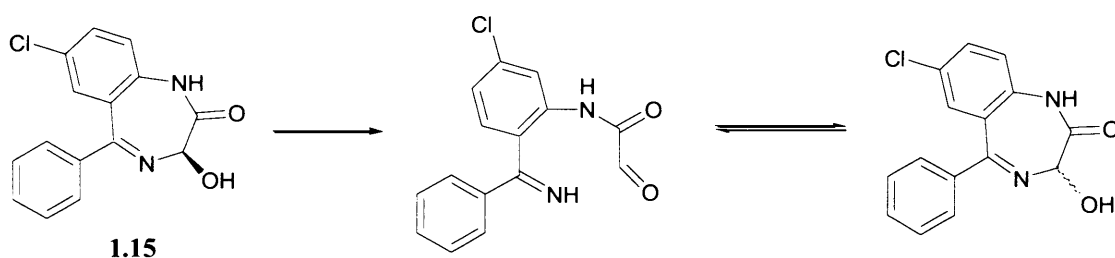
Scheme 1.21: Racemisation of oxazepam (**1.15**).

1.15 undergoes racemisation under acidic and basic aqueous solutions. In acidic solutions, protonation of the imine may catalyse the rearrangement whereas in basic solutions removal of the hydroxyl proton may be base catalysed.

1.6 Acid and Base Catalysis[90]

The aqueous nature of the blood stream and the presence within it of endogenous buffers such as proteins, amines and anions such as thiolates, phosphate and bicarbonate means that any acid or base catalysis of racemisation should be understood.[89]

1.6.1 Acid Catalysis

There are several examples in the literature of racemisation reactions catalysed by acid.[64, 91-93] Catalysis of a reaction by H_3O^+ ions only is referred to as specific-acid catalysis. In aqueous solutions, specific-acid-catalysed reactions are found to have pseudo first-order rate constants (eqn 1.3).

$$-\frac{d[R]}{dt} = k_{obs} \cdot [R] \qquad (1.3)$$

where [R] is the reactant concentration and k_{obs} is the observed rate constant.

The observed rate constant for specific-acid-catalysed reactions can be expressed in the form of eqn (1.4).

$$k_{obs} = k_0 + k_H \cdot [H_3O^+] \qquad (1.4)$$

where k_{obs} is the observed rate constant, k_0 is the rate constant for the uncatalysed reaction and k_H is the rate constant for the reaction catalysed by H_3O^+, and $[H_3O^+]$ is the concentration of H_3O^+.

k_0 and k_H for specific-acid-catalysed reactions can be determined by plotting k_{obs} against $[H_3O^+]$ for the reaction at various acid concentrations. The slope of the line corresponds to k_H and the intercept, where $[H_3O^+]$ equals 0, is k_0.

Catalysis by an un-ionised acid A-H is known as general-acid catalysis. General-acid catalysis will add an extra term to the expression for the rate constant for the reaction for each catalytically active acid present, resulting in eqn (1.5).

$$k_{obs} = k_0 + k_H \cdot [H_3O^+] + \sum k_{AH} \cdot [AH] \qquad (1.5)$$

where k_{obs} is the observed rate constant, k_0 is the rate constant for the uncatalysed reaction, k_H is the rate constant for the reaction catalysed by H_3O^+, k_{AH} is the rate constant for the reaction catalysed by the general acid AH, and $\Sigma k_{AH}.[AH]$ is the sum over the contributions of all catalytically active acids present.

A general-acid-catalysed reaction can be differentiated from a specific-acid-catalysed reaction, by determining the relationship between k_{obs} and [AH] at a constant pH. A specific-acid-catalysed reaction will give a horizontal line, whereas general-acid-catalysed reactions will give a slope. The intercept, where general acid concentration is 0, corresponds to $k_0 + k_H[H_3O^+]$ and the slope of the line corresponds to k_{AH}.

1.6.2 Base Catalysis

Base-catalysed racemisations are well documented in the literature.[40, 57, 61, 85, 94, 95] Base catalysis is generally a result of proton abstraction by base from stereocentres of the type R''R'RC-H through either an S_E1 or S_E2 mechanism (Section 1.3).

A reaction which takes place that is catalysed by OH⁻ but not by any other bases present is described as specific-base catalysed, analogous to specific-acid catalysis. The rate law for such reactions is described in eqn (1.6).

$$-\frac{d[R]}{dt} = k_{obs} \cdot [R] \qquad (1.6)$$

The pseudo first-order rate constant for such reactions can be expressed as eqn (1.7).

$$k_{obs} = k_0 + k_{OH} \cdot [OH^-] \qquad (1.7)$$

where k_{obs} is the observed rate constant, k_0 is the rate constant for the uncatalysed reaction and k_{OH} is the rate constant for the reaction catalysed by OH⁻.

Akin to specific-acid-catalysed reactions, a plot of k_{obs} against [OH⁻] for specific base-catalysed reactions gives a straight line with intercept k_0, and gradient k_{OH}.

If a reaction is catalysed by any base, it is general-base catalysed. The observed rate constant for such reactions is given by eqn (1.8).

$$k_{obs} = k_0 + k_{OH} \cdot [OH^-] + \sum k_B \cdot [B] \qquad (1.8)$$

where k_{obs} is the observed rate constant, k_0 is the rate constant for the uncatalysed reaction, k_{OH} is the rate constant for the reaction catalysed by OH⁻, k_B is the rate constant for the

reaction catalysed by general base B, and $\Sigma k_B.[B]$ is the sum over the contributions of all catalytically active bases present.

A general-base-catalysed reaction is catalysed by any base. As such, each general base present will need to be included in the sum function in eqn (1.8). This is important when a general base may exist in more than form, such as phosphate in different protonation states.

General-base-catalysed reactions are distinguished from specific-base-catalysed reactions in the same manner as specific- and general-acid-catalysed reactions are distinguished. A plot of k_{obs} against [B] at constant pH will give a horizontal line for specific-base-catalysed reactions and a slope for general-base-catalysed reactions with intercept $k_0 + k_{OH}[OH^-]$ and gradient k_B.

1.7 Kinetic Isotope Effects[96]

In studying chemical reactions, the presence of kinetic isotope effects (KIEs) can offer insight into the mechanism by which a reaction can take place. It is known that substitution of an atom within a molecule by an isotope of the same element does not affect the chemistry of the compound. Such a compound will undergo the same chemical reactions, via the same mechanisms, regardless of the change in isotope. However, the rate (or equilibrium) constant for the reaction may become smaller or larger due to the isotopic substitution. It is this change in rate constant, or lack thereof, that provides information on the mechanism of reaction.

The principles behind the KIE are best discussed for the example of a simple diatomic molecule, H-X, the zero-point energy (ε_0) of which is given by eqn (1.9).

$$\varepsilon_0 = 0.5h\nu \qquad (1.9)$$

where ν is the vibrational frequency and h is Planck's constant.

As eqn (1.9) shows, the zero-point energy is dependent on the molecule's vibrational frequency. Although increasing the mass of an atom in a molecule by addition of a neutron to the nucleus has no effect on the bonding within the molecule, it does affect its vibrational properties. The vibrational frequency of H-X (where X is an atom much heavier than hydrogen) is given by eqn (1.10).

$$\nu = \frac{1}{2\pi}\sqrt{\frac{\kappa}{\mu_{HX}}} \qquad (1.10)$$

where κ is the force constant of the bond and μ_{HX} is the reduced mass of the molecule.

The reduced mass for a diatomic molecule H-X is given by eqn (1.11).

$$\mu_{HX} = \frac{m_H \cdot m_X}{\left(m_H + m_X\right)}$$ (1.11)

where m_H is the mass of H and m_X is the mass of X.

If $m_X \gg m_H$, the reduced mass of H-X is approximately equal to 1. However, for the deuterated equivalent (D-X) the reduced mass is approximately equal to 2. From the reduced masses and eqn (1.11), the resulting molecular vibration of DX is lower than that of HX (eqn 1.12).

$$\frac{v_{HX}}{v_{DX}} = \sqrt{\frac{\mu_{DX}}{\mu_{HX}}} \approx \sqrt{2} \approx 1.41$$ (1.12)

This difference in vibrational frequencies is the basis for the KIE. As the vibrational frequency for D-X will be lower than that of H-X (eqn 1.12), the zero-point energy will also be lower (Figure 1.1).
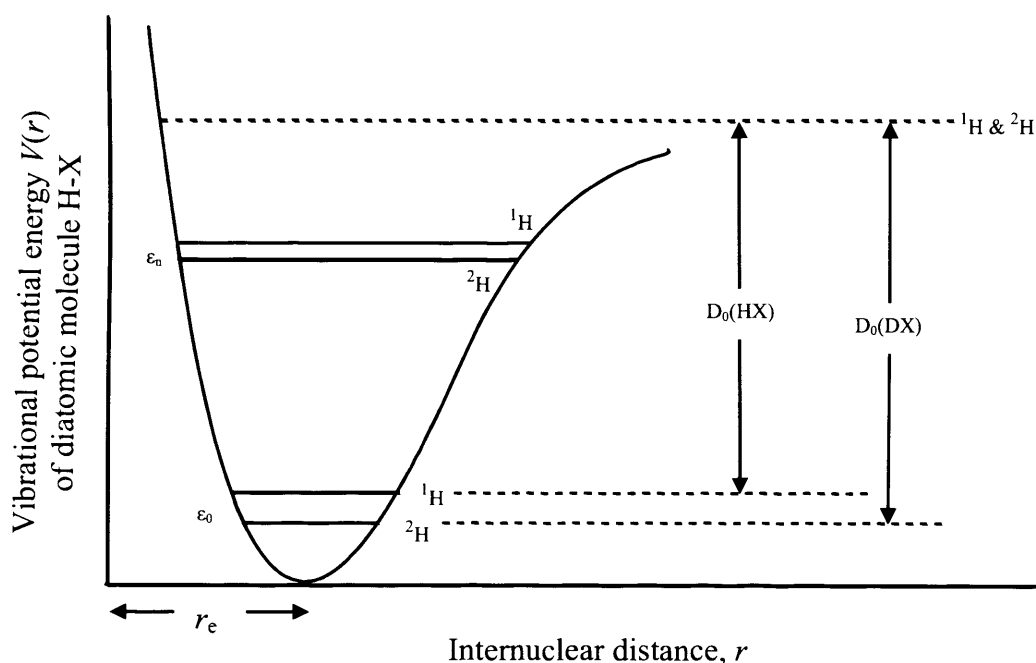
Figure 1.1: Enharmonic oscillator potential-energy diagram for diatomic molecules H-X and D-X (where the mass of X $\gg$ H). $D_0(HX)$ = dissociation energy of H-X, $D_0(DX)$ = dissociation energy of D-X.

Figure 1.1 shows that a greater amount of energy is required to break the D-X bond than is required to break the H-X bond. This is the origin of the KIE. For reactions where the rate-

determining-step involves breaking of a bond to a proton, the ratio k_H / k_D is therefore greater than 1, where k_H is the rate constant for the protonated reaction and k_D is the rate constant for the deuterated reaction. KIEs greater than 1 are known as a normal KIE, and are typically around 2-3. An example of a normal KIE is the dehydrogenation of propanol (Scheme 1.22).
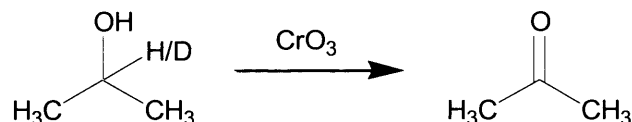
Scheme 1.22: Dehydrogenation of propan-1-ol by chromium trioxide, where $k_H / k_D = 7$.[96]

Instances where $k_H / k_D < 1$ are known as an inverse KIE. These occur when the force field of a vibration involving the isotopically substituted atom increases as the reaction progresses. This results in the vibrational potential energy curve of the activated complex becoming steeper than that of the reactant, and the gap between the ^1H energy level is larger than that between the ^2H energy levels.

Heavy atom KIEs may be observed when an element other than hydrogen is isotopically substituted (e.g. ^{35}Cl and ^{37}Cl). However, as the proportional difference in the reduced masses is far lower for isotopes of heavy atoms than for hydrogen, any KIE will be smaller in magnitude.

Isotopic variation of a molecule in positions other than the site of reaction may also give different rate constants. This is known as a secondary KIE. Magnitudes are generally far lower than for primary KIEs, typically around 0.80-1.25, and are dependent on the distance between the site of reaction and the isotopically varied atom.

KIEs may also be seen when the solvent in which the reaction is taking place is isotopically substituted. A common example is performing a reaction in both H_2O and D_2O. Solvent KIEs may be a result of the solvent being a reagent in the reaction, or result from different solvation properties of the isotopically substituted solvent.

1.8 Linear Free-Energy Relationships

1.8.1 The Brønsted Catalysis Law

The Brønsted catalysis law is a linear free energy relationship (LFER) that describes the relationship between acid or base strength with its catalytic ability in general-acid and –base

catalysis (see Section 1.6). The Brønsted relationship is described by eqn (1.13) for general-acid catalysis and by eqn (1.14) for general-base catalysis.

$$\log k_{AH} = -\alpha \cdot p\,K_{AH} + \text{constant} \qquad (1.13)$$

$$\log k_{B} = \beta \cdot p\,K_{BH} + \text{constant} \qquad (1.14)$$

where k_{AH} is the second-order rate constant for the reaction catalysed by the general acid AH, K_{AH} is the acidity constant of AH, α is the Brønsted factor for catalysis by general acids of the reaction under scrutiny, k_{B} is the rate constant for the reaction catalysed by the general base B, K_{BH} is the acidity constant of the conjugate acid of B and β is the Brønsted factor for catalysis by general bases of the reaction under scrutiny.

Values for α or β are determined by measuring k_{AH} or k_B for reaction for a series of acid or base catalysts. A logarithmic plot of the resulting rate constants against the pK_{AH} or pK_{BH} of the catalyst used in each case should give a straight line with gradient α or β (Figure 1.2).
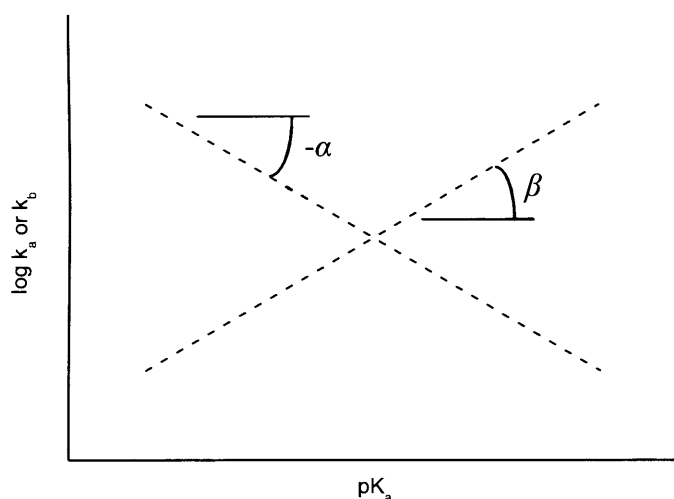
Figure 1.2: Example of a Brønsted plot, with gradient $-\alpha$ or β.

The Brønsted α and β coefficients quantify how sensitive the catalysed reaction is to the strength of the acid or base catalysts, and is typically in the range 0-1 for reactions carried out in water.

When α and β are close to zero or one, the values are difficult to determine experimentally. When close to zero, catalysis is insensitive to the strength of the catalyst, meaning the reaction will take place by pathways in proportion to the relative concentrations of each acid or base present. Therefore, in aqueous conditions the reaction will be almost exclusively

31

solvent induced, any acid or base catalysis will be difficult to observe and the reaction will appear uncatalysed. Conversely, as α and β tend to one the reaction is very sensitive to the catalyst strength. The majority of the reaction will take place by the strongest acid or base present, H_3O^+ or OH^- respectively in water, and the reaction will thus appear to be specific-acid or -base catalysed.

The physical reason for the LFER and the traditional interpretation of Brønsted α or β is illustrated by a potential energy diagram (Figure 1.3).

Reaction Coordinate
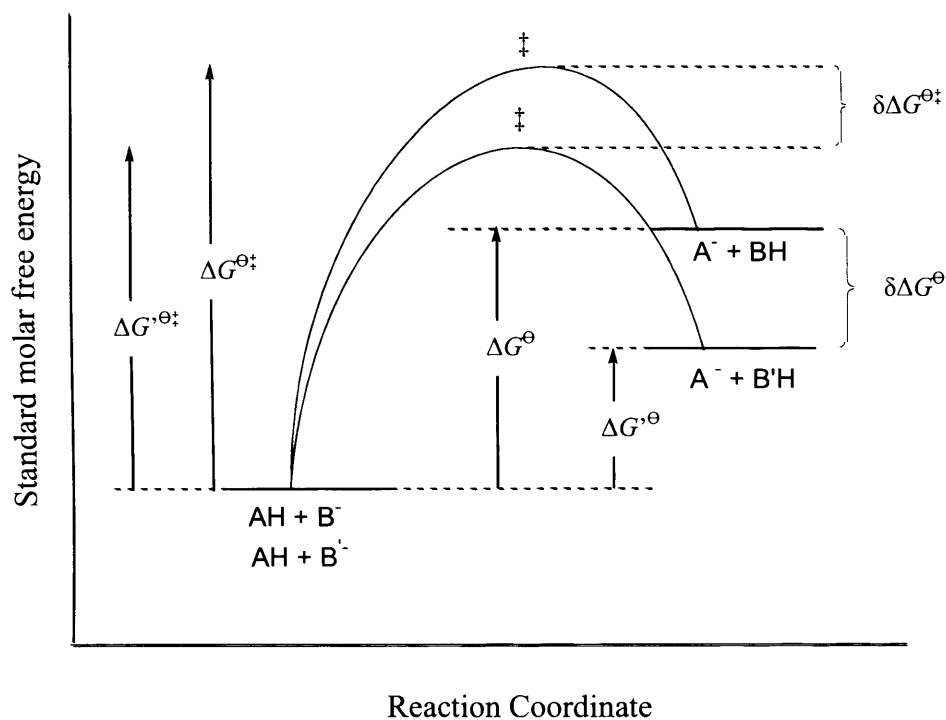
Figure 1.3: Reaction profile for proton abstraction by base. Reactant AH is the same for both curves, with base B modified to a stronger base B'. $\Delta G^{\ominus\ddagger}$ is the standard molar Gibbs energy of activation and $\Delta G^{\ominus}$ is the standard molar Gibbs energy of reaction

Modifying the base results in a lowering of the activation energy. The difference in activation energies for the two bases is denoted in Figure 1.3 by $\delta\Delta G^{\ominus\ddagger}$. The Brønsted parameter (β in this case) is the proportionality constant between $\delta\Delta G^{\ominus}$ and $\delta\Delta G^{\ominus\ddagger}$ (eqn 1.15).

$$\delta\Delta G^{\ominus\ddagger} = \beta \cdot \delta\Delta G^{\ominus} \qquad (1.15)$$

In the traditional interpretation of Brønsted plots, α or β describe the degree of proton transfer taking place at the transition state. As α or β tend to zero, the transition state is similar in structure to reactants and little or no proton transfer has occurred. As α or β tend to one, the transition state is similar in structure to the products and proton transfer is almost complete.

32

1.8.2 The Hammett Equation[97-99]

The Hammett equation is a Linear Free Energy Relationship (LFER) which can provide insight into the mechanism by which a specific reaction of a series of substituted aromatic compounds takes place. A series of compounds, differently substituted in the *meta* and *para* positions but with a common reaction site, will show differences in their reactivity at the common site dependent on the substituent nature. An equation providing a quantitative link between processes sharing a common development of charge was first proposed by Louis P. Hammett in 1937 based on the varying acidities of substituted benzoic acid derivatives.[100]
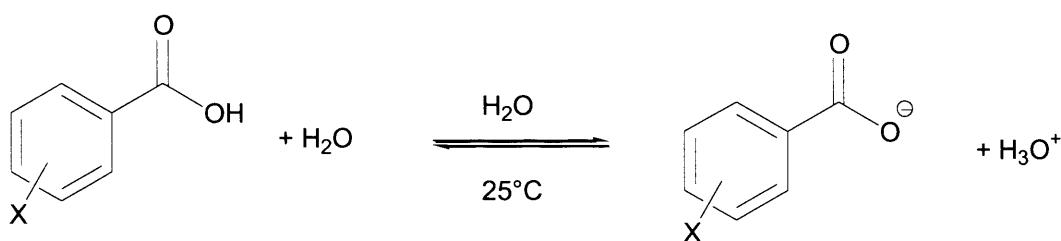
Scheme 1.23: Dissociation of benzoic acid derivatives.

For the deprotonation of benzoic acids, electron-withdrawing substituents stabilise the negative charge on the carboxylate and hence the equilibrium lies further to the right-hand-side of Scheme 1.23. Electron-donating substituents destabilise the negative charge and hence equilibrium lies further to the left. Taking the deprotonation of benzoic acids as a reference reaction, the basic equation describing the relationship between electronic substituent effect and equilibrium constants is given by eqn (1.16).

$$\log\left\{\frac{K_{\mathrm{X}}}{K_0}\right\} = \sigma\rho \qquad\qquad (1.16)$$

where K_{X} is the equilibrium constant of reaction for the compound with aromatic substituent X, K_0 is the equilibrium constant of reaction for the unsubstituted compound, σ is the substituent constant for substituent X and ρ is the reaction constant.

The reaction constant, ρ, was arbitrarily set to 1 for the dissociation of benzoic acids in water at 25 °C. This allows for each substituent X, the assignment of a substituent constant, σ, which quantifies its electron-withdrawing or –donating capability. The same substituent will have a different σ value depending on whether it is in the *meta-* (σ_{m}) or *para*-position (σ_{p}) (*ortho* substituents are excluded as steric effects become a factor as well as the electronic factors). Compared to no substitution, electron-withdrawing substituents have a positive σ value; electron-donating substituents have a negative σ value (Table 1.5).

33

Table 1.5: List of example Hammett substituent constants.[75] The applicability of σ_p^- and σ_p^+ substituent constants is outlined in Sections 1.8.2.2.1 and 1.8.2.2.2.

Substituent	Substituent Constants			
	σ_m	σ_p	σ_p^-	σ_p^+
NO$_2$	0.71	0.78	1.27	0.79
CF$_3$	0.43	0.54	0.65	0.61
COOH	0.37	0.45	0.77	0.42
COOMe	0.37	0.45	0.75	0.49
Cl	0.37	0.23	0.19	0.11
F	0.34	0.06	-0.03	-0.07
OMe	0.12	-0.27	-0.26	-0.78
OH	0.12	-0.37	-0.37	-0.92
H	0.00	0.00	0.00	0.00
Et	-0.07	-0.15	-0.19	-0.30
Me	-0.07	-0.17	-0.17	-0.31
COO$^-$	-0.10	0.00	0.30	-0.02
NH$_2$	-0.16	-0.66	-0.15	-1.30

Using these substituent constants, the ρ value of any reaction can be determined experimentally. A positive ρ value informs us that negative charge is built up during the reaction or a positive charge is removed; a negative value tells us that positive charge is built up or a negative charge is removed.

The Hammett equation is most frequently used for analysis of rate constants for reactions of a series of substituted aromatic compounds (eqn 1.17).

$$\log\left\{\frac{k_X}{k_0}\right\} = \sigma\rho \qquad (1.17)$$

where k_X is the rate constant of reaction for the compound with aromatic substituent X, k_0 is the rate constant of reaction for the unsubstituted compound, σ is the substituent constant for substituent X and ρ is the reaction constant to be determined.

Again, the sign and magnitude of ρ affords information on the nature and magnitude of any charge built up (or removed) on the activated complex during the reaction, and therefore informs us about the mechanism by which the reaction takes place.

The information that can be retrieved from ρ is illustrated by the hydrolysis reaction of substituted phenyl diphenylphosphinates, catalysed by imidazole (Scheme 1.24).[101]
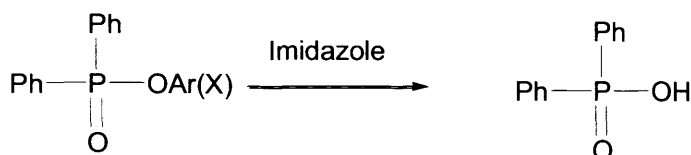
Scheme 1.24: Hydrolysis of substituted phenyl diphenylphosphinates, catalysed by imidazole.

The rate constants for the differently substituted esters are listed in Table 1.6.

Table 1.6: Rates of hydrolysis of substituted phenyl diphenylphosphinates catalysed by imidazole in 10 % dioxane in water, pH 8.12, 55 °C (data from reference 100).

Substituent X	σ	$k \times 10^3$ / M^{-1} s^{-1}	$\log \dfrac{k_X}{k_0}$
p-NO$_2$	0.78	4.880 ± 0.080	2.130
m-NO$_2$	0.71	2.100 ± 0.030	1.764
p-C(O)Me	0.50	0.857 ± 0.008	1.374
p-Cl	0.23	0.141 ± 0.0003	0.590
H	0	0.0362 ± 0.0002	0

A Hammett plot of the data from Table 1.6 is displayed in Figure 1.4.

2.5

2.0

1.5

$\log(k_X / k_H)$ 1.0

0.5

0.0

0.0   0.2   0.4   0.6   0.8

σ
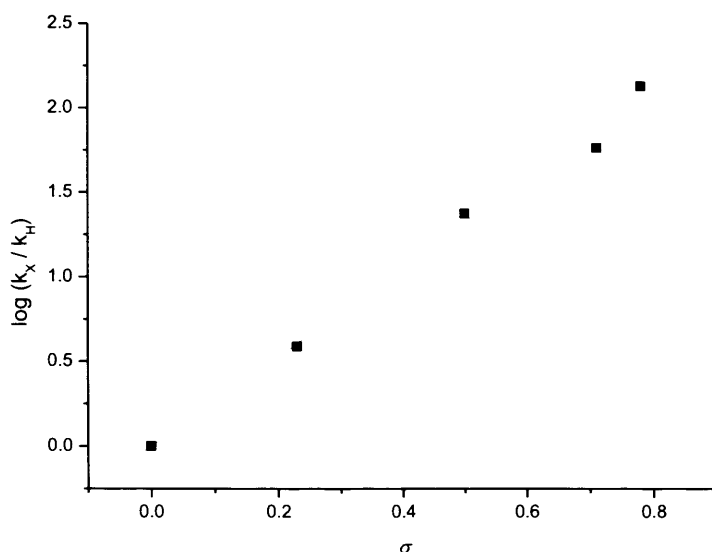
Figure 1.4: Hammett plot for the imidazole catalysed hydrolysis of substituted phenyl diphenylphosphinates in 10 % dioxane in water, pH 8.12, 55 °C, $\rho = 2.64$.

The sign and magnitude of ρ suggests that a significant extent of negative charge is built up on the activated complex during hydrolysis (Scheme 1.25).

Ph | Ph—P—OAr(X) → B, H₂O → [B, H, O, δ⁻, P, Ph, Ph, OAr(X)] → -BH → Ph—P—OH + ⁻OAr(X)
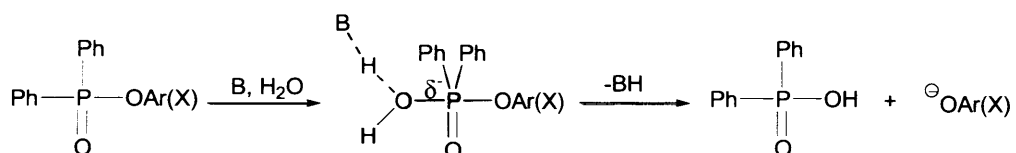
Scheme 1.25: Negative charge build up during hydrolysis of phenyl diphenylphosphinates.

This negative charge is stabilised by electron withdrawing groups. This means $\Delta G^{\ddagger}$ is lowered and hence the reaction takes place with a higher rate constant.

1.8.2.1 Factors Affecting p

1.8.2.1.1 Distance Between Reaction Site and Aromatic Substituent

The number of bonds in a molecule between the site of reaction and the substituted aromatic ring will affect the magnitude of ρ. Increased distance between the reaction site and the substituted aromatic ring will diminish the transmission of any electronic effect, and reduce the magnitude of ρ. This is illustrated by the dissociation of aromatic acids. The original

Hammett σ constants are based on the equilibrium constants for dissociation of benzoic acids in water at 25 °C. Moving the site of dissociation away from the site of substitution lowers the ρ value as displayed in Table 1.7.

Table 1.7: Hammett ρ values for the dissociation of aromatic acids in H_2O at 25 °C.[102]

Acid[a]	ρ
ArCOOH	1.00
ArCH$_2$COOH	0.49
ArCH$_2$CH$_2$COOH	0.21

[a] Ar = X-C$_6$H$_4$- where X is the variable substituent

1.8.2.1.2 Temperature Dependence of ρ

The temperature dependence of ρ has been subject to much debate. Many studies have suggested that the reaction constant ρ varies with temperature,[103-106] in one manner or another. The effect of the reaction medium and temperature on ρ values has been described by eqn (1.18).[100, 107, 108]

$$\rho = \left(\frac{A + (B/D)}{RT} \right)$$ (1.18)

where, A and B describe the susceptibility of the reaction to polar effects independent and dependent on the reaction medium, D is the dielectric constant of the medium, R is the gas constant and T is the temperature.

Eqn (1.18) suggests that the magnitude of ρ is inversely proportional to T. As a result, we would expect to see the ρ value of a reaction decrease if the temperature is increased. However, eqn (1.18) and the dependence of ρ on T^1 has not been unequivocally accepted.[109-111] An example of a lack of temperature dependence of ρ is provided by the racemisation of phenylglycines in aqueous conditions, as studied by Smith and Sivakua.[40] They found identical ρ values of 1.15 for the reaction at both 80 and 110 °C, and concluded that temperature was not a major factor for the ρ value.

1.8.2.1.3 Non-linearity

For some reactions, the Hammett relationship does not apply and a non-linear Hammett plot is found. A non-linear Hammett plot may indicate that the LFER has broken down, potentially

as a result of a change in mechanism, for example from an S_N2 to an S_N1 or S_AN mechanism.[112] The application of modified Hammett substituents in certain circumstances can also be used to explain and circumvent non-linearity in a Hammett plot.

1.8.2.2 Modifications of the Hammett Equation

In some circumstances, the Hammett σ constants require modification for certain substituents. In order for a LFER to be valid, the change from the reference compound to the modified compound (in this case from the unsubstituted to substituted compound) should be qualitatively the same on the test reaction and the reference reaction (dissociation of benzoic acids for σ constants).

1.8.2.2.1 σ^- Substituent Constants

In certain reactions, developing π-electron density can be delocalised directly to a *para*-substituent that can accept a formal negative charge, such as a nitro or aldehyde group. In these circumstances the reference reaction is not directly comparable (as the charge in the dissociation of benzoic acids cannot be delocalised to *para* substituents) and so the σ constants cannot be expected to provide the basis for a good correlation for the new set of circumstances. As a result, a new modified substituent constant, σ^-, was developed to properly account for such situations. The values of σ^- were obtained from the dissociation constants of substituted phenols in H_2O at 25 °C, where a negative charge can be delocalised onto particular *para* substituents, such as a nitro substituent (Scheme 1.26).

a)

b)
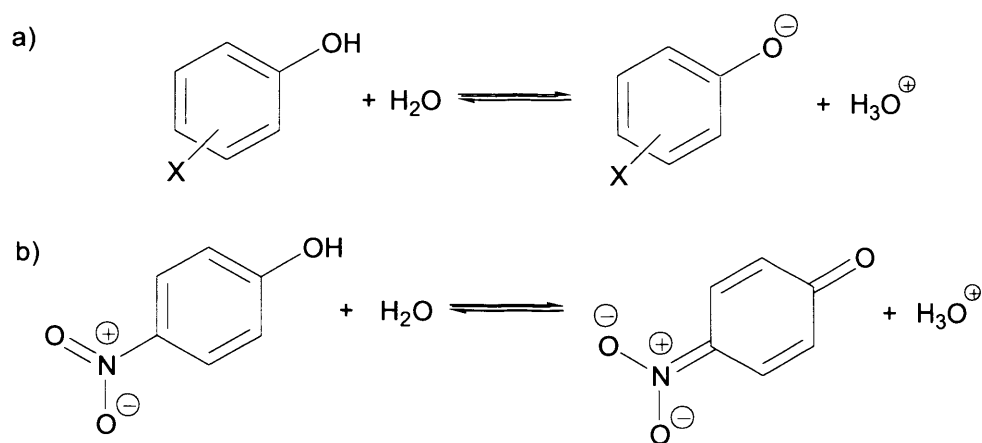
Scheme 1.26: a) Dissociation of substituted phenols at 25 °C, reference reaction for σ^- constant; b) example of stabilisation of negative charge onto a p-NO$_2$ group.

Examples of how some Hammett substituent constants change when a negative charge is built up directly adjacent to the aromatic ring can be seen in Table 1.5.

1.8.2.2.2 σ^+ Substituent Constants

Correspondingly, for reactions where positive charge built up on the reaction centre can be directly stabilised through π-electron donation by a *para* substituent, the alternative substituent constant σ^+ was developed. Values for σ^+ are obtained from rate constants of the solvolyses of substituted cumyl chlorides in 90 % aqueous acetone at 25 °C (Scheme 1.27).

a)

b)
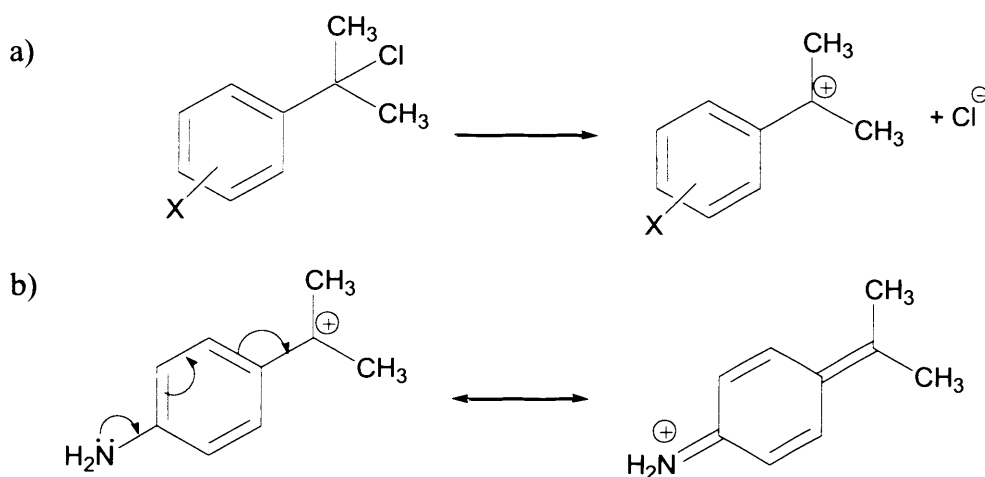
Scheme 1.27: a) Solvolyses of substituted cumyl chlorides in 90 % aqueous acetone at 25 °C, reference reaction for σ^+ constant; b) example of stabilisation of positive charge by p-NH$_2$ group.

Examples of how some Hammett substituent constants change when a positive charge is built up directly adjacent to the aromatic ring can be seen in Table 1.5.

1.8.2.2.3 The Yukawa-Tsuno Equation[113]

The Yukawa-Tsuno equation is an extension of the Hammett equation. Rather than selecting either the parameter for no significant resonance conjugation between the reaction site and the substituent (σ), or the parameter for full conjugation (σ^- or σ^+), the Hammett equation is refined to acknowledge the possible presence of an intermediate degree of resonance interaction. This degree of resonance is denoted by a new parameter, r^- or r^+, depending on whether the substituent is accepting or donating an electron pair, respectively. For electron pair acceptors, adding the extra term gives eqn (1.19).

$$\log\left\{\frac{k_X}{k_0}\right\} = \rho\{\sigma + r^-(\sigma^- - \sigma)\} \qquad (1.19)$$

Analogously, for electron pair donors eqn (1.20) is used.

$$\log\left\{\frac{k_X}{k_0}\right\} = \rho\{\sigma + r^+(\sigma - \sigma^+)\} \qquad (1.20)$$

r^- and r^+ values can be determined by initially determining the ρ value using only *meta*-substituted compounds or *para*-substituted compounds where $\sigma = \sigma^-$ or $\sigma = \sigma^+$. The value of r^- or r^+ can then be found from the gradient of a plot of $\left(\frac{1}{\rho} \cdot \log\left\{\frac{k_X}{k_H}\right\} - \sigma\right)$ against the difference of σ and σ^- / σ^+.

Other extensions of the Hammett equation that will not be discussed include the Taft equation,[114] which introduces steric influences and the Swain-Lupton equation,[115] which divides the substituent constant into field (inductive) and resonance effects.

1.8.2.3 Cross-Interaction Terms[116, 117]

The incorporation of more than one substituted aromatic ring in a reactant can increase the number of terms required in the Hammett equation. For example, Lee *et al.*[118] studied the nucleophilic substitution of substituted benzoyl chlorides with substituted anilines (Scheme 1.28).

X = p-CH$_3$, H, p-Cl, m-NO$_2$
Y = p-CH$_3$, H, p-Cl
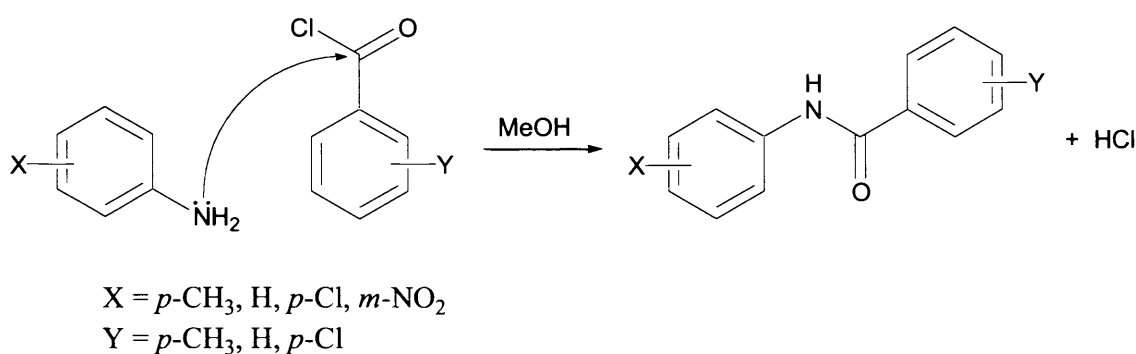
Scheme 1.28: Nucleophilic substitution of substituted benzoyl chlorides with substituted anilines, in methanol at 35 °C.

Variation of either X- or Y- substituent over the full range of substituents in Scheme 1.28 gives a table of 12 rate constants. A value of ρ can be determined from the data in each line and column of the table. One series of ρ will be for variation of the nucleophile with different electrophilic centres and the other series of ρ will be for variation of the electrophilic centre with different nucleophiles. Rather than reporting a range of ρ_X and ρ_Y values, however, the kinetic data can be summarised in terms of eqn (1.21).

$$\log\left\{\frac{k_{XY}}{k_{HH}}\right\} = \rho_X\sigma_X + \rho_Y\sigma_Y + \rho_{XY}\sigma_X\sigma_Y \qquad (1.21)$$

where ρ_X and ρ_Y are the reaction constants for varying the X- and Y-substituent respectively, σ_X and σ_Y are the substituent constants for the X- and Y-substituent respectively and ρ_{XY} is the cross-interaction term.

ρ_{XY} is usually obtained by multiple-regression analysis. The cross-interaction term affords information as to the intensity of the interaction between the two substituents through the reaction system framework. In the example shown in Scheme 1.28, ρ_{XY} = -0.68. The negative sign of ρ_{XY} suggests that a stronger nucleophile (more electron-donating X-substituent) gives a more positive reaction constant when varying the electrophile, resulting from a greater degree of bond-formation in the transition state (i.e. the development of more negative charge on reaction centre).

Other systems have been analysed where three aromatic rings have been included in the reaction centres,[119, 120] but that is beyond the scope of this thesis.

41

1.8.2.4 Application of the Hammett Equation to Heterocycle-Substituted Reactants

It was first suggested that effective substituent constants could be defined for aromatic heterocycles by Jaffé.[108] Since then a range of substituent constants have been proposed for many different heterocycles. Agreement on specific values has proved difficult - Charton[121] lists eight different values of reported σ values for 2-thienyl substitution, ranging from -0.15 to 0.71, determined by correlation with various reference reactions. As the author notes, in order to be useful, substituent constants should be reasonably constant for a range of reactions. As such, the scope for inclusion of heteroaryl groups within the Hammett equation appears limited, and efforts to do so must be viewed in this context. For five-membered heterocycles, the substituent constants used in this thesis were determined by correlation with the pK_a of benzoic acids in water at 25 °C.[122, 123] As they are the second most frequently found aromatic heterocycle in drug databases (after benzene),[124] it is also desirable to obtain σ values for pyridine-substituted compounds. Determining σ values for pyridines is complicated by protonation on the heteroatom, which can also lead to zwitterion formation and tautomerisation when determining σ values from data for nicotinic and isonicotinic acids (which are analogous to benzoic acids).[125] Protonation also makes the pyridine heterocycle much more electron-withdrawing and hence different σ values exist for neutral and protonated pyridine as substituent. The substituent constants used for heterocycles in this thesis are summarised in Table 1.8.

Table 1.8: Hammett σ values of heterocycles determined by correlation with pK_a of benzoic acids in water at 25 °C.[122, 123] Pyridine σ values determined at 22 °C.[125]

Heterocycle	Heteroatom position	
	α	β
thiophene	0.72	0.12
furan	1.08	0.25
pyrrole	-0.24	-0.34
	3	**4**
pyridine	0.45	0.76
protonated pyridine	2.09	2.34

The σ values for pyridines in Table 1.8 are supported by pK_a data for substituted phenyl ketones reported by Richard *et al.*[126] (Scheme 1.29).

| pK_a | 14.8 | 12.7 | 7.0 |
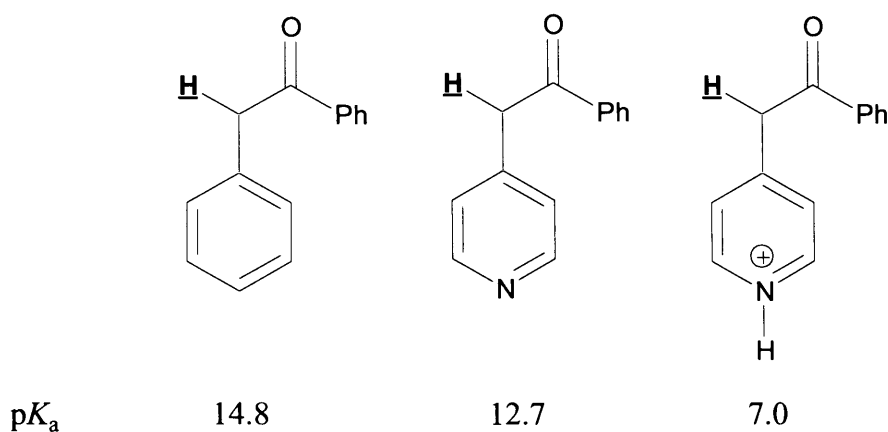
Scheme 1.29: Comparison of pK_a's for substituted phenyl ketones.

Scheme 1.29 shows a decrease of two pK_a units for a carbon acid when an adjacent phenyl group is substituted for a 4-pyridyl group, and a decrease of nearly 8 pK_a units for a carbon acid when an adjacent phenyl group is substituted for a protonated 4-pyridyl group. These figures are consistent with the σ values for pyridine substituents displayed in Table 1.8, which suggest that a 4-pyridyl group is more electron-withdrawing than a phenyl group and that a protonated 4-pyridyl group is far more electron-withdrawing than a phenyl group.

1.9 Thermodynamic Activation Parameters

1.9.1 The Arrhenius Equation

The Arrhenius equation describes the temperature dependence of reaction rate constants. In terms of the Arrhenius equation, each reaction has a pre-exponential factor, A, and an activation energy, E_a, both of which have negligible temperature dependence over small temperature ranges. The Arrhenius equation takes the form of eqn (1.22).[127]

$$k = A \cdot e^{-E_a / RT} \tag{1.22}$$

where k is the rate constant, A is the pre-exponential factor (having the same units as k), E_a is the activation energy, R is the gas constant and T the temperature.

Collision theory suggests that the pre-exponential factor is the constant of proportionality between the concentration of reactants and the rate at which the reactant molecules collide in the correct orientation for reaction. The activation energy is the minimum kinetic energy required for a particular collision to result in reaction, and reflects the temperature dependence of the rate constant.[128] The greater the activation energy, the greater the temperature dependence of the reaction in question.

43

Eqn (1.22) can alternatively be written as eqn (1.23).

$$\ln k = \ln A - \frac{E_a}{RT}$$ (1.23)

Eqn (1.23) shows that a plot of $\ln k$ against $1/T$ should result in a linear graph, with a y-axis intercept equal to $\ln A$ and a gradient of $-E_a/R$. This plot is known as an Arrhenius plot.

1.9.2 The Eyring Equation

The Eyring equation also describes the change in rate constant as a function of temperature. The Eyring equation differs from the Arrhenius equation in that it is based on the standard molar Gibbs energy of activation, $\Delta G^{\ominus\ddagger}$, of a reaction. The Eyring equation can be used to determine the enthalpy and entropy of activation for a chemical reaction. The general form of the equation is given by eqn (1.24).[129-131]

$$k = \left(\frac{k_B T}{h} \right) \cdot e^{-\frac{\Delta G^{\ddagger}}{RT}}$$ (1.24)

where k_B is the Boltzmann constant, h is Planck's constant and $\Delta G^{\ddagger}$ is the Gibbs energy of activation.

Inserting the terms for enthalpy and entropy of activation into eqn (1.24) gives eqn (1.25)

$$k = \left(\frac{k_B T}{h} \right) \cdot e^{-\frac{\Delta H^{\ddagger}}{RT}} \cdot e^{\frac{\Delta S^{\ddagger}}{R}}$$ (1.25)

Eqn (1.25) can be rearranged to the linear form, eqn (1.26).

$$\ln\left(\frac{k}{T} \right) = \left(\frac{-\Delta H^{\ddagger}}{RT} \right) + \ln\left(\frac{k_B}{h} \right) + \left(\frac{\Delta S^{\ddagger}}{R} \right)$$ (1.26)

where $\Delta H^{\ddagger}$ is the enthalpy of activation and $\Delta S^{\ddagger}$ is the entropy of activation

Eqn (1.26) shows that a plot of $\ln k/T$ against $1/T$ should result in a linear plot (Eyring plot). The gradient of this plot equals $-\Delta H^{\ddagger}/R$, and the y-axis intercept equals $\ln (k_B/h) + \Delta S^{\ddagger}/R$.

1.9.3 Interpretation of Eyring Thermodynamic Activation Parameters

Interpretation of $\Delta H^{\ddagger}$ and $\Delta S^{\ddagger}$ values is best done by comparison. Table 1.9 shows a selection of typical literature values of $\Delta H^{\ddagger}$ and $\Delta S^{\ddagger}$.

Table 1.9: Some examples of activation parameters.

Reaction	$\Delta H^{\ddagger}$ / kJ mol^{-1}	$\Delta S^{\ddagger}$ / J K^{-1} mol^{-1}
Hydrolysis of CH_3Cl [132, 133]	100.4	-51.5
Hydrolysis of CH_3Br [132, 133]	96.2	-42.3
Hydrolysis of CH_3I [132, 133]	102.7	-33.9
Hydrolysis of n-C_3H_7Br [132, 133]	92.5	-56.9
Solvolysis of t-Butyl chloride in H_2O [132, 134]	97.15	51.0
Solvolysis of t-Butyl chloride in CH_3OH [132, 134]	104.1	-13.0
Solvolysis of **1.19** in C_2H_5OH [132, 134]	124.0	-9.2
Solvolysis of **1.19** in HCO_2H [132, 134]	104.0	15.0
Solvolysis of **1.20** in H_2O [135]	43.0	-179.0
Thermal decomposition of 1,1'-azobutane [136, 137]	217.6	79.5
Dimerisation of cyclopentadiene [137, 138]	64.9	-142.3
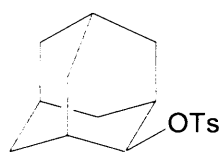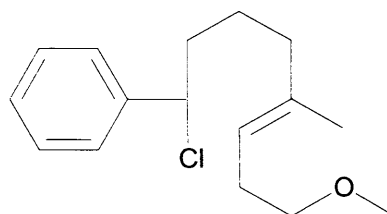
1.19   **1.20**

$\Delta H^{\ddagger}$ corresponds to the energy required for bond reorganisation in formation of the activated complex.[137] The energy cost of breaking a bond means that $\Delta H^{\ddagger}$ will be high if bond breaking is important in the rate-determining step, and low if bond formation is important in the rate-determining step. An example of a large $\Delta H^{\ddagger}$ is the thermal decomposition of 1,1'-azobutane, where the rate-determining step is homolytic breaking of C-N bonds. A large $\Delta H^{\ddagger}$ is found because there is little bond formation to compensate for the bond breaking. The solvolysis of **1.20**, and the dimerisation of cyclopentadiene have low $\Delta H^{\ddagger}$ as both reactions involve concerted cyclisation mechanisms with bond formation simultaneous with bond breaking.

$\Delta S^{\ddagger}$ corresponds to the degree of organisation that results from activated complex formation. Loss of degrees of electronic, rotational or translation freedom in forming the activated complex results in reduced entropy of the system and hence $\Delta S^{\ddagger}$ will be strongly negative. A gain of degrees of electronic, rotational or translation freedom through molecules falling apart will result in $\Delta S^{\ddagger}$ being slightly negative or positive. The values in Table 1.9 for $\Delta S^{\ddagger}$ reflect this. The hydrolysis reactions occurring by an S_N2 mechanism have a negative $\Delta S^{\ddagger}$ as bringing together the molecules for reaction reduces the entropy. The solvolysis reactions of t-butyl chloride and **1.19** have only slightly negative or positive $\Delta S^{\ddagger}$ as the molecule 'falls apart' increasing disorder in the S_N1 mechanism. Slightly negative $\Delta S^{\ddagger}$ in the solvolysis of t-butyl chloride and **1.19** are due to solvent rearrangement giving an increasingly structured solvation of the ionic intermediates. The large positive value of $\Delta S^{\ddagger}$ for thermal decomposition of 1,1'-azobutane is due to the increased entropy resulting from transformation of one molecule to three. Conversely, formation of highly ordered cyclic transition states results in the strongly negative $\Delta S^{\ddagger}$ for solvolysis of **1.20**, and dimerisation of cyclopentadiene.

1.10 Experimental Techniques

1.10.1 ¹H NMR Spectroscopy[139-142]

The technique Nuclear Magnetic Resonance (NMR) spectroscopy relies on protons and neutrons having a property called 'spin'. When placed in a magnetic field, spin will cause protons and neutrons to orientate themselves either with the magnetic field or opposed to it. The small energy gap between these two states is dependent on the interaction between the nucleus and the magnetic field. Application of electromagnetic radiation of a specific frequency will cause the nuclei to switch from the low energy state (aligned with the magnetic field) to the high energy state (against the magnetic field). Each spin-active nucleus has a different resonance frequency and can therefore be distinguished. Furthermore, this resonance frequency is also slightly dependent on the chemical environment in which the nucleus finds itself. This difference in resonance frequency allows distinction between atoms in different chemical environments and allows for elucidation of a molecular structure.

As discussed previously (Section 1.3), proton-deuterium exchange can be used to indirectly investigate the rate constant and mechanism of racemisation. ¹H NMR spectroscopy as a method of determining the rate of H/D exchange has been frequently used to investigate the

racemisation of stereogenic centres of type R''R'RC-H.[33, 39, 57, 59, 143-145] The molecule under investigation is dissolved in a D_2O-based buffer and incubated at the desired temperature. ^1H NMR spectra of the compound are recorded over a period of time. If the protons bound to the stereogenic centre of the molecule exchange with solvent, they will be replaced by deuterons. As a result, the ^1H NMR spectra will show a decrease in the intensity of the peak corresponding to the proton bound to the stereogenic centre. This decrease in intensity can be recorded in relation to peaks in the ^1H NMR spectrum from another part of the molecule (that is assumed not to undergo H/D exchange itself),[146] or relative to an external standard added to the solution.

1.10.2 Mass Spectrometry[147]

Mass Spectrometry (MS) is an important tool in compound characterisation. The procedure to obtain a mass spectrum can be divided into three stages: initial vaporisation of the analyte; production of ions from the gas-phase molecules formed; and subsequent separation and detection of these ions by their mass-to-charge ratio (m/z). Vaporisation is achieved by heating a sample to high temperatures at low pressure. Ionisation is usually achieved through either the electron impact (EI) or chemical ionisation (CI) method. EI proceeds by firing an electron beam at the sample, removing an electron from the sample and leaving a radical-cation (eqn 1.27).

$$M + e \rightarrow M^{\bullet +} + 2e \qquad (1.27)$$

The molecular ions produced through EI can then fragment through well documented fragmentation processes. The pattern of fragment ions can then be used to characterise the compound.

CI proceeds by collision of the sample with ions of a reagent gas to give a protonated sample. Initial ionisation of a sample gas such as methane is done with an electron beam as in EI producing a radical cation (eqn 1.28).

$$CH_4 + e \rightarrow CH_4^{\bullet +} + 2e \qquad (1.28)$$

The radical cation produced will then collide with neutral molecules to yield a cation (eqn 1.29).

$$CH_4^{\bullet +} + CH_4 \rightarrow CH_5^+ + CH_3^{\bullet} \qquad (1.29)$$

47
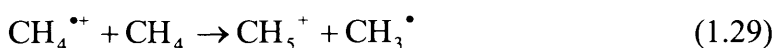
Entering the sample into this mixture will cause CH_5^+ to act as a strong acid and the sample is protonated (eqn 1.30).

$$M + CH_5^+ \rightarrow MH^+ + CH_4 \qquad (1.30)$$

Fragmentation is less common in CI than EI. This makes the molecular weight of the sample easily obtainable, as the observed m/z value will be one unit larger than the sample's molecular weight. Detection of the ions from both ionisation methods is achieved using a mass analyser. The mass analyser separates the ions from the spectrometer by deflection of the ions in a strong magnetic field; ions of greater mass are deflected less than those of a smaller mass. Mass spectrometry can also be enhanced by coupling the technique to gas and liquid chromatographs (GCMS and LCMS). This allows for chemical separation of analytes before characterisation by MS.

As in the case of ^1H NMR spectroscopy, MS has been used to investigate the rate constant and mechanism of racemisation by determining the rate of H/D exchange.[143] Monitoring the reaction over time and determining the ratio of the parent compound ion to its deuterated equivalent from the CI spectra, allows calculation of the rate constant of deuterium incorporation at the stereogenic centre.

1.10.3 Circular Dichroism[148]

Circular Dichroism (CD) is a phenomenon arising from the molecular property of chirality. The technique of CD spectroscopy works through analysis of the sample using plane polarised light. Plane-polarised light consists of two components of circularly polarised light of equal intensity but rotating in opposite directions. These are known as right circularly polarised light (rcpl) and left circularly polarised light (lcpl). Rcpl and lcpl are mirror images of each other. Each component will interact differently with an enantiomer of a chiral molecule.

The absorbance of unpolarised light by a sample is defined in eqn (1.31).

$$A = \log(I_0 / I) \qquad (1.31)$$

where A is the absorbance of unpolarised light, I is the intensity of light after it has travelled a distance l through the sample, I_0 is the intensity before it has travelled through sample

A can also be described by the Beer-Lambert law, eqn (1.32).

$$A = \varepsilon \cdot C \cdot l \qquad\qquad (1.32)$$

where ε is the molar absorption coefficient ($M^{-1}cm^{-1}$), C is the molar concentration (M), l is the sample pathlength (cm)

Similarly, molar absorption coefficients can be defined for rcpl and lcpl. This allows us to calculate the molar circular dichroism (eqn 1.33)

$$\Delta\varepsilon = \varepsilon_L - \varepsilon_R = (A_L - A_R)/Cl \qquad\qquad (1.33)$$

where $\Delta\varepsilon$ is the molar circular dichroism ($M^{-1}cm^{-1}$), ε_L is the molar absorption coefficient of left hand polarised light ($M^{-1}cm^{-1}$), ε_R is the molar absorption coefficient of right hand polarised light ($M^{-1}cm^{-1}$), A_L is the absorbance of left hand polarised light, A_R is the absorbance of right hand polarised light

The CD instrument measures the intensity of rclp and lclp after passing through the sample and from the intensities determines $A_L - A_R$ and then $\Delta\varepsilon$ using the equations above.

CD spectroscopy can be used to determine how enantiomerically pure a compound is. Several examples exist of its use as a method of determining loss of enantiomeric excess and hence rate constants of racemisation.[149, 150]

1.10.4 Computational Chemistry

The use of computers to rapidly perform high-level theoretical chemistry calculations has become widespread. Molecular information such as the most stable configuration of nuclei and the relative energy of such configurations can be theoretically obtained through such calculations.

Calculations in Chapter 5 were performed using Density Functional Theory (DFT).[151] DFT uses approximations of electron interactions to convert the wavefunction into electron density. Differing approximations give rise to different functionals. The functional used in this body of work is RB3LYP.[152]

Also important in computational chemistry is the choice of basis set.[153] The basis set is the set of functions used to model the molecular orbitals. Using a finite basis, only the molecular orbital components along the coordinate axes corresponding to the selected basis are represented. A smaller basis set results in a less computationally expensive calculation, but gives a poorer representation of the molecule. Thus, when choosing a basis set a compromise has to be made between computation time and accuracy. The basis set 6-31+G(d,p) used in

this body of work is frequently used in computational chemistry as it provides a good balance between computation time and accuracy.

Chemistry is usually carried out in a solution, and the interactions between the solvent and solute can greatly affect molecular properties such as molecular geometry or energy. As a result, the effects of solvation are often incorporated into theoretical calculations to provide a better description of the system under analysis. One approach is to include individual solvent molecules in the calculation, and consider changes in the substrate and solvent due to interactions with one another. However, in order to accurately model these interactions hundreds or thousands of solvent molecules need to be included in the calculations, making such an approach very computationally demanding. Therefore an alternative approach based on continuum models has been developed.[154]

In this body of work, the Polarisable Continuum Model (PCM) of Tomasi *et al.*[155] has been used. In the PCM model, a cavity for the molecule is generated based on the van der Waals radii of the atoms in the molecule. A solvent-accessible surface is then manifested by a spherical particle rolling on the surface of the van der Waals surface. This surface is then treated as one continuous dielectric field, and specific solvent-solute interactions are disregarded. This approach provides a relatively cheap computational way of mimicking the effect of a solvent.

1.11 Project Goals

We aim to test the existing kinetic data and substituent effect information on racemisation of stereogenic centres of type R''R'RC-H, and to expand the range of structures for which kinetic data is available. In doing so we aim to:

1. Determine the structures at risk of racemisation

Dependence of racemisation on the types of functional groups adjacent to the stereogenic centre will be tested. The assignments made by Testa *et al.* (Table 1.1) will be considered and may be further refined.

2. Quantify the risk

Quantification of the rate constants of racemisation will allow direct comparison of the risk of racemisation for different structures. By modifying the structures this may allow us to quantify the effect of each particular functional group on racemisation.

3. Establish conditions where racemisation is a threat

By investigating the dependence of racemisation rate constants on pH, temperature and general-acid or -base concentration, we will be able to determine which factors are important for racemisation of individual structures and functional groups.

4. Investigate mechanisms of racemisation

Examination of the mechanism (or mechanisms) by which a molecule undergoes racemisation is an important goal of the project. This aspect of the project runs parallel to the dependence on structural aspects on the molecule. The variation with structure of rate constants for racemisation will allow insight into the mechanism by which racemisation takes place.

5. Explore possible methods for prediction of structures at risk of racemisation

The ability to assess whether a particular molecule is configurationally unstable under pharmacological conditions without having to undertake experimentation would be beneficial. The ability to predict configurational stability depends on knowledge of the mechanisms by which configurational instability occurs, and will allow structural features to be related to rate constants for racemisation. The use of computational chemistry to predict structures at risk will also be investigated.

1.12 References

1.   Perez, S.; Barcelo, D., *Trac-Trends in Analytical Chemistry* **2008**, *27* (10), 836-846.
2.   Ariens, E. J., *Trends in Pharmacological Sciences* **1993**, *14* (2), 68-75.
3.   Miller, C. P.; Ullrich, J. W., *Chirality* **2008**, *20* (6), 762-770.
4.   Agranat, I.; Wainschtein, S. R., *Drug Discovery Today* **2010**, *15* (5-6), 163-170.
5.   Caner, H.; Groner, E.; Levy, L.; Agranat, I., *Drug Discovery Today* **2004**, *9* (3), 105-110.
6.   Agranat, I.; Caner, H., *Drug Discovery Today* **1999**, *4* (7), 313-321.
7.   Agranat, I.; Caner, H.; Caldwell, A., *Nature Reviews Drug Discovery* **2002**, *1* (10), 753-768.
8.   Lovering, F.; Bikker, J.; Humblet, C., *Journal of Medicinal Chemistry* **2009**, *52* (21), 6752-6756.
9.   Testa, B.; Trager, W. F., *Chirality* **1990**, *2* (3), 129-133.
10.   Levy, R. H.; Boddy, A. V., *Pharmaceutical Research* **1991**, *8* (5), 551-556.
11.   Bentley, R., *Chemical Reviews* **2006**, *106* (9), 4099-4112.
12.   Zehnter, R.; Gerlach, H., *Tetrahedron-Asymmetry* **1995**, *6* (11), 2779-2786.
13.   Nunez, M. C.; Garcia-Rubino, M. E.; Conejo-Garcia, A.; Cruz-Lopez, O.; Kimatrai, M.; Gallo, M. A.; Espinosa, A.; Campos, J. M., *Current Medicinal Chemistry* **2009**, *16* (16), 2064-2074.
14.   Lee, E. J. D.; Williams, K.; Day, R.; Graham, G.; Champion, D., *British Journal of Clinical Pharmacology* **1985**, *19* (5), 669-674.
15.   Ariens, E. J., *European Journal of Clinical Pharmacology* **1984**, *26* (6), 663-668.
16.   Mellin, G. W.; Katzenstein, M., *N Engl J Med* **1962**, *267*, 1184-1244.
17.   Blaschke, G.; Kraft, H. P.; Fickentscher, K.; Kohler, F., *Arzneimittel-Forschung/Drug Research* **1979**, *29-2* (10), 1640-1642.
18.   Kasprzyk-Hordern, B., *Chemical Society Reviews* **2010**, *39* (11), 4466-4503.
19.   Fabro, S.; Smith, R. L.; Williams, R. T., *Nature* **1967**, *215* (5098), 296.
20.   Gunzler, V., *Drug Safety* **1992**, *7* (2), 116-134.
21.   Serilevy, A.; Richards, W. G., *Tetrahedron-Asymmetry* **1993**, *4* (8), 1917-1923.
22.   Horn, A. S.; De Ranter, C. J., *X-Ray Crystallography and Drug Action*. Oxford Science Publications: 1984.
23.   Eriksson, T.; Bjorkman, S.; Roth, B.; Fyge, A.; Hoglund, P., *Chirality* **1995**, *7* (1), 44-52.
24.   Knoche, B.; Blaschke, G., *Journal of Chromatography A* **1994**, *666* (1-2), 235-240.
25.   Decamp, W. H., *Chirality* **1989**, *1* (1), 2-6.
26.   Huerta, F. F.; Minidis, A. B. E.; Backvall, J. E., *Chemical Society Reviews* **2001**, *30* (6), 321-331.
27.   Pellissier, H., *Tetrahedron* **2003**, *59* (42), 8291-8327.
28.   Ward, R. S., *Tetrahedron-Asymmetry* **1995**, *6* (7), 1475-1490.
29.   Wolf, C., *Dynamic Stereochemistry of Chiral Compounds: Principles and Applications*. RSC Publishing: 2008; p 30-43.
30.   Reist, M.; Testa, B.; Carrupt, P. A.; Jung, M.; Schurig, V., *Chirality* **1995**, *7* (6), 396-400.
31.   Carpenter, B. K., *Determination of Organic Reaction Mechanisms*. Wiley-Interscience: 1984; p 1-4.
32.   Cram, D. J., *Fundamentals of Carbanion Chemistry*. Academic Press Inc.: 1965; p 85-113.
33.   Reist, M.; Carrupt, P. A.; Testa, B.; Lehmann, S.; Hansen, J. J., *Helvetica Chimica Acta* **1996**, *79* (3), 767-778.

34. Cram, D. J.; Gosser, L., *Journal of the American Chemical Society* **1963**, *85* (23), 3890-3891.

35. Cram, D. J.; Gosser, L., *Journal of the American Chemical Society* **1964**, *86* (24), 5457-5465.

36. Guthrie, R. D.; Nicolas, E. C., *Journal of the American Chemical Society* **1981**, *103* (15), 4637-4638.

37. Hsu, S. K.; Ingold, C. K.; Wilson, C. L., *Journal of the Chemical Society* **1938**, 78-81.

38. Cram, D. J.; Kingsbury, C. A.; Haberfie, P.; Rickborn, B., *Journal of the American Chemical Society* **1961**, *83* (17), 3678-3687.

39. Matsuo, H.; Kawazoe, Y.; Sato, M.; Ohnishi, M.; Tatsuno, T., *Chemical & Pharmaceutical Bulletin* **1967**, *15* (4), 391-398.

40. Smith, G. G.; Sivakua, T., *Journal of Organic Chemistry* **1983**, *48* (5), 627-634.

41. Isaacs, N., *Physical Organic Chemistry*. 2nd ed.; Longman Scientific & Technical: Harlow, 1995; p 140-145.

42. Testa, B.; Carrupt, P. A.; Gal, J., *Chirality* **1993**, *5* (3), 105-111.

43. Reist, M.; Testa, B.; Carrupt, P. A., *Enantiomer* **1997**, *2* (3-4), 147-155.

44. Richard, J. P.; Amyes, T. L., *Current Opinion in Chemical Biology* **2001**, *5* (6), 626-633.

45. Rios, A.; Richard, J. P., *Journal of the American Chemical Society* **1997**, *119* (35), 8375-8376.

46. Richard, J. P.; Amyes, T. L.; Toteva, M. M., *Accounts of Chemical Research* **2001**, *34* (12), 981-988.

47. Amyes, T. L.; Richard, J. P., *Journal of the American Chemical Society* **1996**, *118* (13), 3129-3141.

48. Richard, J. P.; Williams, G.; Gao, J. L., *Journal of the American Chemical Society* **1999**, *121* (4), 715-726.

49. Chiang, Y.; Griesbeck, A. G.; Heckroth, H.; Hellrung, B.; Kresge, A. J.; Meng, Q.; O'Donoghue, A. C.; Richard, J. P.; Wirz, J., *Journal of the American Chemical Society* **2001**, *123* (37), 8979-8984.

50. Rios, A.; Amyes, T. L.; Richard, J. P., *Journal of the American Chemical Society* **2000**, *122* (39), 9373-9385.

51. Rios, A.; Crugeiras, J.; Amyes, T. L.; Richard, J. P., *Journal of the American Chemical Society* **2001**, *123* (32), 7949-7950.

52. Richard, J. P.; Williams, G.; O'Donoghue, A. C.; Amyes, T. L., *Journal of the American Chemical Society* **2002**, *124* (12), 2957-2968.

53. Amyes, T. L.; Richard, J. P., *Journal of the American Chemical Society* **1992**, *114* (26), 10297-10302.

54. Perrin, D. D.; Dempsey, B.; Serjeant, E. P., *pK_a Prediction for Organic Acids and Bases*. Chapman and Hall: 1981; p 1-11.

55. Ali, I.; Gupta, V. K.; Aboul-Enein, H. Y.; Singh, P.; Sharma, B., *Chirality* **2007**, *19* (6), 453-463.

56. Ebbers, E. J.; Ariaans, G. J. A.; Houbiers, J. P. M.; Bruggink, A.; Zwanenburg, B., *Tetrahedron* **1997**, *53* (28), 9417-9476.

57. Reist, M.; Christiansen, L. H.; Christoffersen, P.; Carrupt, P. A.; Testa, B., *Chirality* **1995**, *7* (6), 469-473.

58. Mills, A. K.; Smith, A. E. W., *Helvetica Chimica Acta* **1960**, *43* (7), 1915-1927.

59. Reist, M.; Roy-De Vos, M.; Montseny, J. P.; Mayer, J. M.; Carrupt, P. A.; Berger, Y.; Testa, B., *Drug Metabolism and Disposition* **2000**, *28* (12), 1405-1410.

60. Pepper, C.; Smith, H. J.; Barrell, K. J.; Nicholls, P. J.; Hewlins, M. J. E., *Chirality* **1994**, *6* (5), 400-404.

61. Danel, C.; Foulon, C.; Goossens, J. F.; Bonte, J. P.; Vaccher, C., *Tetrahedron-Asymmetry* **2006,** *17* (16), 2317-2321.

62. Danel, C.; Azaroual, N.; Brunel, A.; Lannoy, D.; Odou, P.; Decaudin, B.; Vermeersch, G.; Bonte, J. P.; Vaccher, C., *Tetrahedron-Asymmetry* **2009,** *20* (10), 1125-1131.

63. Lambert, W. J.; Timmer, P. G., *Pharmaceutical Research* **1991,** *8* (11), 1444-1447.

64. Lambert, W. J.; Timmer, P. G.; Walters, R. R.; Hsu, C. Y. L., *Journal of Pharmaceutical Sciences* **1992,** *81* (10), 1028-1031.

65. Venter, D. P., *Tetrahedron* **1991,** *47* (27), 5019-5024.

66. Kahn, K.; Tipton, P. A., *Bioorganic Chemistry* **2000,** *28* (2), 62-72.

67. Brandl, M.; Conley, D.; Johnson, D., *Journal of Pharmaceutical Sciences* **1995,** *84* (9), 1045-1048.

68. Yang, S. K.; Lu, X. L., *Chirality* **1992,** *4* (7), 443-446.

69. Lamparter, E.; Blaschke, G.; Schluter, J., *Chirality* **1993,** *5* (5), 370-374.

70. Caldwell, J.; Hutt, A. J.; Fournel-Gigleux, S., *Biochemical Pharmacology* **1988,** *37* (1), 105-114.

71. Gu, L.; Strickley, R. G., *Pharmaceutical Research* **1987,** *4* (5), 392-397.

72. Kirkwood, J. G.; Westheimer, F. H., *Journal of Chemical Physics* **1938,** *6* (9), 506-512.

73. Westneimer, F. H.; Kirkwood, J. G., *Journal of Chemical Physics* **1938,** *6* (9), 513-517.

74. Hine, J., *Structural Effects on Equilibria in Organic Chemistry*. Wiley-Interscience: 1975; p 98.

75. Hansch, C.; Leo, A.; Taft, R. W., *Chemical Reviews* **1991,** *91* (2), 165-195.

76. Narduolo, S., Unpublished results.

77. Tan, S. C.; Patel, B. K.; Jackson, S. H. D.; Swift, C. G.; Hutt, A. J., *Enantiomer* **1999,** *4* (3-4), 195-203.

78. Landoni, M. F.; Soraci, A., *Current Drug Metabolism* **2001,** *2* (1), 37-51.

79. Porubek, D. J.; Sanins, S. M.; Stephens, J. R.; Grillo, M. P.; Kaiser, D. G.; Halstead, G. W.; Adams, W. J.; Baillie, T. A., *Biochemical Pharmacology* **1991,** *42* (1).

80. Leipold, D. D.; Kantoci, D.; Murray, D.; Quiggle, D. D.; Wechter, W. J., *Chirality* **2004,** *16* (6), 379-387.

81. Berry, B. W.; Jamali, F., *Journal of Pharmacology and Experimental Therapeutics* **1991,** *258* (2), 695-701.

82. Knihinicki, R. D.; Williams, K. M.; Day, R. O., *Biochemical Pharmacology* **1989,** *38* (24), 4389-4395.

83. Knihinicki, R. D.; Day, R. O.; Williams, K. M., *Biochemical Pharmacology* **1991,** *42* (10), 1905-1911.

84. Noorduin, W. L.; Kaptein, B.; Meekes, H.; van Enckevort, W. J. P.; Kellogg, R. M.; Vlieg, E., *Angewandte Chemie-International Edition* **2009,** *48* (25), 4581-4583.

85. Yuchun, X.; Huizhou, L.; Jiayong, C., *International Journal of Pharmaceutics* **2000,** *196* (1), 21-26.

86. Wolf, C., *Dynamic Stereochemistry of Chiral Compounds: Principles and Applications*. RSC Publishing: 2008; p 58-70.

87. Aso, Y.; Yoshioka, S.; Shibazaki, T.; Uchiyama, M., *Chemical and Pharmaceutical Bulletin* **1988,** *36* (5), 1834-1840.

88. Aso, Y.; Yoshioka, S.; Takeda, Y., *Chemical and Pharmaceutical Bulletin* **1990,** *38* (1), 180-184.

89. Reist, M.; Testa, B.; Carrupt, P.-A., Drug Racemization and Its Significance in Pharmaceutical Research. In *Handbook of Experimental Pharmacology*, Springer: 2003; Vol. 153, pp 91-112.

90. Maskill, H., *The Physical Basis of Organic Chemistry*. Oxford Science Publications: 1985; p 315-366.

91. Schroeter, L. C.; Higuchi, T., *Journal of the American Pharmaceutical Association* **1958,** *47* (6), 426-430.

92. Mohan, A. G.; Conley, R. T., *Journal of Organic Chemistry* **1969,** *34* (11), 3259-3263.

93. Alibrandi, G.; Coppolino, S.; D'Aliberti, S.; Ficarra, P.; Micali, N.; Villari, A., *Journal of Pharmaceutical and Biomedical Analysis* **2002,** *29* (6), 1025-1029.

94. Youssef, A. A.; Sharaf, S. M., *Journal of Organic Chemistry* **1974,** *39* (12), 1705-1707.

95. Sato, M.; Tatsuno, T.; Matsuo, H., *Chemical & Pharmaceutical Bulletin* **1970,** *18* (9), 1794-1798.

96. Isaacs, N., *Physical Organic Chemistry*. 2nd ed.; Longman Scientific & Technical: Harlow, 1995; p 287-318.

97. Carpenter, B., *Determination of Organic Reaction Mechanisms*. Wiley-Interscience: 1984; p 142-156.

98. Maskill, H., *The Physical Basis of Organic Chemistry*. Oxford Science Publications: 1985; p 442-466.

99. Shorter, J., *Pure and Applied Chemistry* **1995,** *67* (5), 835-840.

100. Hammett, L. P., *Journal of the American Chemical Society* **1937,** *59*, 96-103.

101. Williams, A.; Naylor, R. A., *Journal of the Chemical Society B-Physical Organic* **1971,** (10), 1967-1972.

102. Maskill, H., *The Physical Basis of Organic Chemistry*. Oxford Science Publications: Oxford, 1985; p 202-211.

103. Hansen, L. D.; Hepler, L. G., *Canadian Journal of Chemistry* **1972,** *50* (7), 1030-1035.

104. Hepler, L. G., *Canadian Journal of Chemistry* **1971,** *49* (17), 2803-2807.

105. Linert, W.; Sapunov, V. N., *Chemical Physics* **1988,** *119* (2-3), 265-274.

106. Wells, P. R., *Chemical Reviews* **1963,** *63* (2), 171-219.

107. Bowden, K., *Canadian Journal of Chemistry* **1963,** *41* (11), 2781-2793.

108. Jaffe, H. H., *Chemical Reviews* **1953,** *53* (2), 191-261.

109. Bitterwolf, T. E.; Linder, R. E.; Ling, A. C., *Journal of the Chemical Society B-Physical Organic* **1970,** (9), 1673-1674.

110. Charton, M., *Journal of Organic Chemistry* **1964,** *29* (5), 1222-1227.

111. Johnson, C. D., *The Hammett Equation*. Cambridge University Press: Cambridge, 1973; p 144-150.

112. Arcoria, A.; Ballistreri, F. P.; Spina, E.; Tomaselli, G. A.; Maccarone, E., *Journal of the Chemical Society-Perkin Transactions 2* **1988,** (10), 1793-1798.

113. Yukawa, Y.; Tsuno, Y., *Bulletin of the Chemical Society of Japan* **1959,** *32* (9), 971-981.

114. Taft, R. W., *Journal of the American Chemical Society* **1952,** *74* (12), 3120-3128.

115. Swain, C. G.; Lupton, E. C., *Journal of the American Chemical Society* **1968,** *90* (16), 4328-4337.

116. Isaacs, N., *Physical Organic Chemistry*. 2nd ed.; Longman Scientific & Technical: Harlow, 1995; p 186-187.

117. Lee, I., *Chemical Society Reviews* **1990,** *19* (3), 317-333.

118. Lee, I.; Shim, C. S.; Chung, S. Y.; Kim, H. Y.; Lee, H. W., *Journal of the Chemical Society-Perkin Transactions 2* **1988,** (11), 1919-1923.

119. Sung, D. D.; Jang, H. M.; Il Jung, D.; Lee, I., *Journal of Physical Organic Chemistry* **2008,** *21* (11), 1014-1019.

120.	Lee, I.; Sohn, S. C.; Kang, C. H.; Oh, Y. J., *Journal of the Chemical Society-Perkin Transactions 2* **1986,** (10), 1631-1634.

121.	Charton, M., Applications of Linear Free Energy Relationships to Polycyclcic Arenes and to Heterocyclic Compounds. In *Correlation Analysis in Chemistry: Recent Advances,* Chapman, N. B.; Shorter, J., Eds. Plenum: New York, 1978; pp 175-268.

122.	Jaffe, H. H.; Jones, H. L., *Advances in Heterocyclic Chemistry* **1964,** *3,* 209-261.

123.	Perrin, D. D.; Dempsey, B.; Serjeant, E. P., *pK_a Prediction for Organic Acids and Bases.* Chapman and Hall: London, 1981; p 82-95.

124.	Lameijer, E. W.; Kok, J. N.; Back, T.; Ijzerman, A. P., *Journal of Chemical Information and Modeling* **2006,** *46* (2), 553-562.

125.	Johnson, C. D., *The Hammett Equation.* Cambridge University Press: Cambridge, 1973; p 99-103.

126.	Crugeiras, J.; Rios, A.; Riveiros, E.; Richard, J. P., *Journal of the American Chemical Society* **2011,** *133* (9), 3173-3183.

127.	Laidler, K. J., *Chemical Kinetics.* 3rd ed.; Harper & Row: New York, 1987; p 39-48.

128.	Atkins, P. W., *The Elements of Physical Chemistry.* 3rd ed.; Oxford University Press: Oxford, 2001; p 229-237.

129.	Maskill, H., *The Physical Basis of Organic Chemistry.* Oxford Science Publications: Oxford, 1985; p 247-249.

130.	Eyring, H., *Chemical Reviews* **1935,** *17* (1), 65-77.

131.	Laidler, K. J.; King, M. C., *Journal of Physical Chemistry* **1983,** *87* (15), 2657-2664.

132.	Maskill, H., *The Physical Basis of Organic Chemistry.* Oxford Science Publications: Oxford, 1985; p 249-261.

133.	Robertson, R. E., *Progress in Physical Organic Chemistry* **1967,** *4,* 213-280.

134.	Bentley, T. W.; Schleyer, P. v. R., *Advances in Physical Organic Chemistry* **1977,** *14,* 1-57.

135.	Juric, S.; Kronja, O., *Journal of Physical Organic Chemistry* **2005,** *18* (4), 368-372.

136.	Blackham, A. U.; Eatough, N. L., *Journal of the American Chemical Society* **1962,** *84* (15), 2922-2930.

137.	Carey, F. A.; Sundberg, R. J., *Advanced Organic Chemistry. Part A: Structure and Mechanisms.* 5th ed.; Springer: New York, 2007; p 270-285.

138.	Wassermann, A., *Monatshefte Fur Chemie* **1952,** *83* (2), 543-544.

139.	Williams, D. H.; Fleming, I., *Spectroscopic Methods in Organic Chemistry.* 5th ed.; McGraw-Hill: London, 1995; p 63-169.

140.	Banwell, C. N.; McCash, E. M., *Fundamentals of Molecular Spectroscopy.* 4th ed.; McGraw-Hill: London, 1994; p 199-256.

141.	Friebolin, H., *Basic One- and Two-Dimensional NMR Spectroscopy.* 3rd ed.; Wiley-VCH: Weinheim, 1998.

142.	Hore, P. J., *Nuclear Magnetic Resonance.* Oxford University Press: Oxford, 1995.

143.	Williams, G.; Maziarz, E. P.; Amyes, T. L.; Wood, T. D.; Richard, J. P., *Biochemistry* **2003,** *42* (27), 8354-8361.

144.	Matsuo, H.; Kawazoe, Y.; Sato, M.; Ohnishi, M.; Tatsuno, T., *Chemical & Pharmaceutical Bulletin* **1970,** *18* (9), 1788-1793.

145.	Yonetani, K.; Hirotsu, Y.; Shiba, T., *Bulletin of the Chemical Society of Japan* **1975,** *48* (11), 3302-3305.

146.	Kawazoe, Y.; Ohnishi, M., *Chemical & Pharmaceutical Bulletin* **1964,** *12* (7), 846-848.

147.	Williams, D. H.; Fleming, I., *Spectroscopic Methods in Organic Chemistry.* 5th ed.; McGraw-Hill: London, 1995; p 170-225.

148. Charney, E., *The Molecular Basis of Optical Activity: Optical Rotary Dispersion and Circular Dichroism*. Wiley-Interscience: New York, 1979.

149. Saito, H.; Mori, T.; Origane, Y.; Wada, T.; Inoue, Y., *Chirality* **2008,** *20* (3-4), 278-281.

150. Yang, S. K., *Chirality* **1999,** *11* (3), 179-186.

151. Jensen, F., *Introduction to Computational Chemistry*. John Wiley & Sons: Chichester, 1999; p 177-194.

152. Becke, A. D., *Journal of Chemical Physics* **1993,** *98* (7), 5648-5652.

153. Cramer, C., *Essentials of Computational Chemistry: Theories and Models*. John Wiley and Sons: Chichester, 2002; p 154-168.

154. Tomasi, J.; Persico, M., *Chemical Reviews* **1994,** *94* (7), 2027-2094.

155. Cossi, M.; Barone, V.; Cammi, R.; Tomasi, J., *Chemical Physics Letters* **1996,** *255* (4-6), 327-335.

2 Database Mining

2.1 Introduction

Our interest in racemisation is primarily from a pharmaceutical perspective. It is therefore important to have some perspective on the types of compounds, and more specifically the types of stereogenic centres commonly found in pharmacologically-active compounds. As a result, a body of data regarding different functional groups that are found adjacent to a stereogenic centre in compounds of interest was obtained and analysed. Of specific interest is to gather information on which functional groups appear, the frequency at which they are seen, and the combinations in which they are found. Such information on functional groups will also make it possible to classify combinations of functional groups as 'at risk' of racemisation (either through base or acid catalysis) and to see the frequency at which such combinations occur.

AstraZeneca possess large databases of compounds of different origin. Here, two databases were examined; the ISAC database, containing details of all compounds registered as of interest by AstraZeneca over the history of the company and its predecessors; and the IBEX database, an externally managed database, comprising of any compounds that appear in the medicinal chemistry literature. Both databases are very large; ISAC contains over 1 million compounds and IBEX over half a million. The trends found in such large libraries of molecules provide insight into which types of stereogenic centre have been most frequently investigated as potential drugs and how often these stereogenic centres appear to be configurationally unstable.*

The information in the IBEX and ISAC databases is recorded using the SMILES[1-8] (Simplified Molecular Input Line Entry Syntax) chemical language. SMILES syntax enables molecules and reactions to be represented using a series of ASCII characters. The basic structure of the language is outlined in the appendix (Section 2.6.1.1).

An important tool in cheminformatics is sub-structure targeting of compounds in molecular databases to find a desired chemical 'motif'. The SMARTS[9, 10] (Smiles Arbitrary Target Specification) chemical language is an extension of SMILES that enables searching for specific patterns within molecules and was used for that purpose in this chapter. A brief overview of SMARTS can be found in the experimental (Section 2.6.1.2). SMARTS have been used in studies filtering out molecules with detrimental ADMET† properties,[11, 12]

---

* Details of specific molecules cannot be discussed due to confidentiality agreements.

† ADMET – Absorption, Distribution, Metabolism, Excretion and Toxicity.

assessing risk of undesired reactivity between compounds in pooled screening studies,[13] identifying commonly occurring molecular fragments found in on-the-market drugs[14] and quantifying the effects of structural changes on pharmaceutical properties.[15]

2.2 Analysis

2.2.1 'Chiral Chopper'

In order to separately classify each substituent bound to a stereogenic centre in each molecule listed in the databases, it was first necessary to identify each stereogenic centre and separate the substituents around it. This was achieved using a program developed in-house by AstraZeneca named 'Chiral Chopper'. The program analyses a database of SMILES strings and detects any stereogenic centres within chiral molecules in the database. The program then performs an operation on the molecule which outputs a SMILES string representing the molecule divided around the stereogenic centre, with the stereogenic centre replaced by a Xenon atom. An example of the operation of the 'Chiral Chopper' program on a simple molecule is displayed in Scheme 2.1.

NC(C(=O)O)CC $\xrightarrow{\text{'Chiral Chopper'}}$ [Xe]N.[Xe]C(=O)O.[Xe]CC.[XeH]
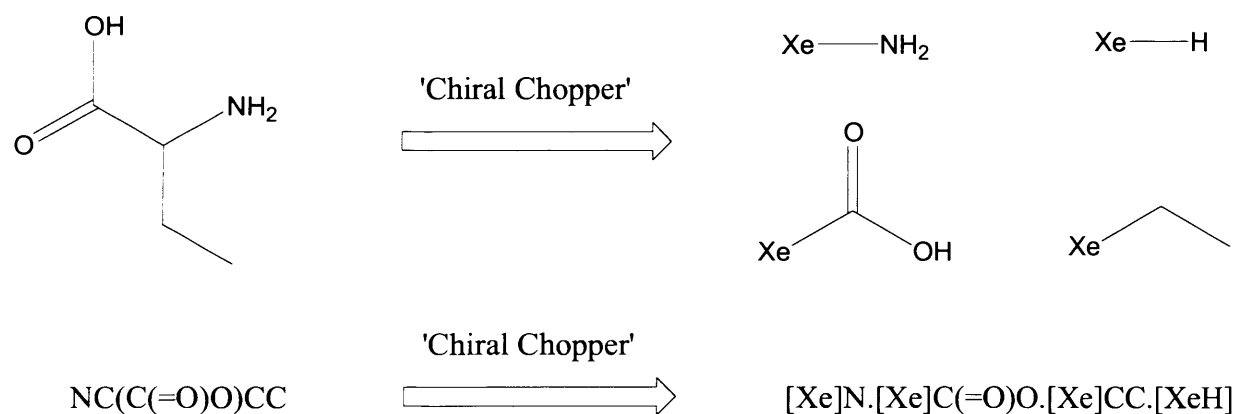
Scheme 2.1: Illustration of operation of 'Chiral Chopper' program on 2-aminobutanoic acid.

The Xenon atom is inserted as a marker for the stereogenic centre, as it allows for recognition through SMARTS queries. It is now possible to define various types of substituent and analyse each newly divided molecule to see which substituents are present on the various stereogenic centres.

2.2.2 Classification of Substituents

In order to analyse the substituents on each stereogenic centre in the databases it is necessary to choose how substituents are to be defined and how specific each definition is to be. For

example, it might be sufficient to define a substituent simply as an amide but primary and secondary amides could also be defined differently. The orientation of certain functional groups with respect to the stereogenic centre may also impact whether the group facilitates racemisation or not.

The categories of amides and amines were divided into primary, secondary and tertiary. This is because different substitution patterns can be expected to have different inductive effects. Also important is the nature of the substituents. Some amides and amines were classified as acidic or nonacidic. Amide substituents with a labile proton (Scheme 2.2) will affect an adjacent stereocentre differently from those where the proton is constantly bound.
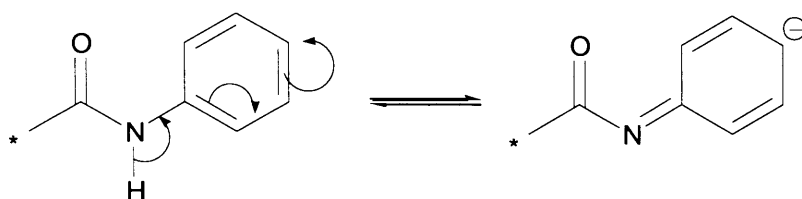
Scheme 2.2: Illustration of acidic secondary amide substituent classification.

If the aromatic group in Scheme 2.2 was to be replaced by an alkyl group the acidic nature of the amide proton would not be retained. The difference in inductive effects of differently substituted amides is illustrated by their σ_I values (Scheme 2.3), quantifying the electron-withdrawing nature of the substituent.

$\sigma_I =$ 0.26   0.35   0.17
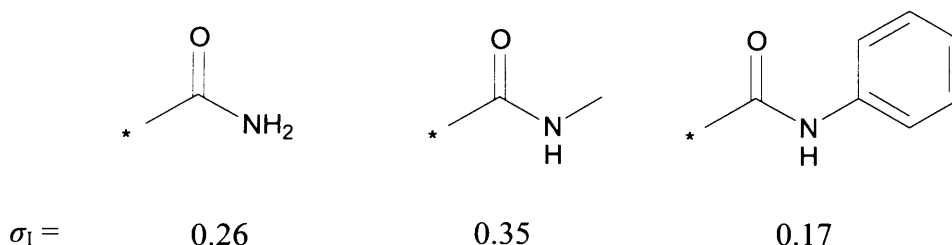
Scheme 2.3: Inductive effect constants for three different amides.[16]

Amide substituents which did not fall into either the aromatic ('acidic') or alkyl ('nonacidic') were classified in a separate category (amide 'other'). Tertiary amides and amines were similarly divided into separate categories dependent on the nature of the groups bound to the nitrogen atom.

Amine groups were defined in the same manner as amides. Although the proton on a secondary amine cannot be said to be 'acidic' in the same manner as for an amine, the same terminology has been used. In this instance, the term 'acidic' refers to the conjugate acid of the secondary amine, which will be more acidic if the amine is aromatic substituted rather than alkyl substituted.

The orientation of an amide with respect to the stereogenic centre is also of interest. Stabilisation of a carbanion by an amide can occur in a different manner dependent on the orientation of the amide. If the carbonyl is adjacent, stabilisation occurs through delocalisation of charge onto the oxygen. If the nitrogen is adjacent, stabilisation occurs through electrostatic interactions between the carbanion and the partial positive charge on the nitrogen (Section 1.4). Amides bound to the stereogenic centre through nitrogen were therefore categorised separately as 'reverse amides', and were also separated into secondary and tertiary classifications.

Because we are essentially interested in the effects on the stability of a carbanion, aromatic groups also require subdivision into more specific categories. Initially, categories were created for five- and six-membered aromatics, with three-, four- and seven-membered groups categorised in 'other'. However, it became apparent that most of the aromatic groups fell in the six-membered category. As a result it was decided to split this group into different types of aromatic, with benzene and various nitrogen-containing heterocycles classified separately.

The SMARTS output for each stereogenic centre consists of a series of numbers each corresponding to a different category. The number denotes how many of the substituents on the stereogenic centre are classified in that category. For example, 2-aminobutanoic acid (Scheme 2.1) will return a '1' in the categories of proton, alkyl, primary amine and carboxylic acid. Every other category will return '0'. In order to check that most substituents are recognised, the sum of the substituents was calculated and any molecules not adding up to 4 were scrutinised. If necessary the SMARTS query was then modified to be more specific and run again.

After this iterative process was complete, a total of 52 different categories for substituents were established. These are listed in Table 2.1. For details on how each was coded, see the experimental (Section 2.5.1). Many of these substituents are fairly common, such as protons, alkyls and halogens. Other less commonly found groups include epoxides, ammonium salts and thioethers. Numerous very rare groups such as thiols, azides and sulfiniums were grouped together as 'other'.

Table 2.1: Substituent categories defined in SMARTS query.

		Amides	Amines	Aromatics	
Proton	Carboxylic acid	Primary	Primary	Benzene	Hydroxylamine
Halogen	Ketone	Secondary with non-acidic proton	Secondary with non-acidic proton	Ortho pyridine	Hydroxamic acid
Hydroxyl	Ester	Secondary with acidic proton	Secondary with acidic proton	Meta pyridine	Thioether
Alkyl	'Reverse' Ester	Other secondary	Other secondary	Para pyridine	Imide
Alkene	Ether	Tertiary with two alkyl groups	Tertiary with two alkyl groups	2,4-pyrimidine	Imine
Alkyne	Aromatic ether	Tertiary with two aromatic groups	Tertiary with two aromatic groups	2,6-pyrimidine	'Reverse' imine
Nitrile	Ether and double bond	Tertiary with one aromatic, one alkyl group	Tertiary with one aromatic, one alkyl group	3,5-pyrimidine	Quaternary ammonium
Nitro	Epoxide	Other tertiary	Other tertiary	2,3-pyradizine	Sulfoxide
		'Reverse' secondary		3,4-pyradizine	Sulfilimine
		'Reverse' tertiary		Pyrazine	Isonitrile
		Double bonded amide		Triazine	Thiocarbonyl
				Other six membered aromatic	Other
				Five membered aromatic	

2.3 Results and Discussion

The sheer number of stereogenic centres analysed in this work (over 1 million in the ISAC database alone) means that there are likely to be a few examples of any type of stereogenic centre that can be formed by combining the substituent categories listed in Table 2.1. Because of this, the focus of our analysis has been on the 250 most frequently occurring combinations of substituents.

2.3.1 Overview of Most Frequently Occurring Combinations of Substituents

The most frequently occurring combinations of substituents around stereogenic centres in the ISAC database are displayed in Table 2.2.

Table 2.2: Details of 20 most common combinations of substituents on stereogenic centres found in the ISAC database.

	Combination of substituents on stereocentre	No. stereocentres[a]
1	1 proton, 3 alkyl	134476
2	1 proton, 1 hydroxyl, 2 alkyl	108097
3	1 proton, 1 alkyl, 1 nonacidic sec. amide, 1 reverse sec. amide	85149
4	1 proton, 2 alkyl, 1 ether	73318
5	1 proton, 2 alkyl, 1 dialkyl tert. amine	58810
6	1 proton, 2 alkyl, 1 reverse tert. amide	45324
7	1 proton, 2 alkyl, 1 reverse sec. amide	45034
8	1 proton, 2 alkyl, 1 benzene	36976
9	1 proton, 1 alkyl, 1 nonacidic sec. amide, 1 reverse tert. amide	28017
10	1 proton, 1 reverse tert. amide, 1 benzene, 1 thioether	25241
11	1 proton, 1 alkyl, 1 dialkyl tert. amide, 1 reverse sec. amide	24437
12	1 proton, 1 alkyl, 1 benzene, 1 reverse tert. amide	21560
13	1 proton, 1 alkyl, 1 benzene, 1 dialkyl tert. amine	20388
14	1 proton, 2 alkyl, 1 reverse ester	20342
15	1 proton, 2 alkyl, 1 nonacidic sec. amine	20100
16	1 proton, 2 alkyl, 1 aromatic ether	20065
17	1 proton, 1 alkyl, 1 benzene, 1 reverse sec. amide	19871
18	1 proton, 2 alkyl, 1 alkene	19031
19	1 proton, 2 alkyl, 1 five membered aromatic	17887
20	1 proton, 1 hydroxyl, 1 alkyl, 1 benzene	16882

[a] from a total of 1,607,343 stereogenic centres

Immediately apparent from Table 2.2, is that all of the top 20 (and 90 of the top 100) most frequently occurring combinations have a proton as one of the substituents. This feature

potentially makes them susceptible to racemisation by proton abstraction by base, as discussed in Section 1.3. As a result it becomes important to assess whether other substituents on these stereogenic centres can stabilise a negative charge, as the ability to do so will make the stereogenic centre more vulnerable to racemisation through the S_E1 and S_E2 mechanisms (Section 1.3).

All bar one of the combinations displayed in Table 2.2 have at least one alkyl substituent. Alkyl substituents were defined by Testa *et al.*[17-19] (Table 1.1) as being neutral towards stabilising a carbanion. Stereocentres with a neutral substituent are thought to require two other acid-strengthening groups, one strongly so, in order for configurational instability to be of pharmaceutical or pharmacological significance. The strongly acid-strengthening groups designated in Table 1.1 are ester and aryl ketone groups, which none of the combinations in Table 2.2 contain. As a result, by the definitions in Table 1.1, none of the most frequent occurring stereogenic 'motifs' would be anticipated to be configurationally unstable. Similar conclusions can be drawn from the results of the IBEX database, illustrated in the Appendix to the Chapter (Section 2.6). This conclusion is perhaps a reassuring one, although it may also be a self-fulfilling prophecy if compounds thought or found to be unstable have been avoided. It is preferable that all stereocentres in chiral drug molecules retain configuration to avoid the potentially disastrous consequences discussed in Section 1.1. However, although these very frequently occurring combinations do not appear to be at risk, looking further down the lists examples of stereogenic centres which are at risk of configurational instability start to appear.

2.3.2 Analysis of Most Frequently Occurring 'At Risk' Combinations of Substituents

The top 250 most frequently occurring combinations from the ISAC database were analysed and classified as either at risk from base-catalysed racemisation, acid-catalysed racemisation, not at risk or unknown. Table 2.3 shows how many combinations of substituents around a stereogenic centre fell into each risk category.

Table 2.3: Number of combinations of substituents in each classification of racemisation risk, from top 250 most frequently occurring combinations from the ISAC database.

Type of risk			
Not at risk	Base-catalysed	Acid-catalysed	Unknown
188	38	10	14

As seen in several examples in Chapter 1,[20-22] molecules with an alcohol group bound to the stereogenic centre can be susceptible to acid-catalysed racemisation via protonation of the alcohol followed by dehydration then rehydration, as illustrated in Scheme 1.18. Of the top 250 combinations there were 10 which are potentially susceptible to acid catalysed racemisation, corresponding to 30,517 individual stereogenic centres (Appendix Table 2.8). Many more fit the criteria outlined in Table 1.1 which may make them susceptible to base-catalysed racemisation through proton abstraction. Of the top 250 combinations, 38 are classified as susceptible to base-catalysed racemisation (78,360 stereogenic centres) and are displayed in Table 2.4 (overleaf). Combinations with one or more substituent with an unknown effect on configurational stability (from Table 1.1 and chemical intuition) such as a thioether substituent, are classified as of 'unknown' risk (appendix Table 2.9).

Table 2.4 illustrates that many molecules investigated as potential drugs contain scaffolds with stereogenic centres that are potentially unstable under physiological conditions. Table 2.4 shows that many of the combinations thought at risk of racemisation through base catalysis contain a carbonyl adjacent to the stereogenic centre. A carbonyl can stabilise a carbanion through delocalisation of charge onto the oxygen and facilitate racemisation, as discussed in Section 1.4.

Also frequently appearing in Table 2.4 are variously-substituted amine and amide groups bonded to the stereogenic centre through nitrogen. Both are designated in Table 1.1 as decreasing configurational stability suggesting that both groups will stabilise an adjacent carbanion. This is due to the formal or partial positive charge on the nitrogen and the stabilising effect this will have on an adjacent carbanion (Section 1.4).

Table 2.4 shows that a combination of an adjacent carbonyl-containing group with an amine or amide bound through nitrogen is found 17 times within the top 250 most common combinations. Within these 17 different combinations, breakdown of the adjacent carbonyl groups shows that 6 are ester groups, 9 are amide groups and 2 are ketones. Of the adjacent nitrogen containing groups, 11 are amides and 7 are amines. These results are summarised in Table 2.5 (page 67).

65

Table 2.4: Details of all combinations of substituents within the most common 250 in ISAC, considered at risk of base-catalysed racemisation

	Combination of substituents on stereocentre, excluding proton	No. stereocentres[a]
29	1 alkyl, 1 ester, 1 reverse sec. amide	11628
35	1 benzene, 1 nonacidic sec. amide, 1 reverse tert. amide	8622
40	1 benzene, 1 reverse sec. amide, 1 reverse tert. amide	7125
55	1 benzene, 2 alkene	4861
57	1 alkyl, 1 ester, 1 reverse tert. amide	4618
60	2 benzene, 1 dialkyl tert. amine	4319
67	1 alkyl, 1 ester, 1 dialkyl tert. amine	3419
70	1 alkyl, 1 ketone, 1 reverse sec. amide	3387
98	1 alkyl and aromatic sub. tert. amide, 1 reverse sec. amide, 1 imine	2143
102	1 alkyl, 1 ketone, 1 ester	2013
103	1 benzene, 1 five membered aromatic, 1 dialkyl tert. amine	1980
106	1 five membered aromatic, 1 nonacidic sec. amide, 1 reverse tert. amide	1885
130	1 alkyl and aromatic sub. tert. amide, 1 imine, 1 sec. amine (other)	1483
138	1 alkyl, 1 ester, 1 nonacidic sec. amine	1383
141	1 alkyl, 1 ester, 1 ether	1374
164	1 alkyl, 2 ketone	1132
166	1 para pyridine, 1 nonacidic sec. amide, 1 reverse tert. amide	1117
170	1 meta pyridine, 1 alkyl, 1 reverse tert. amide	1067
176	1 benzene, 1 acidic sec. amide, 1 reverse tert. amide	1040
179	1 benzene, 1 reverse sec. amide, 1 tert. amine (other)	984
185	1 alkyl, 1 benzene , 1 ester	920
188	1 alkyl, 1 ester, 1 prim. amine	904
190	1 benzene, 1 five membered aromatic, 1 nonacidic sec. amine	900
191	1 benzene, 1 alkyl and aromatic sub. tert. amide, 1 reverse tert. amide	899
192	1 nonacidic sec. amide, 1 reverse sec. amide	897
199	1 alkyl, 1 benzene , 1 ketone	816
210	1 benzene, 1 reverse tert. amide, 1 dialkyl tert. amine	756
215	1 five membered aromatic, 2 alkenes	699
217	2 benzene, 1 reverse sec. amide	666
221	1 hydroxyl, 1 alkyl, 1 ester	645
226	1 benzene, 1 acidic sec. amide, 1 reverse sec. amide	627
230	1 meta pyridine, 1 five membered aromatic, 1 dialkyl tert. amine	611
234	1 alkyl, 1 ester, 1 sec. amine (other)	603
237	1 alkyl, 1 benzene , 1 halogen	594
241	2 benzene, 1 reverse tert. amide	580
244	1 alkyl, 1 ketone, 1 dialkyl tert. amine	561
246	1 benzene, 1 alkene, 1 reverse tert. amide	559
250	1 alkyl, 1 alkene, 1 ketone	543

[a] from a total of 1,607,343 stereogenic centres

Table 2.5: Combinations of substituents within the most common 250 combinations from the ISAC database, with one substituent containing a carbonyl group adjacent to the stereocentre and one substituent with nitrogen adjacent to the stereocentre.

Combination of substituents on stereocentre (excluding proton), listed by carbonyl group type		No. stereocentres[a]
Esters		
29 1 alkyl, 1 ester, 1 reverse sec. amide		11628
57 1 alkyl, 1 ester, 1 reverse tert. amide		4618
67 1 alkyl, 1 ester, 1 dialkyl tert. amine	*	3419
138 1 alkyl, 1 ester, 1 nonacidic sec. amine	*	1383
188 1 alkyl, 1 ester, 1 prim. amine	*	904
234 1 alkyl, 1 ester, 1 sec. amine (other)	*	603
Amides		
35 1 benzene, 1 nonacidic sec. amide, 1 reverse tert. amide		8622
98 1 alkyl and aromatic sub. tert. amide, 1 reverse sec. amide, 1 imine		2143
106 1 five membered aromatic, 1 nonacidic sec. amide, 1 reverse tert. amide		1885
130 1 alkyl and aromatic sub. tert. amide, 1 imine, 1 sec amine (other)	*	1483
166 1 para pyridine, 1 nonacidic sec. amide, 1 reverse tert. amide		1117
176 1 benzene, 1 acidic sec. amide, 1 reverse tert. amide		1040
191 1 benzene, 1 alkyl and aromatic sub. tert. amide, 1 reverse tert. amide		899
192 1 benzene, 1 nonacidic sec. amide, 1 reverse sec. amide		897
226 1 benzene, 1 acidic sec. amide, 1 reverse sec. amide		627
Ketones		
70 1 alkyl, 1 ketone, 1 reverse sec. amide		3387
244 1 alkyl, 1 ketone, 1 dialkyl tert. amine	*	561

[a] from a total of 1,607,343 stereogenic centres
* denotes adjacent amine groups

Also noticeable is the frequent occurrence of aromatic groups in combinations that appear configurationally unstable. Of the 38 combinations that appear in Table 2.4, 22 contain at least one aromatic group substituent. Of these, 17 contain a benzene substituent. Heterocycles are a less common occurrence, with only three pyridine derivatives seen. This observation is consistent with that made by Ghose *et al.*[23] In an extensive study of drug databases classifying functional groups found anywhere in drug molecules, they observed that benzene was the most frequently found aromatic group, outnumbering all other heterocycles (aromatics and non-aromatics) combined. The observation of pyridines as the most frequently seen aromatic

group after benzene is consistent with the observations of Lameijer et al.[24] in their analysis of the database of the National Cancer Institute.

Analysis of the data from the IBEX database was carried out in the same manner as for the ISAC database. As in the ISAC database, none of the 20 most frequently occurring combinations of substituents on a stereogenic centre in the IBEX appear susceptible to base-catalysed racemisation (Table 2.10). Risk-of-racemisation assessment of the top 250 most frequently occurring combinations are shown in Table 2.6.

Table 2.6: Number of combinations of substituents in each classification of racemisation risk, from top 250 most frequently occurring combinations from the IBEX database.

Type of risk			
Not at risk	**Base-catalysed**	**Acid-catalysed**	**Unknown**
193	22	16	19

Although the number of combinations deemed not at risk in Table 2.6 is approximately the same as for the ISAC database, the number deemed at risk of base-catalysed racemisation is much lower and the numbers in the other two risk categories slightly higher. The manner in which the two databases are compiled suggests potential explanations for this difference. The ISAC database is comprised of any compound that has ever been of interest AZ (or its precursor companies), as opposed to IBEX which only contains compounds that have appeared in the medicinal chemistry literature. The discretionary nature of compound registration into the ISAC database may have resulted in some entries being far removed from the types of compound which generally end up making it into literature. It may also be the case that other organisations are developing drugs for different illnesses than AstraZeneca, and so the types of molecules required may be completely different. Alternatively, other organisations maybe approaching the same diseases but with a completely different solution.

The combination of a carbonyl substituent with a nitrogen-adjacent substituent (as outlined in Table 2.5 for the ISAC database) occurs often in the IBEX database (Table 2.12). The frequent occurrence of benzene groups in the ISAC database is also seen in the IBEX database. This is illustrated in Table 2.11, where all the aromatic groups found in combinations susceptible to base-catalysed racemisation are benzene rings.

2.4 Conclusions

The results from this chapter allow three main conclusions to be drawn.

Primarily, the vast majority of the stereogenic centres analysed have one proton substituent. This illustrates the importance of understanding the factors required for proton abstraction by base to occur and which substituents promote and supress it.

Secondly, following the definitions from Table 1.1, the vast majority of stereogenic centres found in the compounds investigated are not at risk from base-catalysed racemisation via proton abstraction. This is largely due to the presence on most stereogenic centres of an alkyl substituent which is unable to stabilise a negative charge.

Finally, of those frequently observed combinations of substituents on a stereogenic centre which do appear susceptible to racemisation, adjacent carbonyl, nitrogen and aromatic groups are commonly found. As a result the experimental studies that will follow this chapter were based around the following scaffold (Scheme 2.4).

X = OR, NHR
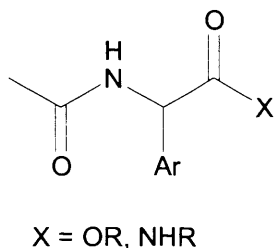
Scheme 2.4: Compounds to be investigated in Chapters 3 and 4.

2.5 Experimental

2.5.1 SMARTS Used for Analysis of Substituents

The SMARTS syntax used for substituent analysis is shown below. The recursive SMARTS definitions called upon in several categories are shown after the category definitions.

```
PROTON [XeH1] 1 1
HYDROXYL [Xe][OH1] 1 1
HALOGEN [Xe][F,Cl,Br,I] 1 1
ALKYL [Xe][CX4] 1 1
ALKENE [Xe]C=[C,c] 1 1
ALKYNE [Xe]C#C 1 1
NITRILE [Xe]C#N 1 1
NITRO [Xe]N(=O)(=O) 1 1
CARBOXYLIC_ACID [Xe]C(=O)[OD1] 1 1
KETONE [Xe]C(=O)[C,c] 1 1
ESTER [Xe]C(=O)[OD2][A,a] 1 1
REVERSE_ESTER [Xe][OD2][$CARBONYL] 1 1
ETHER [Xe][OD2][CX4;!$C_NEXT_TO_CHIRAL] 1 1
AROMATIC_ETHER [Xe][OD2][c] 1 1
ETHER_DB [Xe][OD2][$ALKENE_DEF,$ALK_ETHER_N_DEF,$ALK_ETHER_S_DEF] 1 1
EPOXIDE [Xe][OD2][$C_NEXT_TO_CHIRAL] 1 1
PRIM_AMIDE [Xe]C(=O)[ND1] 1 1
SEC_AMIDE_NONACIDIC [Xe]C(=O)[ND2][$ALKYL_DEF] 1 1
SEC_AMIDE_ACIDIC [Xe]C(=O)[ND2][$CARBONYL,$AROMATIC_DEF] 1 1
SEC_AMIDE_OTHER [Xe]C(=O)[ND2][!$SEC_AMIDE_OTHER_DEF] 1 1
TERT_AMIDE_DIALKYL [Xe]C(=O)[ND3]([$ALKYL_DEF])[$ALKYL_DEF] 1 1
TERT_AMIDE_DIAROMATIC [Xe]C(=O)[ND3]([$AROMATIC_DEF])[$AROMATIC_DEF] 1 1
TERT_AMIDE_ALKYL_AROMATIC [Xe]C(=O)[ND3]([$ALKYL_DEF])[$AROMATIC_DEF] 1 1
TERT_AMIDE_OTHER
[Xe][$TERT_AROMATIC_AMIDE_DEF,$TERT_AMIDE_OTHER_DEF,$TERT_AMIDE_ALKYL_OTHER
_DEF,$TERT_AMIDE_AROMATIC_OTHER_DEF] 1 1
REVERSE_SEC_AMIDE [Xe][ND2][$CARBONYL] 1 1
REVERSE_TERT_AMIDE [Xe][ND3]([A,a;!$CARBONYL])[$CARBONYL] 1 1
AMIDE_DB [Xe][$CARBONYL]N=[A,a] 1 1
PRIM_AMINE [Xe][ND1] 1 1
SEC_AMINE_NONACIDIC [Xe][ND2][$ALKYL_DEF] 1 1
SEC_AMINE_ACIDIC [Xe][ND2][$AROMATIC_DEF;!$CARBONYL] 1 1
SEC_AMINE_OTHER [Xe][ND2][!$AROMATIC_DEF;!$CARBONYL;!$ALKYL_DEF] 1 1
TERT_AMINE_DIALKYL [Xe][ND3]([$ALKYL_DEF])[$ALKYL_DEF] 1 1
TERT_AMINE_ALKYL_AROMATIC [Xe][ND3]([$ALKYL_DEF])[$AROMATIC_DEF] 1 1
TERT_AMINE_DIAROMATIC [Xe][ND3]([$AROMATIC_DEF])[$AROMATIC_DEF] 1 1
```

```
TERT_AMINE_OTHER
[$TERT_AMINE_OTHER_DEF,$TERT_AMINE_ALKYL_OTHER_DEF,$TERT_AMINE_AROMATIC_OTH
ER_DEF] 1 1
BENZENE [Xe]c1ccccc1 1 1
PYRIDINE_ORTH [Xe]c1ncccc1 1 1
PYRIDINE_META [Xe]c1cnccc1 1 1
PYRIDINE_PARA [Xe]c1ccncc1 1 1
PYRIMIDINE_2_6 [Xe]c1ncccn1 1 1
PYRIMIDINE_2_4 [Xe]c1ncncc1 1 1
PYRIMIDINE_3_5 [Xe]c1cncnc1 1 1
PYRADIZINE_2_3 [Xe]c1nnccc1 1 1
PYRADIZINE_3_4 [Xe]c1cnncc1 1 1
PYRAZINE [Xe]c1nccnc1 1 1
TRIAZINE [Xe]c1ncncn1 1 1
SIX_MEMBERED_GENERAL
[$SIX_MEMBERED_GENERAL_DEF;!$BENZENE;!$TRIAZINE;!$PYRADIZINE_3_4;!$PYRADIZI
NE_2_3;!$PYRAZINE;!$PYRIMIDINE_3_5;!$PYRIMIDINE_2_4;!$PYRIMIDINE_2_6;!$PYRI
DINE_PARA;!$PYRIDINE_META;!$PYRIDINE_ORTH] 1 1
FIVE_MEM_AROMATIC [Xe][$FIVE_MEMBERED_AROMATIC_DEF] 1 1
O_HYDROXYLAMINE [Xe][OD2][N,n] 1 1
IMIDE [Xe][ND3]([$CARBONYL])[$CARBONYL] 1 1
IMINE [Xe][ND2]=[CX3,c] 1 1
REVERSE_IMINE [Xe]C=[N+0] 1 1
HYDROXAMIC_ACID [Xe]C(=O)[ND2][OD1] 1 1
QUAT_AMMONIUM [Xe][NX4;!$QA_DEF] 1 1
SULFOXIDE [Xe]=O 1 1
SULFILIMINE [Xe]=N 1 1
THIOETHER [Xe][SD2]-[A,a] 1 1
ISONITRILE [Xe][$ISONITRILE_1DEF,$ISONITRILE_2DEF] 1 1
THIOCARBONYL [Xe]C=[SD1] 1 1
OTHER
[$OTHER_ATOM,$N3,$N_C_OS,$NN_DB,$THIOESTER,$ACID_CHLORIDE,$ALDEHYDE,$PHOSPH
OROUS_DERIV,$THIOL,$ETHER_OTHER,$S_N_DB,$OXOIMINIUM,$ASULFINIUM,$SULFINIUM,
$IMINIUM,$REV_IMINIUM,$THREE_MEM_RING,$FOUR_MEM_RING,$SULFUR_OXIDE_DEF,$SEV
EN_MEM_RING] 1 1

CARBONYL C(=O) 1 0
C_NEXT_TO_CHIRAL C[Xe] 1 0
ALKENE_DEF C=C 1 0
ALK_ETHER_N_DEF C=N 1 0
ALK_ETHER_S_DEF C=S 1 0
ALKYL_DEF [CX4] 1 0
```

71

```
FIVE_MEMBERED_AROMATIC_DEF a1aaaa1 1 0
SIX_MEMBERED_AROMATIC_DEF a1aaaaa1 1 0
AROMATIC_DEF [$FIVE_MEMBERED_AROMATIC_DEF,$SIX_MEMBERED_AROMATIC_DEF] 1 0
SEC_AMIDE_OTHER_DEF [$CARBONYL,$AROMATIC_DEF,$ALKYL_DEF,OD1] 1 0
TERT_AMIDE_OTHER_DEF
C(=O)[ND3]([!$AROMATIC_DEF;!$ALKYL_DEF])[!$AROMATIC_DEF;!$ALKYL_DEF] 1 0
TERT_AMIDE_ALKYL_OTHER_DEF
C(=O)[ND3]([$ALKYL_DEF])[!$AROMATIC_DEF;!$ALKYL_DEF] 1 0
TERT_AMIDE_AROMATIC_OTHER_DEF
C(=O)[ND3]([$AROMATIC_DEF])[!$AROMATIC_DEF;!$ALKYL_DEF] 1 0
TERT_AROMATIC_AMIDE_DEF C(=O)n 1 0
TERT_AMINE_OTHER_DEF
[Xe][ND3]([!$AROMATIC_DEF;!$ALKYL_DEF;!$CARBONYL])[!$AROMATIC_DEF;!$ALKYL_D
EF;!$CARBONYL] 1 0
TERT_AMINE_ALKYL_OTHER_DEF
[Xe][ND3]([$ALKYL_DEF])[!$AROMATIC_DEF;!$CARBONYL;!$ALKYL_DEF] 1 0
TERT_AMINE_AROMATIC_OTHER_DEF
[Xe][ND3]([$AROMATIC_DEF])[!$AROMATIC_DEF;!$ALKYL_DEF;!$CARBONYL] 1 0
SIX_MEMBERED_GENERAL_DEF [Xe]a1aaaaa1 1 0
QA_DEF [NH2;D2]=C 1 0
ISONITRILE_1DEF [N+]#C 1 0
ISONITRILE_2DEF N=[CD1;H0] 1 0
ETHER_OTHER [Xe][OD2][!C;!c;!N;!n] 1 0
THIOL [Xe][SH1] 1 0
SULFUR_OXIDE_DEF [Xe]S(=O) 1 0
SEVEN_MEM_RING [Xe]a1aaaaaa1 1 0
FOUR_MEM_RING [Xe]a1aaa1 1 0
THREE_MEM_RING [Xe]a1aa1 1 0
IMINIUM [Xe]C=[N+1] 1 0
REV_IMINIUM [Xe][N+1]=C 1 0
SULFINIUM [Xe][SH1]=A 1 0
ASULFINIUM [Xe]C=[SH1;D2] 1 0
OXOIMINIUM [Xe]N(=O)=C 1 0
S_N_DB [Xe]S=N 1 0
PHOSPHOROUS_DERIV [Xe]P 1 0
ALDEHYDE [Xe][CD2]=O 1 0
ACID_CHLORIDE [Xe][$CARBONYL][Cl,F] 1 0
THIOESTER [Xe][$CARBONYL]S 1 0
NN_DB [Xe]N=[N+0] 1 0
N3 [Xe]N=[N+1]=[N-1] 1 0
N_C_OS [Xe]N=C=[O,S] 1 0
OTHER_ATOM [Xe][Se,Na,B,Sn,Si,As] 1 0
```

2.5.2 SMARTS Queries

The definitions in the SMARTS code shown in Section 2.5.1 were used to interpret the SMILES strings from the AZ databases after processing using the 'chiral chopper' program (Section 2.2.1). The stereogenic centre in each molecule is replaced by a 'marker' Xenon atom and, as can be seen in the SMARTS code, this is used to identify the location of the stereogenic centre within each substituent.

The use of recursive SMARTS is well illustrated by the category 'other six-membered aromatic'. This category contains all six-membered aromatic groups other than benzene and the nitrogen-containing heterocycles displayed in Table 2.1. After initial SMARTS were written for each of these aromatics, a 'catch all' six-membered aromatic definition was written:

```
SIX_MEMBERED_GENERAL_DEF [Xe]alaaaaa1 1 0
```

A SMARTS definition was then written for 'other six-membered aromatic', which looks for SMILES strings which fit the definition of a six-membered aromatic group but are not any of the specific groups defined previously (benzene, pyridines etc.):

```
SIX_MEMBERED_GENERAL
[$SIX_MEMBERED_GENERAL_DEF;!$BENZENE;!$TRIAZINE;!$PYRADIZINE_3_4;!$PYRADIZI
NE_2_3;!$PYRAZINE;!$PYRIMIDINE_3_5;!$PYRIMIDINE_2_4;!$PYRIMIDINE_2_6;!$PYRI
DINE_PARA;!$PYRIDINE_META;!$PYRIDINE_ORTH] 1 1
```

Similar examples of recursive SMARTS were used in the definitions for differently substituted amide groups, as well as the 'other' category.

The 'chiral chopper' program also recognises the chirality found on sulphur atoms in sulfoxide and sulfilimine functional groups, on account of the sulphur lone pair (Scheme 2.5).

Sulfoxide   Sulfilimine
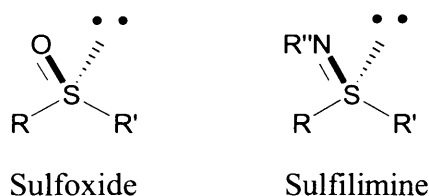
Scheme 2.5: Chirality in sulfoxide and sulfilimine functional groups.

When the 'chiral chopper' program encounters molecules containing these functional groups, it results in SMILES denoting a Xenon atom double bonded to either an oxygen (sulfoxide) or a nitrogen (sulfilimine). Therefore, when analysing the output of the SMARTS query it has to be taken into account that SMILES strings for these molecules will only have three substituents.

73

2.5.3 SMARTS Output

The output from the SMARTS query consists of a large .txt file with a molecule number for every compound listed in the database queried followed by a series of numbers, corresponding to each of the 52 categories of substituent tested for and how many instances of that group the compound contains. In order to check that the SMARTS code was recognising every substituent as one of the designated categories, the sum of the substituents was calculated for each molecule. If every substituent of a molecule has been categorised the sum is equal to 4, except in cases where the stereogenic centre is not a carbon atom such as sulfoxides and sulfilimines (Section 2.5.2). This worked as an iterative process; the SMARTS output was analysed for cases where the sum of the groups was more or less than four and the structure of the original molecule was analysed. The SMARTS code was then rewritten to either 'tighten up' certain definitions (so it did not record substituents in more than one category) or new functional groups were coded for (either as a stand-alone category or to be classified as 'other').

Each stereogenic centre in the SMARTS output was given an identifier code, produced by stringing together the series of numbers corresponding to each substituent category. This results in all stereogenic centres with the same combinations of substituents having the same identifying code. The number of stereogenic centres bearing each combination of substituents could then be totalled.

The most frequently occurring combinations of substituents were then analysed, and using chemical intuition and the guidelines set by Testa *et al.* (Table 1.1) assessed for susceptibility to acid- or base-catalysed racemisation.

2.6 Appendix

2.6.1 Explanation of Syntax Used
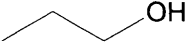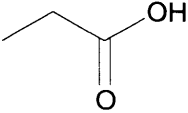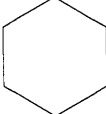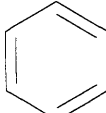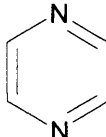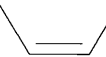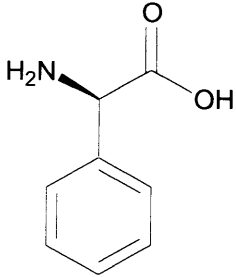
2.6.1.1 SMILES

The information in the ISAC and IBEX databases is recorded using the SMILES[1-8] (Simplified Molecular Input Line Entry Syntax) chemical language. Using SMILES, molecules and reactions can be represented using a series of ASCII characters. The basic structure of the language is as follows:

- Atoms within a molecule are represented by their atomic symbol inside square brackets.

- For elements within the 'organic subset' (Boron, Nitrogen, Carbon, Oxygen, Phosphorous, Sulphur and the halogens), the square brackets are not necessary if the number of hydrogens conforms to the lowest normal valence.

- Within square brackets, any attached hydrogens or formal charge must be specified.

- Aromaticity is signified by lowercase lettering.

- Bonds are assumed to be single unless specified otherwise. Molecular branches can be specified by enclosure within parentheses.

- Cyclic structures are represented by assigning a number to an atom and then referring back to it.

- Chirality is indicated by either @ or @ @ designation of stereogenic centre.

Some examples of simple molecules represented by SMILES syntax are shown in Table 2.7.

Table 2.7: Examples of SMILES syntax.

Compound name	Graphical Depiction	SMILES notation
Propane		CCC
Propan-1-ol		CCCO
Propanoic acid		CCC (=O) O
Cyclohexane		C1CCCCC1
Benzene		c1ccccc1
Pyrazine		c1nccnc1
Cis-2-butene		C\C=C/C
L-Phenylglycine		N[C@@H] (c1ccccc1) C (=O) O
Sodium Chloride	NaCl	[Na+].[Cl-]

2.6.1.2 SMARTS

The SMARTS[9, 10] (Smiles Arbitrary Target Specification) chemical language is an extension of SMILES that enables sub-structure targeting of compounds in molecular databases to find a desired chemical 'motif'. All SMILES characters and properties are valid terms in SMARTS, which also includes logical operators (such as 'and', 'or' and 'not'). This allows queries to be made with the desired level of specificity. For example, using SMILES, methane can be written as C or [CH4]. A SMARTS search of C would result in a match for methane, but would also match for ethane, propane, or any compound in the database containing an aliphatic carbon. A SMARTS search of [CH4] would match only for methane. If one wanted to search for carbonyl containing compounds, the following SMARTS searches would give varying results:

- C=O   would return molecules containing a carbonyl (ketone, amide, etc.)

- CC(=O)C   would only return ketones

- CC(=O)O   would return all esters and carboxylic acids

- CC(=O)OC   would only return esters

Some other important features of SMARTS are described below:

- "a" is any aromatic atom, "A" is any aliphatic

- "D" is any heavy atom (i.e. not hydrogen)

  o E.g.   [OD2] is oxygen bonded to any two heavy atoms

- "#" can be used to define any atom of a specified atomic number

  o E.g.   [#7] is any aromatic or aliphatic nitrogen

- "!" is the "not" logical operator

  o E.g.   [!C] is any atom that is not an aliphatic carbon

- "," is the "or" logical operator

  o E.g.   [O,N] is any atom that is an aliphatic oxygen or carbon

- "&" and ";" are both "and" logical operators. "&" is higher precedence than the "or" operator (","), ";" is lower precedence than "or". High precedence "and" is the default operator and may be omitted.

  o [C&+1,+0] is an aliphatic carbon with +1 charge or any neutral atom

o   `[C;+1,+0]` is an aliphatic carbon with +1 or neutral charge

The examples below show the range of specificity possible with SMARTS.

Aliphatic oxygen attached to carbon with any bond:

- `C~O`

Oxygen or nitrogen, with at least one hydrogen attached and not in a ring:

- `[O,N;!H0;!R]`

Oxygen double bonded to aliphatic carbon or nitrogen:

- `[O]=[C,N]`   or   `[#6]=[C,N]`

Oxygen double bonded to aliphatic carbon or nitrogen, single bonded to an aromatic ring, with a halogen in meta position:

- `[#6]=[C,N]-aaa[F,Cl,Br,I]`

It is also possible to define SMARTS and then refer back to them. So-called recursive SMARTS are used to define an atomic environment which can be called upon using the $ symbol. In the following example, a carbonyl group is defined and then referred back to when searching for a primary amide group:

```
CARBONYL_DEF          C(=O) 1 0

PRIM_AMIDE            [$CARBONYL_DEF][ND1] 1 1
```

Recursive SMARTS were used in writing the search criteria for the analysis in this chapter. The numbers after the definition determine whether the SMARTS desire output or not. '1 0' after SMARTS code is used when something is defined to be called upon later and does not give any output. '1 1' after SMARTS code instructs the program to output whether the SMARTS have been found or not. It does this in the form of a '1' for yes, '0' for no.

2.6.2 Data Tables

Table 2.8: Details of all combinations of substituents within the most common 250 in ISAC, considered at risk of acid-catalysed racemisation.

	Combination of substituents on stereocentre	No. stereocentres[a]
20	1 proton, 1 hydroxyl, 1 benzene, 1 alkyl	16882
72	1 hydroxyl, 1 benzene, 2 alkyl	3291
77	1 proton, 1 hydroxyl, 1 alkyl, 1 alkene	2866
115	1 hydroxyl, 2 benzene, 1 alkyl	1717
127	1 hydroxyl, 2 benzene, 1 alkyl and aromatic sub. tert. amide	1502
134	1 proton, 1 hydroxyl, 1 five-membered aromatic, 1 alkyl	1398
196	1 proton, 1 hydroxyl, 1 benzene, 1 dialkyl tert. amide	861
203	1 proton, 1 hydroxyl, 1 benzene, 1 five-membered aromatic	795
219	1 hydroxyl, 1 benzene, 1 alkyl, 1 dialkyl tert. amide	661
249	1 proton, 1 hydroxyl, 1 alkyl, 1 ether	544

[a] from a total of 1,607,343 stereogenic centres

Table 2.9: Details of all combinations of substituents within the most common 250 in ISAC, with unknown risk of racemisation.

	Combination of substituents on stereocentre	No. stereocentres[a]
10	1 proton, 1 benzene, 1 reverse tert. amide, 1 thioether	25241
33	1 proton, 1 alkyl, 1 dialkyl tert. amide, 1 thioether	9631
39	1 proton, 2 alkyl, 1 thioether	7286
53	1 proton, 2 alkyl, 1 other	5215
61	1 proton, 1 alkyl, 1 reverse tert. amide, 1 thioether	4152
62	1 proton, 1 benzene, 1 alkyl, 1 thioether	4140
89	1 proton, 2 alkyl, 1 epoxide	2426
186	1 proton, 1 alkyl, 1 ester, 1 thioether	913
200	1 proton, 1 alkyl, 1 nitrile, 1 reverse sec. amide	814
208	1 proton, 1 five-membered aromatic, 1 nitrile, 1 reverse sec. amide	768
224	1 proton, 1 alkyl, 1 ester, 1 other	639
225	chiral sulfoxide, 1 hydroxyl, 1 ether	631
229	1 proton, 1 benzene, 1 meta pyridine, 1 ether	613
245	1 proton, 1 meta pyridine, 1 alkyl, 1 ether	561

[a] from a total of 1,607,343 stereogenic centres

Table 2.10: Details of 20 most common combinations of substituents on stereogenic centres found in IBEX database.

	Combination of substituents on stereocentre	No. stereocentres[a]
1	1 proton, 3 alkyl	107820
2	1 proton, 1 hydroxyl, 2 alkyl	76213
3	1 proton, 2 alkyl, 1 dialkyl tert. amine	59925
4	1 proton, 2 alkyl, 1 benzene	37118
5	1 proton, 2 alkyl, 1 ether	35557
6	1 proton, 2 alkyl, 1 reverse sec. amide	35398
7	1 proton, 2 alkyl, 1 nonacidic sec. amine	30963
8	1 proton, 2 alkyl, 1 reverse tert. amide	26833
9	1 proton, 1 alkyl, 1 nonacidic sec. amide, 1 reverse sec. amide	14696
10	1 proton, 2 alkyl, 1 aromatic ether	14505
11	1 proton, 2 alkyl, 1 five membered aromatic	13379
12	1 proton, 1 hydroxyl, 1 alkyl, 1 benzene	13005
13	1 proton, 2 alkyl, 1 prim. amine	12870
14	1 proton, 1 alkyl, 1 benzene, 1 reverse sec. amide	10623
15	1 proton, 2 alkyl, 1 reverse ester	10601
16	3 alkyl, 1 benzene	10392
17	1 proton, 1 alkyl, 1 benzene, 1 dialkyl tert. amine	10202
18	1 proton, 2 alkyl, 1 acidic sec. amine	9642
19	1 proton, 2 alkyl, 1 alkyl and aromatic sub. tert. amine	9408
20	1 proton, 2 alkyl, 1 nonacidic sec. amide	8821

[a] from a total of 989,125 stereogenic centres

Table 2.11: Details of all combinations of substituents within the most common 250 in IBEX, considered at risk of base-catalysed racemisation.

	Combination of substituents on stereocentre, excluding proton	No. stereocentres[a]
26	1 alkyl, 1 ketone, 1 reverse sec. amide	7003
60	1 alkyl, 1 ester, 1 reverse sec. amide	2430
71	1 alkyl, 1 ketone, 1 reverse tert. amide	1971
74	1 benzene, 2 alkene	1900
83	1 alkyl and aromatic sub. tert. amide, 1 reverse sec. amide, 1 imine	1540
87	1 alkyl, 1 ester, 1 reverse tert. amide	1454
95	1 alkyl, 1 ester, 1 nonacidic sec. amine	1231
106	1 alkyl, 1 benzene, 1 ester	1143
107	2 benzene, 1 dialkyl tert. amine	1140
132	1 alkyl, 1 benzene, 1 ketone	801
141	1 benzene, 1 dialkyl tert. amide, 1 reverse sec. amide	756
149	1 alkyl, 1 ketone, 1 ester	694
162	1 alkyl, 2 ketone	618
176	1 benzene, 1 five-membered aromatic, 1 dialkyl tert. amine	551
184	1 alkyl, 1 ester, 1 prim. amine	508
196	1 alkyl, 1 ketone, 1 nonacidic sec. amine	467
210	2 benzene, 1 reverse tert. amide	435
220	1 benzene, 1 acidic sec. amide, 1 reverse sec. amide	417
234	1 benzene, 1 nonacidic sec. amide, 1 reverse sec. amide	386
244	2 benzene, 1 alkene	364
246	1 alkyl, 1 ester, 1 dialkyl tert. amine	360
247	1 alkyl, 1 ester, 1 sec. amine (other)	359

[a] from a total of 989,125 stereogenic centres

Table 2.12: Details of combinations of substituents within the most common 250 with one substituent with carbonyl group adjacent to stereocentre and one substituent with nitrogen adjacent to stereocentre (IBEX database).

Combination of substituents on stereocentre, excluding proton		No. stereocentres[a]
Esters		
60 1 alkyl, 1 ester, 1 reverse sec. amide		2430
87 1 alkyl, 1 ester, 1 reverse tert. amide		1454
95 1 alkyl, 1 ester, 1 nonacidic sec. amine	*	1231
184 1 alkyl, 1 ester, 1 prim. amine	*	508
246 1 alkyl, 1 ester, 1 dialkyl tert. amine	*	360
247 1 alkyl, 1 ester, 1 sec. amine (other)	*	359
Amides		
83 1 alkyl and aromatic sub. tert. amide, 1 reverse sec. amide, 1 imine		1540
141 1 benzene, 1 dialkyl tert. amide, 1 reverse sec. amide		756
220 1 benzene, 1 acidic sec. amide, 1 reverse sec. amide		417
234 1 benzene, 1 nonacidic sec. amide, 1 reverse sec. amide		386
Ketones		
26 1 alkyl, 1 ketone, 1 reverse sec. amide		7003
71 1 alkyl, 1 ketone, 1 reverse tert. amide		1971
196 1 alkyl, 1 ketone, 1 nonacidic sec. amine	*	467

[a] from a total of 989,125 stereogenic centres
* denotes adjacent amine groups

Table 2.13: Details of all combinations of substituents within the most common 250 in IBEX, considered at risk of acid-catalysed racemisation.

	Combination of substituents on stereocentre	No. stereocentres[a]
12	1 proton, 1 hydroxyl, 1 benzene, 1 alkyl	13005
45	1 proton, 1 hydroxyl, 1 alkyl, 1 alkene	3628
51	1 hydroxyl, 1 benzene, 2 alkyl	2864
70	1 proton, 1 hydroxyl, 1 five-membered aromatic, 1 alkyl	1981
110	1 proton, 1 hydroxyl, 1 meta pyridine, 1 alkyl	1132
135	1 hydroxyl, 2 alkyl, 1 alkyne	784
143	1 hydroxyl, 1 benzene, 1 alkyl, 1 nonacidic sec. amide	747
170	1 hydroxyl, 1 benzene, 1 alkyl, 1 ester	568
177	1 hydroxyl, 2 benzene, 1 alkyl	544
178	1 proton, 1 hydroxyl, 2 benzene	536
191	1 hydroxyl, 1 five-membered aromatic, 2 alkyl	490
192	1 proton, 1 hydroxyl, 1 alkyl, 1 ether	488
201	1 proton, 1 hydroxyl, 1 ortho pyridine, 1 alkyl	460
203	1 hydroxyl, 1 para pyridine, 1 alkyl, 1 ester	450
206	1 proton, 1 hydroxyl, 1 para pyridine, 1 alkyl	442
242	1 hydroxyl, 2 benzene, 1 reverse tert. amide	366

[a] from a total of 989,125 stereogenic centres

Table 2.14: Details of all combinations of substituents within the most common 250 in IBEX, with unknown risk of racemisation.

	Combination of substituents on stereocentre	No. stereocentres[a]
43	1 proton, 2 alkyl, 1 hydroxamic acid	4024
46	1 proton, 1 alkyl, 1 tert. amine (other), 1 hydroxamic acid	3497
48	1 proton, 1 alkyl, 1 nitrile, 1 reverse tert. amide	3260
63	1 proton, 2 alkyl, 1 thioether	2307
86	1 proton, 2 alkyl, 1 other	1504
92	1 proton, 2 alkyl, 1 hydroxylamine	1368
113	1 proton, 1 benzene, 1 alkyl, 1 thioether	1086
114	1 proton, 1 benzene, 1 reverse tert. amide, 1 thioether	1083
118	1 proton, 1 alkyl, 1 acidic sec. amide 1 thioether	1008
136	1 proton, 1 alkyl, 1 nitrile, 1 reverse sec. amide	783
142	1 proton, 1 alkyl, 1 reverse tert. amide, 1 hydroxamic acid	754
148	1 proton, 2 benzene, 1 ether	709
164	1 proton, 1 benzene, 1 alkyl, 1 other	587
165	1 proton, 1 alkyl, 1 ketone, 1 aromatic ether	582
206	1 proton, 1 alkyl, 1 reverse tert. amide, 1 thioether	445
217	1 proton, 1 alkyl, 1 ketone, 1 thioether	421
226	1 proton, 1 hydroxyl, 1 alkyl, 1 hydroxamic acid	406
232	1 proton, 1 alkyl, 1 ester, 1 aromatic ether	390
233	1 proton, 1 meta pyridine, 1 alkyl, 1 thioether	388

[a] from a total of 989,125 stereogenic centres

2.7 References

1.   http://www.daylight.com/dayhtml_tutorials/languages/smiles/index.html   (accessed 19/01/2011).

2.   Weininger, D., *Journal of Chemical Information and Computer Sciences* **1988,** *28* (1), 31-36.

3.   Weininger, D.; Weininger, A.; Weininger, J. L., *Journal of Chemical Information and Computer Sciences* **1989,** *29* (2), 97-101.

4.   Weininger, D., *Journal of Chemical Information and Computer Sciences* **1990,** *30* (3), 237-243.

5.   Engel, T., *Journal of Chemical Information and Modeling* **2006,** *46* (6), 2267-2277.

6.   Gasteiger, J.; Engel, T., *Chemoinformatics: a textbook*. Wiley-VCH: 2003; p 26-27.

7.   Leach, A. R., *Molecular Modelling: Principles and Applications*. 2nd ed.; Prentice Hall: 2001; p 642-647.

8.   Velingkar, V. S.; Pokharna, G.; Kohle, N. S., *International Journal of Current Pharmaceutical Research* **2011,** *3* (1), 71-75.

9.   http://www.daylight.com/dayhtml_tutorials/languages/smarts/index.html   (accessed 19/01/2011).

10.   Schneider, G.; Baringhaus, K.-H., *Molecular Design: Concepts and Applications*. Wiley-VCH: 2008; p 25-29.

11.   Lagorce, D.; Sperandio, O.; Galons, H.; Miteva, M. A.; Villoutreix, B. O., *BMC Bioinformatics* **2008,** *9:396*.

12.   Walters, W. P.; Murcko, M. A., *Advanced Drug Delivery Reviews* **2002,** *54* (3), 255-271.

13.   Hann, M.; Hudson, B.; Lewell, X.; Lifely, R.; Miller, L.; Ramsden, N., *Journal of Chemical Information and Computer Sciences* **1999,** *39* (5), 897-902.

14.   Vieth, M.; Siegel, M. G.; Higgs, R. E.; Watson, I. A.; Robertson, D. H.; Savin, K. A.; Durst, G. L.; Hipskind, P. A., *Journal of Medicinal Chemistry* **2004,** *47* (1), 224-232.

15.   Leach, A. G.; Jones, H. D.; Cosgrove, D. A.; Kenny, P. W.; Ruston, L.; MacFaul, P.; Wood, J. M.; Colclough, N.; Law, B., *Journal of Medicinal Chemistry* **2006,** *49* (23), 6672-6682.

16.   Hansch, C.; Leo, A.; Taft, R. W., *Chemical Reviews* **1991,** *91* (2), 165-195.

17.   Reist, M.; Testa, B.; Carrupt, P. A., *Enantiomer* **1997,** *2* (3-4), 147-155.

18.   Testa, B.; Carrupt, P. A.; Gal, J., *Chirality* **1993,** *5* (3), 105-111.

19.   Reist, M.; Testa, B.; Carrupt, P.-A., Drug Racemization and Its Significance in Pharmaceutical Research. In *Handbook of Experimental Pharmacology*, Springer: 2003; Vol. 153, pp 91-112.

20.   Lambert, W. J.; Timmer, P. G., *Pharmaceutical Research* **1991,** *8* (11), 1444-1447.

21.   Lambert, W. J.; Timmer, P. G.; Walters, R. R.; Hsu, C. Y. L., *Journal of Pharmaceutical Sciences* **1992,** *81* (10), 1028-1031.

22.   Venter, D. P., *Tetrahedron* **1991,** *47* (27), 5019-5024.

23.   Ghose, A. K.; Viswanadhan, V. N.; Wendoloski, J. J., *Journal of Combinatorial Chemistry* **1999,** *1* (1), 55-68.

24.   Lameijer, E. W.; Kok, J. N.; Back, T.; IJzerman, A. P., *Journal of Chemical Information and Modeling* **2006,** *46* (2), 553-562.

3 Kinetic Studies on the Configurational Instability of *N*-Acetyl Arylglycine Esters

3.1 Introduction

The literature on instability of stereogenic centres (Chapter 1) combined with chemical intuition gives an insight into the structural features that may facilitate racemisation of drugs under physiological conditions. This information, in conjunction with the results from the analysis of AstraZeneca's compound libraries (Chapter 2), suggested several structures of interest. The focus in this chapter will be on the set of *N*-acetyl arylglycine ester derivatives illustrated in Scheme 3.1.
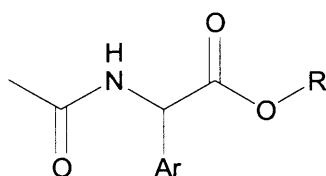
Scheme 3.1: Structures to be investigated in this chapter. R = methyl, ethyl and isopropyl esters, Ar = substituted benzenes and 2- and 3-thienyl groups.

N-acetyl arylglycine esters are of type R''R'RC-H, and hence could be susceptible to racemisation through base-catalysed proton abstraction mechanisms, as discussed in Chapter 1. All three substituents around the stereogenic centre can help stabilise a developing negative charge. Esters and aromatic groups can do this through delocalisation of the negative charge (Scheme 1.10). The amide group can do this through electrostatic interactions of a partial positive charge on the amide nitrogen with the negative charge built up during racemisation (Scheme 1.11b). By the guidelines set out by Testa *et al.*,[1-3] (Table 1.1) we would expect to see pharmaceutically relevant configurational instability due to the presence of three 'acid-strengthening' groups, one of which is classified as strongly so (ester).

Database mining studies showed that stereogenic centres deemed susceptible to base-catalysed racemisation commonly possess adjacent carbonyl, nitrogen and aromatic groups (Chapter 2). The particular combination of an adjacent ester, 'reverse' secondary amide and a benzene group is only the 437th most frequently occurring combination of substituents in the ISAC database (appearing in 225 stereocentres).[*] However, each substituent appears frequently in compounds considered susceptible to base-catalysed racemisation. As a result, the effect of each substituent on the process of base-catalysed racemisation is of importance.

---

[*] 354th most frequently occurring combination of substituents in the IBEX database, appearing in 205 stereocentres.

Several of the top selling pharmaceutical drugs on the market have stereogenic centres similar to that shown in Scheme 3.1. Stereogenic centres similar to the those under investigation in this chapter are found in the platelet aggregate inhibitor Clopidogrel,[4, 5] cholesterol regulator Ezetimibe,[6] psychostimulant Methylphenidate[7, 8] and ACE[†] inhibitor Perindopril[9] (Scheme 3.2).
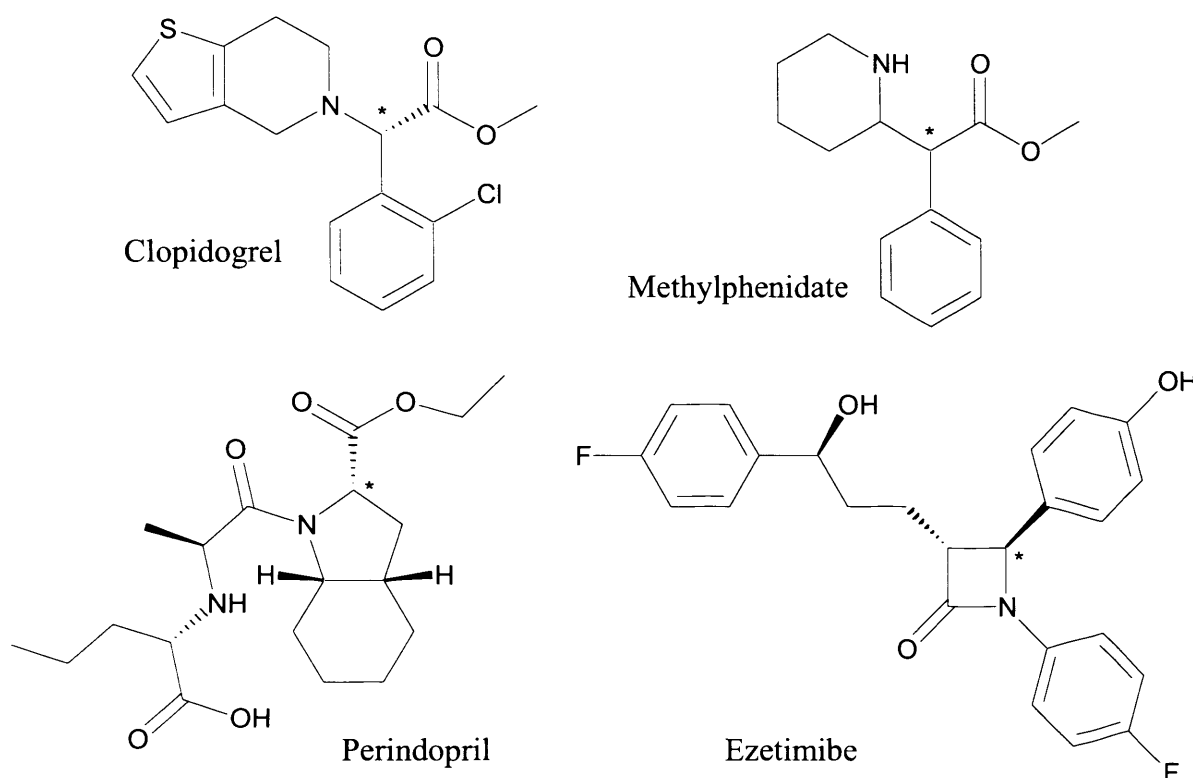
Scheme 3.2: Drugs with similar stereogenic centres to the scaffold shown in Scheme 3.1.

Mining studies of drug databases have shown that, although not as abundant as benzene rings, aromatic heterocycles are commonly found in drug molecules.[10] Nitrogen-containing heterocycles are the most commonly found, followed by oxygen-containing and sulphur-containing heterocycles.[11] Pyridine was found to be the second most frequently occurring ring system in the National Cancer Institute drug database (after benzene), appearing in 2.7 % of molecules (> 250,000 drugs analysed).[12] Thiophene is the most common sulphur-containing heterocycle found in the Comprehensive Medicinal Chemistry database.[11] An example of a thiophene containing drug is the antidepressant Duloxetine[13] (Scheme 3.3).

[†] ACE – Angiotensin-Converting Enzyme.
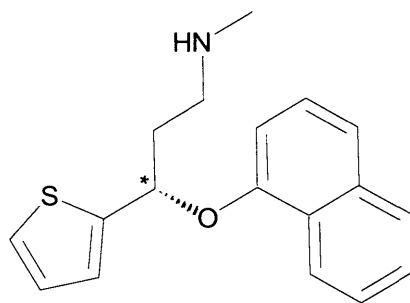
Scheme 3.3: Structure of Duloxetine.

Because of their abundance in drug molecules, it is desirable to incorporate compounds containing heterocycles into our analysis. Thiophenes were chosen for analysis in this chapter due to the commercial availability of appropriate starting materials. Although thiophenes are not the most desired heteroaromatics for study, analysis of their behaviour will allow insight into how the effect of heteroaromatic substituents on a stereogenic centre may differ from the effect of benzene derivatives.

3.2 Aims

This chapter has five main aims.

First, to determine the rates of racemisation and proton-deuterium exchange (H/D exchange) for compounds of general structure illustrated in Scheme 3.1, under conditions analogous to those found in the body. Evaluation of these rates will inform as to whether or not stereogenic centres such as those found in the compounds under analysis are at risk of configurational instability in the body.

Second, to analyse the effect changes in conditions have on the rate constants of configurational instability.

Third, resulting from the previous point, to determine whether configurational instability is general- or specific-base catalysed.

Fourth, to investigate the effects each substituent has on configurational stability. Quantifying the effect of slight changes in molecular structure on the rate constants of H/D exchange will afford insight into the importance of each substituent in the process.

Fifth, to determine the mechanism by which racemisation and H/D exchange takes place. This will also be informed by the effect of different substituents on the rate constants for racemisation and H/D exchange.

3.3 Synthesis of Compounds for Analysis

A set of *N*-acetyl arylglycine methyl esters **3a-l** was selected for analysis (Scheme 3.4).

3a-h

X = **a)** H, **b)** *p*-OH, **c)** *p*-Me, **d)** *p*-F,
e) *p*-Cl, **f)** *m*-F, **g)** *m*-F, **h)** *p*-CF$_3$

3i-j

R = **i)** Et, **j)** ^{i}Pr

3k

3l
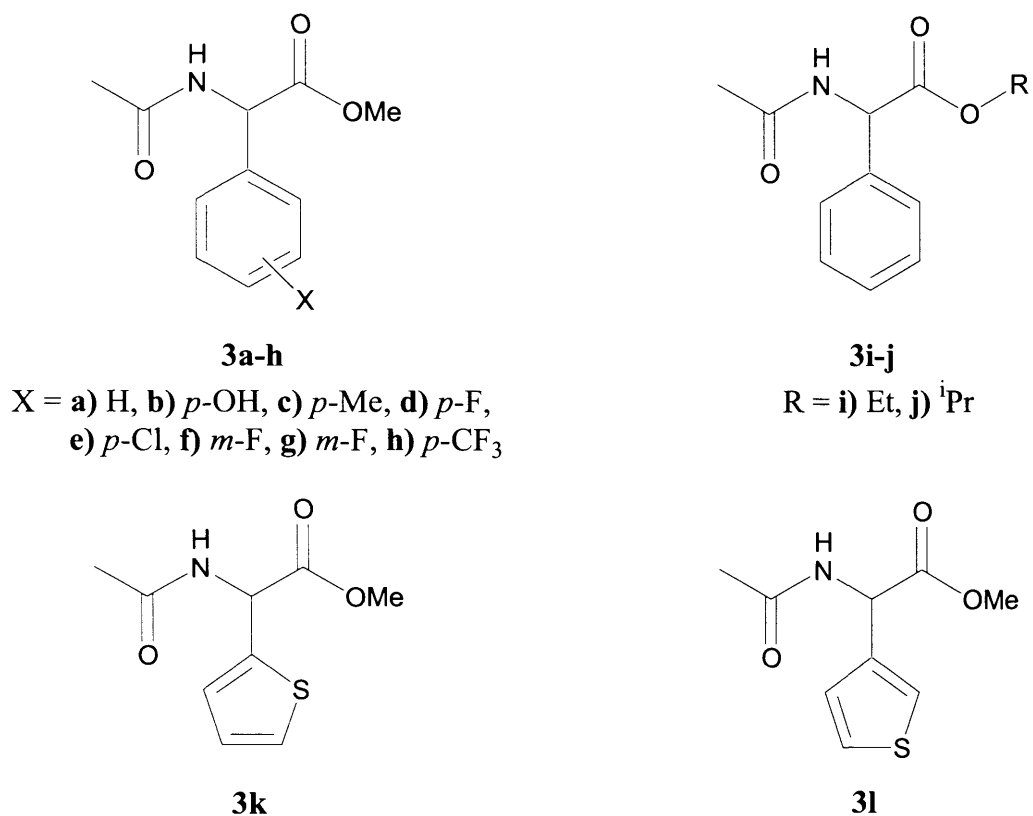
Scheme 3.4: *N*-Acetyl arylglycine methyl esters **3a-l**.

Compounds **3a-l** were synthesised from commercially available arylglycine starting materials (Scheme 3.5).

1a-h, k, l　　　　　　**2a-l**　　　　　　**3a-l**
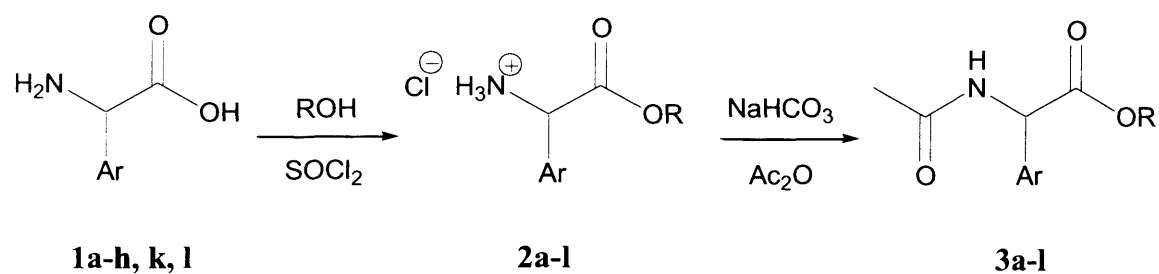
Scheme 3.5: Synthetic route to compounds **3a-l**.

For comparison, a set of *N*-acetyl phenylglycines, **4a, c-e, g-h**, was also synthesised for analysis (Scheme 3.6).
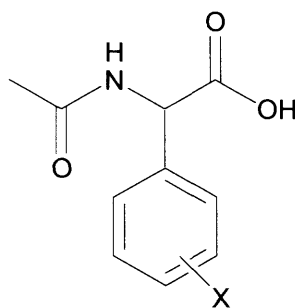
4a, c-e, g-h

X = **a)** H, **c)** *p*-Me, **d)** *p*-F,
e) *p*-Cl, **g)** *m*-F, **h)** *p*-CF$_3$

Scheme 3.6: *N*-acetyl phenylglycines **4a, c-e, g-h**.

These compounds were also synthesised from commercially available arylglycine starting materials, as displayed in Scheme 3.7.

1a, c-e, i-h   **4a, c-e, i-h**
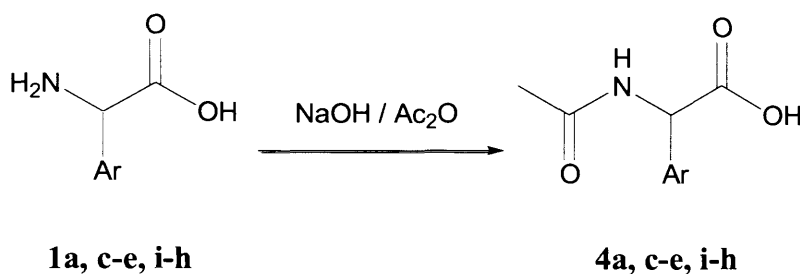
Scheme 3.7: Synthetic route to compounds **4a, c-e, g-h**.

Enantiopure analogues of **3a, 3e, 4a** and **4e** were synthesised in the same manner from enantiopure starting materials.

3.4 Results and Discussion

3.4.1 Initial Proton-Deuterium Exchange Experiments

As discussed in Chapter 1, configurational instability for stereogenic centres of type R''R'RC-H can be monitored through H/D exchange experiments. If deuterium incorporation at the stereogenic centre is observed then this strongly suggests that the compound is not configurationally stable. The use of H/D exchange experiments as a model for racemisation also has the advantage that enantiopure or enantioenriched compounds do not need to be used.

Compounds **3a-j** were placed in deuterated buffers and incubated at 37 °C. A range of different phosphate buffer strengths were used. Generally, buffers with pH** 7.4 were used.[‡][14-16] Some experiments were undertaken at pH** 7.8, in order to evaluate the relative involvement of the different phosphate species present ($H_2PO_4^-$ and HPO_4^{2-}) in H/D exchange. A constant ionic strength of 1 M was used. The reaction was monitored over time using ^1H NMR spectroscopy. The extent of H/D exchange at the stereogenic centre is measured by looking for a decrease in the intensity of the peak corresponding to the proton bound to the stereogenic centre. The intensity of the peak is calculated relative to the peak for the protons on the benzene ring. It is assumed that no deuterium incorporation takes place on the benzene ring and, thus, that the intensity of the aromatic protons remains constant over time.

3.4.2 Reaction Scheme

H/D exchange at the stereogenic centre was observed for all compounds **3a-l**. Ester hydrolysis was also seen for each compound. As the ester was being hydrolysed, a new peak in the ^1H NMR spectrum appeared. This peak corresponds to a proton bound to the stereogenic centre for the relevant hydrolysis products **4a-h, k-l**. Confirmation that this new peak was a result of ester hydrolysis was obtained by comparison of the chemical shift of the new peak in the ^1H NMR spectrum, with that seen for the synthesised corresponding *N*-acetyl phenylglycine.

---

‡ When reporting the acidity of D_2O-based solutions, the term 'pH*' is often used to denote the value recorded on a standard electrode. It is widely accepted that deuterium isotope effects cause the actual pD of D_2O solutions to equal pH* + 0.4 units. However, the value of pH* is commonly used as a deuterium isotope effect also alters the position of equilibrium between buffer components, generally raising the pK_a by 0.5-0.7 units. This approximately offsets the error from the uncorrected pH meter reading. The term 'pH**' adds the extra caveat that the buffers used are not temperature corrected, i.e. the values displayed were determined at 25 °C and the buffers were used at 37 °C.

Following ester hydrolysis, no further H/D exchange is seen at the stereogenic centre. Confirmation that no H/D exchange at the stereogenic centre occurs for **4a-h, k-l** was obtained by monitoring **4h** under the same conditions. No decrease in the intensity of the peak corresponding to the proton bound to the stereogenic centre was seen after 30 days for compound **4h**, indicating no H/D exchange occurs. As the p-CF$_3$ aromatic substituent in **4h** is the most electron withdrawing substituent analysed, it can be concluded that if H/D exchange does not occur for this compound, it will not for any of the N-acetyl phenylglycines **4a-h, k-l** (*cf.* Section 1.8.2). The observation that no further H/D exchange occurs is consistent with the classification of a carboxylate group as enhancing configurational stability, because of unfavourable interactions between the carboxylate anion and negative charge built up during H/D exchange (Scheme 1.15). Therefore, the reaction scheme for compound **3a** in deuterated buffers can be summarised as in Scheme 3.8.
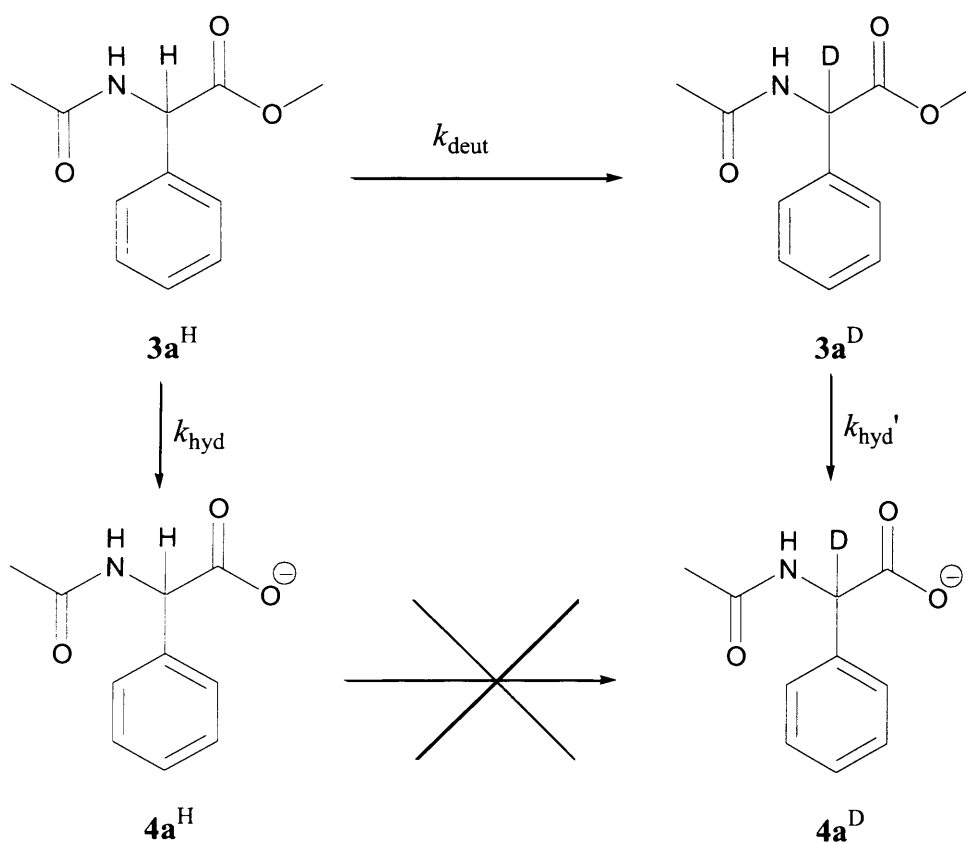
Scheme 3.8: Reaction of **3a** in deuterated buffer. Superscript letters in compound numbering refer to the nature of the hydron bound to the stereogenic centre in molecule.

The reaction profile in Scheme 3.8 also applies to compounds **3b-j**.

Despite ester hydrolysis, there is negligible difference in the chemical shift of the protons bound to the benzene ring between compounds **3** and **4**. The total intensity of the peaks from

the aromatic groups remains constant over time. Thus, when calculating relative integrals for protons bound to the stereogenic centre for both compounds, they are relative to the intensity of aromatic protons from both species.

3.4.3 Determination of Rate Constants of H/D Exchange and Hydrolysis

Observed rate constants for the disappearance of start material protonated at the stereogenic centre were obtained for compounds **3a-h**. Each compound was analysed at a range of buffer concentrations and pH**'s, at an ionic strength of 1 M and temperature of 37 °C. Rate constants for H/D exchange and hydrolysis were derived from the observed rate constants as described in the experimental (Section 3.6.3.3). The observed rate constants and the derived rate constants for H/D exchange and hydrolysis of **3a** are summarised in Table 3.1.

Table 3.1: Rate constants for H/D exchange and for hydrolysis of **3a** in D_2O buffers at 37 °C, $I = 1$ M.

pH**	phosphate conc. / M	[HPO$_4^{2-}$] conc. / M	k_{obs} x 10^6 / s^{-1}	k_{deut} x 10^6 / s^{-1}	k_{hyd} x 10^6 / s^{-1}
7.4	0.050	0.030	3.47 ± 0.15	1.36 ± 0.18	2.11 ± 0.09
7.4	0.100	0.061	4.10 ± 0.13	1.82 ± 0.15	2.28 ± 0.08
7.4	0.200	0.122	4.91 ± 0.08	2.80 ± 0.09	2.11 ± 0.04
7.4	0.250	0.152	5.52 ± 0.16	3.25 ± 0.17	2.27 ± 0.07
7.8	0.200	0.159	7.03 ± 0.14	3.57 ± 0.16	3.46 ± 0.07
7.4	0.300	0.182	6.16 ± 0.11	3.64 ± 0.12	2.53 ± 0.05
7.8	0.355	0.282	10.22 ± 0.18	5.61 ± 0.19	4.61 ± 0.08

Tables analogous to Table 3.1 for **3b-h** can be found in the appendix (Section 3.7.1.1).

To confirm the method of analysis, the rate constant for hydrolysis of **3a** was also determined through HPLC. The rate constant of hydrolysis (k_{hyd}) of **3a** in D_2O buffer of pH** 7.4, phosphate concentration 0.2 M, $I = 1$M at 37 °C was determined to be $(2.14 ± 0.05)$ x 10^{-6} s^{-1} (see experimental Section 3.6.5). This value compares favourably with the value of k_{hyd} determined under these conditions through ^1H NMR spectroscopy, of $(2.11 ± 0.04)$ x 10^{-6} s^{-1}.

3.4.4 Nature of Base-Catalysis

For each compound **3a-h**, the rate constant for deuteration was plotted as a function of the concentration of the basic component of the buffer (Figure 3.1 for **3a**).
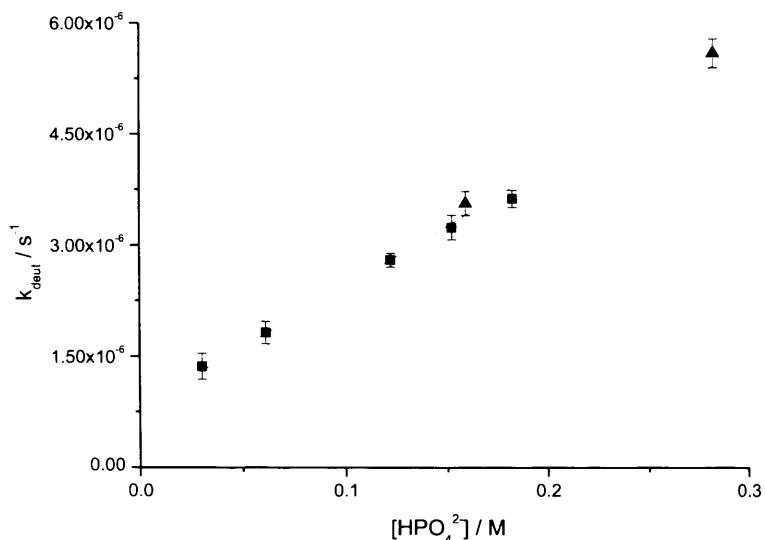
Figure 3.1: Variation of k_{deut} of **3a** with $[HPO_4^{2-}]$ at 37 °C, $I = 1$ M, (■) pH** 7.4, (▲) pH** 7.8.

Figure 3.1 shows a linear increase in the rate constant for H/D exchange as a function of the concentration of the basic buffer component. This linear increase suggests that H/D exchange is subject to general-base catalysis by phosphate dianion. The experimental rate constant for deuteration follows the rate law given by eqn (3.1).

$$k_{deut} = k_0 + k_{OH}[OH^-] + k_{gb}[HPO_4^{2-}]$$ (3.1)

where k_{deut} is the observed rate constant for deuteration, k_0 is the rate constant of the uncatalysed reaction, k_{OH} is the rate constant of the hydroxide-catalysed deuteration reaction and k_{gb} is the rate constant of the phosphate dianion-catalysed deuteration reaction.

The gradient of the line in Figure 3.1 corresponds to the rate constant for H/D exchange by general-base catalysis. The intercept with the y-axis corresponds to the sum of the uncatalysed and hydroxide-catalysed H/D exchange reaction, k_0' (eqn 3.2).

$$k_0' = k_0 + k_{OH}[OH^-]$$ (3.2)

For **3a**, the non-zero y-axis intercept suggests a degree of H/D exchange proceeding by non-general-base catalysed pathways. As Figure 3.2 shows, not all compounds **3b-h** display this non-zero y-axis intercept.
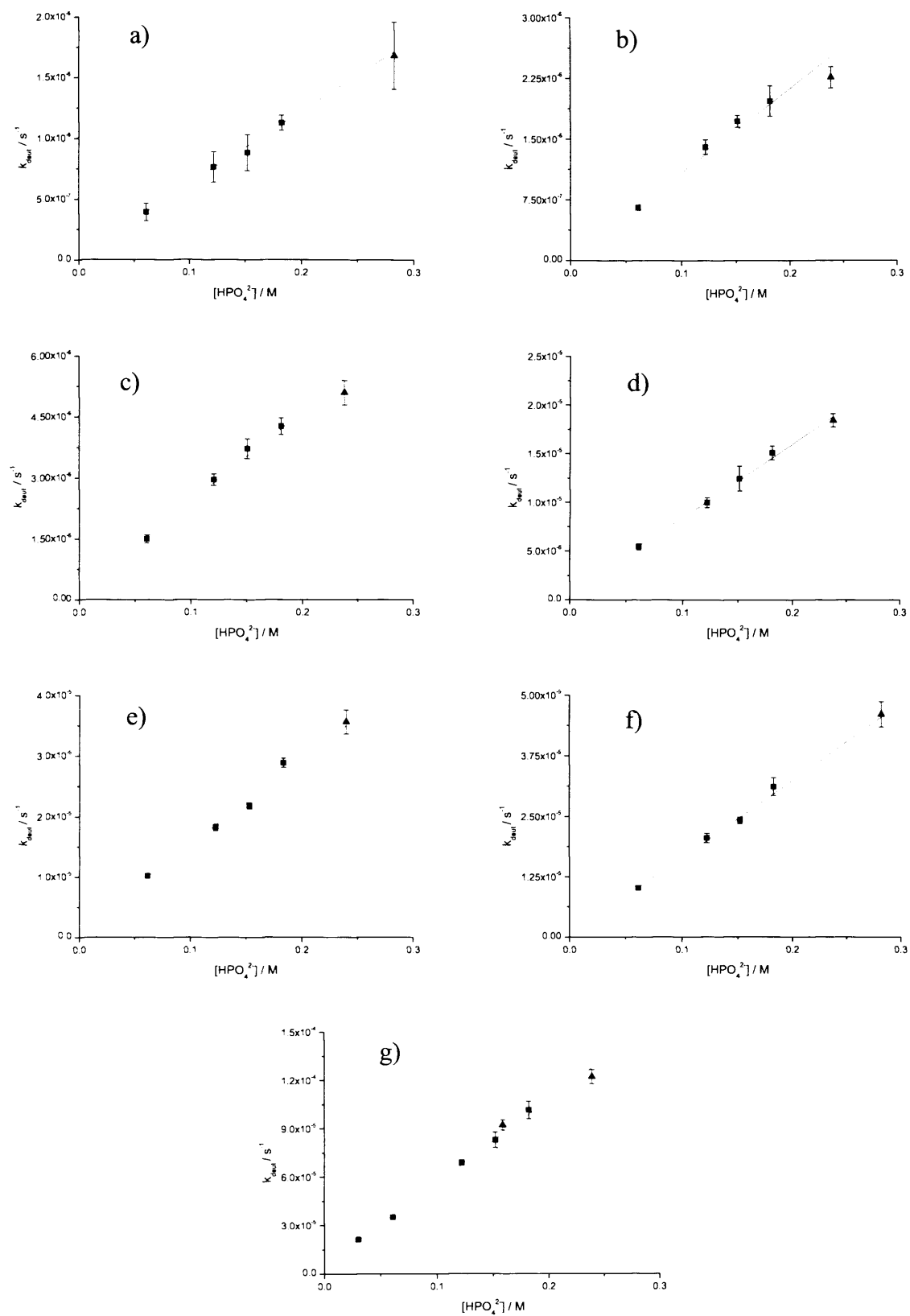
Figure 3.2: Relationship between k_{deut} and basic buffer component for a) **3b**, b) **3c**, c) **3d**, d) **3e**, e) **3f**, f) **3g**, g) **3h**, at (■) pH** 7.4 and (▲) pH** 7.8 at 37 °C, I = 1 M.

The data from Figure 3.1 and Figure 3.2 is summarised in Table 3.2.

Table 3.2: k_{gb} and k_0' for **3a-h**, at pH** 7.4 and 7.8, 37 °C, I = 1 M.

Compound	k_{gb} / $s^{-1}M^{-1}$	k_0'/ s^{-1}
3a	$(1.64 \pm 0.09) \times 10^{-5}$	$(8.05 \pm 1.28) \times 10^{-7}$
3b	$(6.01 \pm 0.72) \times 10^{-6}$	$(0.24 \pm 1.05) \times 10^{-7}$
3c	$(1.03 \pm 0.06) \times 10^{-5}$	$(4.47 \pm 5.92) \times 10^{-7}$
3d	$(2.20 \pm 0.13) \times 10^{-5}$	$(1.92 \pm 1.54) \times 10^{-7}$
3e	$(7.47 \pm 0.38) \times 10^{-5}$	$(9.37 \pm 4.71) \times 10^{-7}$
3f	$(1.40 \pm 0.05) \times 10^{-4}$	$(1.48 \pm 0.50) \times 10^{-6}$
3g	$(1.60 \pm 0.06) \times 10^{-4}$	$(4.68 \pm 4.53) \times 10^{-7}$
3h	$(5.15 \pm 0.13) \pm 10^{-4}$	$(5.01 \pm 0.98) \times 10^{-7}$

Table 3.2 shows that for **3b** and **3c**, k_0' is zero within error margins and most other compounds are not too far away from this. A significant value for k_0' is only seen for **3a** and **3h**. If specific-base catalysis were occurring to a significant extent, data from the experiments undertaken at pH** 7.8 would not fall on the same line of best fit with the experiments at pH** 7.4, but would appear above the others. However, for all compounds **3a-h** the data points obtained at pH** 7.8 fit with those seen at pH** 7.4. As a result, specific-base catalysis can be ignored for the pH** tested here, and analysis will focus on general-base catalysis by HPO_4^{2-} ions.

Table 3.2 shows that the rate constants for H/D exchange are greater for compounds with more electron-withdrawing substituents. Approximate half-lives of deuteration in 0.3 M D_2O phosphate buffers at pH** 7.4, I = 1 M at 37 °C, are given in Table 3.3.

Table 3.3: Half-lives of H/D exchange for **3a-h** in D_2O 0.3 M phosphate buffers of pH** 7.4, $I = 1$ M, 37 °C.

Compound	Aryl Substituent	$t_{1/2}$ of deuteration / h
3a	-	62.7
3b	*p*-OH	175.9
3c	*p*-Me	94.7
3d	*p*-F	48.0
3e	*p*-Cl	14.2
3f	*m*-F	7.1
3g	*m*-Cl	6.7
3h	*p*-CF$_3$	2.0

Table 3.3 shows that H/D exchange at the stereogenic centre, and hence racemisation, of **3a-h** takes place on a pharmaceutically relevant timescale. This is particularly true for compounds with electron-withdrawing ring substituents.

3.4.5 Hydrolysis

In contrast to H/D exchange, hydrolysis appears much more dependent on OH⁻ concentration. Plots of k_{hyd} against [HPO$_4$$^{2-}$] (Figure 3.3) do not show a good correlation for all compounds. This is especially true for experiments undertaken at pH** 7.8, for which k_{hyd} is generally much higher than for experiments at pH** 7.4. The data from Figure 3.3 is summarised in Table 3.4

Figure 3.3: Relationship between k_{hyd} and basic buffer component for a) **3a**, b) **3b**, c) **3c**, d) **3d**, e) **3e**, f) **3f**, g) **3g**, h) **3h**, at (■) pH** 7.4 and (▲) pH** 7.8 at 37 °C, I = 1 M. (—) fitted solely with pH** 7.4 data points.

Table 3.4: $k_{gb(hyd)}$ and $k_0{'}_{(hyd)}$ for **3a-h**, at pH** 7.4, 37 °C, $I = 1$ M.

Compound	$k_{gb(hyd)}$ / s^{-1}M^{-1}	$k_0{'}_{(hyd)}$ / s^{-1}
3a	$(2.66 \pm 0.55) \times 10^{-6}$	$(1.92 \pm 0.08) \times 10^{-6}$
3b	$(2.35 \pm 0.47) \times 10^{-6}$	$(1.52 \pm 0.07) \times 10^{-6}$
3c	$(7.07 \pm 0.38) \times 10^{-6}$	$(8.27 \pm 0.38) \times 10^{-7}$
3d	$(1.29 \pm 0.08) \times 10^{-5}$	$(1.43 \pm 0.09) \times 10^{-6}$
3e	$(2.05 \pm 0.18) \times 10^{-5}$	$(1.69 \pm 0.20) \times 10^{-6}$
3f	$(1.30 \pm 0.11) \times 10^{-5}$	$(2.73 \pm 0.14) \times 10^{-6}$
3g	$(1.05 \pm 0.16) \times 10^{-5}$	$(2.74 \pm 0.13) \times 10^{-6}$
3h	$(4.62 \pm 0.25) \pm 10^{-6}$	$(7.19 \pm 3.57) \times 10^{-6}$

Table 3.4 shows that, although there appears to be some general-base catalysis of hydrolysis for **3a-h**, it is less than that seen for H/D exchange. It is also noticeable that general-base catalysed hydrolysis shows no apparent increase for the structures with more electron-withdrawing aromatic substituents. A possible explanation for this is that the reaction site for hydrolysis is further away from the aromatic ring than the site of H/D exchange. The values of $k_0{'}$ are larger in magnitude for the hydrolysis of **3a-h** than for H/D exchange. It was observed that the values of k_{hyd} at pH** 7.8 are larger than would be expected if hydrolysis was solely general-base catalysed, suggesting a significant degree of specific-base catalysis by hydroxide ions.

3.4.6 Hammett Analysis

Hammett plots of the rate constants of general base-catalysed H/D exchange for **3a-h** (from Table 3.2) as a function of σ- and σ^--constants were constructed (Figure 3.4).

Figure 3.4: Hammett plots for data from Table 3.2 for general base-catalysed H/D exchange at the stereogenic centres of **3a-h**, in D_2O phosphate buffers of I = 1 M at 37 °C a) as a function of σ-values (—) line of best fit for all data points, ρ = 2.50 ± 0.03, R^2 = 0.979 , (—) line of best fit for data points where $\sigma \geq 0$, ρ = 2.79 ± 0.04, R^2 = 0.998. b) as a function of σ^--values, (—) ρ = 2.07 ± 0.02, R^2 = 0.984. Hammett constants from Table 1.5.[17]

The linear nature of both plots in Figure 3.4 suggests a common mechanism of H/D exchange for compounds **3a-h**. The positive gradients seen in Figure 3.4 confirms that negative charge is built up on the reaction centre during H/D exchange. Using σ-constants, the data shows a good linear correlation for electron-withdrawing substituents ($\sigma > 0$) but this does not hold for electron-donating substituents **3b** and **3c** (*p*-OH and *p*-Me). Figure 3.4 shows a better overall correlation to σ^--values than with standard σ-values. The better correlation with σ^- is attributed to direct conjugation of the site of reaction to the aromatic ring. Negative charge built up during H/D exchange can be resonance-delocalised through the phenyl group onto the substituent.

Although Figure 3.4 shows a better correlation with σ^--values than with σ-values for general base-catalysed H/D exchange of **3a-h**, it should be noted that for most of the substituents analysed there is not a great deal of difference between σ and σ^-. Of the eight different compounds, only three have different σ- and σ^--values and the largest difference (*p*-CF₃) is only 0.11 units. This small difference makes conclusively determining whether the data correlates better with one set of substituent constants or with another difficult. Ideally, a substituent such as a nitro group (σ- and σ^--values 0.78 and 1.27 respectively) would be included in the Hammett analysis, to simplify determination of which set of substituent constants is best for the data. Unfortunately, the appropriately substituted phenylglycine starting material is not commercially available and efforts to synthesise it were unsuccessful.

In circumstances where data appears to fit somewhere in between σ- and σ^--values (or indeed σ- and σ^+-values) the Yukawa-Tsuno equation (Section 1.8.2.2.3) is used, to acknowledge the possible presence of an intermediate degree of resonance interaction. However, as the difference in σ- and σ^--values for **3a-h** is only small there is little value in carrying out an analysis in terms of the Yukawa-Tsuno equation for the current dataset.

The magnitude of ρ from Figure 3.4 gives us an insight into the degree of negative charge built up on the reaction centre during H/D exchange. The value of $\rho = 2.07$ can be contrasted with that of $\rho = 1.15$ for the racemisation of arylglycines in phosphate buffers, determined by Smith and Sivakua.[18] The authors consider this ρ value for arylglycine racemisation to be quite low, suggesting little charge stabilisation is derived from the aryl group. This is because either very little charge is built up on the reaction centre or, as considered more likely by the authors, stabilisation results from moieties other than the aryl substituents. They conclude that major stabilisation comes from the reaction medium (water) and the adjacent $-NH_3^+$ group.[§] The S_E1 mechanism was proposed as the mechanism of racemisation for arylglycines, based on the relative ratio of the rate constants of racemisation and H/D exchange (Section 1.3). A similarly small ρ of 0.83 was determined for the ionisation of arylnitromethanes ($ArCH_2NO_2$) in water at 25 °C by Bordwell and Boyle.[19, 20] The small ρ value was believed to be a result of the adjacent nitro group providing major stabilisation.

Conversely, a ρ value of 3.58 for the racemisation of profen thioesters catalysed by trioctylamine in isooctane at 45 °C was determined by Chen *et al.* (Scheme 3.9).[21]

Scheme 3.9: Racemisation of profen thioesters in isooctane via proton abstraction with trioctylamine base. $\rho = 3.58$.

The higher ρ value for the reaction in Scheme 3.9 can be attributed to two factors. Firstly, the methyl group adjacent the site of negative charge build-up (the stereogenic centre) cannot stabilise a charge in the manner that an $-NHAc$ group (compounds **3a-h**), an $-NH_3^+$ group (reference 18) or an $-NO_2$ group (reference 19) does. Therefore the reliance on charge

---

[§] The experiments discussed from reference 18 were undertaken at pH 10, where the ratio of arylglycine free base (anion) to zwitterion is approximately 100:1. However, the rate constant of racemisation for the zwitterion over the free base is approximately 100,000:1, suggesting that the zwitterion is the major species undergoing racemisation and supporting the assertion of stabilisation from $-NH_3^+$.

102

stabilisation by the aryl substituent is greater. Secondly, the reaction medium in this case is isooctane. This nonpolar alkane cannot stabilise a charge in the manner that water can in the other cited examples, giving even greater importance to the stabilisation by the aryl substituent.

3.4.7 Variation of Ester Substituent

The effect of the nature of the ester substituent was investigated through comparison of rate constants of H/D exchange and hydrolysis for compounds **3a**, **3i** and **3j**. The rate constants are summarised in Table 3.5.

Table 3.5: Rate constants of **3a**, **3i** and **3j** in pH** 7.4 D_2O buffers of 0.3 M phosphate concentration, at 37 °C, $I = 1$ M.

Compound	$k_{obs} \times 10^6 / s^{-1}$	$k_{deut} \times 10^6 / s^{-1}$	$k_{hyd} \times 10^6 / s^{-1}$
3a	6.16 ± 0.11	3.64 ± 0.12	2.53 ± 0.05
3i	2.85 ± 0.08	1.91 ± 0.08	0.95 ± 0.03
3j	0.98 ± 0.04	0.88 ± 0.04	0.10 ± 0.01

As expected, rate constants of hydrolysis were found to decrease as the ester substituent increased in size. This decrease is attributed to steric hindrance disfavouring general- and specific- base catalysed hydrolysis by blocking attack at the carbonyl carbon.[22, 23] Rate constants of H/D exchange also decreased with increasing size of alkyl ester substituent. As with hydrolysis, this decrease is likely due to steric hindrance blocking base-catalysed proton abstraction at the stereogenic centre. As many drug molecules are much larger in molecular weight and have a much larger 'framework' than those analysed here, the observation that racemisation can be retarded by steric bulk may become important when assessing the racemisation risk of prototype drugs.

The rate constant for hydrolysis shows a larger decrease with increasing bulk of the ester substituent than the rate constant for H/D exchange. The rate constant of hydrolysis drops by an approximate factor of 25 when the methyl ester is replaced by an isopropyl ester (**3a** to **3j**), whereas the rate constant for H/D exchange drops by an approximate factor of 4. This observation is probably due to the proximity of the ester alkyl substituent being varied to the site of reaction, which is closer for hydrolysis (carbonyl carbon) than for H/D exchange (stereogenic centre). As a result, the increasing steric hindrance from the ester group will have

a greater impact on the rate constant of hydrolysis than it will on the rate constant of H/D exchange.

3.4.8 Mechanism of Racemisation

Comparison between the rate constants for racemisation and H/D exchange can inform as to by which mechanism racemisation is occurring. The two most likely mechanisms of racemisation are known as S_E1 and S_E2. Previous studies on compounds similar to **3a-h** have generally concluded that racemisation occurs through an S_E1 mechanism,[18, 24, 25] although an example of racemisation by the S_E2 mechanism has been reported.[26] The S_E1 and S_E2 mechanisms can be distinguished by comparison of the rate constants of racemisation and H/D exchange (Section 1.3).

Ester hydrolysis of **3a-h** is a problem when trying to determine the rate constant of racemisation. The hydrolysis reaction results in the presence of more than one species (ester and carboxylate) in the reaction mixture at the same time. Ideally, chiral HPLC is used to determine the concentration of each of the enantiomers of ester and carboxylate throughout the reaction, however this technique was unavailable. Multiple species in the reaction mixture makes analysis through spectroscopy difficult, as distinguishing between the signals from the ester and carboxylate species is a problem. However, a way around this problem is to only look at the final composition of the reaction mixture, once hydrolysis is complete. The enantiomeric excess of the final, fully hydrolysed product can be determined through CD spectroscopy (Section 1.10.3). Comparison of the *ee* of the fully hydrolysed compound with the final proportion of molecules deuterated at the stereogenic centre (i.e. proportion that have undergone H/D exchange prior to hydrolysis) affords information on the mechanism by which H/D exchange is taking place. The expected observations for the S_E1 and S_E2 mechanisms are outlined in eqns (3.3) and (3.4), respectively.

$$Q_f^H = ee_f \qquad\qquad (3.3)$$

$$Q_f^H > ee_f \qquad\qquad (3.4)$$

where Q_f^H is the percentage of molecules protonated at the stereogenic centre after hydrolysis is complete and ee_f is the enantiomeric excess of hydrolysed species after hydrolysis is complete. The theoretical basis for equations 3.3 and 3.4 is outlined in Appendix Section 3.7.1.

3.4.8.1 Comparison of Data from CD and ¹H NMR Spectroscopy Experiments

H/D exchange/racemisation experiments in deuterated buffer were undertaken for enantiopure (R)-3a and (S)-3e. H/D exchange was monitored through ^{1}H NMR spectroscopy and hydrolysis was followed by HPLC. Once hydrolysis was complete, the final *ee* was determined through CD spectroscopy. Comparisons of Q_f^H with ee_f for **3a** and **3e** are displayed in Table 3.6.

Table 3.6: Comparison of Q_f^H with ee_f for **3a** and **3e** in D_2O buffers of pH** 7.4, 0.3 M phosphate concentration, I = 1 M at 37 °C.

Compound	X-substituent	Q_f^H	ee_f
3a	-	41.1 ± 0.3 %	45.5 ± 2.1 %
3e	p-Cl	26.8 ± 0.6 %	30.2 ± 1.4 %

Table 3.6 shows that Q_f^H and ee_f for both **3a** and **3e** are approximately the same. This strongly suggests that H/D exchange, and hence racemisation, occur via an S_E1 mechanism. Although the values determined for Q_f^H and ee_f for both compounds do not exactly match, in both cases ee_f is slightly higher than Q_f^H. If the S_E2 mechanism were taking place, Q_f^H would be higher than ee_f, and significantly so given the comparative rates of k_{deut} and k_{hyd} determined by ^{1}H NMR and HPLC for **3a** and **3e**. As discussed in Section 1.3, there are known examples where deuteration can proceed with retention of stereochemistry (isoinversion).[27, 28] The small discrepancy between Q_f^H and ee_f may be due to isoinversion or experimental error.

Although the ee_f could only be determined for **3a** and **3e**, it seems safe to extrapolate this result to all differently substituted **3** compounds. This is based on the conclusion from the linear Hammett plot (Figure 3.4) that all compounds **3a-h** share a common mechanism of H/D exchange.

3.4.8.2 Mechanistic Conclusions

Overall, it can be concluded that general-base catalysed H/D exchange and racemisation of **3a-h** proceed through the S_E1 mechanism, under the conditions studies here. This is based on three observations.

First, the value of ρ of 2.07 determined from Figure 3.4 is compatible with an S_E1 mechanism. The positive value of ρ confirms that negative charge is built up during H/D

exchange. The magnitude of ρ is also suggestive of an S_E1 mechanism; a large ρ value means that a considerable amount of negative charge is built up during H/D exchange, which is more characteristic of an S_E1 mechanism than of an S_E2 mechanism.

Second, Hammett plots of the rate constants for general base-catalysed H/D exchange of **3a-h** show a better correlation with σ^- constants than with standard σ constants (Figure 3.4). This suggests that the negative charge is built up on the reaction centre during H/D exchange, as it can be directly conjugated with the aromatic ring substituents. This location of charge is consistent with the S_E1 mechanism, although it does not rule out an S_E2 mechanism.

Third, CD and ^{1}H NMR analysis of the final, fully hydrolysed products of **3a** and **3e** show the proportion of material protonated at the stereogenic centre is almost equivalent with the enantiomeric excess. This observation rules out H/D exchange by the S_E2 mechanism.

3.4.9 Analysis of Thiophene Derivatives

As described in Section 3.3, *N*-acetyl thienylglycine methyl esters **3k** and **3l** (Scheme 3.10) were also synthesised for analysis of H/D exchange reactions.

3k　　　　　　**3l**

Scheme 3.10: Structure of compounds **3k** and **3l**.

Of specific interest is the possibility of incorporating heteroaromatic groups into the Hammett plots depicted in Figure 3.4. The application of the Hammett equation to heterocycles is discussed in Section 1.8.2.4. If it is shown that the kinetics of racemisation of compounds **3k** and **3l** can be accounted for by the Hammett analysis, it may then be possible to extend this relationship to predict the rate constants of H/D exchange for other heteroaromatic *N*-acetyl arylglycine methyl esters.

3.4.9.1 Kinetics of H/D Exchange for 3k and 3l

Reactions of compounds **3k** and **3l** in deuterated buffers were monitored via ^{1}H NMR spectroscopy. Rate constants of H/D exchange and hydrolysis were determined for **3l**.

Hydrolysis of **3k** was negligible compared to H/D exchange (< 4 %). Rate constants of H/D exchange were plotted as a function of basic buffer component (Figure 3.5).

Figure 3.5: Relationship between k_{deut} and concentration of the basic buffer component for a) **3k** b) **3l**. Experiments carried out at 37 °C with $I = 1$ M.

Values for k_0', k_{gb} and approximate half-lives of deuteration are collected in Table 3.7.

Table 3.7: k_{gb} and k_0' values for **3k** and **3l**, approximate half-lives of deuteration at stereocentre of **3k-l** determined in D_2O 0.3 M phosphate buffers of pH** 7.4, $I = 1$ M, 37 °C.

Compound	k_{gb} / $s^{-1}M^{-1}$	k_0'/ s^{-1}	$t_{1/2}$ of deuteration / h
3k	$(2.74 \pm 0.10) \times 10^{-3}$	$(-2.28 \pm 1.32) \times 10^{-5}$	0.4
3l	$(5.62 \pm 0.35) \times 10^{-5}$	$(1.16 \pm 0.41) \times 10^{-6}$	16.5

As was the case for compounds **3a-h**, the values of k_0' displayed in Table 3.7 show that specific base-catalysed or non-catalysed H/D exchange of compounds **3k** and **3l** is negligible.

3.4.9.2 Hammett Analysis

Data for compounds **3k** and **3l** were added to the Hammett analysis displayed in Figure 3.4, using the σ-values displayed in Table 1.8 (Figure 3.6).

Figure 3.6: Hammett plots of data from Table 3.2 and Table 3.7 for general base-catalysed H/D exchange at the stereogenic centre of **3a-h** and **3k-l**, in D_2O phosphate buffers of $I = 1$ M at 37 °C. a) as a function of σ-values (—) line of best fit for all data points, $\rho = 2.70 \pm 0.02$, $R^2 = 0.968$, (—) line of best fit for data points were $\sigma \geq 0$, $\rho = 2.95 \pm 0.03$, $R^2 = 0.980$. b) as a function of to σ^--values (—) $\rho = 2.35 \pm 0.02$, $R^2 = 0.928$.

Figure 3.6 shows that the Hammett σ-constants for thiophene heterocycles displayed in Table 1.8 are in reasonable agreement with the experimental rate constants determined for compounds **3k-l**. The value of k_{gb} for **3k** shows best correlation using σ-constants with electron withdrawing compounds only. The value of k_{gb} for **3l** shows best correlation using σ^--constants. Although neither k_{gb} value for **3k-l** fits exactly with the data obtained for compounds **3a-h**, the general characterisation of a 2-thienyl heterocycle as a strongly electron-withdrawing substituent and 3-thienyl heterocycle as a moderately electron-withdrawing substituent is supported by this data. The reasonable fit with Hammett plots for **3a-h** suggests that H/D exchange for compounds **3k-l** also follows the S_E1 mechanism proposed for **3a-h**.

Using the σ-constants displayed in Table 1.8, we can extrapolate the Hammett plots to predict the susceptibility to racemisation of compounds containing other heterocycles. A compound based on the general scaffold displayed in Scheme 3.1 with a 2-furyl aromatic substituent ($\sigma =$ 1.08), would therefore be expected to undergo H/D exchange at a rate faster than that seen for **3k**. Such a compound would therefore be at particular risk of racemisation under pharmacological conditions. Based on these σ-constants, a 3-furyl substituted analogue would be expected to undergo H/D exchange at a rate similar to that seen for **3e** (p-Cl substituted benzene). Pyrrole-substituted analogues would be expected to undergo H/D exchange at much slower rates, similar to that seen for **3b** (p-OH substituted benzene). A pyridine substituted analogue would be at a high risk of physiological racemisation. The pK_a of pyridine is 5.23,[29]

108

so the heteroatom would not be protonated at pH 7.4. However, the σ-values in Table 1.8 still suggest that at this pH pyridine substituents are very electron-withdrawing (σ = 0.45 for 3-pyridine, σ = 0.76 for 4-pyridine) and would hence make racemisation a significant risk. Although rates of H/D exchange have not been determined at pH < 5.23, conditions like this do of course exist in the body. The very high σ-value of a pyridine protonated at the heteroatom would be cause for concern even though general-base catalysis at low pH would be far weaker than under conditions investigated in this chapter.

3.5 Conclusions

Rate constants for H/D exchange and hydrolysis of compounds **3a-l** have been determined under aqueous conditions in phosphate buffers at physiological pH and temperature. From this data the following conclusions can be drawn.

First, H/D exchange of **3a-l** is general-base catalysed by the basic species of the phosphate buffer at pH** 7.4 (HPO_4^{2-}).

Second, H/D exchange of **3a-l** is of pharmacological relevance, particularly for those compounds with more electron-withdrawing aromatic groups.

Third, for compounds **3a** and **3e**, studies suggest an S_E1 mechanism for H/D exchange and racemisation. Hammett correlations imply the same mechanism for **3b-d, f-l**.

Fourth, results for **3k-l** show that Hammett plots can be used to extend the scope of our results, allowing assessment of racemisation risks for other heterocyclic compounds.

3.6 Experimental

3.6.1 General Experimental

All reagents were purchased from Acros Organics, Alfa Aesar, Fluorochem or Sigma-Aldrich. ^{1}H NMR and ^{13}C NMR spectra were recorded on a Bruker DPX 400 or DPX 500 spectrometer. δ values are reported in ppm downfield from trimethylsilane. HPLC was performed using an Agilent Technologies 1200 series instrument. Infrared spectra were obtained using a Varian 7000 FT-IR spectrometer. Samples were applied directly to the diamond tip. Circular Dichroism spectra were recorded using an Applied Photophysics Chirascan CD spectrometer. High-resolution mass spectra were obtained on a Waters LCT Premier XE mass spectrometer.

3.6.2 Synthesis of Compounds

3.6.2.1 Synthesis of Arylglycine Ester Hydrochloride Salts (2a-l)

Compounds **2a-l** were synthesised from commercially available starting materials **1a-h, 1k** and **1l** according to the method outlined by Kudelko and Zieliński (Scheme 3.11).[30]

Scheme 3.11: Synthesis of compounds **2a-l**.

The general method outlined below in the synthesis of **2a** was used in the synthesis of all compounds **2a-l**, with the appropriate arylglycine starting material and alcohol used.

Phenylglycine methyl ester hydrochloride (2a)

A suspension of phenylglycine (5 g, 33.1 mmol) in methanol (25 ml) was cooled to 0 °C and thionyl chloride (6.5 ml, 3.97 g, 33.3 mmol) was added dropwise. The reaction mixture was allowed to warm to room temperature and left to stir overnight, then solvent was removed using a rotary evaporator. The crude product was washed with diethyl ether (30 ml) and dried under reduced pressure to give phenylglycine methyl ester hydrochloride as a white solid (6.38 g, 31.7 mmol, 96 %).

^{1}H NMR (400 MHz, D$_2$O) δ = 7.32-7.39 (m, 5H, -C$_6$H$_5$), 5.15 (s, 1H, -CH(C$_6$H$_5$)-), 3.77 (s, 3H, -COOCH$_3$).

^{13}C NMR (100 MHz, D$_2$O) δ = 169.90 (1C, -C(O)OCH$_3$), 131.26 (1C, aromatic), 130.76 (1C, aromatic), 130.01 (2C, aromatics), 128.32 (2C, aromatics), 56.68 (1C, -CHNH$_3^+$), 54.20 (1C, -OCH$_3$).

IR (ss) v/cm^{-1}: 3082, 1744, 1552

Found m/z (AP$^+$) = 166.0870, calculated 166.0868

M.p. = 190-192 °C

(*R*)-(-)-Phenylglycine methyl ester hydrochloride (2a)

Yield: 95 %, $[\alpha]_D^{20}$ = -122.0° (*c* 1.0, H$_2$O). Spectroscopic data as for racemate.

M.p. = 191-192 °C

(*S*)-(+)-Phenylglycine methyl ester hydrochloride (2a)

Yield: 93 %, $[\alpha]_D^{20}$ = +124.4° (*c* 1.0, H$_2$O). Spectroscopic data as for racemate.

M.p. = 191-192 °C

(*p*-Hydroxyphenyl)glycine methyl ester hydrochloride (2b)

Yield: 99 %

^{1}H NMR (500 MHz, D$_2$O) δ = 7.19 (d, 2H, aromatic **CH** meta to hydroxyl, $^3J_{H-H}$ = 8.65 Hz), 6.81 (d, 2H, aromatic **CH** ortho to hydroxyl, $^3J_{H-H}$ = 8.60 Hz), 5.08 (s, 1H, -**CH**(C$_6$H$_4$OH)-), 3.65 (s, 3H, -COO**CH$_3$**).

^{13}C NMR (125 MHz, D$_2$O) δ = 169.83 (1C, -**C**(O)OCH$_3$), 157.27 (1C, aromatic carbon ipso to hydroxyl), 129.87 (2C, aromatic carbon meta to hydroxyl), 122.75 (1C, aromatic carbon para to hydroxyl), 116.41 (2C, aromatic carbon ortho to hydroxyl), 55.95 (1C, -**CH**NH$_3^+$), 53.90 (1C, -O**CH$_3$**).

IR (ss) v/cm^{-1}: 3285, 3098, 1738, 1541

Found m/z (AP$^+$) = 182.0814, calculated 182.0817

M.p. = 206-208 °C

(*p*-Methylphenyl)glycine methyl ester hydrochloride (2c)

Yield: 92 %

^{1}H NMR (500 MHz, D$_2$O) δ = 7.23 (s, 4H, -C$_6$H$_4$CH$_3$), 5.13 (s, 1H, -CH(-C$_6$H$_4$CH$_3$)-), 3.69 (s, 3H, -OCH$_3$), 2.24 (s, 3H, -C$_6$H$_4$CH$_3$).

^{13}C NMR (100 MHz, D$_2$O) δ = 170.08 (1C, -C(O)OCH$_3$), 141.41 (1C, aromatic carbon ipso to methyl substituent), 130.55 (2C, aromatic carbon ortho to methyl substituent), 128.29 (1C, aromatic carbon para to methyl substituent), 128.26 (2C, aromatic carbon meta to methyl substituent), 56.46 (1C, -CHNH$_3^+$), 54.17 (1C, -OCH$_3$), 20.64 (1C, -C$_6$H$_4$CH$_3$).

Found m/z (AP$^+$) = 180.1030, calculated 180.1025

IR (ss) v/cm^{-1}: 3031, 1744, 1533

M.p. = 210-211 °C

(p-Fluorophenyl)glycine methyl ester hydrochloride (2d)

Yield: 92 %

^{1}H NMR (500 MHz, D$_2$O) δ = 7.37 (dd, 2H, -C$_6$H$_4$F (aromatic **CH** meta to fluorine), $^3J_{H-H}$ = 7.04 Hz, $^4J_{H-F}$ = 4.12 Hz), 7.13 (t, 2H, -C$_6$H$_4$F (aromatic **CH** ortho to fluorine), $^3J_{H-H}$ = $^3J_{H-F}$ = 7.04 Hz), 5.19 (s, 1H, -**CH**(C$_6$H$_4$F)-), 3.70 (s, 3H, -COOCH$_3$).

^{13}C NMR (100 MHz, D$_2$O) δ = 169.78 (1C, -C(O)OCH$_3$), 163.77 (d, 1C, aromatic carbon ipso to fluorine, $^1J_{C-F}$ = 246.18 Hz), 130.75 (d, 1C, aromatic carbon meta to fluorine, $^3J_{C-F}$ = 8.86 Hz), 127.37 (d, 1C, aromatic carbon para to fluorine, $^4J_{C-F}$ = 3.20 Hz), 116.96 (d, 1C, aromatic carbon ortho to fluorine, $^2J_{C-F}$ = 22.08 Hz), 56.05 (1C, -CHNH$_3^+$), 54.35 (1C, -OCH$_3$).

Found m/z (AP$^+$) = 184.0777, calculated 184.0774

IR (ss) v/cm^{-1}: 3069, 1758, 1732, 1550

M.p. = 192-193 °C

(p-Chlorophenyl)glycine methyl ester hydrochloride (2e)

Yield: 90 %

^{1}H NMR (400 MHz, D$_2$O) δ = 7.37 (d, 2H, aromatic **CH**, $^3J_{H-H}$ = 8.60 Hz), 7.30 (d, 2H, aromatic **CH**, $^3J_{H-H}$ = 8.60 Hz), 5.17 (s, 1H, -**CH**(C$_6$H$_4$Cl)-), 3.67 (s, 3H, -COOCH$_3$).

^{13}C NMR (100 MHz, D$_2$O) δ = 169.56 (1C, -C(O)OCH$_3$), 136.22 (1C, aromatic), 130.01 (2C, aromatics), 129.95 (2C, aromatics), 129.85 (1C, aromatic), 56.02 (1C, -CHNH$_3^+$), 54.31 (1C, -OCH$_3$).

IR (ss) v/cm^{-1}: 3055, 1746, 1548

Found m/z (AP$^+$) = 200.0476, calculated 200.0478

M.p. = 201-202 °C

(S)-(+)-(p-Chlorophenyl)glycine methyl ester hydrochloride (2e)

Yield: 99 %, $[\alpha]_D^{20}$ = +120.8° (c 1.0, H_2O). ^1H and ^{13}C NMR spectra as for racemate.

M.p. = 198-199 °C

(*m*-Fluorophenyl)glycine methyl ester hydrochloride (2f)

Yield: 82 %

^1H NMR (400 MHz, D_2O) δ = 7.41 (dt, 1H, $-C_6H_4F$ (aromatic CH meta to fluorine), $^3J_{H\text{-}H}$ = 7.90 Hz, $^4J_{H\text{-}F}$ = 6.00 Hz), 7.13-7.19 (m, 3H, $-C_6H_4F$ (aromatic CH ortho and para to fluorine), 5.20 (s, 1H, $-CH(C_6H_4F)$-), 3.70 (s, 3H, $-COOCH_3$).

^{13}C NMR (100 MHz, D_2O) δ = 169.11 (1C, $-C(O)OCH_3$), 162.71 (d, 1C, aromatic carbon ipso to fluorine $^1J_{C\text{-}F}$ = 245.61 Hz), 132.95 (d, 1C, aromatic carbon meta to fluorine, ipso to rest of molecule, $^3J_{C\text{-}F}$ = 7.53 Hz), 131.68 (d, 1C, aromatic carbon meta to fluorine, $^3J_{C\text{-}F}$ = 8.30 Hz), 124.00 (1C, aromatic carbon para to fluorine), 117.43 (d, 1C, aromatic carbon ortho to fluorine and rest of molecule $^2J_{C\text{-}F}$ = 20.75 Hz), 115.18 (d, 1C, aromatic carbon ortho to fluorine $^2J_{C\text{-}F}$ = 23.00 Hz), 55.85 (1C, $-CHNH_3^+$), 54.08 (1C, $-OCH_3$).

Found m/z (AP^+) = 184.0775, calculated 184.0774

IR (ss) v/cm^{-1}: 3061, 1749, 1560

M.p. = 207-208 °C

(*m*-Chlorophenyl)glycine methyl ester hydrochloride (2g)

Yield: 90 %

^1H NMR (400 MHz, D_2O) δ = 7.26-7.42 (m, 4H, $-C_6H_4Cl$), 5.18 (s, 1H, $-CH(C_6H_4Cl)$-), 3.69 (s, 3H, $-COOCH_3$).

^{13}C NMR (100 MHz, D_2O) δ = 169.38 (1C, $-C(O)OCH_3$), 135.08 (1C, aromatic carbon), 133.03 (1C, aromatic carbon), 131.46 (1C, aromatic carbon), 130.81 (1C, aromatic carbon), 128.40 (1C, aromatic carbon), 126.74 (1C, aromatic carbon), 56.10 (1C, $-CHNH_3^+$), 54.35 (1C, $-OCH_3$).

Found m/z (AP^+) = 200.0476, calculated 200.0482

IR (ss) v/cm^{-1}: 3045, 1780, 1590

M.p. = 209-210 °C

(*p*-Trifluoromethylphenyl)glycine methyl ester hydrochloride (2h)

Yield = 92 %

^{1}H NMR (400 MHz, D$_2$O) δ = 7.70 (d, 2H, -C$_6$H$_4$CF$_3$ (aromatic CH ortho to trifluoromethyl), $^3J_{H-H}$ = 8.12 Hz), 7.53 (d, 2H, -C$_6$H$_4$CF$_3$ (aromatic CH meta to trifluoromethyl), $^3J_{H-H}$ = 8.12 Hz), 5.30 (s, 1H, -CH(C$_6$H$_4$CF$_3$)-), 3.70 (s, 3H, -COOCH$_3$).

^{13}C NMR (100 MHz, D$_2$O) δ = 169.28 (1C, -C(O)OCH$_3$), 135.15 (s, 1C, aromatic carbon para to trifluoromethyl), 131.90 (q, 1C, aromatic carbon ipso to trifluoromethyl, $^2J_{C-F}$ = 32.24 Hz), 129.06 (s, 2C, aromatic carbon meta to trifluoromethyl), 126.88 (q, 2C, aromatic carbon ortho to trifluoromethyl, $^3J_{C-F}$ = 3.68 Hz), 124.00 (q, 1C, -CF$_3$, $^1J_{C-F}$ = 270.04 Hz), 56.18 (1C, -CHNH$_3$$^+$), 54.39 (1C, -OCH$_3$).

Found m/z (AP$^+$) = 234.0741, calculated 234.0742

IR (ss) v/cm^{-1}: 3091, 1730, 1540

M.p. = 180-181 °C

Phenylglycine ethyl ester hydrochloride (2i)

Yield: 91 %

^{1}H NMR (400 MHz, D$_2$O) δ = 7.32-7.39 (m, 5H, -C$_6$H$_5$), 5.12 (s, 1H, -CH(C$_6$H$_5$)-), 4.08-4.21 (dq, 2H, -COOCH$_2$CH$_3$), 1.06 (t, 3H, OCH$_2$CH$_3$, $^3J_{H-H}$ = 7.16 Hz).

^{13}C NMR (100 MHz, D$_2$O) δ = 169.42 (1C, -C(O)OCH$_3$), 131.38 (1C, aromatic), 130.76 (1C, aromatic), 130.03 (2C, aromatics), 128.36 (2C, aromatics), 64.30 (1C, -OCH$_2$CH$_3$), 56.68 (1C, -CHNH$_3$$^+$), 13.39 (1C, -OCH$_2CH_3$).

IR (ss) v/cm^{-1}: 3085, 1740, 1566

Found m/z (ES$^+$) = 180.1033, calculated 180.1025

M.p. = 214-215 °C

Phenylglycine isopropyl ester hydrochloride (2j)

Yield: 83 %

^{1}H NMR (500 MHz, D$_2$O) δ = 7.33-7.40 (m, 5H, -C$_6$H$_5$), 5.10 (s, 1H, -CH(C$_6$H$_5$)-), 5.01 (sept, 1H, -COOCH(CH$_3$)$_2$, $^3J_{H-H}$ = 6.30 Hz), 1.14 (d, 3H, -OCH(CH$_3$)$_A$(CH$_3$)$_B$, $^3J_{H-H}$ = 6.30 Hz), 1.04 (d, 3H, -OCH(CH$_3$)$_A$(CH$_3$)$_B$, $^3J_{H-H}$ = 6.25 Hz).

^{13}C NMR (100 MHz, D$_2$O) δ = 169.60 (1C, -C(O)OCH$_3$), 131.20 (1C, aromatic), 130.46 (1C, aromatic), 129.76 (2C, aromatics), 128.06 (2C, aromatics), 72.77 (1C, -OCH(CH$_3$)$_2$), 56.65 (1C, -CHNH$_3$$^+$), 20.71 (1C, -OCH(CH$_3$)$_A$(CH$_3$)$_B$), 20.47 (1C, -OCH(CH$_3$)$_A$(CH$_3$)$_B$).

Found m/z (AP$^+$) = 194.1181, calculated 194.1181

IR (ss) v/cm^{-1}: 3098, 1738, 1550

M.p. = 222-223 °C

(2-Thienyl)glycine methyl ester hydrochloride (2k)

Yield: 87 %

^{1}H NMR (400 MHz, D$_2$O) δ = 7.46 (d, 1H, aromatic **CH** in 3 position, $^3J_{H-H}$ = 5.08 Hz), 7.16 (d, 1H, aromatic **CH** in 5 position, $^3J_{H-H}$ = 4.20 Hz), 7.00 (t, 1H, aromatic **CH** in 4 position, $^3J_{H-H}$ = 5.00 Hz), 5.50 (s, 1H, -**CH**NH$_3^+$), 3.71 (s, 3H, -O**CH$_3$**).

^{13}C NMR (100 MHz, D$_2$O) δ = 169.08 (1C, -**C**(O)OCH$_3$), 131.83 (1C, aromatic **C** in 1 position), 130.10 (1C, aromatic **C** in 4 position), 129.36 (1C, aromatic **C** in 5 position), 128.20 (1C aromatic **C** in 3 position), 54.43 (1C, -**C**HNH$_3^+$), 51.79 (1C, -O**C**H$_3$).

IR (ss) ν/cm^{-1}: 3051, 1745, 1530

Found *m/z* (AP$^+$) = 172.0430, calculated 172.0432

M.p. = 189-190 °C

(3-Thienyl)glycine methyl ester hydrochloride (2l)

Yield: 90 %

^{1}H NMR (500 MHz, D$_2$O) δ = 7.60 (m, 1H, aromatic **CH** in 4 position), 7.51 (m, 1H, aromatic **CH** in 2 position), 7.12 (m, 1H, aromatic **CH** in 5 position), 5.38 (s, 1H, -**CH**NH$_3^+$), 3.76 (s, 3H, -O**CH$_3$**).

^{13}C NMR (125 MHz, D$_2$O) δ = 169.35 (1C, -**C**(O)OCH$_3$), 130.75 (1C, aromatic **C** in 1 position), 128.67 (1C, aromatic **C** in 5 position), 127.14 (1C, aromatic **C** in 2 position), 126.06 (1C, aromatic **C** in 4 position), 54.12 (1C, -**C**HNH$_3^+$), 51.91 (1C, -O**C**H$_3$).

IR (ss) ν/cm^{-1}: 3042, 1740, 1560

Found *m/z* (ES$^+$) = 172.0429, calculated 172.0432

M.p. = 197-198 °C

3.6.2.2 Synthesis of N-Acetyl Arylglycine Esters (3a-l)

Compounds **3a-l** were synthesised from compounds **2a-l** according to the method outlined by Kudelko and Zieliński (Scheme 3.12).[30]
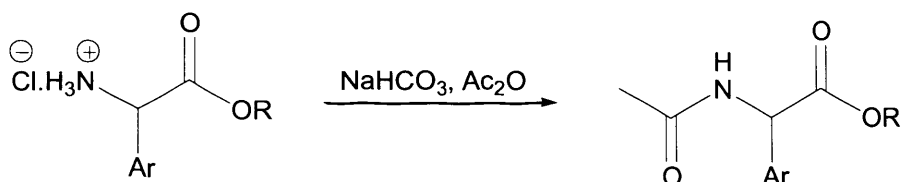
Scheme 3.12: Synthesis of compounds **3a-l**.

The general method outlined below in the synthesis of **3a** was used in synthesis of all compounds **3a-l**.

N-Acetyl phenylglycine methyl ester (3a)

Phenylglycine methyl ester hydrochloride (2 g, 9.9 mmol) was dissolved in cold water (20 ml). Sodium hydrogen carbonate (2.13 g, 2.5 equiv., 25 mmol) was added and the mixture was stirred until carbon dioxide liberation was complete. Acetic anhydride (1 ml, 10.5 mmol) was added dropwise and the mixture stirred for 1 hour. The solution was cooled to 0 °C and the precipitate filtered off and recrystallised from isopropanol to give *N*-acetyl phenylglycine methyl ester as a white solid (1.67 g, 8.1 mmol, 82 %).

^{1}H NMR (400 MHz, d^6-DMSO) δ = 8.74 (d, 1H, -NH-, $^3J_{H-H}$ = 6.96 Hz), 7.34-7.39 (m, 5H, -C$_6$H$_5$), 5.39 (d, 1H, -CH(C$_6$H$_5$)-, $^3J_{H-H}$ = 7.12 Hz), 3.62 (s, 3H, -OCH$_3$), 1.90 (s, 3H, CH$_3$C(O)-).

^{13}C NMR (100 MHz, d^6-DMSO) δ = 171.57 (1C, CH$_3$C(O)-), 169.68 (1C, -C(O)OCH$_3$), 136.63 (1C, aromatic), 129.07 (2C, aromatics), 128.63 (1C, aromatic), 128.15 (2C, aromatics), 56.63 (1C, - CH(C$_6$H$_5$)-), 52.55 (1C, -OCH$_3$), 22.50 (1C, -C(O)CH$_3$).

IR (ss) v/cm^{-1}: 3311, 1746, 1650, 1523

Found m/z (EI$^+$) = 207.0897, calculated 207.0895

M.p. = 81-82 °C

(*R*)-(-)-*N*-Acetyl phenylglycine methyl ester (3a)

Yield: 70 %, $[\alpha]_D^{20}$ = -174.8° (*c* 1.0, MeOH). Spectroscopic data as for racemate.

M.p. = 80-82 °C

(*S*)-(+)-*N*-Acetyl phenylglycine methyl ester (3a)

Yield: 76 %, $[\alpha]_D^{20}$ = +169.4° (*c* 1.0, MeOH). Spectroscopic data as for racemate.

M.p. = 81-82 °C

N-Acetyl (*p*-hydroxy phenyl)glycine methyl ester (3b)

Yield: 63 %

^{1}H NMR (400 MHz, d^6-DMSO) δ = 9.60 (s, 1H, -C$_6$H$_4$**OH**), 8.59 (d, 1H, -N**H**-, $^3J_{\text{H-H}}$ = 6.76 Hz), 7.17 (d, 2H, aromatic C**H** meta to hydroxy, $^3J_{\text{H-H}}$ = 8.56 Hz), 6.76 (d, 2H, aromatic C**H** ortho to hydroxy, $^3J_{\text{H-H}}$ = 8.48 Hz), 5.23 (d, 1H, -C**H**(C$_6$H$_4$OH)-, $^3J_{\text{H-H}}$ = 6.76 Hz), 3.60 (s, 3H, -OC**H**$_3$), 1.88 (s, 3H, C**H**$_3$C(O)-).

^{13}C NMR (125 MHz, d^6-DMSO) δ = 171.49 (1C, CH$_3$**C**(O)-), 169.21 (1C, -**C**(O)OCH$_3$), 157.38 (1C, aromatic carbon ipso to hydroxyl), 128.93 (2C, aromatic carbons meta to hydroxyl), 126.14 (1C, aromatic carbon para to hydroxyl), 115.27 (2C, aromatic carbons ortho to hydroxyl), 55.72 (1C, - **C**H(C$_6$H$_4$OH)-), 51.86 (1C, -O**C**H$_3$), 21.97 (1C, -C(O)**C**H$_3$).

IR (ss) ν/cm^{-1}: 3353, 1732, 1612, 1539, 1515

Found m/z (EI$^+$) = 223.0842, calculated 223.0845

M.p. = 176-177 °C

N-Acetyl (*p*-methyl phenyl)glycine methyl ester (3c)

Yield: 80 %

^{1}H NMR (500 MHz, d^6-DMSO) δ = 8.68 (d, 1H, -N**H**-, $^3J_{\text{H-H}}$ = 7.00 Hz), 7.26 (d, 2H, aromatic C**H** meta to methyl group, $^3J_{\text{H-H}}$ = 8.05 Hz), 7.19 (d, 2H, aromatic C**H** ortho to methyl group, $^3J_{\text{H-H}}$ = 7.90 Hz), 5.33 (d, 1H, -C**H**(C$_6$H$_4$CH$_3$)-, $^3J_{\text{H-H}}$ = 7.05 Hz), 3.61 (s, 3H, -OC**H**$_3$), 2.30 (s, 3H, -C$_6$H$_4$C**H**$_3$), 1.89 (s, 3H, C**H**$_3$C(O)-).

^{13}C NMR (125 MHz, d^6-DMSO) δ = 171.28 (1C, CH$_3$**C**(O)-), 169.24 (1C, -**C**(O)OCH$_3$), 137.57 (1C, aromatic), 133.27 (1C, aromatic), 129.16 (2C, aromatics), 127.62 (2C, aromatics), 55.97 (1C, - **C**H(C$_6$H$_4$CH$_3$)-), 52.07 (1C, -O**C**H$_3$), 22.11 (1C, -C(O)**C**H$_3$), 20.63 (1C, -C$_6$H$_4$**C**H$_3$).

IR (ss) ν/cm^{-1}: 3278, 1748, 1648, 1537, 1514

Found m/z (EI$^+$) = 221.1051, calculated 221.1052

M.p. = 110-111 °C

N-Acetyl (*p*-fluoro phenyl)glycine methyl ester (3d)

Yield: 71 %

^{1}H NMR (500 MHz, d^6-DMSO) δ = 8.76 (d, 1H, -N**H**-, $^3J_{\text{H-H}}$ = 7.00 Hz), 7.44 (dd, 2H, - C$_6$H$_4$F (aromatic C**H** meta to fluorine), $^3J_{\text{H-H}}$ = 8.50 Hz, $^4J_{\text{H-F}}$ = 5.50 Hz), 7.23 (t, 2H, (aromatic C**H** ortho to fluorine), $^3J_{\text{H-H}}$ = $^3J_{\text{H-F}}$ = 8.80 Hz), 5.42 (d, 1H, -C**H**(C$_6$H$_4$F)-, $^3J_{\text{H-H}}$ = 7.10 Hz), 3.62 (s, 3H, -OC**H**$_3$), 1.90 (s, 3H, C**H**$_3$C(O)-).

^{13}C NMR (125 MHz, d^6-DMSO) δ = 171.04 (1C, CH$_3$C(O)-), 169.24 (1C, -C(O)OCH$_3$), 161.88 (d, 1C, aromatic carbon ipso to fluorine, $^1J_{C-F}$ = 243.06 Hz), 132.61 (d, 1C, aromatic carbon para to fluorine, $^4J_{C-F}$ = 3.1 Hz), 129.87 (d, 2C, aromatic carbon meta to fluorine, $^3J_{C-F}$ = 8.36 Hz), 115.45 (d, 2C, carbon ortho to fluorine, $^2J_{C-F}$ = 21.59 Hz) , 55.44 (1C, -CH(C$_6$H$_4$F)-), 52.22 (1C, -OCH$_3$), 22.12 (1C, -C(O)CH$_3$).

IR (ss) v/cm^{-1}: 3308, 1756, 1734, 1650, 1533, 1507

Found m/z (EI$^+$) = 225.0807, calculated 225.0801

M.p. = 96-97 °C

N-Acetyl (p-chloro phenyl)glycine methyl ester (3e)

Yield: 74 %

^{1}H NMR (500 MHz, d^6-DMSO) δ = 8.79 (d, 1H, -NH-, $^3J_{H-H}$ = 6.12 Hz), 7.46 (d, 2H, aromatic CH, $^3J_{H-H}$ = 7.92 Hz), 7.41 (d, 2H, aromatic CH, $^3J_{H-H}$ = 6.64 Hz), 5.43 (d, 1H, -CH(C$_6$H$_4$Cl)-, $^3J_{H-H}$ = 7.04 Hz), 3.62 (s, 3H, -OCH$_3$), 1.90 (s, 3H, CH$_3$C(O)-).

^{13}C NMR (125 MHz, d^6-DMSO) δ = 171.24 (1C, CH$_3$C(O)-), 169.68 (1C, -C(O)OCH$_3$), 135.74 (1C, aromatic), 133.28 (1C, aromatic), 130.04 (2C, aromatics), 129.00 (2C, aromatics), 55.83 (1C, - CH(C$_6$H$_4$Cl)-), 52.69 (1C, -OCH$_3$), 22.47 (1C, -C(O)CH$_3$).

IR (ss) v/cm^{-1}: 3289, 1754, 1738, 1650, 1533

Found m/z (EI$^+$) = 241.0506, calculated 241.0506

M.p. = 126-128 °C

(S)-(+)-N-Acetyl (p-chloro phenyl)glycine methyl ester (3e)

Yield: 73 %, $[\alpha]_D^{20}$ = +166.0° (c 1.0, MeOH). Spectroscopic data as for racemate.

M.p. = 117-119 °C

N-Acetyl (m-fluoro phenyl)glycine methyl ester (3f)

Yield: 61 %

^{1}H NMR (400 MHz, d^6-DMSO) δ = 8.81 (d, 1H, -NH-, $^3J_{H-H}$ = 7.32 Hz), 7.44 (q, 1H, aromatic CH meta to fluorine, $^3J_{H-H}$ = $^4J_{H-F}$ = 6.92 Hz), 7.17-7.25 (m, 3H, aromatic CH ortho and para to fluorine), 5.47 (d, 1H, -CH(C$_6$H$_4$F)-, $^3J_{H-H}$ = 7.32 Hz), 3.63 (s, 3H, -OCH$_3$), 1.91 (s, 3H, CH$_3$C(O)-).

^{13}C NMR (125 MHz, d^6-DMSO) δ = 170.71 (1C, CH$_3$C(O)-), 169.30 (1C, -C(O)OCH$_3$), 162.03 (d, 1C, aromatic carbon ipso to fluorine $^1J_{C-F}$ = 242.28 Hz), 139.01 (d, 1C, aromatic

carbon meta to fluorine, ipso to rest of molecule, $^3J_{C\text{-}F}$ = 7.11 Hz), 130.64 (d, 1C, aromatic carbon meta to fluorine, $^3J_{C\text{-}F}$ = 8.25 Hz), 123.93 (d, 1C, aromatic carbon para to fluorine, $^4J_{C\text{-}F}$ = 1.68 Hz), 115.07 (d, 1C, aromatic carbon ortho to fluorine and rest of molecule $^2J_{C\text{-}F}$ = 20.56 Hz), 114.57 (d, 1C, aromatic carbon ortho to fluorine $^2J_{C\text{-}F}$ = 22.33 Hz), 55.61 (1C, -CH(C$_6$H$_4$Cl)-), 52.34 (1C, -OCH$_3$), 22.13 (1C, CH$_3$C(O)-).

IR (ss) v/cm^{-1}: 3291, 1746, 1646, 1530

Found m/z (EI$^+$) = 225.0799, calculated 225.0801

M.p. = 89-91 °C

_N_-Acetyl (_m_-chloro phenyl)glycine methyl ester (3g)

Yield: 61 %

^{1}H NMR (500 MHz, d^6-DMSO) δ = 8.83 (d, 1H, -NH-, $^3J_{H\text{-}H}$ = 7.15 Hz), 7.35-7.48 (m, 4H, -C$_6$H$_4$Cl), 5.47 (d, 1H, -CH(C$_6$H$_4$Cl)-, $^3J_{H\text{-}H}$ = 7.30 Hz), 3.64 (s, 3H, -OCH$_3$), 1.91 (s, 3H, CH$_3$C(O)-).

^{13}C NMR (125 MHz, d^6-DMSO) δ = 170.67 (1C, CH$_3$C(O)-), 169.29 (1C, -C(O)OCH$_3$), 138.78 (1C, aromatic), 133.17 (1C, aromatic), 130.50 (1C, aromatic), 128.18 (1C, aromatic), 127.52 (1C, aromatic), 126.57 (1C, aromatic), 55.58 (1C, - CH(C$_6$H$_4$Cl)-), 52.37 (1C, -OCH$_3$), 22.13 (1C, -C(O)CH$_3$).

IR (ss) v/cm^{-1}: 3278, 1499, 1655, 1531

Found m/z (EI$^+$) = 241.0499, calculated 241.0506

M.p. = 66-67 °C

_N_-Acetyl (_p_-trifluoromethyl phenyl)glycine methyl ester (3h)

Yield: 80 %

^{1}H NMR (400 MHz, d^6-DMSO) δ = 8.90 (d, 1H, -NH-, $^3J_{H\text{-}H}$ = 7.28 Hz), 7.77 (d, 2H, aromatic CH, $^3J_{H\text{-}H}$ = 8.24 Hz), 7.62 (d, 2H, aromatic CH, $^3J_{H\text{-}H}$ = 8.16 Hz), 5.58 (d, 1H, -CH(C$_6$H$_4$CF$_3$)-, $^3J_{H\text{-}H}$ = 7.28 Hz), 3.64 (s, 3H, -OCH$_3$), 1.91 (s, 3H, CH$_3$C(O)-).

^{13}C NMR (100 MHz, DMSO) δ = 170.93 (1C, CH$_3$C(O)-), 169.73 (1C, -C(O)OCH$_3$), 141.51 (s, 1C, aromatic carbon para to trifluoromethyl), 129.13 (q, 1C, aromatic carbon ipso to trifluoromethyl, $^2J_{C\text{-}F}$ = 31.79 Hz), 129.03 (s, 2C, aromatic carbon meta to trifluoromethyl), 125.89 (q, 2C, aromatic carbon ortho to trifluoromethyl, $^3J_{C\text{-}F}$ = 3.68 Hz), 124.44 (q, 1C, -CF$_3$, $^1J_{C\text{-}F}$ = 270.56 Hz), 56.11 (1C, - CH(C$_6$H$_4$CF$_3$)-), 52.79 (1C, -OCH$_3$), 22.49 (1C, -C(O)CH$_3$).

IR (ss) v/cm^{-1}: 3309, 1739, 1643, 1531

Found m/z (EI$^+$) = 275.0776, calculated 275.0769

M.p. = 96-98 °C

N-Acetyl phenylglycine ethyl ester (3i)

Yield: 83 %

^{1}H NMR (400 MHz, d^6-DMSO) δ = 8.73 (d, 1H, -NH-, $^3J_{H-H}$ = 7.08 Hz), 7.32-7.39 (m, 5H, -C$_6$H$_5$), 5.36 (d, 1H, -CH(C$_6$H$_5$)-, $^3J_{H-H}$ = 7.12 Hz), 4.03-4.14 (dq, 2H, -OCH$_2$CH$_3$), 1.90 (s, 3H, CH$_3$C(O)-), 1.12 (t, 3H, OCH$_2$CH$_3$, $^3J_{H-H}$ = 7.16 Hz).

^{13}C NMR (100 MHz, d^6-DMSO) δ = 171.05 (1C, CH$_3$C(O)-), 169.67 (1C, -C(O)OCH$_3$), 136.67 (1C, aromatic), 129.04 (2C, aromatics), 128.59 (1C, aromatic), 128.11 (2C, aromatics), 61.19 (1C, -OCH$_2$CH$_3$), 56.73 (1C, - CH(C$_6$H$_5$)-), 22.50 (1C, -C(O)CH$_3$), 14.29 (1C, -OCH$_2$CH$_3$).

IR (ss) v/cm^{-1}: 3314, 1731, 1649, 1535

Found m/z (AP$^+$) = 222.1138, 222.1130

M.p. = 85-86 °C

N-Acetyl phenylglycine isopropyl ester (3j)

Yield: 82 %

^{1}H NMR (500 MHz, d^6-DMSO) δ = 8.69 (d, 1H, -NH-, $^3J_{H-H}$ = 7.05 Hz), 7.32-7.39 (m, 5H, -C$_6$H$_5$), 5.34 (d, 1H, -CH(C$_6$H$_5$)-, $^3J_{H-H}$ = 7.20 Hz), 4.90 (sept, 1H, -OCH(CH$_3$)$_2$, $^3J_{H-H}$ = 6.20 Hz), 1.90 (s, 3H, CH$_3$C(O)-), 1.19 (d, 3H, -OCH(CH$_3$)$_A$(CH$_3$)$_B$, $^3J_{H-H}$ = 6.20 Hz), 1.04 (d, 3H, -OCH(CH$_3$)$_A$(CH$_3$)$_B$, $^3J_{H-H}$ = 6.20 Hz).

^{13}C NMR (125 MHz, d^6-DMSO) δ = 170.11 (1C, CH$_3$C(O)-), 169.25 (1C, -C(O)OCH$_3$), 136.41 (1C, aromatic), 128.58 (2C, aromatic), 128.10 (1C, aromatic), 127.61 (2C, aromatic), 68.28 (1C, -OCH(CH$_3$)$_2$), 56.46 (1C, - CH(C$_6$H$_5$)-), 22.11 (1C, -C(O)CH$_3$), 21.40 (1C, - OCH(CH$_3$)$_A$(CH$_3$)$_B$), 21.15 (1C, -OCH(CH$_3$)$_A$(CH$_3$)$_B$).

IR (ss) v/cm^{-1}: 3302, 1723, 1648, 1538

Found m/z (EI$^+$) = 235.1208, calculated 235.1208

M.p. = 102-104 °C

N-Acetyl (2-thienyl)glycine methyl ester (3k)

Yield: 69 %

^{1}H NMR (400 MHz, d^6-DMSO) δ = 8.87 (d, 1H, -NH-, $^3J_{H\text{-}H}$ = 7.04 Hz), 7.53 (dd, 1H, aromatic **CH** in 3 position, $^3J_{H\text{-}H}$ = 5.12 Hz, $^4J_{H\text{-}H}$ = 1.12 Hz), 7.11 (d, 1H, aromatic **CH** in 5 position, $^3J_{H\text{-}H}$ = 3.40 Hz), 7.02 (dd, **CH** in 4 position, $^3J_{H\text{-}H}$ = 5.08 Hz, $^3J_{H\text{-}H}$ = 3.60 Hz), 5.64 (d, 1H, -C**H**NH$_3$$^+$, $^3J_{H\text{-}H}$ = 7.08 Hz), 3.67 (s, 3H, -OC**H$_3$**), 1.90 (s, 3H, -COC**H$_3$**).

^{13}C NMR (100 MHz, d^6-DMSO) δ = 170.77 (1C, CH$_3$**C**O-), 169.69 (1C, -**C**OOCH$_3$), 138.36 (1C, aromatic **C**H in 1 position), 127.29 (2C, aromatic **C**H in 4 and 5 positions), 126.92 (1C, aromatic **C**H in 3 position), 52.82 (1C, -**C**NHAc), 52.02 (1C, -O**C**H$_3$), 22.40 (1C, -C(O)**C**H$_3$).

IR (ss) v/cm^{-1}: 3239, 1746, 1641, 1540

Found m/z (AP$^+$) = 214.0532, calculated 214.0538

M.p. = 91-93 °C

N-Acetyl (3-thienyl)glycine methyl ester (3l)

Yield: 73 %

^{1}H NMR (500 MHz, d^6-DMSO) δ = 8.72 (d, 1H, -NH-, $^3J_{H\text{-}H}$ = 7.20 Hz), 7.56 (dd, 1H, aromatic **CH** in 4 position, $^3J_{H\text{-}H}$ = 4.95 Hz, $^4J_{H\text{-}H}$ = 2.95 Hz), 7.53 (m, 1H, aromatic **CH** in 2 position), 7.12 (dd, 1H, aromatic **CH** in 5 position, $^3J_{H\text{-}H}$ = 4.95 Hz, $^4J_{H\text{-}H}$ = 1.65 Hz), 5.49 (d, 1H, -C**H**NHAc, $^3J_{H\text{-}H}$ = 7.25 Hz), 3.64 (s, 3H, -OC**H$_3$**), 1.90 (s, 3H, -COC**H$_3$**).

^{13}C NMR (125 MHz, d^6-DMSO) δ = 170.94 (1C, CH$_3$**C**O-), 169.29 (1C, -**C**OOCH$_3$), 136.29 (1C, aromatic **C**H in 1 position), 127.04 (1C, aromatic **C**H in 5 position), 126.81 (1C, aromatic **C**H in 2 position), 123.78 (1C, aromatic **C**H in 4 position), 52.14 (1C, -**C**NHAc), 52.02 (1C, -O**C**H$_3$), 22.09 (1C, -C(O)**C**H$_3$).

IR (ss) v/cm^{-1}: 3237, 1746, 1636, 1541

Found m/z (AP$^+$) = 214.0545, calculated 214.0538

M.p. = 108-109 °C

3.6.2.3 Synthesis of N-Acetyl Phenylglycines (4a, c-e, i-h)

Compounds **4a, c-e, i-h** were synthesised from compounds **1a, c-e, i-h** according to the method outlined by de Boer *et al.*[31]

Scheme 3.13: Synthesis of compounds **4a, c-e, i-h**.

The general method outlined below in the synthesis of **4a** was used in synthesis of all compounds **4a, c-e, i-h**.

N-Acetyl phenylglycine (4a)

Phenylglycine (2 g, 13.2 mmol) was suspended in H_2O (30 ml) and cooled to 0 °C. Sodium hydroxide (0.53 g, 13.2 mmol) was added and the cooled solution stirred until all solid had dissolved. Acetic anhydride (2.5 ml, 26.4 mmol) was added dropwise, followed by a solution of sodium hydroxide (1.59 g, 39.8 mmol) in H_2O (8 ml) and the mixture was left to stir for 15 mins at 0 °C. The mixture was acidified to pH 1 using concentrated hydrochloric acid and the colourless precipitate formed was filtered off and washed on the filter with ice cold water. A portion was recrystallised from a 1:1 mixture of water and ethanol to give needle-like crystals (1.86 g, 9.6 mmol, 73 %).

^{1}H NMR (400 MHz, d^6-DMSO) δ = 8.62 (d, 1H, -NH-, $^3J_{H-H}$ = 7.48 Hz), 7.32-7.39 (m, 5H, -C$_6$H$_5$), 5.31 (d, 1H, -CH(C$_6$H$_5$)-, $^3J_{H-H}$ = 7.52 Hz), 1.89 (s, 3H, CH$_3$C(O)-).

^{13}C NMR (100 MHz, d^6-DMSO) δ = 172.42 (1C, CH$_3$CO-), 169.49 (1C, -COOCH$_3$), 137.59 (1C, aromatic), 128.89 (2C, aromatics), 128.30 (1C, aromatic), 128.03 (2C, aromatics), 56.63 (1C, - CH(C$_6$H$_5$)-), 22.62 (1C, -C(O)CH$_3$).

IR (ss) v/cm^{-1}: 3347, 1710, 1607, 1542

Found *m/z* (EI$^+$) = 193.0733, calculated 193.0739

M.p. = 187-188 °C

(*R*)-(-)-*N*-Acetyl phenylglycine (4a)

Yield: 73 %, $[\alpha]_D^{20}$ = -206.4 (*c* 1.0, MeOH). ^{1}H and ^{13}C NMR spectra as for racemate.

M.p. = 185-187 °C

(*S*)-(+)-*N*-Acetyl phenylglycine (4a)

Yield: 56 %, $[\alpha]_D^{20}$ = +210.4 (*c* 1.0, MeOH). ^{1}H and ^{13}C NMR spectra as for racemate.

M.p. = 186-187 °C

N-Acetyl (*p*-methyl phenyl)glycine (4c)

Yield: 94 %

^{1}H NMR (400 MHz, d^6-DMSO) δ = 8.56 (d, 1H, -NH-, $^3J_{\text{H-H}}$ = 7.48 Hz), 7.26 (d, 2H, aromatic CH meta to methyl group, $^3J_{\text{H-H}}$ = 8.08 Hz), 7.18(d, 2H, aromatic CH ortho to methyl group, $^3J_{\text{H-H}}$ = 8.00 Hz), 5.25 (d, 1H, -CHNHAc, $^3J_{\text{H-H}}$ = 7.44 Hz), 2.29 (s, 3H, -C$_6$H$_4$CH$_3$), 1.88 (s, 3H, CH$_3$C(O)-).

^{13}C NMR (100 MHz, d^6-DMSO) δ = 172.54 (1C, CH$_3$CO-), 169.42 (1C, -COOCH$_3$), 137.56 (1C, aromatic), 134.58 (1C, aromatics), 129.39 (2C, aromatic), 127.92 (2C, aromatics), 56.34 (1C, - CH(C$_6$H$_4$CH$_3$)-), 22.61 (1C, -C(O)CH$_3$), 21.04 (1C, C$_6$H$_4$CH$_3$).

IR (ss) v/cm^{-1}: 3332, 1713, 1592, 1541

Found m/z (EI$^+$) = 207.0891, calculated 207.0895

M.p. = 235-236 °C

N-Acetyl (p-fluoro phenyl)glycine (4d)

Yield: 64 %

^{1}H NMR (400 MHz, d^6-DMSO) δ = 8.69 (d, 1H, -NH-, $^3J_{\text{H-H}}$ = 7.48 Hz), 7.48 (dd, 2H, - C$_6$H$_4$F (aromatic CH meta to fluorine), $^3J_{\text{H-H}}$ = 8.72 Hz, $^4J_{\text{H-F}}$ = 5.52 Hz), 7.27 (t, 2H, (aromatic CH ortho to fluorine), $^3J_{\text{H-H}}$ ≈ $^3J_{\text{H-F}}$ = 8.84 Hz), 5.39 (d, 1H, -CH(C$_6$H$_4$F)-, $^3J_{\text{H-H}}$ = 7.52 Hz), 1.95 (s, 3H, CH$_3$C(O)-).

^{13}C NMR (100 MHz, d^6-DMSO) δ = 172.30 (1C, CH$_3$C(O)-), 169.45 (1C, -C(O)OCH$_3$), 162.10 (d, 1C, aromatic carbon ipso to fluorine, $^1J_{\text{C-F}}$ = 242.38 Hz), 133.92 (d, 1C, aromatic carbon para to fluorine, $^4J_{\text{C-F}}$ = 3.08 Hz), 130.08 (d, 2C, aromatic carbon meta to fluorine, $^3J_{\text{C-F}}$ = 8.23 Hz), 115.68 (d, 2C, carbon ortho to fluorine, $^2J_{\text{C-F}}$ = 21.37 Hz) , 55.84 (1C, - CH(C$_6$H$_4$F)-), 22.61 (1C, -C(O)CH$_3$).

IR (ss) v/cm^{-1}: 3337, 1719, 1607, 1540, 1507

Found m/z (EI$^+$) = 211.0640, calculated 211.0645

M.p. = 194-195 °C

N-Acetyl (p-chloro phenyl)glycine (4e)

Yield: 86 %

^{1}H NMR (400 MHz, d^6-DMSO) δ = 8.67 (d, 1H, -NH-, $^3J_{\text{H-H}}$ = 7.48 Hz), 7.45 (d, 2H, aromatic CH, $^3J_{\text{H-H}}$ = 8.52 Hz), 7.41 (d, 2H, aromatic CH, $^3J_{\text{H-H}}$ = 8.44 Hz), 5.35 (d, 1H, - CH(C$_6$H$_4$Cl)-, $^3J_{\text{H-H}}$ = 7.52 Hz), 1.89 (s, 3H, CH$_3$C(O)-).

^{13}C NMR (100 MHz, d^6-DMSO) δ = 172.06 (1C, CH$_3$C(O)-), 169.48 (1C, -C(O)OCH$_3$), 136.75 (1C, aromatic), 132.93 (1C, aromatic), 129.88 (2C, aromatics), 128.85 (2C, aromatics), 55.90 (1C, - CH(C$_6$H$_4$Cl)-), 22.62 (1C, -C(O)CH$_3$).

IR (ss) v/cm^{-1}: 3333, 1714, 1593, 1537

Found m/z (EI$^+$) = 227.0345, calculated 227.0349

M.p. = 208-210 °C

(*S*)-(+)-*N*-Acetyl (*p*-chloro phenyl)glycine (4e)

Yield: 80 %, $[\alpha]_D^{20}$ = +206.2° (*c* 1.0, MeOH)

M.p. = 189 °C

N-Acetyl (*m*-chloro phenyl)glycine (4g)

Yield: 66 %

^{1}H NMR (500 MHz, d^6-DMSO) δ = 8.74 (d, 1H, -NH-, $^3J_{H-H}$ = 7.64 Hz), 7.39-7.50 (m, 4H, - C$_6$H$_4$Cl), 5.41 (d, 1H, -CH(C$_6$H$_4$Cl)-, $^3J_{H-H}$ = 7.64 Hz), 1.94 (s, 3H, CH$_3$C(O)-).

^{13}C NMR (100 MHz, d^6-DMSO) δ = 171.89 (1C, CH$_3$C(O)-), 169.51 (1C, -C(O)OCH$_3$), 140.15 (1C, aromatic), 133.43 (1C, aromatic), 130.77 (1C, aromatic), 128.25 (1C, aromatic), 127.74 (1C, aromatic), 126.85 (1C, aromatic), 56.03 (1C, - CH(C$_6$H$_4$Cl)-), 22.63 (1C, - C(O)CH$_3$).

IR (ss) v/cm^{-1}: 3342, 1718, 1601, 1533

Found m/z (EI$^+$) = 227.0348, calculated 227.0349

M.p. = 173-174 °C

N-Acetyl (*p*-trifluoromethyl phenyl)glycine (4g)

Yield: 85 %

^{1}H NMR (400 MHz, d^6-DMSO) δ = 8.81 (d, 1H, -NH-, $^3J_{H-H}$ = 7.60 Hz), 7.80 (d, 2H, aromatic CH, $^3J_{H-H}$ = 8.24 Hz), 7.66 (d, 2H, aromatic CH, $^3J_{H-H}$ = 8.12 Hz), 5.52 (d, 1H, - CH(C$_6$H$_4$CF$_3$)-, $^3J_{H-H}$ = 7.64 Hz), 1.96 (s, 3H, CH$_3$C(O)-).

^{13}C NMR (100 MHz, DMSO) δ = 171.73 (1C, CH$_3$C(O)-), 169.52 (1C, -C(O)OCH$_3$), 142.54 (s, 1C, aromatic carbon para to trifluoromethyl), 128.84 (s, 2C, aromatic carbon meta to trifluoromethyl), 128.80 (q, 1C, aromatic carbon ipso to trifluoromethyl, $^2J_{C-F}$ = 31.83 Hz), 125.78 (q, 2C, aromatic carbon ortho to trifluoromethyl, $^3J_{C-F}$ = 3.75 Hz), 124.72 (q, 1C, -CF$_3$, $^1J_{C-F}$ = 270.12 Hz), 56.19 (1C, - CH(C$_6$H$_4$CF$_3$)-), 22.62 (1C, -C(O)CH$_3$).

IR (ss) v/cm^{-1}: 3355, 1724, 1598, 1535

Found m/z (EI⁻) = 260.0533, calculated 260.0535

M.p. = 202-203 °C

3.6.3 Proton-Deuterium Exchange Reactions Followed by ¹H NMR Spectroscopy

3.6.3.1 Experimental Procedure

Buffers for H/D exchange experiments were prepared as follows. The appropriate quantity of NaH_2PO_4 for the desired buffer concentration was dissolved in D_2O. The ionic strength was made to 1 M using NaCl. The desired pH** was obtained through adding portions of $NaOD/D_2O$ solution whilst monitoring the pH.

H/D exchange experiments were carried out as follows. 1 ml solutions of approximately 0.005 M concentration of the compound for analysis in the appropriate buffer solution were prepared in Eppendorf vials. The vial was vortexed to aid dissolution, and the contents filtered to ensure no solid remained. The resulting solution was then placed in a sealed NMR tube which was maintained at 37 °C using a thermostatted water bath. The tube was removed from the water bath at intervals as required for analysis by ¹H NMR spectroscopy, then returned to the water bath. The hydrolysis reaction of compounds **3a-l** produces the carboxylic acid, which lowers the pH**. As a result, the pH** of the reaction mixture was monitored using a micro pH meter and maintained at the desired pH** ± 0.05 by addition of aliquots of a 0.01 M $NaOD/D_2O$ solution as required. Initial experiments showed that H/D exchange and hydrolysis reactions obeyed pseudo-first-order rate law and hence rate constants are independent of initial concentration.

Compound **3k** underwent H/D exchange too rapidly to adequately monitor the reaction through the previously described method. As such, the compound was dissolved in the appropriate buffer in an NMR tube as described previously, and the NMR tube was placed in the probe of the NMR spectrometer, which was maintained at 37 °C and spectra were recorded every 15 minutes. As hydrolysis rates for **3k** were small in respect to H/D exchange, pH** adjustments were not required.

3.6.3.2 Interpretation of ¹H NMR Spectra

Spinworks 2.5.5 was used to analyse ¹H NMR spectra. The analysis in this chapter was based on the integration of the peaks corresponding to the protons bound to the stereogenic centre in

compounds **3a-l** and **4a-h, k-l**. The integration of these peaks was relative to the peaks for the aromatic protons. The data was 'normalised' according to the number of aromatic protons. For example, when analysing compounds **3a, i-j**, the integrations of the stereogenic-centre-bound proton relative to the aromatic protons were multiplied by five, as **3a** has five aromatic protons. For compounds **3c-h**, the signal was multiplied by four. As the two aromatic peaks in compound **3b** have rather different chemical shifts (~0.4 ppm), it was decided to base the integration on only the farthest upfield peak (7.17 ppm) to avoid errors resulting from integrating over large stretches of baseline. As such the signal was normalised by a factor of two. Integrals for **3k** were normalised based on the aromatic thiophene peak at 7.53 ppm. Integrals for **3l** were normalised based on the aromatic thiophene peak at 7.12 ppm.

3.6.3.3 Interpretation of Data

The analysis of the data for compound **3a** in deuterated buffer shall be used as an example to illustrate the method by which the data was interpreted for all compounds **3a-l**.

The relative peak integration corresponding to the proton bound to the stereogenic centre for both **3a** and **4a** can be used to calculate the proportion of molecules which have been deuterated at the stereogenic centre. This value can be obtained by subtracting the relative intensity of both from the initial relative intensity of the protons bound to the stereogenic centre (eqn 3.5).

$$[3a^D] + [4a^D] = [3a^H]_0 - \{[3a^H] + [4a^H]\} \qquad (3.5)$$

where $[3a^D]$ is the concentration of **3a** with a deuteron bound to the stereogenic centre, $[4a^D]$ is the concentration of **4a** with a deuteron bound to the stereogenic centre, $[3a^H]$ is the concentration of **3a** with a proton bound to the stereogenic centre, $[4a^H]$ is the concentration of **4a** with a proton bound to the stereogenic centre and $[3a^H]_0$ is the starting concentration of **3a** with a proton bound to the stereogenic centre.

$[3a^H]$, $[4a^H]$ and $\{[3a^D] + [4a^D]\}$ were plotted as a function of time (Figure 3.7).

Figure 3.7: Relative integration of (■) [3a^H], (●) [4a^H] and (▲){[3a^D] + [4a^D]} as a function of time in 0.2 M D$_2$O phosphate buffer, I = 1 M, at 37 °C.

First-order rate constants were obtained by data analysis according to eqn (3.6).

$$S_t = S_f - \left(\Delta S \times e^{(-k \times t)}\right)$$

(3.6)

where S_t is the relative peak intensity at time t, S_f is the final peak intensity, ΔS is the change in peak intensity, k is the observed first-order rate constant and t is the elapsed time in seconds.

This data was plotted using OriginPro 8, and analysed using the 'global fit' function. All three curves in Figure 3.7 were defined to fit to the same observed rate constant. This observed rate constant is the sum of the rate constants of H/D exchange and of hydrolysis (eqn 3.7).

$$k_{obs} = k_{deut} + k_{hyd}$$

(3.7)

where k_{obs} is the observed rate constant for disappearance of 3a^H, k_{deut} is the rate constant of H/D exchange and k_{hyd} is the rate constant of hydrolysis.

The concentration of 3a^H decreases by both H/D exchange and hydrolysis. Therefore, the rate constant for the disappearance of 3a^H is the sum of the rate constants for both H/D exchange and hydrolysis reactions. The formation of both 4a^H and {3a^D + 4a^D} is dependent on the concentration of 3a^H, as it is the starting material for both. Therefore, the observed rate constants of formation for 4a^H and {3a^D + 4a^D} are the same as that for disappearance of 3a^H.

The individual rate constants for the H/D exchange and hydrolysis reactions can then be determined from the relative final amounts of 4a^H and {3a^D + 4a^D}. The ratio of these products will be equal to the ratio of the relative rate constants k_{deut} and k_{hyd} (eqn 3.8).

128

$$\frac{k_{\text{deut}}}{k_{\text{hyd}}} = \frac{S_{\text{f (deut)}}}{S_{\text{f (hyd)}}} \qquad (3.8)$$

Where $S_{\text{f (deut)}}$ is the final proportion of compound deuterated at the stereogenic centre and $S_{\text{f (hyd)}}$ is the final proportion of carboxylate protonated at the stereogenic centre.

Eqns (3.7) and (3.8) can then be combined, allowing k_{hyd} to be determined from the observed rate constant (eqn 3.9).

$$k_{\text{deut}} = \frac{S_{\text{f (deut)}}}{S_{\text{f (hyd)}}} \cdot k_{\text{hyd}}$$

therefore,

$$k_{\text{obs}} = \frac{S_{\text{f (deut)}}}{S_{\text{f (hyd)}}} \cdot k_{\text{hyd}} + k_{\text{hyd}}$$

$$k_{\text{obs}} = k_{\text{hyd}} \{ \frac{S_{\text{f (deut)}}}{S_{\text{f (hyd)}}} + 1 \} \qquad (3.9)$$

k_{deut} is then determined by substituting k_{hyd} back into eqn (3.7).

3.6.4 Determination of Enantiomeric Excess

As described in Section 3.4.8.1, Circular Dichroism spectroscopy was used to determine the ee_f of compounds **4a** and **4e** after hydrolysis of **3a** and **3e**. Comparison of ee_f with Q_f^H allowed the determination of the mechanism of H/D exchange. The ee_f was determined *via* the method described by Reetz *et al.*[32] Normalisation of the circular dichroism with respect to UV absorbance gives the anisotropy factor, also known as the g factor (eqn 3.10)

$$g = \frac{\theta}{A} \qquad (3.10)$$

where g is the anisotropy factor, θ is the ellipticity and A is the UV absorbance.

If the g factor can be shown to be independent of concentration and linear with respect to the ee, the ee of a solution of unknown concentration can be determined. Calibration curves for the g factor of **4a** and **4e** can be found in the Appendix (Section 3.7.2).

The ee of compounds **4a** and **4e** after full hydrolysis from enantiopure **3a** and **3e** starting materials (ee_f) was determined as follows.

A stock solution was made of 0.026 g (R)-(-)-**3a** in 20 ml of D_2O buffer of pH** 7.4, 0.3 M phosphate concentration and $I = 1$ M (6.28 mM in **3a**). The solution was incubated in a water

bath at 37 °C. Intermittently, a 0.5 ml portion was removed and analysed through ^{1}H NMR, to monitor hydrolysis. pH** 7.4 ± 0.05 was maintained through addition of aliquots of a 0.01 M NaOD/D_2O solution as required. After 350 hrs, the ^{1}H NMR spectrum suggested no **3a** remained in solution (disappearance of peak corresponding to methyl ester protons). To ensure full hydrolysis, the solution was kept incubated for a further 150 hrs. HPLC analysis (see Section 3.6.5) confirmed that no **3a** remained in solution. The solution was then analysed using CD spectroscopy. The g factor was determined for the fully hydrolysed solution, at 6 concentrations between 0.123 and 0.355 mM (dilution with H_2O). The g factor was found to be -40.391 ± 1.828, corresponding to ee_f = -45.499 ± 2.133 (from Figure 3.10).

The experiment for hydrolysis of **3e** to **4e** was carried out in an analogous fashion. The original stock solution used was 0.010 g (S)-(+)-**3e** in 20 ml of D_2O buffer of pH** 7.4, 0.3 M phosphate concentration and I = 1 M (2.07 mM in **3e**). After 60 hrs incubation at 37 °C the ^{1}H NMR spectrum suggested no **3e** remained in solution. The solution was incubated for a further 150 hrs before CD spectroscopy was used to determine the g factor at 223 nm for 6 different concentrations between 0.058 and 0.141 mM (dilution with H_2O). The average g factor was found to be 15.856 ± 0.732, corresponding to ee_f = +30.166 ± 1.387 (from Figure 3.12).

3.6.5 HPLC

Reverse-phase HPLC was used to confirm k_{hyd} as determined by ^{1}H NMR spectroscopy. Experiments were carried out using an Eclipse column (XD8-C18, 5 μm, 4.6 × 150 mm). A method to separate ester **3a** from hydrolysis product **4a** was developed. Flow rate was 1 ml / minute and UV detection of products was at 260 nm with 40 nm bandwidth. The eluents and the gradient used in the LC method are as follows:

Channel A = H_2O, Channel B = CH_3CN, Channel C = 0.02 % TFA in H_2O (pH 1.67).

Table 3.8: Gradient used for HPLC experiments.

Time (mins)	% A	% B	% C
0.0	90	0	10
4.0	50	40	10
7.0	50	40	10
9.0	90	0	10

Carboxylic acid **4a** eluted between 5-5.25 minutes, ester **3a** eluted between 6.15-6.3 minutes. HPLC calibration curves for **3a** and **4a** can be found in the Appendix (Section 3.7.3).

k_{hyd} of **3a** in D_2O buffer of pH** 7.4, phosphate concentration 0.2 M, $I = 1$ M was determined according to the following method.

0.013 g of **3a** was dissolved in 10 ml of D_2O buffer. The sample tube was incubated at 37 °C. pH** 7.4 ± 0.05 was maintained through addition of small portions of 0.01 M $NaOD/D_2O$ solution as required. Intermittently, a 0.5 ml portion of this stock solution was withdrawn and placed in a HPLC vial. A 10 μl injection from this vial was made into the HPLC instrument and the previously described HPLC method run. The remaining material was returned to the stock solution for further injections to be made. Results of the HPLC run were compared with the calibration curves to determine the quantity of each species. These results are displayed in Figure 3.8.

Figure 3.8: Change in quantity of (●) **3a** and (■) **4a** in 10 μl injections over time.

Each curve produced the same rate constant of $(2.14 ± 0.05) \times 10^{-6}$ s^{-1}. This compares favourably with the k_{hyd} value determined under the same conditions through ^1H NMR spectroscopy.

3.6.6 Miscellaneous

The data presented in Figure 3.9 (Appendix Section 3.7.1.2) was modelled numerically using Microsoft Excel 2010. Calculations modelled the kinetic scheme shown in Scheme 3.15. Initial concentrations were set at 100 for (R)-**3a**^{H} and 0 for all other species. The concentration of each species is displayed in eqns (3.11)-(3.16), where [ ]$_{pt}$ refers to the concentration of the denoted species at the previous time point, k_{inv} is the rate constant for

131

proton deuterium exchange at the stereogenic centre with chiral inversion, k_{hyd} is the rate constant of hydrolysis, KIE is the kinetic isotope effect on k_{inv} and dt refers to the time step since the previous time point.

$$[(R)\text{-}\mathbf{3a}^H] = [(R)\text{-}\mathbf{3a}^H]_{pt} \cdot \{ 1 - (k_{inv} + k_{hyd}) \cdot \mathrm{d}t \} \qquad (3.11)$$

$$[(S)\text{-}\mathbf{3a}^D] = [(S)\text{-}\mathbf{3a}^D]_{pt} \cdot \{ 1 - (k_{hyd} + (k_{inv} / \text{KIE})) \cdot \mathrm{d}t \} + [(R)\text{-}\mathbf{3a}^H]_{pt} \cdot k_{inv} \cdot \mathrm{d}t$$

$$+ [(R)\text{-}\mathbf{3a}^D]_{pt} \cdot (k_{inv} / \text{KIE}) \cdot \mathrm{d}t \qquad (3.12)$$

$$[(R)\text{-}\mathbf{3a}^D] = [(R)\text{-}\mathbf{3a}^D]_{pt} \cdot \{ 1 - (k_{hyd} + (k_{inv} / \text{KIE})) \cdot \mathrm{d}t \} + [(S)\text{-}\mathbf{3a}^D]_{pt} \cdot (k_{inv} / \text{KIE}) \cdot \mathrm{d}t$$

$$(3.13)$$

$$[(R)\text{-}\mathbf{4a}^H] = [(R)\text{-}\mathbf{3a}^H]_{pt} \cdot k_{hyd} \cdot \mathrm{d}t \qquad (3.14)$$

$$[(S)\text{-}\mathbf{4a}^D] = [(S)\text{-}\mathbf{3a}^D]_{pt} \cdot k_{hyd} \cdot \mathrm{d}t \qquad (3.15)$$

$$[(R)\text{-}\mathbf{4a}^D] = [(R)\text{-}\mathbf{3a}^D]_{pt} \cdot k_{hyd} \cdot \mathrm{d}t \qquad (3.16)$$

k_{inv}, k_{hyd} and KIE are all variables, and the time step dt was chosen to be as short as practically possible. Modification of k_{inv}, k_{hyd} and KIE produced the different values for Q_f^H and ee_f shown in Table 3.9.

3.7 Appendix

3.7.1 Theoretical Background for Equations 3.3 and 3.4

3.7.1.1 S_E1 Mechanism (Eqn 3.3)

If the experiments outlined in Section 3.4.1 are undertaken with a chiral starting material, (R)-**3a**, and H/D exchange proceeds through the S_E1 mechanism, the reaction profile shown in Scheme 3.8 is altered to that shown in Scheme 3.14.

Scheme 3.14: Reaction scheme of (R)-**3a** in deuterated buffers, if mechanism of H/D exchange/racemisation is S_E1.

Because the carbanion intermediate formed from deprotonation of (R)-**3a** can be deuterated on either face, the portion of the final, fully hydrolysed product **4a** which is deuterated at the stereogenic centre will also be racemic. The portion of final product **4a** which is protonated at the stereogenic centre will be enantiopure; once hydrolysis has occurred no H/D exchange or racemisation will take place due to the negative charge on the carboxylate. Therefore, if the *ee* of **4a** (after hydrolysis is complete) is equal to the percentage of **4a** which is protonated at the stereogenic centre, the data is consistent with an S_E1 mechanism (eqn 3.3).

$$Q_f^{\;H} = ee_f \qquad\qquad (3.3)$$

where Q_f^H is the percentage of **4a** molecules protonated at the stereogenic centre after hydrolysis is complete and ee_f is the enantiomeric excess of **4a** after hydrolysis is complete.

133

3.7.1.2 S_E2 Mechanism (Eqn 3.4)

If H/D exchange/racemisation of (R)-**3a** proceeds via the S_E2 mechanism, the reaction scheme will be as depicted in Scheme 3.15.

Scheme 3.15: Reaction scheme of (R)-**3a** in deuterated buffers, if mechanism of H/D exchange/racemisation is S_E2. k_{inv} is the rate constant of H/D exchange at stereogenic centre with chiral inversion. KIE is the primary kinetic isotope effect on k_{inv} as a result of deuteration on the stereogenic centre. Secondary kinetic isotope effects on k_{hyd} due to deuteration on the stereogenic centre were considered negligible.

A kinetic analysis of how the concentrations of each species shown in Scheme 3.15 changes with time if an S_E2 mechanism is occurring is displayed in Figure 3.9.

Figure 3.9: Kinetic profile for reaction scheme displayed in Scheme 3.15, where (■) (R)-$\mathbf{3a}^{H}$, (●) (S)-$\mathbf{3a}^{D}$, (▲) (R)-$\mathbf{3a}^{D}$, (▼) (R)-$\mathbf{4a}^{H}$, (◄) (S)-$\mathbf{4a}^{D}$, (►) (R)-$\mathbf{4a}^{D}$. The time units in Figure 3.9 are arbitrary. The ratio of k_{inv}: k_{hyd} is set to 1 : 0.7,[**] and the kinetic isotope effect on k_{inv} of a deuterated stereogenic centre set to 2.5. Details of the construction of this plot are provided in the experimental (Section 3.6.6).

Figure 3.9 can be used to predict what would be the expected ratio of final *ee* to the proportion of molecules protonated at the stereogenic centre for the fully hydrolysed product **4a**. The only final product protonated at the stereogenic centre is (R)-$\mathbf{4a}^{H}$ (▼ in Figure 3.9). Therefore, the proportion of molecules deuterated at the stereogenic centre for the fully hydrolysed product **4a**, is equal to the proportion of (R)-$\mathbf{4a}^{H}$ in the reaction mixture after the reaction is complete (i.e. the proportion of molecules that undergo hydrolysis before H/D deuteration). This is the same as previously described for the $S_{E}1$ mechanism. However, because the $S_{E}2$ mechanism deuterates with chiral inversion, the $\mathbf{3a}^{D}$ molecules formed from the starting material will be of (S) stereochemistry (unlike the racemate formed from $S_{E}1$ mechanism). This means that a far higher proportion of the final **4a** product is of (S) stereochemistry and the *ee* will be lower than the proportion of protonated final product. Eqns (3.17)-(3.19) illustrate this for the $S_{E}2$ mechanism.

$$Q_{f}^{H} = [(R) - \mathbf{4a}^{H}] \qquad (3.17)$$

$$ee_{f} = [(R) - \mathbf{4a}^{H}] - \left\{ [(S) - \mathbf{4a}^{D}] - [(R) - \mathbf{4a}^{D}] \right\} \qquad (3.18)$$

[**] Experimentally determined ratio of k_{deut}:k_{hyd} for **3a** in 0.3 M buffer, displayed in Table 3.1.

$$ee_f = Q_f^H - \left\{ [(S) - 4\mathbf{a}^D] - [(R) - 4\mathbf{a}^D] \right\}$$ (3.19)

Eqns (3.17)-(3.19) show that, as the molecules of **4a** deuterated on the stereogenic centre will have a higher proportion of (S) than (R) configuration, the value for Q_f^H will be higher than ee_f if an S_E2 mechanism is occurring. The ratio of k_{inv} to k_{hyd} and the KIE used in formulation of Figure 3.9 would give $Q_f^H = 41$ % and $ee_f = 14$ %.

Using different ratios of k_{inv} to k_{hyd} and a different KIE will alter the ratio of Q_f^H to ee_f. However, Q_f^H will always be greater than ee_f for an S_E2 mechanism except in cases where k_{inv} is far greater than k_{hyd}. In circumstances where $k_{inv} >> k_{hyd}$, deuterated **3a** will equilibrate before any can be 'siphoned-off' by hydrolysis resulting in $Q_f^H = ee_f$. The relationship between Q_f^H and ee_f for the S_E2 mechanism is therefore described by eqn (3.4).

$$Q_f^H > ee_f$$ (3. 4)

except where $k_{inv} >> k_{hyd}$.

Values of Q_f^H and ee_f for scenarios of different k_{inv}, k_{hyd} and KIE are displayed in Table 3.9.

Table 3.9: Expected values of Q_f^H and ee_f based on values of k_{inv}, k_{hyd} and KIE, if an S_E2 mechanism of racemisation is taking place.

Input			Output	
k_{inv}	k_{hyd}	KIE	Q_f^H	ee_f
1	0.7	2.5	41 %	14 %
1	1.5	2.5	60 %	34 %
1	0.7	1	41 %	26 %
1	1.5	1	60 %	43 %
1	5	2.5	83 %	69 %
1	0.01	2.5	1 %	0 %

3.7.2 Circular Dichroism Calibrations

3.7.2.1 CD Calibration for the ee Determination of 4a

To calibrate for determination of *ee* of solutions of **4a**, 0.163 mM solutions of **4a** in water were made with *ee* (+)-100, (+)-80, (+)-40, (+)-20, 0, (-)-20, (-)-40, (-)-80 and (-)-100. The absorbance and circular dichroism were determined at 217 nm for each solution, using a 1 cm pathlength cuvette. After baseline subtraction, these values were used to determine the *g* factor for each solution (Figure 3.10).
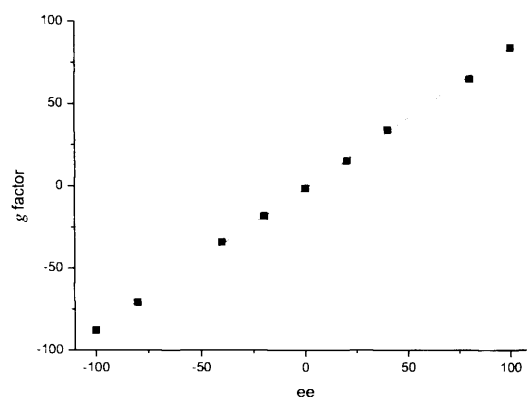
Figure 3.10: Calibration graph of *g* factor against *ee* for **4a**, determined at 217 nm for 0.163 mM solutions. Gradient = 0.857 ± 0.006, intercept = -1.399 ± 0.378. R^2 = 0.9996.

It was necessary to confirm that the *g* factor is independent of concentration for **4a**. The *g* factor was determined for solutions of **4a** for a range of concentrations between 0.033 and 0.319 mM, all with *ee* = (-)-40 (Figure 3.11).
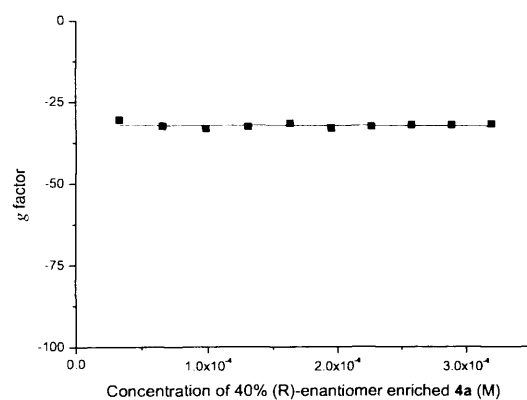
Figure 3.11: Dependency of the *g* factor at 217 nm on concentration for **4a** solutions with *ee* = (-)-40, standard deviation = 2.45 %.

137

Figure 3.11 clearly shows that the *g* factor for **4a** is independent of concentration.

3.7.2.2 CD Calibration for the ee Determination of 4e

The *ee* determination for **4e** was calibrated in the same manner as for **4a**. Absorbance and circular dichroism were determined at 223 nm. As only (S)-(+)-**4e** was available, the *g* factor was only determined for (+)-*ee* values (Figure 3.12)
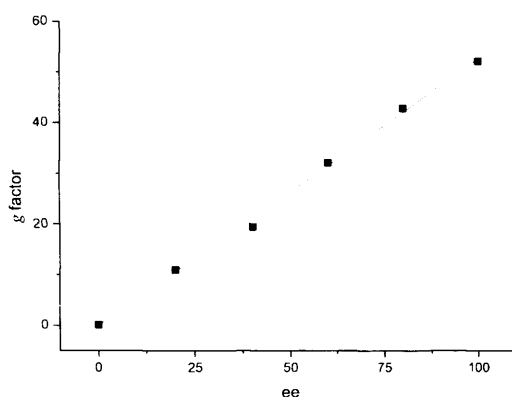
Figure 3.12: Calibration graph of *g* factor against *ee* for **4e**, determined at 223 nm for 0.086 mM solutions. Gradient = 0.528 ± 0.012, intercept = - 0.072 ± 0.743. R^2 = 0.997.

The *g* factor was determined for solutions of **4e** at a range of concentrations between 0.052 and 0.185 mM, all with *ee* = (+)-40 (Figure 3.13).
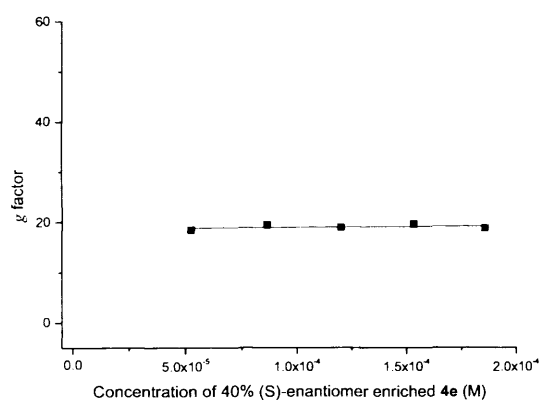
Figure 3.13: Dependency of *g* factor at 223 nm on concentration for **4e** solutions with *ee* = (-)-40, standard deviation = 2.62 %.

Figure 3.13 clearly shows that the *g* factor of **4e** is independent of concentration.

3.7.3 HPLC Calibrations for 3a and 4a

Solutions of 4 and 2 gL^{-1} of **3a** and **4a** were made up. Each solution was then diluted by ¼, ½, and ¾. HPLC calibration graphs were obtained using 5 and 10 μl injections of each solution (Figure 3.14 and Figure 3.15).
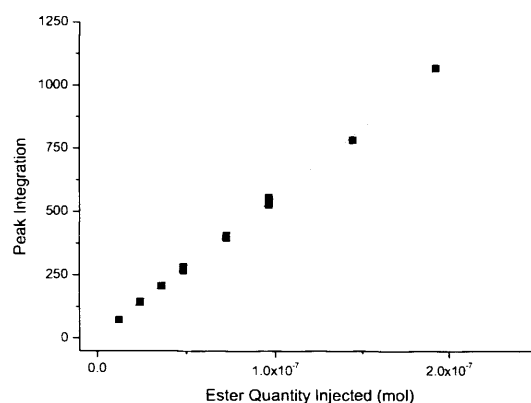
Figure 3.14: HPLC calibration for **3a**. Gradient = (5.46 ± 0.05) x 10^9, intercept = 11.28 ± 3.87. R^2 = 0.999.
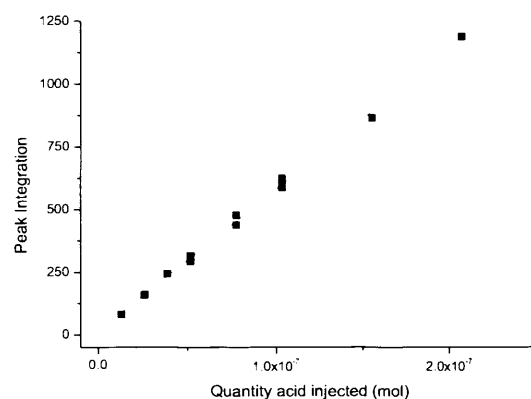
Figure 3.15: HPLC calibration of **4a**. Gradient = (5.64 ± 0.07) x 10^9, intercept = 15.94 ± 6.22. R^2 = 0.998.

3.7.4 Data Tables from ¹H NMR Spectroscopy Kinetic Experiments

The kinetic data from ^1H NMR spectroscopy from which Figure 3.2 and Figure 3.3 were constructed is listed in the tables displayed in the following pages.

Table 3.10: Rate constant data for compound **3a** in D_2O buffers at 37 °C, $I = 1$ M.

pH**	phosphate conc. / M	[HPO_4^{2-}] conc. / M	k_{obs} x 10^6 / s^{-1}	k_{deut} x 10^6 / s^{-1}	k_{hyd} x 10^6 / s^{-1}	$S_{f(deut)}$	$S_{f(hyd)}$
7.4	0.050	0.030	3.47 ± 0.15	1.36 ± 0.18	2.11 ± 0.09	0.378 ± 0.009	0.584 ± 0.010
7.4	0.100	0.061	4.10 ± 0.13	1.82 ± 0.15	2.28 ± 0.08	0.437 ± 0.007	0.546 ± 0.007
7.4	0.200	0.122	4.91 ± 0.08	2.80 ± 0.09	2.11 ± 0.04	0.569 ± 0.004	0.428 ± 0.003
7.4	0.250	0.152	5.52 ± 0.16	3.25 ± 0.17	2.27 ± 0.07	0.588 ± 0.006	0.411 ± 0.005
7.8	0.200	0.159	7.03 ± 0.14	3.57 ± 0.16	3.46 ± 0.07	0.502 ± 0.003	0.485 ± 0.003
7.4	0.300	0.182	6.16 ± 0.11	3.64 ± 0.12	2.53 ± 0.05	0.590 ± 0.003	0.411 ± 0.003
7.8	0.355	0.282	10.22 ± 0.18	5.61 ± 0.19	4.61 ± 0.08	0.547 ± 0.003	0.450 ± 0.003

$k_{gb} = (1.64 \pm 0.09) \times 10^{-5}\ s^{-1}\ M$, $\qquad k_0' = (8.05 \pm 1.28) \times 10^{-7}\ s^{-1}$

Table 3.11: Rate constant data for compound **3b** in D_2O buffers at 37 °C, $I = 1$ M.

pH**	phosphate conc. / M	$[HPO_4^{2-}]$ conc. / M	k_{obs} x 10^6 / s^{-1}	k_{deut} x 10^6 / s^{-1}	k_{hyd} x 10^6 / s^{-1}	$S_{f\,(deut)}$	$S_{f\,(hyd)}$
7.4	0.100	0.061	2.07 ± 0.06	0.39 ± 0.07	1.68 ± 0.05	0.186 ± 0.005	0.800 ± 0.006
7.4	0.200	0.122	2.62 ± 0.10	0.76 ± 0.13	1.86 ± 0.07	0.289 ± 0.007	0.705 ± 0.008
7.4	0.250	0.152	2.45 ± 0.12	0.88 ± 0.15	1.57 ± 0.08	0.361 ± 0.009	0.642 ± 0.010
7.4	0.300	0.182	3.11 ± 0.05	1.14 ± 0.06	1.98 ± 0.03	0.362 ± 0.004	0.637 ± 0.004
7.8	0.355	0.282	9.38 ± 0.21	1.69 ± 0.28	7.70 ± 0.18	0.178 ± 0.006	0.814 ± 0.006

$k_{gb} = (6.01 \pm 0.72)$ x 10^{-6} s^{-1} M, $\qquad k_0' = (0.24 \pm 1.01)$ x 10^{-7} s^{-1}

Table 3.12: Rate constant data for compound **3c** in D_2O buffers at 37 °C, $I = 1$ M.

pH**	phosphate conc. / M	$[HPO_4^{2-}]$ conc. / M	k_{obs} x 10^6 / s^{-1}	k_{deut} x 10^6 / s^{-1}	k_{hyd} x 10^6 / s^{-1}	$S_{f\,(deut)}$	$S_{f\,(hyd)}$
7.4	0.100	0.061	1.91 ± 0.03	0.65 ± 0.03	1.26 ± 0.02	0.350 ± 0.003	0.673 ± 0.004
7.4	0.200	0.122	3.08 ± 0.08	1.40 ± 0.09	1.68 ± 0.04	0.450 ± 0.005	0.541 ± 0.005
7.4	0.250	0.152	3.62 ± 0.07	1.72 ± 0.07	1.90 ± 0.04	0.472 ± 0.003	0.521 ± 0.004
7.4	0.300	0.182	4.12 ± 0.17	1.97 ± 0.19	2.14 ± 0.09	0.478 ± 0.009	0.521 ± 0.009
7.8	0.300	0.239	5.30 ± 0.11	2.26 ± 0.13	3.04 ± 0.07	0.424 ± 0.005	0.573 ± 0.006

$k_{gb} = (1.03 \pm 0.06)$ x 10^{-5} s^{-1} M, $\qquad k_0' = (4.47 \pm 5.92)$ x 10^{-8} s^{-1}

Table 3.13: Rate constant data for compound **3d** in D_2O buffers at 37 °C, I = 1 M.

pH**	phosphate conc. / M	$[HPO_4^{2-}]$ conc. / M	k_{obs} x 10^6 / s^{-1}	k_{deut} x 10^6 / s^{-1}	k_{hyd} x 10^6 / s^{-1}	$S_{f\,(deut)}$	$S_{f\,(hyd)}$
7.4	0.100	0.061	3.79 ± 0.08	1.49 ± 0.10	2.29 ± 0.05	0.392 ± 0.005	0.602 ± 0.005
7.4	0.200	0.122	5.74 ± 0.13	2.95 ± 0.14	2.79 ± 0.06	0.510 ± 0.004	0.482 ± 0.004
7.4	0.250	0.152	7.04 ± 0.22	3.72 ± 0.25	3.33 ± 0.11	0.524 ± 0.005	0.469 ± 0.005
7.4	0.300	0.182	8.32 ± 0.18	4.26 ± 0.20	4.06 ± 0.09	0.509 ± 0.005	0.485 ± 0.005
7.8	0.300	0.239	10.20 ± 0.27	5.09 ± 0.30	5.11 ± 0.14	0.501 ± 0.006	0.504 ± 0.006

k_{gb} = (2.20 ± 0.13) x 10^{-5} s^{-1} M, k_0' = (1.92 ± 1.54) x 10^{-7} s^{-1}

Table 3.14: Rate constant data for compound **3e** in D_2O buffers at 37 °C, I = 1 M.

pH**	phosphate conc. / M	$[HPO_4^{2-}]$ conc. / M	k_{obs} x 10^6 / s^{-1}	k_{deut} x 10^6 / s^{-1}	k_{hyd} x 10^6 / s^{-1}	$S_{f\,(deut)}$	$S_{f\,(hyd)}$
7.4	0.100	0.061	0.84 ± 0.03	0.55 ± 0.03	0.29 ± 0.01	0.659 ± 0.010	0.353 ± 0.009
7.4	0.200	0.122	1.43 ± 0.05	1.00 ± 0.05	0.43 ± 0.02	0.699 ± 0.007	0.303 ± 0.007
7.4	0.250	0.152	1.67 ± 0.12	1.25 ± 0.13	0.42 ± 0.04	0.746 ± 0.015	0.252 ± 0.014
7.4	0.300	0.182	2.06 ± 0.07	1.51 ± 0.07	0.55 ± 0.02	0.741 ± 0.006	0.268 ± 0.006
7.8	0.300	0.239	2.43 ± 0.07	1.84 ± 0.07	0.59 ± 0.02	0.763 ± 0.006	0.245 ± 0.006

k_{gb} = (7.47 ± 0.37) x 10^{-5} s^{-1} M, k_0' = (9.37 ± 4.71) x 10^{-7} s^{-1}

Table 3.15: Rate constant data for compound **3f** in D_2O buffers at 37 °C, $I = 1$ M.

pH**	phosphate conc. / M	$[HPO_4^{2-}]$ conc. / M	k_{obs} x 10^6 / s^{-1}	k_{deut} x 10^6 / s^{-1}	k_{hyd} x 10^6 / s^{-1}	$S_{f(deut)}$	$S_{f(hyd)}$
7.4	0.100	0.061	1.36 ± 0.03	1.02 ± 0.03	0.35 ± 0.01	0.740 ± 0.004	0.251 ± 0.004
7.4	0.200	0.122	2.30 ± 0.05	1.82 ± 0.05	0.48 ± 0.01	0.786 ± 0.005	0.209 ± 0.004
7.4	0.250	0.152	2.64 ± 0.05	2.18 ± 0.05	0.46 ± 0.01	0.819 ± 0.004	0.174 ± 0.003
7.4	0.300	0.182	3.38 ± 0.07	2.89 ± 0.08	0.49 ± 0.01	0.852 ± 0.004	0.144 ± 0.003
7.8	0.300	0.239	4.61 ± 0.19	3.56 ± 0.20	1.05 ± 0.06	0.770 ± 0.014	0.228 ± 0.012

$k_{gb} = (1.40 ± 0.05)$ x 10^{-4} s^{-1} M, $k_0' = (1.48 ± 0.49)$ x 10^{-6} s^{-1}

Table 3.16: Rate constant data for compound **3g** in D_2O buffers at 37 °C, $I = 1$ M.

pH**	phosphate conc. / M	$[HPO_4^{2-}]$ conc. / M	k_{obs} x 10^6 / s^{-1}	k_{deut} x 10^6 / s^{-1}	k_{hyd} x 10^6 / s^{-1}	$S_{f(deut)}$	$S_{f(hyd)}$
7.4	0.100	0.061	1.36 ± 0.02	1.02 ± 0.02	0.34 ± 0.01	0.751 ± 0.003	0.247 ± 0.003
7.4	0.200	0.122	2.54 ± 0.09	2.05 ± 0.10	0.49 ± 0.02	0.820 ± 0.009	0.196 ± 0.008
7.4	0.250	0.152	2.82 ± 0.07	2.42 ± 0.07	0.41 ± 0.02	0.867 ± 0.006	0.146 ± 0.005
7.4	0.300	0.182	3.58 ± 0.18	3.11 ± 0.19	0.47 ± 0.04	0.876 ± 0.012	0.131 ± 0.010
7.8	0.355	0.282	6.81 ± 0.25	4.60 ± 0.26	2.21 ± 0.09	0.676 ± 0.007	0.325 ± 0.007

$k_{gb} = (1.60 ± 0.06)$ x 10^{-4} s^{-1} M, $k_0' = (4.68 ± 4.53)$ x 10^{-7} s^{-1}

Table 3.17: Rate constant data for compound **3h** in D_2O buffers at 37 °C, $I = 1$ M.

pH**	phosphate conc. / M	[HPO$_4^{2-}$] conc. / M	k_{obs} x 10^6 / s^{-1}	k_{deut} x 10^6 / s^{-1}	k_{hyd} x 10^6 / s^{-1}	$S_{f(deut)}$	$S_{f(hyd)}$
7.4	0.050	0.030	2.61 ± 0.08	2.12 ± 0.08	0.48 ± 0.02	0.805 ± 0.007	0.184 ± 0.006
7.4	0.100	0.061	4.01 ± 0.09	3.50 ± 0.09	0.51 ± 0.02	0.879 ± 0.005	0.127 ± 0.005
7.4	0.200	0.122	7.44 ± 0.17	6.89 ± 0.18	0.54 ± 0.04	0.921 ± 0.006	0.073 ± 0.005
7.4	0.250	0.152	8.91 ± 0.47	8.30 ± 0.48	0.61 ± 0.10	0.919 ± 0.013	0.067 ± 0.011
7.8	0.200	0.159	10.48 ± 0.31	9.24 ± 0.32	1.24 ± 0.08	0.875 ± 0.008	0.118 ± 0.007
7.4	0.300	0.182	10.74 ± 0.54	10.16 ± 0.54	0.59 ± 0.08	0.933 ± 0.008	0.054 ± 0.007
7.8	0.300	0.239	13.26 ± 0.44	12.24 ± 0.44	1.02 ± 0.09	0.924 ± 0.008	0.077 ± 0.007

$k_{gb} = (5.15 \pm 0.13) \times 10^{-4}$ s^{-1} M, $\qquad$ $k_0' = (5.01 \pm 0.98) \times 10^{-6}$ s^{-1}

3.7.5 Figures from ¹H NMR Kinetic Experiments

The graphs from which the data in the tables in Section 3.7.1.1 was obtained are displayed in the figures in the following pages. All experiments were carried out at 37 °C, $I = 1$ M. pH** 7.4 unless denoted. (■) $3x^H$, (●) $4x^H$, (▲) $\{[3x^D] + [4x^D]\}$, where x refers to the specific compound denoted in the heading for that section.
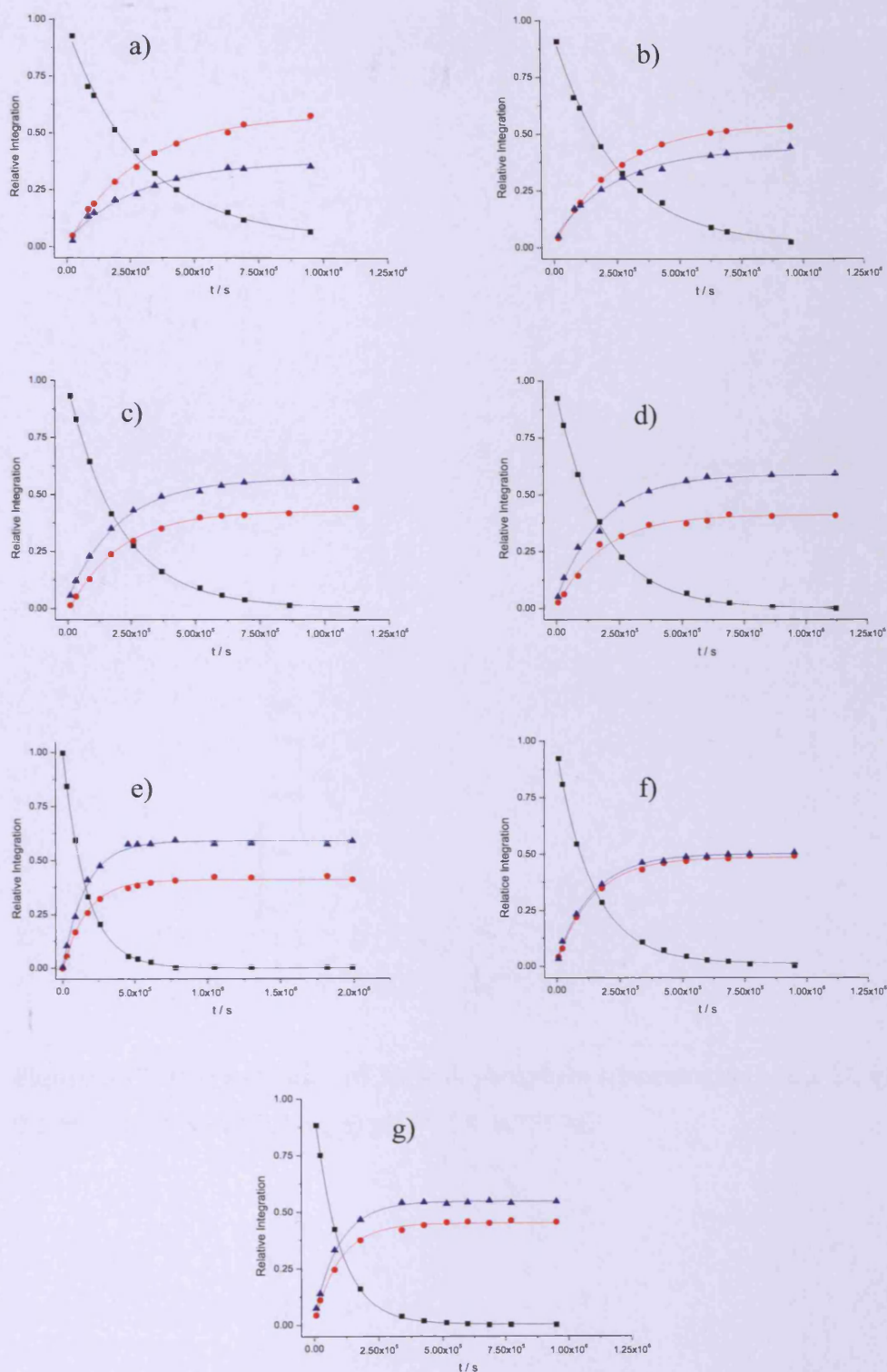
Figure 3.16: H/D exchange of **3a**, with phosphate concentration a) 0.05 M, b) 0.1 M, c) 0.2 M, d) 0.25 M, e) 0.3 M, f) pH** 7.8, 0.2 M, g) pH** 7.8, 0.355 M.
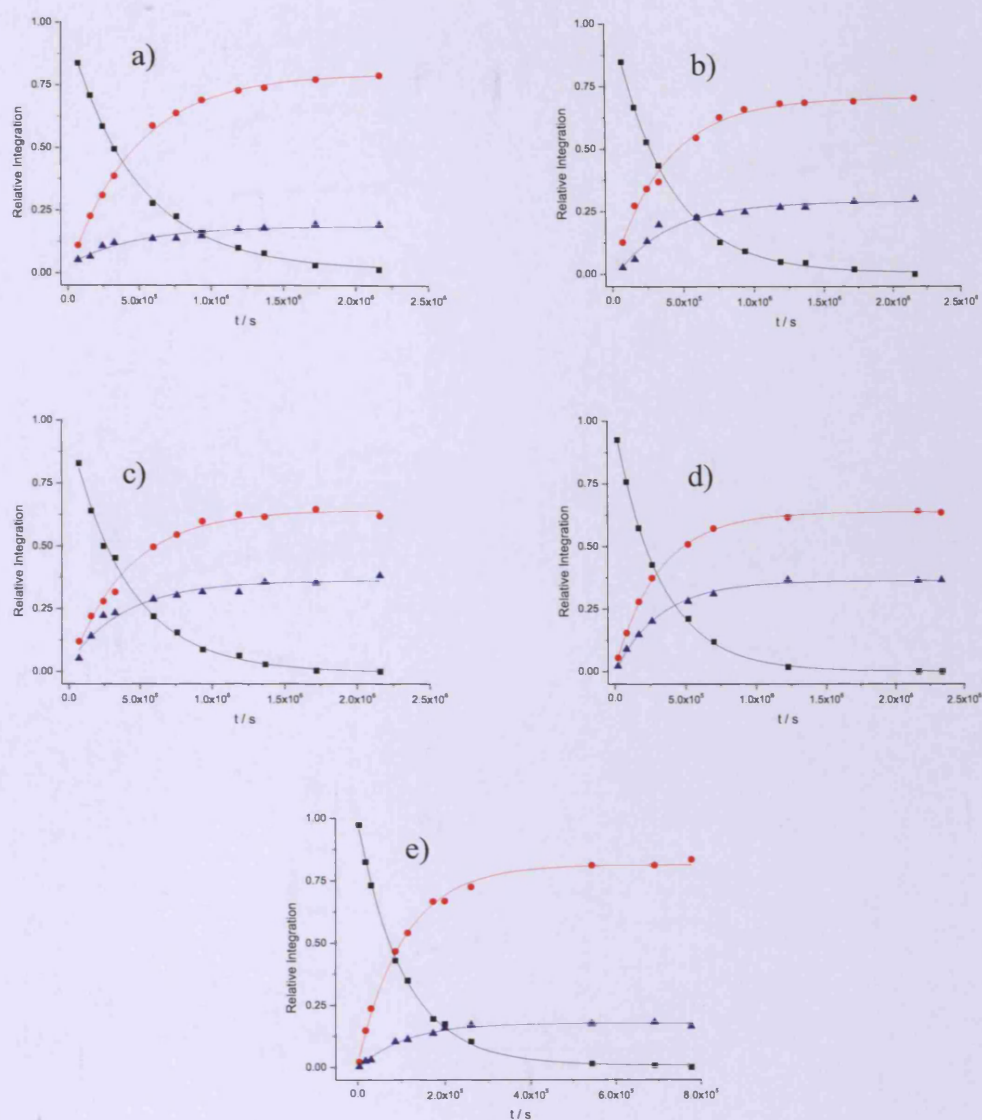
Figure 3.17: H/D exchange of **3b** with phosphate concentration a) 0.1 M, b) 0.2 M, c) 0.25 M, d) 0.3 M, e) pH** 7.8, 0.355 M.

3.7.5.3 Compound 3c
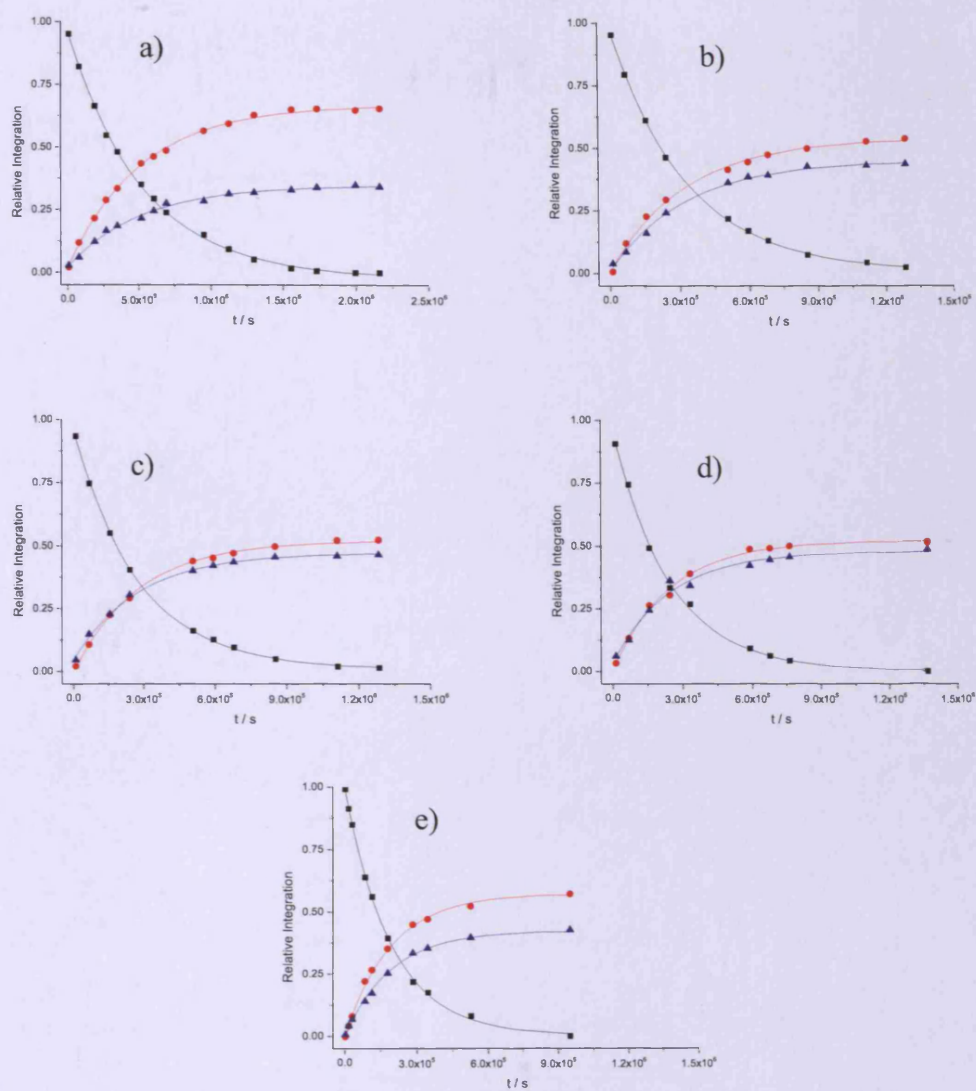
Figure 3.18: H/D exchange of **3c** with phosphate concentration a) 0.1 M, b) 0.2 M, c) 0.25 M, d) 0.3 M, e) pH** 7.8, 0.3 M.

3.7.5.4 Compound 3d
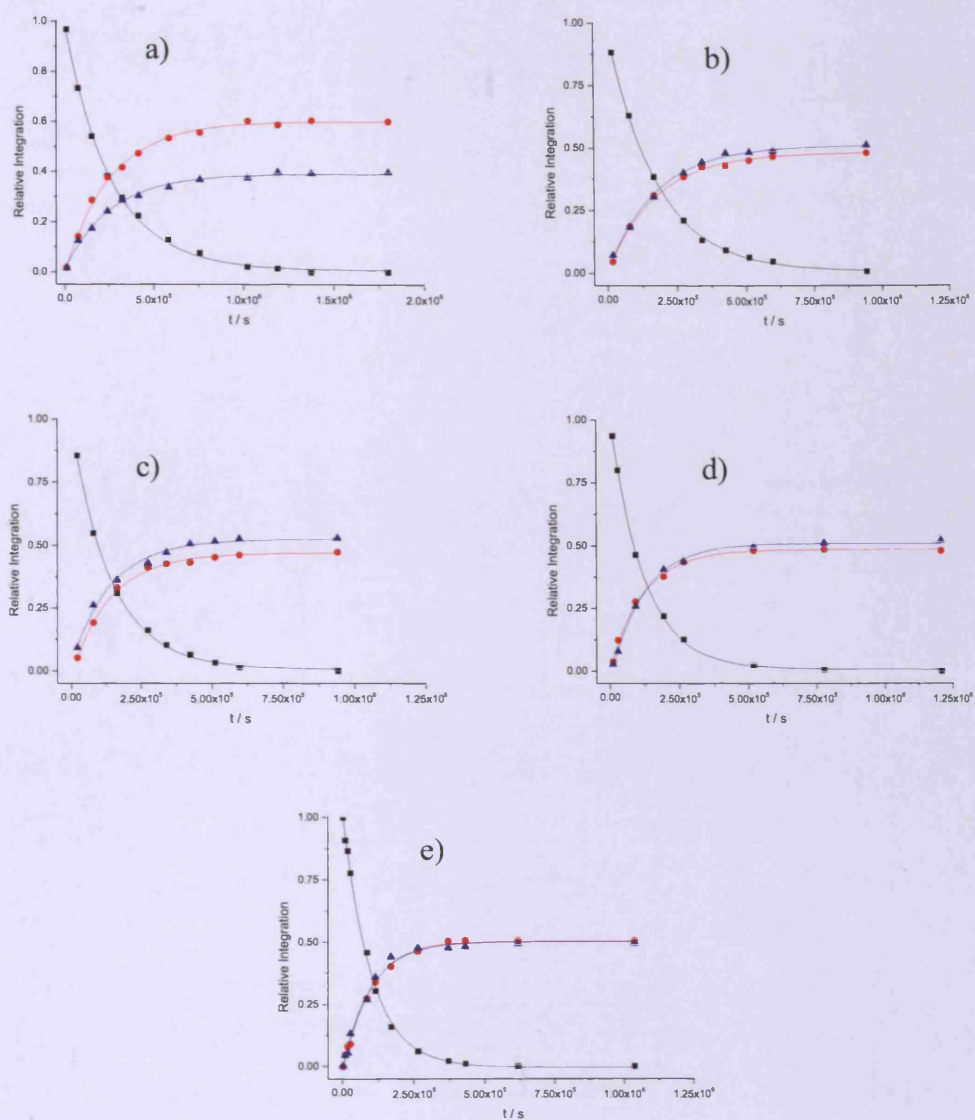
Figure 3.19: H/D exchange of **3d** with phosphate concentration a) 0.1 M, b) 0.2 M, c) 0.25 M, d) 0.3 M, e) pH** 7.8, 0.3 M
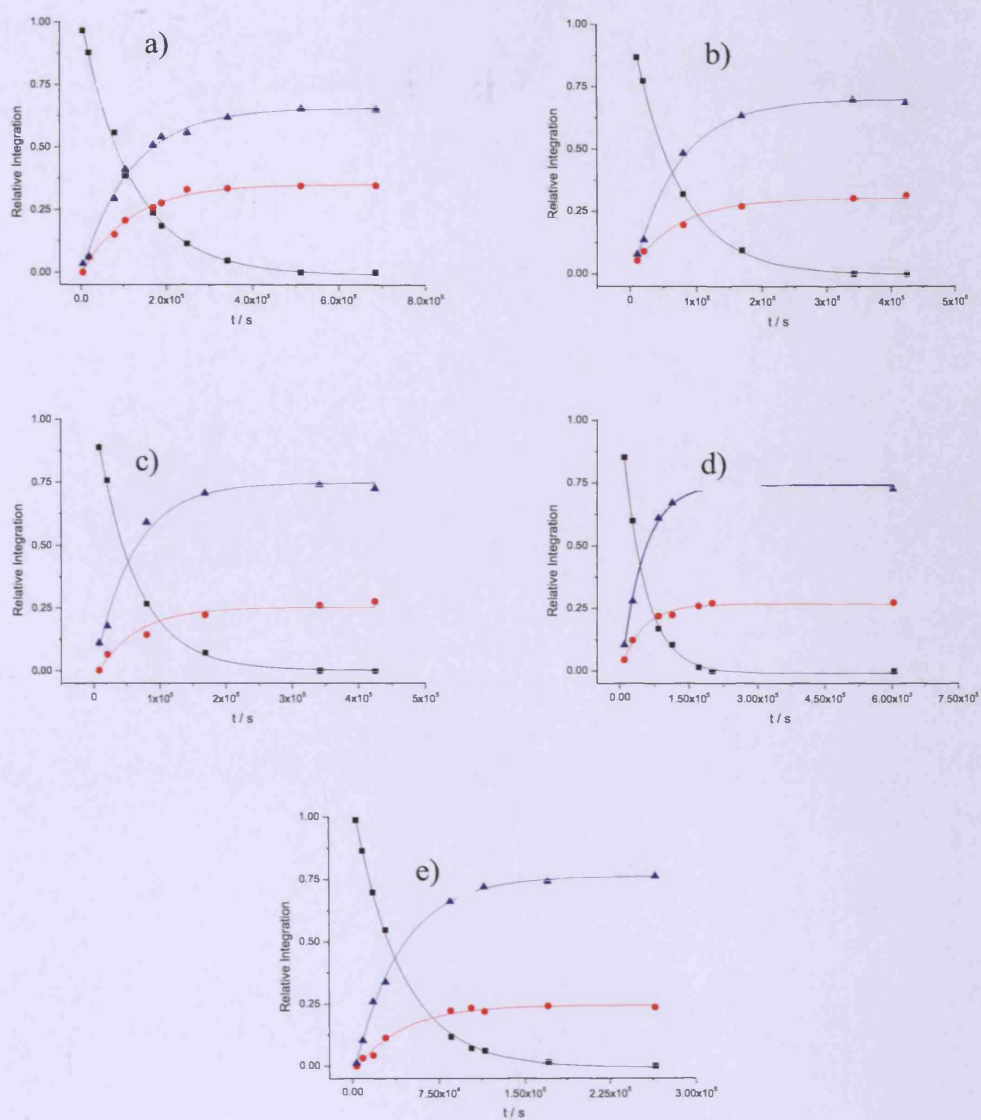
Figure 3.20: H/D exchange of **3e** with phosphate concentration a) 0.1 M, b) 0.2 M, c) 0.25 M, d) 0.3 M, e) pH** 7.8, 0.3 M.
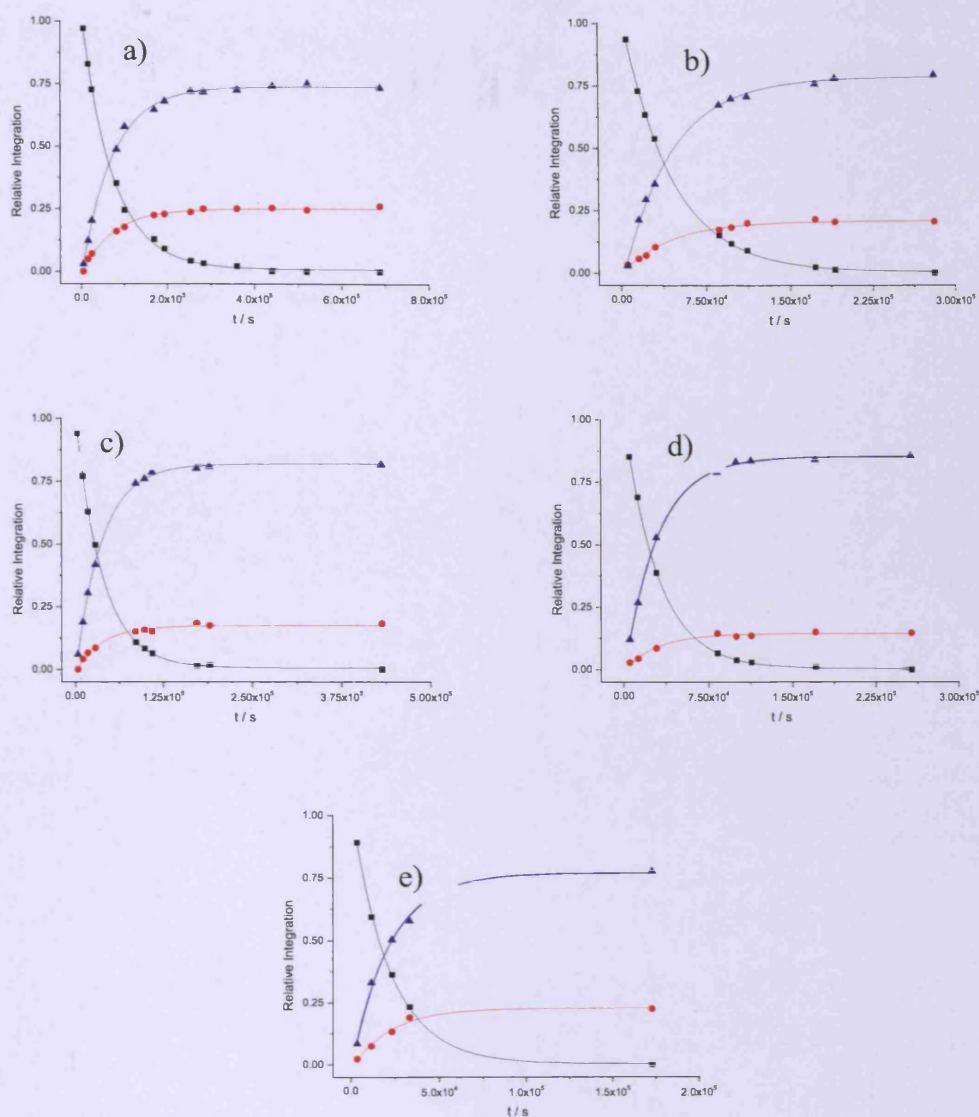
Figure 3.21: H/D exchange of **3f** with phosphate concentration a) 0.1 M, b) 0.2 M, c) 0.25 M, d) 0.3 M, e) pH** 7.8, 0.3 M.
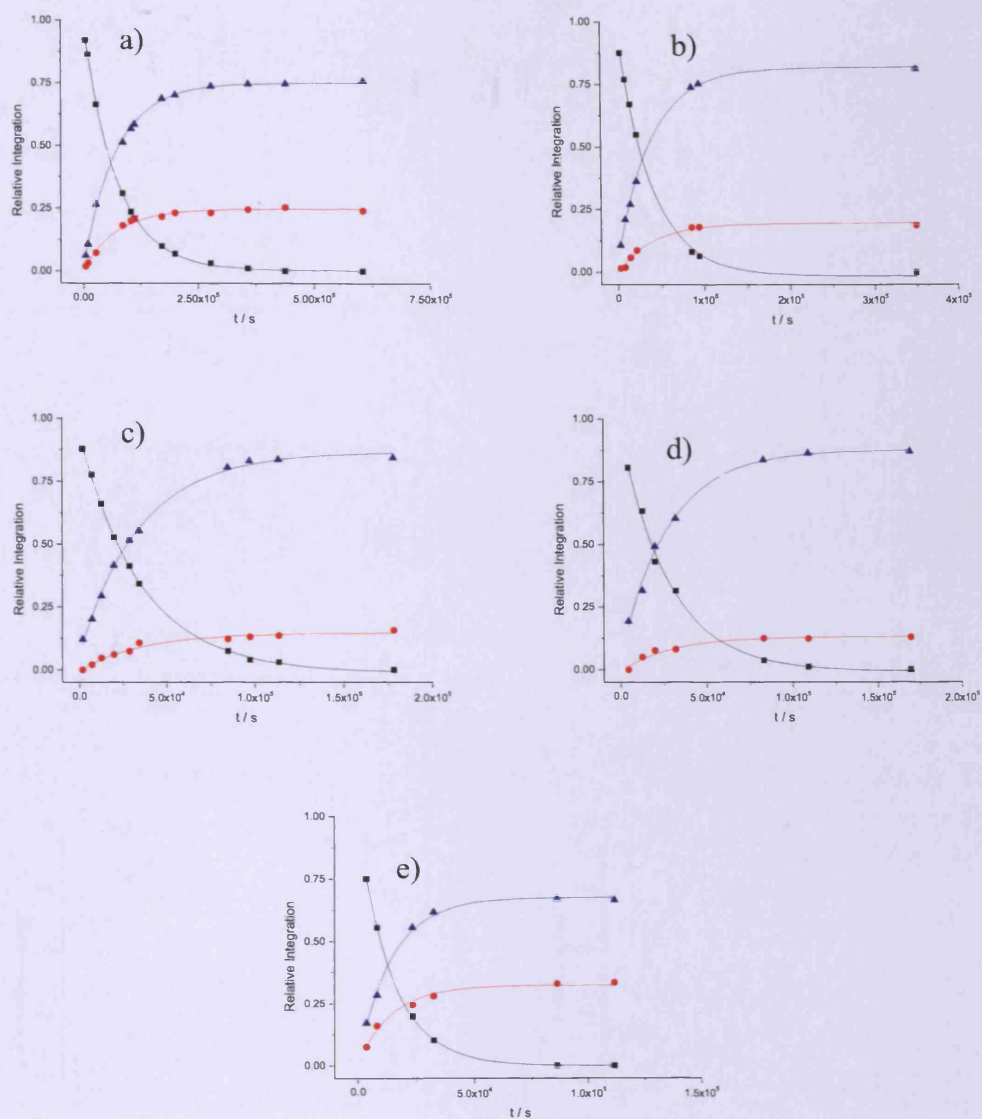
Figure 3.22: H/D exchange of **3g** with phosphate concentration a) 0.1 M, b) 0.2 M, c) 0.25 M, d) 0.3 M, e) pH** 7.8, 0.355 M.

3.7.5.8 Compound 3h
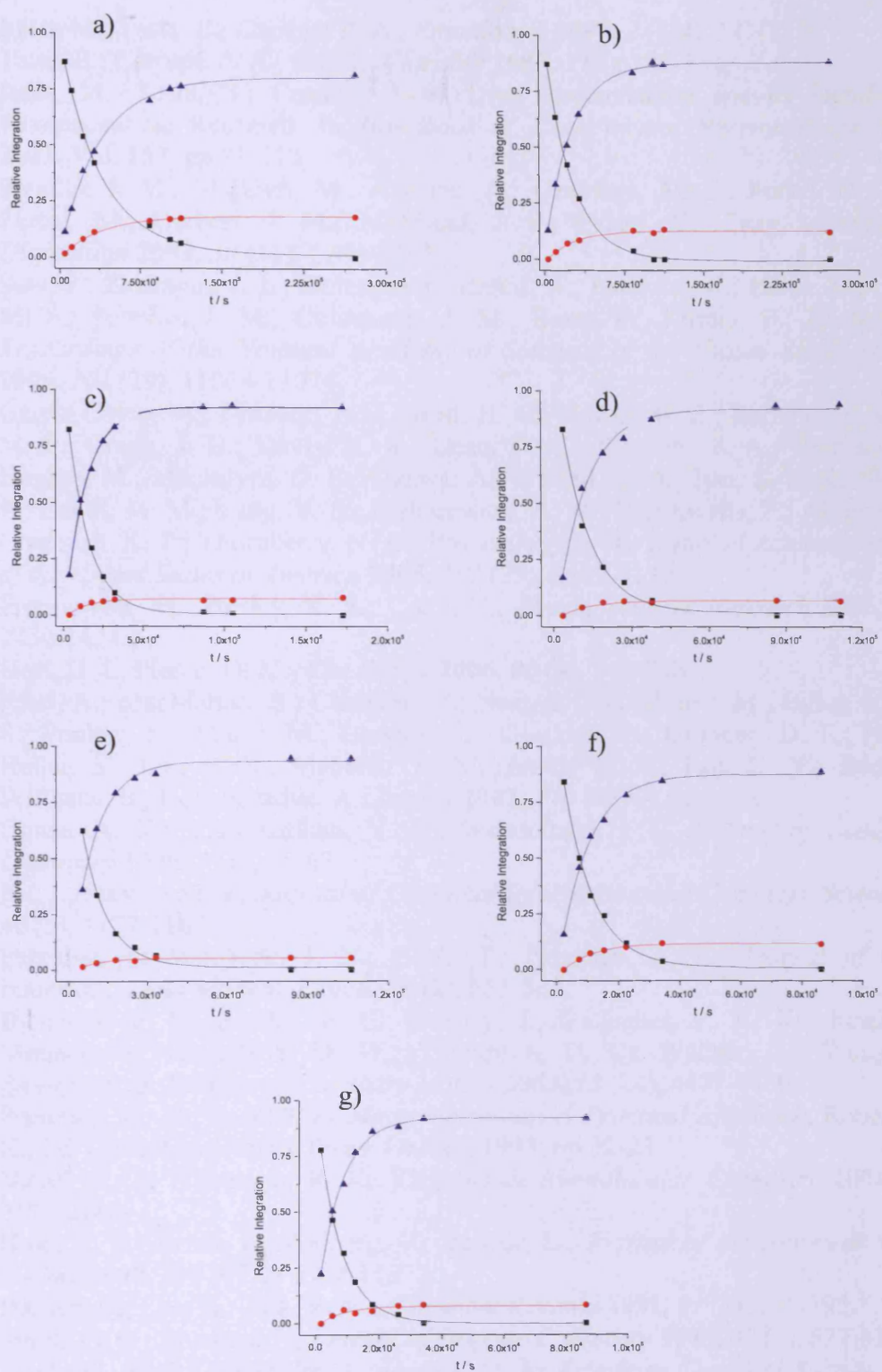
Figure 3.23: H/D exchange of **3h** with phosphate concentration a) 0.05 M, b) 0.1 M, c) 0.2 M, d) 0.25 M, e) 0.3 M, f) pH** 7.8, 0.2 M, g) pH** 7.8, 0.355 M.

3.8 References

1. Reist, M.; Testa, B.; Carrupt, P. A., *Enantiomer* **1997**, *2* (3-4), 147-155.
2. Testa, B.; Carrupt, P. A.; Gal, J., *Chirality* **1993**, *5* (3), 105-111.
3. Reist, M.; Testa, B.; Carrupt, P.-A., Drug Racemization and Its Significance in Pharmaceutical Research. In *Handbook of Experimental Pharmacology*, Springer: 2003; Vol. 153, pp 91-112.
4. Pereillo, J. M.; Maftouh, M.; Andrieu, A.; Uzabiaga, M. F.; Fedeli, O.; Savi, P.; Pascal, M.; Herbert, J. M.; Maffrand, J. P.; Picard, C., *Drug Metabolism and Disposition* **2002**, *30* (11), 1288-1295.
5. Savi, P.; Zachayus, J. L.; Delesque-Touchard, N.; Labouret, C.; Herve, C.; Uzabiaga, M. F.; Pereillo, J. M.; Culouscou, J. M.; Bono, F.; Ferrara, P.; Herbert, J. M., *Proceedings of the National Academy of Sciences of the United States of America* **2006**, *103* (29), 11069-11074.
6. Garcia-Calvo, M.; Lisnock, J. M.; Bull, H. G.; Hawes, B. E.; Burnett, D. A.; Braun, M. P.; Crona, J. H.; Davis, H. R.; Dean, D. C.; Detmers, P. A.; Graziano, M. P.; Hughes, M.; MacIntyre, D. E.; Ogawa, A.; O'Neill, K. A.; Iyer, S. P. N.; Shevell, D. E.; Smith, M. M.; Tang, Y. S.; Makarewicz, A. M.; Ujjainwalla, F.; Altmann, S. W.; Chapman, K. T.; Thornberry, N. A., *Proceedings of the National Academy of Sciences of the United States of America* **2005**, *102* (23), 8132-8137.
7. Froimowitz, M.; Patrick, K. S.; Cody, V., *Pharmaceutical Research* **1995**, *12* (10), 1430-1434.
8. Heal, D. J.; Pierce, D. M., *Cns Drugs* **2006**, *20* (9), 713-738.
9. Patel, A.; MacMahon, S.; Chalmers, J.; Neal, B.; Woodward, M.; Billot, L.; Harrap, S.; Poulter, N.; Marre, M.; Cooper, M.; Glasziou, P.; Grobbee, D. E.; Hamet, P.; Heller, S.; Liu, L. S.; Mancia, G.; Mogensen, C. E.; Pan, C. Y.; Rodgers, A.; Williams, B.; Collaborative, A., *Lancet* **2007**, *370* (9590), 829-840.
10. Ghose, A. K.; Viswanadhan, V. N.; Wendoloski, J. J., *Journal of Combinatorial Chemistry* **1999**, *1* (1), 55-68.
11. Xu, J.; Stevenson, J., *Journal of Chemical Information and Computer Sciences* **2000**, *40* (5), 1177-1187.
12. Lameijer, E. W.; Kok, J. N.; Back, T.; Ijzerman, A. P., *Journal of Chemical Information and Modeling* **2006**, *46* (2), 553-562.
13. Bymaster, F. P.; Beedle, E. E.; Findlay, J.; Gallagher, P. T.; Krushinski, J. H.; Mitchell, S.; Robertson, D. W.; Thompson, D. C.; Wallace, L.; Wong, D. T., *Bioorganic & Medicinal Chemistry Letters* **2003**, *13* (24), 4477-4480.
14. Primrose, W. U., In *NMR of Macromolecules: A Practical Approach*, Roberts, G. C. K., Ed. Oxford University Press: Oxford, 1993; pp 22-23.
15. Nicoll, A. J.; Allemann, R. K., *Organic & Biomolecular Chemistry* **2004**, *2* (15), 2175-2180.
16. Broo, K. S.; Brive, L.; Ahlberg, P.; Baltzer, L., *Journal of the American Chemical Society* **1997**, *119* (47), 11362-11372.
17. Hansch, C.; Leo, A.; Taft, R. W., *Chemical Reviews* **1991**, *91* (2), 165-195.
18. Smith, G. G.; Sivakua, T., *Journal of Organic Chemistry* **1983**, *48* (5), 627-634.
19. Bordwell, F. G.; Boyle, W. J., *Journal of the American Chemical Society* **1972**, *94* (11), 3907-3911.
20. Bordwell, F. G.; Boyle, W. J., *Journal of the American Chemical Society* **1971**, *93* (2), 511-512.
21. Chen, C. Y.; Chang, Y. S.; Lin, S. A.; Wen, H. I.; Cheng, Y. C.; Tsai, S. W., *Journal of Organic Chemistry* **2002**, *67* (10), 3323-3326.
22. Hammett, L. P.; Pfluger, H. L., *Journal of the American Chemical Society* **1933**, *50* (10), 4079-4089.

23. Hilal, S. H.; Karickhoff, S. W.; Carreira, L. A.; Shrestha, B. P., *Qsar & Combinatorial Science* **2004,** *22* (9-10), 917-925.

24. Matsuo, H.; Kawazoe, Y.; Sato, M.; Ohnishi, M.; Tatsuno, T., *Chemical & Pharmaceutical Bulletin* **1970,** *18* (9), 1788-1793.

25. Reist, M.; Christiansen, L. H.; Christoffersen, P.; Carrupt, P. A.; Testa, B., *Chirality* **1995,** *7* (6), 469-473.

26. Reist, M.; Carrupt, P. A.; Testa, B.; Lehmann, S.; Hansen, J. J., *Helvetica Chimica Acta* **1996,** *79* (3), 767-778.

27. Cram, D. J.; Gosser, L., *Journal of the American Chemical Society* **1964,** *86* (24), 5457-5465.

28. Guthrie, R. D.; Nicolas, E. C., *Journal of the American Chemical Society* **1981,** *103* (15), 4637-4638.

29. Albert, A.; Serjeant, E. P., *Ionization Constants of Acids and Bases*. Methuen & Co: London, 1962; p 143-146.

30. Kudelko, A.; Zielinski, W., *Tetrahedron* **2009,** *65* (6), 1200-1206.

31. de Boer, J. W.; Browne, W. R.; Harutyunyan, S. R.; Bini, L.; Tiemersma-Wegman, T. D.; Alsters, P. L.; Hage, R.; Feringa, B. L., *Chemical Communications* **2008,** (32), 3747-3749.

32. Reetz, M. T.; Kuhling, K. M.; Hinrichs, H.; Deege, A., *Chirality* **2000,** *12* (5-6), 479-482.

4 Kinetic Studies on the Configurational Instability of N-Substituted Phenylglycine Amides

4.1 Introduction

The database mining studies reported in Chapter 2 showed the frequent occurrence of amide functional groups adjacent to stereogenic centres deemed at risk of configurational instability under physiological conditions, according to the assignments by Testa et al.[1-3] (Table 1.1). In particular, the combination of a proton, an aromatic group, an amide bound through the carbonyl and an amide bound through nitrogen appeared 7 times in the 250 most frequently occurring combinations of substituents around a stereogenic centre for compounds in the ISAC database (Table 2.5). Stereogenic centres such as these, of the type R''R'RC-H with R groups that can stabilise a negative charge, are susceptible to base-catalysed proton abstraction mechanisms as discussed in Chapter 1. This chapter will therefore focus on molecules based on the 'chiral motif' exhibited in Scheme 4.1.
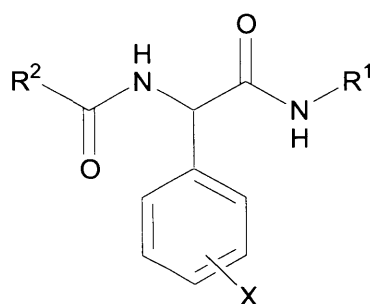
Scheme 4.1: Structures to be investigated in this chapter. R^1 = -H, -C$_6$H$_4$X,
R^2 = -CH$_3$, -C$_6$H$_4$X, X = various substituents.

In comparison to the related ester compounds discussed in Chapter 3, it was expected that the compounds analysed in this chapter would display lower rate constants for H/D exchange and racemisation. This expectation is based on the classification by Testa et al. (Table 1.1) of an amide substituent as 'acid-strengthening', rather than the 'strongly acid-strengthening' classification attributed to ester substituents. All else being equal, the molecules displayed in Scheme 4.1 should therefore have greater configurational stability than those investigated in Chapter 3.

Resonance delocalisation of the amide lone pair may be the reason for the reduced degree of 'acid-strengthening' displayed by amides in comparison to esters. Amides are known to display partial carbon-nitrogen double-bond character,[4-8] as shown in Scheme 4.2.
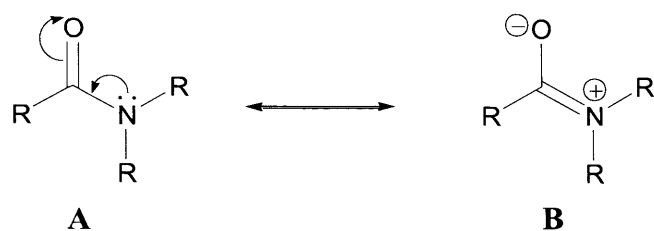
Scheme 4.2: Amide resonance structures.

An adjacent carbonyl group can favour H/D exchange and racemisation via an S_E1 reaction by delocalisation of negative charge onto the carbonyl oxygen. However, for amide substituents the presence of resonance structure **B** diminishes delocalisation onto the carbonyl oxygen, as the carbonyl is already carrying an enhanced partial negative charge through delocalisation of the nitrogen lone pair.

Many drugs on the market contain stereogenic centres similar to those shown in Scheme 4.1 and those investigated in this chapter. These drugs include the antibiotic Cephalexin,[9] anti-epileptic Levetiracetam[10] and proteasome inhibitors Bortezomib[11] and Lenalidomide.[12]

Cefalexin

Leviracetam

Bortezomib

Lenalidomide
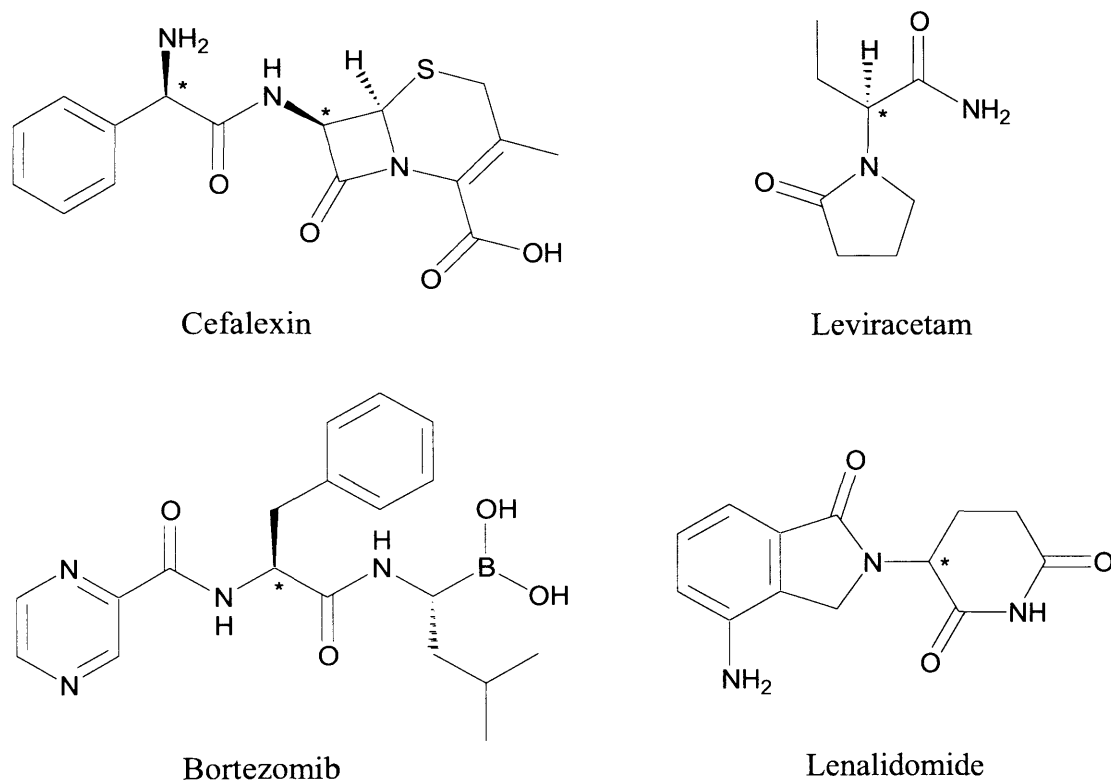
Scheme 4.3: Drugs with stereocentres alike the scaffold in Scheme 4.1.

4.2 Aims

There are 3 mains aims for this chapter.

First, to determine the rate constants of H/D exchange for the compounds illustrated in Scheme 4.1, under conditions mimicking physiological conditions. These kinetic studies will clarify whether stereogenic centres such as those in Scheme 4.1 are at risk of racemisation if administered as a drug.

Second, to understand the effect of changes in buffer concentration and temperature on the kinetics of H/D exchange. The former will inform us as to whether the process is general- or specific-base catalysed; the latter will allow determination of thermodynamic activation parameters for the H/D exchange reaction.

Third, to investigate the effects each moiety on the stereogenic centre has on configurational stability. Quantification of the effect that alterations in molecular structure have on rate constants of H/D exchange will provide information on the role of each substituent. Comparisons can also be made with the results presented in Chapter 3 for *N*-acetyl arylglycine esters. These comparisons may inform as to the mechanism by which H/D exchange occurs.

4.3 Synthesis of Compounds for Analysis

N-Substituted phenylglycine amides **6a-e**, **7a-d** and **8a-m** (Scheme 4.4) were synthesised from commercially available starting materials. Phenylglycine amides **5a-e** (Scheme 4.4) were also synthesised as intermediates.

5a-e

6a-e

7a-d

X = **a)** H, **b)** *p*-Me, **c)** *p*-F,   X = **a)** H, **b)** *p*-Me, **c)** *p*-F,   X = **a)** H, **b)** *p*-OMe,
    d) *p*-Cl, **e)** *p*-CF$_3$ **d)** *p*-Cl, **e)** *p*-CF$_3$ **c)** *p*-OCF$_3$, **d)** *p*-CF$_3$

a) X = H, Y = H   **g)** X = *p*-Me, Y = H
b) X = H, Y = *p*-Me   **h)** X = *p*-Me, Y = *m*-Cl
c) X = H, Y = *m*-Me   **i)** X = *p*-Cl, Y = H
d) X = H, Y = *p*-Cl   **j)** X = *m*-Cl, Y = *p*-Me
e) X = H, Y = *m*-Cl   **k)** X = *m*-Cl, Y = H
f) X = *p*-Me, Y = *m*-Me   **l)** X = *p*-CF$_3$, Y = H

8a-l
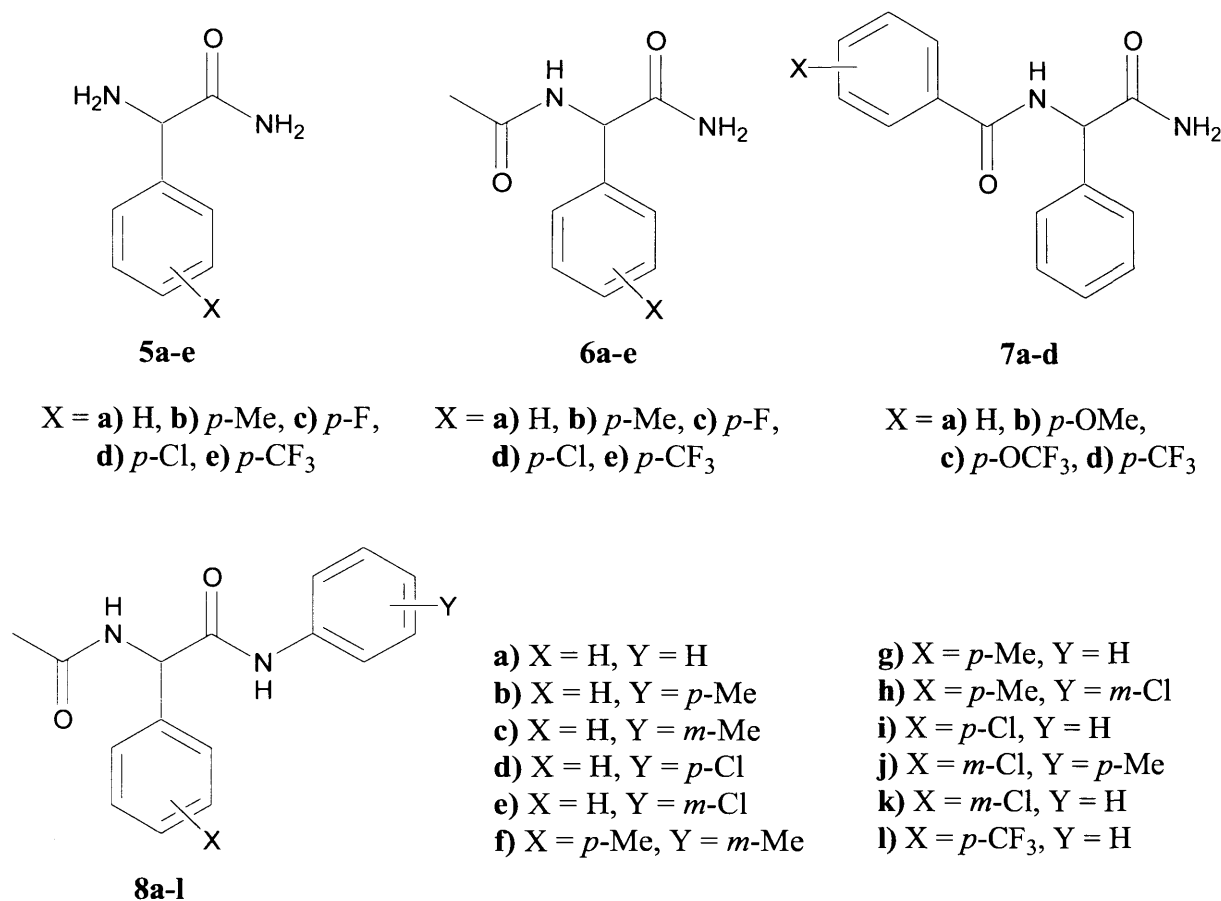
Scheme 4.4: Phenylglycine amides **6a-g**, **7a-d** and **8a-l**.

Phenylglycine amides **5a-e** were synthesised (Scheme 4.5), from the corresponding phenylglycine methyl ester hydrochlorides **2a, c-e, h** (see Chapter 3).

2a, c-e, h

5a-e
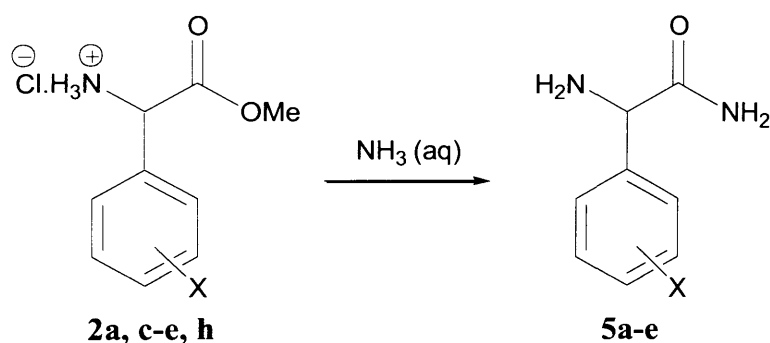
Scheme 4.5: Synthesis of phenylglycine amides **5a-e**.

N-Substituted phenylglycine amides **6a-e** and **7a-d** were then synthesised from the appropriate phenylglycine amide **5a-e**.

159
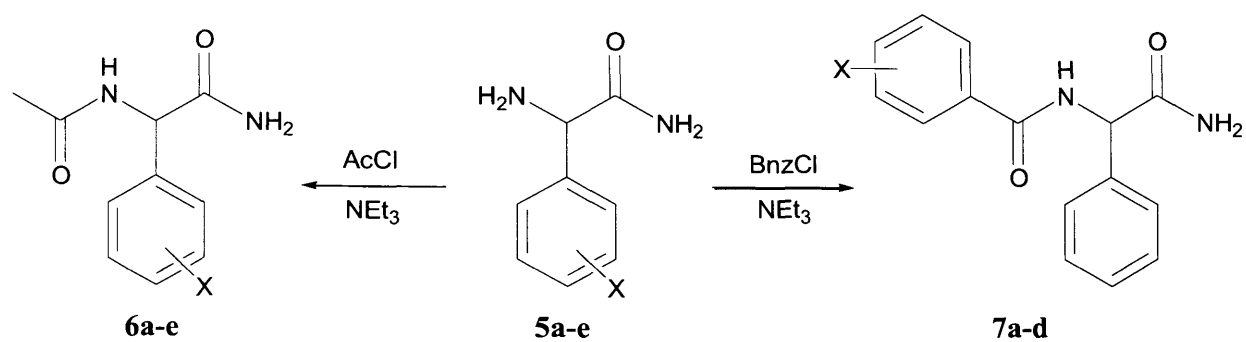
Scheme 4.6: Synthesis of *N*-substituted phenylglycine amides **6a-e**, **7a-d**.

The synthesis of *N*-acetyl phenylglycines **4a, c, e, h** was described in Chapter 3. From these, *N*-acetyl phenylglycine amides **8a-l** were synthesised (Scheme 4.7).
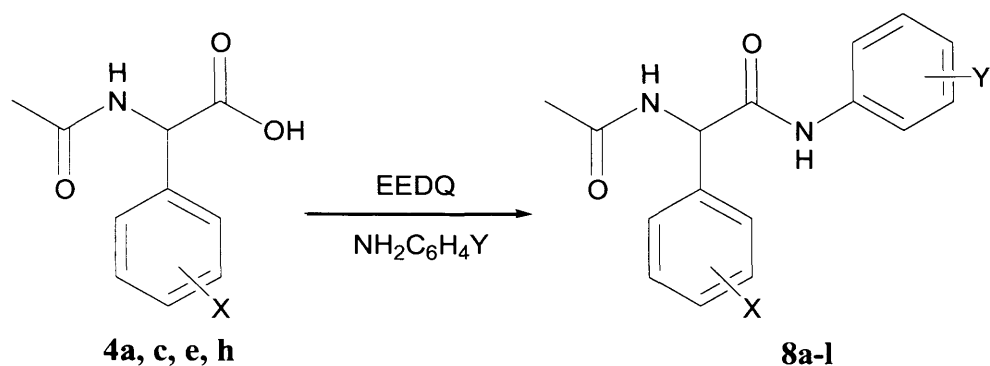
Scheme 4.7: Synthesis of *N*-substituted phenylglycine amides **8a-l**.

Details of procedures used in synthesis and characterisation of products can be found in the experimental (Section 4.6.2).

4.4 Results and Discussion

4.4.1 *N*-Acetyl Phenylglycine Primary Amides 6a-e

4.4.1.1 Initial H/D Exchange Kinetic Experiments at 37 °C

Preliminary H/D exchange studies focused on compound **6a**. The compound was dissolved in D_2O phosphate buffers, incubated at 37 °C and monitored over time using ^1H NMR spectroscopy, looking for a decrease in the normalised integration of the peak corresponding to the proton bound to the stereogenic centre (as in Chapter 3). For amide **6a** at 37 °C and pH** 7.4, H/D exchange does occur, but at a far lower rate than that observed for ester **3a** under identical conditions. The normalised integration after 28 days incubation at a variety of buffer strengths is displayed in Table 4.1.

Table 4.1: Normalised integration of **6a** after 28 days in D_2O phosphate buffers of pH** 7.4, $I = 1$ M, 37 °C.

Total buffer concentration / M	0.1	0.2	0.25	0.3
Normalised Integration	0.93	0.88	0.87	0.82

Because of the lengths of time that experiments would have to be monitored for in order to get accurate rate constants of deuteration for **6a** at 37 °C, it was deemed unfeasible to follow H/D exchange in this manner for **6a**. The only compound in the series **6a-e** for which H/D exchange occurred rapidly enough to be monitored in this manner was **6e**, as the *p*-CF_3 substituent is the most electron-withdrawing (has the highest Hammett σ constant) of those synthesised. Rate constants of H/D exchange at 37 °C for **6e** are displayed in Table 4.2.

Table 4.2: Rate constants of H/D exchange of **6e** in D_2O phosphate buffers of pH** 7.4, $I = 1$ M, 37 °C, determined by ^1H NMR spectroscopy.

phosphate conc. / M	$[HPO_4^{2-}]$ conc. / M	$k_{deut} \times 10^7 / s^{-1}$
0.1	0.061	5.05 ±0.39
0.2	0.122	8.73 ± 0.37
0.3	0.182	14.74 ± 0.43

These were plotted as a function of basic buffer component from which k_{gb} (as defined in Section 3.4.4) was determined (Figure 4.1).
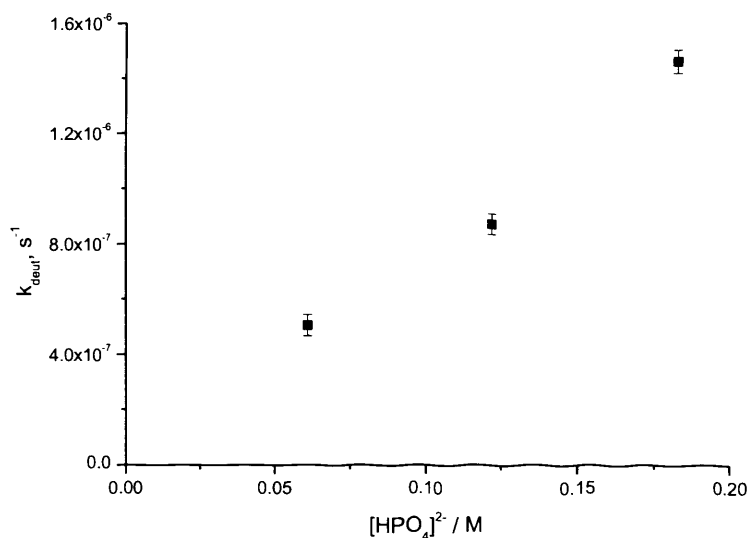
Figure 4.1: k_{deut} of **6e** at 37 °C, pH** 7.4, $I = 1$ M, plotted as a function of basic buffer component. $k_{gb} = (7.87 \pm 0.48) \times 10^{-6}\ s^{-1}$ M.

Figure 4.1 shows a slightly negative intercept with the y-axis, suggesting that there is negligible amount of specific-base catalysed or uncatalysed reaction under the conditions at which the experiments were performed. Contrasting the value of k_{gb} obtained for **6e** with that of **3h** (Chapter 3), provides a direct comparison of the effect on H/D exchange/racemisation of a methyl ester compared to a primary amide (Table 4.3).

Table 4.3: Comparison of k_{gb} at 37 °C, pH** 7.4, $I = 1$ M of compounds **3h** and **6e**.

R group	k_{gb} x 10^6 / s^{-1} M
-OMe (3h)	514.73 ± 13.00
-NH$_2$ (6e)	7.87 ± 0.48

General-base catalysis as quantified by k_{gb} for methyl ester **3h** is nearly 2 orders of magnitude more efficient than for primary amide **6e**. This difference is likely due to the propensity of the amide nitrogen to donate its lone pair, resulting in a negative charge on the carbonyl group (Section 4.1, Scheme 4.2). This also corroborates the assignment in Table 1.1 of ester groups as more strongly configurationally destabilising in comparison with amides. The observation that k_{gb} for methyl ester **3h** is nearly 2 orders of magnitude greater than for primary amide **6e** also fits with the pK_a values of carbon acids determined by Richard *et al.*[13] (Table 1.2). They

162

found that the pK_a of the α-carbon of methyl acetate was over two pK_a units lower than that of acetamide.

Because of the longer periods of time required for H/D exchange experiments of **6a-d**, it was not deemed possible to analyse them in the same way as compounds **3a-l** or **6e**. It was also impossible to analyse compounds **7a-d** and **8a-l** in this manner, as these compounds are too insoluble in D$_2$O to allow sufficient concentrations for analysis through ^{1}H NMR spectroscopy. To avoid these problems, rate constants of H/D exchange were obtained using LCMS at higher temperatures. The higher temperatures increased the rate of the reactions and the greater sensitivity of the LCMS (compared with ^{1}H NMR spectroscopy) allowed for lower concentrations of analyte to be used. As in Chapter 3, analysis was undertaken in D$_2$O phosphate buffers. The solution was monitored over time using LCMS. Deuterium-incorporation was monitored by changes in the mass spectrogram over time (see Experimental Section 4.6.3.2).

4.4.1.2 LCMS Hammett Analysis at 90 °C

Rate constants of H/D exchange for **6b**, **6d** and **6e** were determined in D$_2$O buffers of pH* 7.4† at 90 °C at a range of buffer concentrations using LCMS. Compounds **6a** and **6c** could not be analysed in the same way, as neither was sufficiently retained on the LCMS column. The greater lipophilicity of **6b**, **6d** and **6e** (as expected from Hansch π-values[14, 15]) gave retention times long enough for analysis. Details of how rate constants were obtained using the LCMS instrument are outlined in the experimental (Section 4.6.3.2). Individual kinetic traces are displayed in the Appendix. Rate constants for H/D exchange as a function of basic buffer component for compounds **6b**, **6d** and **6e** are displayed in Figure 4.2.

---

† The term 'pH*' is used in this chapter for the experiments carried out at 60, 70, 80 and 90 °C as the pH of the buffers used was corrected for temperature, so that the buffers were at the desired pH at the temperature at which experiments were carried out. See experimental (Section 4.6.3.2) for further details.
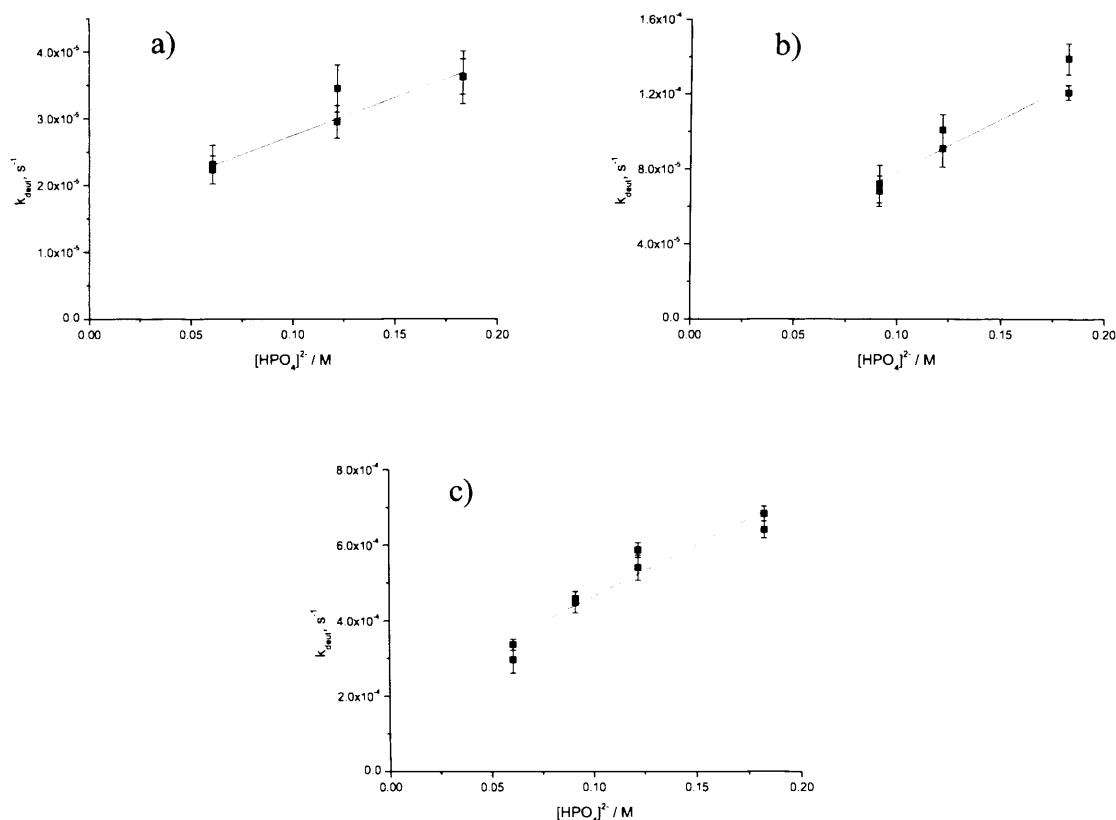
Figure 4.2: Rate constants of H/D exchange as a function of basic buffer component for a) **6b**, b) **6d**, c) **6e** in D_2O phosphate buffers of pH* 7.4, $I = 1$ M at 90 °C.

From Figure 4.2, k_{gb} and k_0' were obtained for compounds **6b**, **6d** and **6e** (Table 4.4).

Table 4.4: k_{gb} and k_0' for compounds **6b**, **6d** and **6e** in D_2O phosphate buffers of pH* 7.4, $I = 1$ M at 90 °C.

Compound	k_{gb} / $s^{-1}M^{-1}$	k_0' / s^{-1}
6b	$(1.15 \pm 0.23) \times 10^{-4}$	$(1.60 \pm 0.27) \times 10^{-5}$
6d	$(5.63 \pm 0.73) \times 10^{-4}$	$(2.24 \pm 1.15) \times 10^{-5}$
6e	$(2.73 \pm 0.16) \times 10^{-3}$	$(1.91 \pm 0.19) \times 10^{-4}$

The results displayed in Table 4.4 show that k_0' is much more significant in H/D exchange of amides **6b**, **6d** and **6e** at 90 °C, than it was for methyl esters **3a-h** or amide **6e** at 37 °C and suggests a substantial degree of specific-base catalysis by OH^- ions and/or uncatalysed reaction.

Hammett plots were constructed, correlating the values of k_{gb} displayed in Table 4.4, with both σ and σ^- substituent constants (Figure 4.3).

164
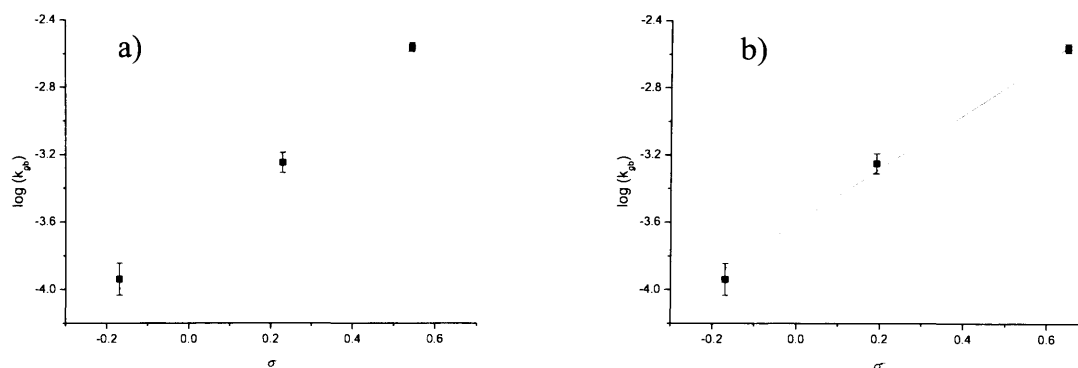
Figure 4.3: Hammett plots of k_{gb} of **6b**, **6d** and **6e** at 90 °C, pH* = 7.4, I = 1 M, fitted to a) σ constants, ρ = 2.02 ± 0.12, R^2 = 0.990 and b) σ^- constants, ρ = 1.61 ± 0.10, R^2 = 0.992.

Figure 4.3 shows that the values determined for k_{gb} correlate reasonably well with both σ and σ^- values. As in the case of the methyl esters (Section 3.4.6), distinguishing between the two sets of substituent constants is difficult as none of the substituents analysed have drastically different σ and σ^- values, leaving little difference between graphs. This similarity between substituent constants results in similar ρ values for both sets of substituent constants. These ρ values are compared with those found for methyl ester compounds **3a-h** in Table 4.5.

Table 4.5: ρ values determined from k_{gb} of **6b, d, e** at 90 °C and **3a-h** at 37 °C, pH* = 7.4, I = 1 M (from Figure 3.4).

Series	σ	σ^-
6b, d, e	2.02 ± 0.12	1.61 ± 0.10
3a-h	2.50 ± 0.03	2.07 ± 0.02

It should be noted that the ρ values for the two series displayed in Table 4.5 were determined at different temperatures. As discussed in Section 1.8.2.1.2, reaction constants have been observed to be temperature dependent. Eqn 1.18 suggests ρ values are dependent on T^{-1}. This temperature dependence is a potential explanation for the greater magnitude of ρ determined for the series **3a-h**, and suggests that a greater ρ value would be obtained for **6b, d, e** if the experiments were to be carried out at 37 °C. However, as discussed in Section 1.8.2.1.2, a definitive relationship between ρ and T^{-1} has not been conclusively proven. In any case, assuming that ρ would be equal for **6b, d, e** and **3a-h** at a specific temperature seems unwise.

Ignoring the effect of temperature, it would generally be expected that the magnitude of ρ for the primary amides would be higher than that seen for the methyl esters. As discussed in

Section 4.1 and illustrated in Scheme 4.2, electron-pair donation by the amide nitrogen results in a substantial negative charge build up on the carbonyl oxygen. This means that a negative charge built up on the stereogenic centre of **6b, d, e** during H/D exchange cannot be stabilised through delocalisation onto the carbonyl oxygen as much as it can for **3a-h**. As a result it would be expected that the stabilising effect of the aromatic group would be more important for H/D exchange of **6b, d, e** than for **3a-l**, and larger ρ values would be seen. An increased dependence on the aromatic group for stabilisation is the proposed cause for the large magnitude of ρ = 3.58 seen for profen thioesters, as discussed in Section 3.4.6 (Scheme 3.9).[16]

The ρ value of 1.61, from k_{gb} values of **6b, d, e** (using σ^- constants) at 90 °C, sits between the ρ values of 2.07 and 1.15 determined from k_{gb} values of **3a-h** (using σ^- constants) at 37 °C and for the racemisation of phenylglycines at 80 °C (Smith and Sivakua[17]) respectively. In both of the latter cases, an S_E1 mechanism was concluded based on equivalent rate constants of racemisation and H/D exchange (see Section 1.3). These ρ values and the similarities in molecular structure between the three sets of compounds suggest that an S_E1 mechanism is also likely for H/D exchange of **6b, d, e**. Computational studies providing further evidence towards this conclusion will be presented in Chapter 5.

4.4.1.3 Determination of Thermodynamic Activation Parameters for H/D Exchange Reactions of 6e

In order to determine the activation energy and pre-exponential factor according to the Arrhenius equation (Section 1.9.1), and enthalpy and entropy of activation according to the Eyring equation (Section 1.9.2) for the general-base catalysed H/D exchange of **6e**, k_{gb} was determined at 60, 70 and 80 °C using the LCMS method. These rate constants were combined with the values of k_{gb} determined at 90 °C using the LCMS method and the rate constant at 37 °C using the ^{1}H NMR spectroscopic method to produce Arrhenius and Eyring plots, which were used to obtain the activation parameters. Rate constants of H/D exchange as a function of basic buffer component for compound **6e** at 60, 70 and 80 °C are displayed in Figure 4.4.
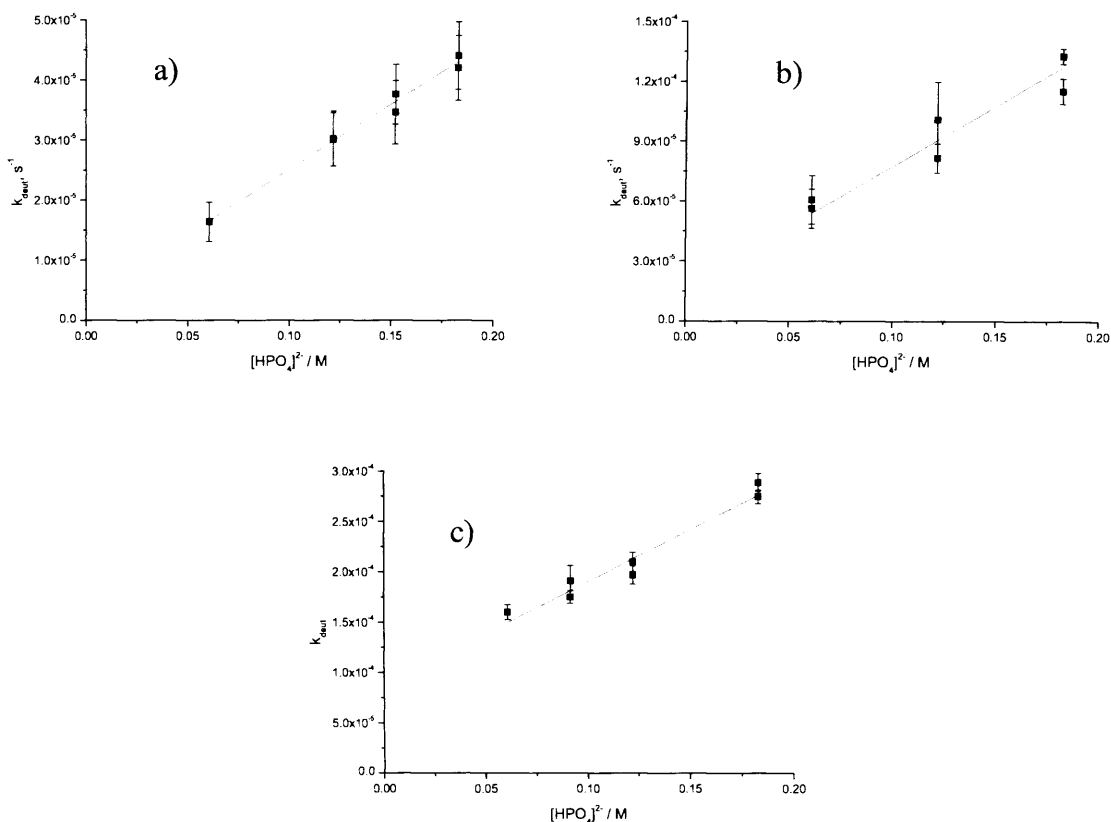
Figure 4.4: Rate constants of H/D exchange as a function of basic buffer component for **6e** in D_2O phosphate buffers of pH* 7.4, $I = 1$ M at a) 60 °C, b) 70 °C and c) 80 °C.

The values of k_{gb} and k_0' determined for **6e** from Figure 4.4 along with those determined at 37 and 90 °C are displayed in Table 4.6.

Table 4.6: values of k_{gb} and k_0' for **6e** in D_2O phosphate buffers of pH** 7.4, $I = 1$ M.

Temperature / °C	k_{gb} / $s^{-1}M^{-1}$	k_0' / s^{-1}
37	$(7.87 \pm 0.48) \times 10^{-6}$	$(-1.23 \pm 6.10) \times 10^{-8}$
60	$(2.19 \pm 0.39) \times 10^{-4}$	$(3.20 \pm 5.11) \times 10^{-6}$
70	$(6.05 \pm 0.64) \times 10^{-4}$	$(1.72 \pm 1.04) \times 10^{-5}$
80	$(1.04 \pm 0.07) \times 10^{-3}$	$(8.61 \pm 0.88) \times 10^{-5}$
90	$(2.73 \pm 0.16) \times 10^{-3}$	$(1.91 \pm 0.19) \times 10^{-4}$

An Arrhenius plot of the data in Table 4.6 is shown in Figure 4.5.
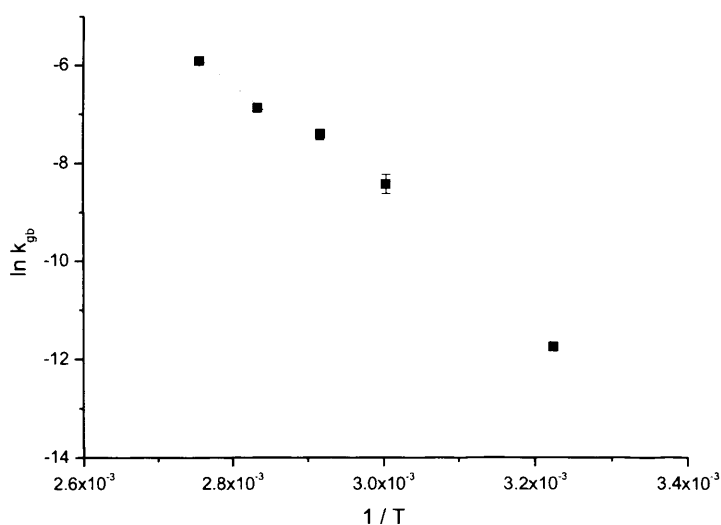
Figure 4.5: Arrhenius plot for general-base catalysed H/D exchange of **6e**, in D_2O phosphate buffers at pH* 7.4, $I = 1$ M. y-axis intercept $= \ln A = 28.38 \pm 1.44$. Gradient $= -E_a/R = -12428.02 \pm 490.636$ K.

From the intercept and gradient of Figure 4.5, an activation energy (E_a) of 103.33 ± 4.08 kJ mol^{-1} and a pre-exponential factor (A) of 2.12×10^{12} s^{-1} M^{-1} (min 5.01×10^{11} s^{-1} M^{-1}, max 8.98×10^{12} s^{-1} M^{-1}) were determined for general-base catalysed H/D exchange of **6e**.

An Eyring plot of the data in Table 4.6 is displayed in Figure 4.6.
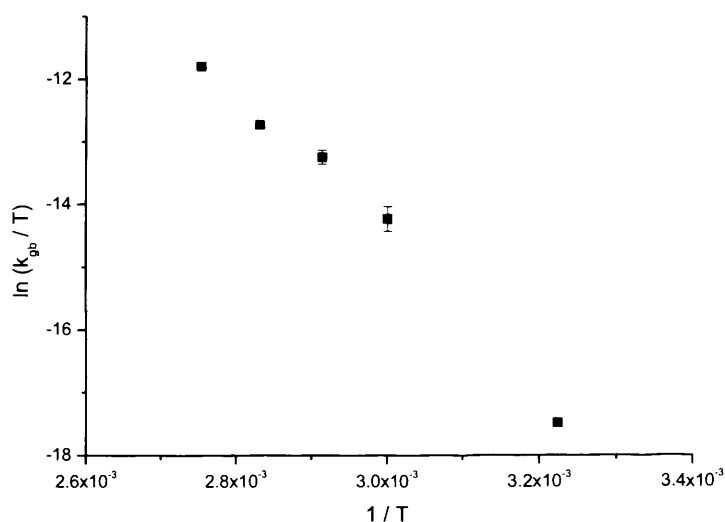
Figure 4.6: Eyring plot of general-base catalysed H/D exchange of **6e**, in D_2O phosphate buffers at pH* 7.4, $I = 1$ M. y-axis intercept $= \ln (k_B/h) + \Delta S^{\ddagger}/R = 21.57 \pm 1.45$. Gradient $= -\Delta H^{\ddagger}/R = -12094.01 \pm 492.97$ K.

From the intercept and gradient of Figure 4.6, an enthalpy of activation ($\Delta H^{\ddagger}$) of 100.55 $\pm$ 4.10 kJ mol^{-1} and entropy of activation ($\Delta S^{\ddagger}$) of -18.21 $\pm$ 12.06 J K^{-1} mol^{-1} for general-base catalysed H/D exchange of **6e** were determined.

It is notable that the percentage error margins on the value determined for A from Figure 4.5 and $\Delta S^{\ddagger}$ from Figure 4.6 are both very large. This is because each value was obtained from the intercept with the y-axis, which involves a relatively long extrapolation from a small cluster of points. This long extrapolation magnifies any error in the calculation. As an alternative, both A and $\Delta S^{\ddagger}$ were calculated at each individual data point using the values of E_a and $\Delta H^{\ddagger}$ calculated from Figure 4.5 and Figure 4.6 respectively by substituting into eqn (1.23) and (1.26). These values are summarised in Table 4.7.

Table 4.7: A and $\Delta S^{\ddagger}$ calculated at individual data points, using the values of E_a and $\Delta H^{\ddagger}$ determined from Figure 4.5 and Figure 4.6.

T / °C	k_{gb} / s^{-1} M^{-1}	A / s^{-1} M^{-1}	$\Delta S^{\ddagger}$ / J K^{-1} mol^{-1}
37	$(7.87 \pm 0.48) \times 10^{-6}$	1.97×10^{12}	-18.86
60	$(2.19 \pm 0.39) \times 10^{-4}$	3.44×10^{12}	-14.17
70	$(6.05 \pm 0.64) \times 10^{-4}$	3.21×10^{12}	-14.76
80	$(1.04 \pm 0.07) \times 10^{-3}$	1.98×10^{12}	-18.79
90	$(2.73 \pm 0.16) \times 10^{-3}$	1.97×10^{12}	-18.83

Table 4.7 shows that calculated A and $\Delta S^{\ddagger}$ values are very similar for experiments at 37, 80 and 90 °C. These are the data points with the smallest error margins from the original experiments and hence should be the most accurate values for A and $\Delta S^{\ddagger}$. Using these values gives $\Delta S^{\ddagger}$ = -17.08 $\pm$ 2.40 J K^{-1} mol^{-1} (errors calculated from standard deviation).

It is of interest to compare the activation parameters for general-base catalysed H/D exchange of **6e** to other examples. Some values of $\Delta H^{\ddagger}$ and $\Delta S^{\ddagger}$ for racemisation reactions thought to proceed through similar mechanism are listed in Table 4.8, 4.9 and 4.10.

Table 4.8: Activation parameters for racemisation of amino acids by Smith *et al.*[17, 18]

Amino Acid	$\Delta H^{\ddagger}$ / kJ mol^{-1}	$\Delta S^{\ddagger}$ / J K^{-1} mol^{-1}
alanine	115.5 ± 2.5	-78.2 ± 5.4
valine	116.6 ± 1.3	-85.4 ± 2.9
isoleucine	113.4 ± 2.5	-90.4 ± 5.9
leucine	114.2 ± 2.1	-84.5 ± 4.6
phenylalanine	97.1 ± 0.8	-117.2 ± 2.1
phenylglycine	83.3 ± 0.0	-121.3 ± 0.4
m-nitrophenylglycine	84.1 ± 0.4	-102.5 ± 1.7
m-chlorophenylglycine	83.3 ± 1.3	-110.9 ± 3.8
p-chlorophenylglycine	82.0 ± 1.3	-118.8 ± 3.3
p-methylphenylglycine	85.4 ± 0.4	-118.4 ± 1.3
p-methoxyphenylglycine	84.9 ± 0.4	-120.9 ± 1.3

Table 4.9: Activation parameters for racemisation of 5-monosubstituted hydantoins from Reist *et al.*[19]

Hydantoin C(5) Substituent	$\Delta H^{\ddagger}$ / kJ mol^{-1}	$\Delta S^{\ddagger}$ / J K^{-1} mol^{-1}
-Ph	72.3 ± 4.0	-68.2 ± 5.0
-CH$_2$OH	76.7 ± 2.8	-86.6 ± 4.6
-NHONH$_2$	94.1 ± 2.1	-39.3 ± 1.3
-CH$_2$Ph	94.3 ± 2.5	-43.1 ± 1.7
-CH$_3$	85.3 ± 2.1	-77.0 ± 2.9
-CH$_2$COOH	98.4 ± 3.2	-42.3 ± 2.1
-CH(CH$_3$)$_2$	80.7 ± 3.0	-105.4 ± 6.7

Table 4.10: Activation parameters for general-base catalysed racemisation of *N*-substituted 5-benzylhydantoins by phosphate buffer at pH 7.2.[20]

Hydantoin *N*- Substituent	$\Delta H^{\ddagger}$ / kJ mol^{-1}	$\Delta S^{\ddagger}$ / J K^{-1} mol^{-1}
-CH$_3$	83.7 ± 0.8	-55.2 ± 2.9
-CH$_2$CH$_2$OCH$_3$	87.9 ± 2.9	-44.8 ± 10.0
-CH$_2$CH$_2$N$^+$(CH$_3$)$_3$	93.7 ± 2.1	-13.4 ± 6.7

It should be noted that the values in Table 4.8 and 4.9 appear to have been calculated from k_{obs} at a single buffer concentration, rather than from the second-order rate constants obtained from the gradient of k_{obs} plotted against buffer concentration. This means that the results have not been normalised to a standard state concentration of 1 mol L^{-1}, and this will result in an incorrect entropy of activation. If an extent of specific-base catalysis contributes to the overall rate constant as well, the problem is made worse as the enthalpy of activation is a combination of two separate reactions (specific- and general-base catalysed).

The values determined for $\Delta H^{\ddagger}$ for H/D exchange of **6e** are of similar magnitude to those displayed in Table 4.8, 4.9 and 4.10. This value is indicative of bond breaking being important in the rate-determining step, which is consistent with an S$_E$1 mechanism.

The negative value of $\Delta S^{\ddagger}$ seen for **6e** is to be expected, as bringing molecules together for reaction reduces the degrees freedom. Increased solvation (and hence negative $\Delta S^{\ddagger}$) from the formation of a negative charge is counterbalanced by the dispersal of the doubly negative charge from the phosphate ion. However, the value determined for $\Delta S^{\ddagger}$ of H/D exchange of **6e** seems remarkably small in comparison with those in Table 4.10.

The entropies of activation in Table 4.10 for N-substituted 5-benzylhydantoins have been corrected in the same manner as for **6e**. Of the three entries displayed in Table 4.10, the quaternary amine substituted hydantoin has a less negative value of $\Delta S^{\ddagger}$ than the other entries. This is thought to be partially because of intramolecular stabilisation of a negative charge built up during H/D exchange by the positively charged amine, but mainly due to solvation differences. As there is already a positive charge on the hydantoin the solvation shell is already tightly ordered, meaning less reorganisation necessary upon deprotonation at the stereogenic centre and hence a smaller $\Delta S^{\ddagger}$. The value of -13.4 J K^{-1} mol^{-1} observed for the quaternary amine substituted hydantoin is the most similar to that observed for **6e**. As no such positive charge exists in **6e** it would be expected to exhibit a $\Delta S^{\ddagger}$ closer to those displayed by the N-methyl and N-ethyl methoxy substituted hydantoins in Table 4.10. The differences between these values and that determined for **6e** may be due to the extent to which proton transfer is complete in the activated complex. One manner in which this could be resolved is through determination and comparison of the Brønsted β-coefficients.

4.4.1.4 High Temperature Kinetic Experiments as a Predictive Tool for Physiological Temperatures

Alongside its use in the determination of thermodynamic activation parameters, the data in Table 4.6 can be used to assess the potential for using experiments at high temperatures as a guide for potential configurational instability under physiological conditions. If accurate predictions of unknown rate constants of H/D exchange at physiological temperatures could be made based on high temperature experiments, experimentation on a potential drug molecule could be carried out at higher temperatures, giving results more quickly and the process of analysis more amenable.

An Eyring plot for H/D exchange of **6e**, with the data point at 37 °C omitted, was constructed. The extrapolated line of best fit was used to make a 'prediction' for the value of k_{gb} at 37 °C, giving a 'predicted' k_{gb} at 37 °C of 2.39 x 10^{-5} s^{-1} M^{-1}. The experimental k_{gb} at 37 °C is (7.87 ± 0.48) x 10^{-6} s^{-1} M^{-1}.

The 'predicted' value of k_{gb} is approximately 3 times higher than the experimentally determined value. Although this is not particularly accurate, it is within an order of magnitude. This type of approximation could therefore be of use in drug development to determine whether a molecule may be of a high risk of being configurationally unstable under physiological conditions.[‡]

4.4.2 *N*-Acetyl Phenylglycine Anilides 8a-l

Compounds **8a-l** (Scheme 4.8) were also studied using LCMS to obtain rate constants of H/D exchange.

[‡] As discussed in Section 4.4.1.2, k_{deut} values determined at 90 °C include a substantial degree of specific base-catalysis by OH⁻ ions and/or uncatalysed reaction not observed at 37 °C. Therefore, extrapolation to predict rate constants of H/D exchange at high temperature from experimental data obtained at 37 °C will exclude any contribution from k_0', and hence is unlikely to be accurate.

8a-l

Scheme 4.8: Phenylglycine amides **8a-l**.

Because of the number of compounds to analyse, it was not possible to analyse these compounds at a range of different buffer concentrations, as was done for **6b, d, e**. Therefore, each compound **8a-l** was only analysed at a single buffer concentration and temperature. Data for all experiments are collected in the appendix. The results for each compound are summarised in Table 4.11.

Table 4.11: Rate constants for H/D exchange of **8a-l** in D_2O 0.3 M phosphate buffers, pH* 7.4, I = 1 M at 90 °C, determined by LCMS analysis.

Compound	X-substituent	Y-substituent	k_{deut} / s^{-1} [a]
8a	-	-	$(5.45 \pm 0.25) \times 10^{-5}$
8b	-	p-Me	$(3.32 \pm 0.35) \times 10^{-5}$
8c	-	m-Me	$(4.24 \pm 0.69) \times 10^{-5}$
8d	-	p-Cl	$(6.41 \pm 0.43) \times 10^{-5}$
8e	-	m-Cl	$(8.86 \pm 0.25) \times 10^{-5}$
8f	p-Me	m-Me	$(2.22 \pm 0.46) \times 10^{-5}$
8g	p-Me	-	$(2.61 \pm 0.44) \times 10^{-5}$
8h	p-Me	m-Cl	$(4.54 \pm 0.25) \times 10^{-5}$
8i	p-Cl	-	$(1.18 \pm 0.05) \times 10^{-4}$
8j	m-Cl	p-Me	$(1.44 \pm 0.04) \times 10^{-4}$
8k	m-Cl	-	$(2.12 \pm 0.04) \times 10^{-4}$
8l	p-CF$_3$	-	$(6.00 \pm 0.52) \times 10^{-4}$

[a] average of two experiments

Because experiments were only carried out at one buffer concentration, it is not possible to separate out rate constants for general- and specific- base catalysis. As a result, comparisons

between the values should be made with care. Nevertheless, a Hammett analysis of the data in Table 4.11 is still of interest.

4.4.2.1 Hammett Analysis of Phenylglycine Aromatic Substituents

Hammett plots of the data displayed in Table 4.11 for compounds **8a**, **8g**, **8i**, **8k** and **8l** (varying substituents on phenylglycine ring, no substituents on aniline ring) were constructed, using both σ and σ^- substituent constants (Figure 4.7).
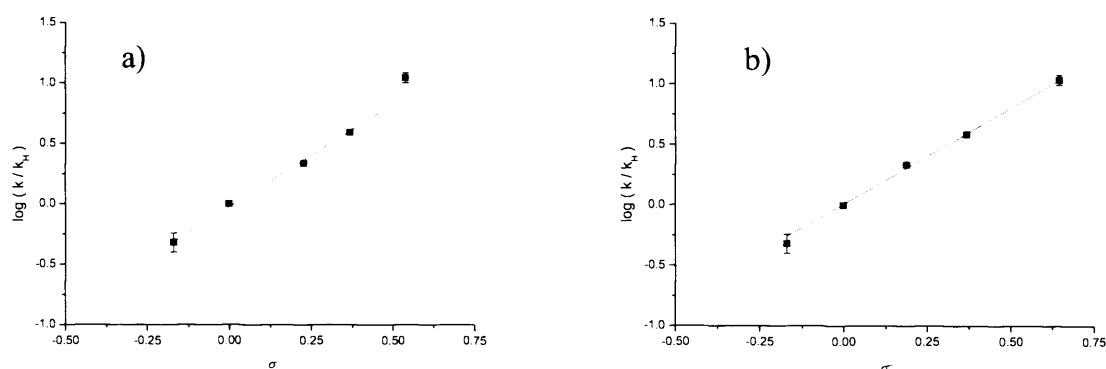
Figure 4.7: Hammett plots of k_{deut} for compounds **8a**, **8g**, **8i**, **8k** and **8l** determined at 0.3 M phosphate concentration, pH* 7.4, I = 1 M, 90 °C, correlated with a) σ substituent constants, ρ = 1.69 ± 0.14, R^2 = 0.975 and b) σ^- substituent constants, ρ = 1.58 ± 0.05, R^2 = 0.997.

Figure 4.7 shows that the data in Table 4.1 correlates reasonably well with both σ and σ^- substituent constants. Again, the small differences between σ and σ^- for the substituents available make distinguishing between the two sets of substituent constants difficult. Nevertheless, both the size of the error margin of ρ and the R^2 values suggest a slightly better correlation with the σ^- substituent constants. A better correlation with σ^- is consistent with negative charge being built up on the carbon at the stereogenic centre, where it can be directly resonance-delocalised onto the Hammett substituent.

The value of ρ of 1.58 found for k_{deut} of **8a**, **g**, **i**, **k**, **l** is very similar to that of 1.61 found from k_{gb} of **6b**, **d**, **e** suggesting a similar mechanism of H/D exchange between the two sets of compounds. Hence, the S_E1 mechanism is the probable mechanism of H/D exchange of **8a**, **g**, **i**, **k**, **l**.

4.4.2.2 Hammett Analysis of Aniline Aromatic Substituents

A Hammett plot was also constructed for the H/D exchange reaction of compounds **8a-e**. In all five of these compounds the phenylglycine ring remains unsubstituted, whilst the substituent on the aniline ring is varied. This provides an indication as to the amount of stabilisation of negative charge provided by the aniline aromatic group. As no direct resonance delocalisation of a negative charge built up on the stereogenic centre onto substituents on the aniline ring is possible, the data was only correlated with Hammett σ constants (Figure 4.8).
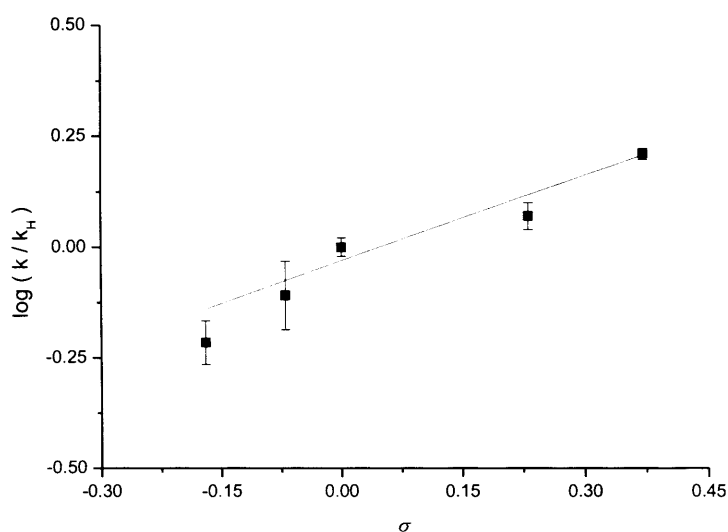
Figure 4.8: Hammett plot of k_{deut} for compounds **8a-e**, at 0.3 M phosphate concentration, pH* 7.4, I = 1 M, 90 °C. ρ = 0.65 ± 0.09, R^2 = 0.933.

Figure 4.8 shows that the Hammett ρ value for H/D exchange of **8a-e** is significantly lower than that seen for the series **8a, g, i, k, l**. The difference in ρ values is attributed to the number of bonds between the site of H/D exchange and the aromatic group upon which the substituents are being varied. The position of the aromatic ring with substituents in the series **8a-e** is three bonds away from the reaction site, as opposed to only one bond in the series **8a, g, i, k, l**, meaning the transmission of any electronic effect is attenuated. This results in the lower observed ρ value (*cf.* Section 1.8.2.1.1, Table 1.7).

The ρ value of 0.65 obtained for H/D exchange of the series is of a similar magnitude to other examples where the reaction site is more than one bond away from the substituted aromatic ring, and is not in direct conjugation. Some examples are shown in Table 4.12.

Reaction [a]	Conditions	p
$ArCH_2COOC_2H_5 + OH^- \rightarrow ArCH_2COO^-$	88 % EtOH, 30 °C	0.82
$ArCH_2CH_2COOC_2H_5 + OH^- \rightarrow ArCH_2CH_2COO^-$	88 % EtOH, 30 °C	0.49
$ArCH_2Cl + I^- \rightarrow ArCH_2I$	Acetone, 20 °C	0.79
$ArCH_2F + OH^- \rightarrow ArCH_2OH$	95 % EtOH, 76 °C	0.45

[a] $Ar = X\text{-}C_6H_4\text{-}$ where X is the variable substituent

The values of $p < 1$ in the examples shown in Table 4.12 and in the H/D exchange of **8a-e**, suggests that the amount of negative charge delocalised onto the aromatic ring in these examples is less than that found in the dissociation of benzoic acids.

Transmission of electron-withdrawing effects through a secondary amide bond in the manner shown for **8a-e** has been observed through ^1H, ^{13}C and ^{15}N NMR spectroscopy.[22-24] Electron-withdrawing substituents on the anilide ring in benzanilides cause an upfield chemical shift of the proton and carbon signals of the acyl aromatic group in good agreement with Hammett σ values.

The effect of varying substitution patterns on the aromatic ring of anilide compounds was investigated by Bergon and Calmon[25] on the rate constants of hydrolysis of methyl carbanilates at 25 °C (Scheme 4.9).
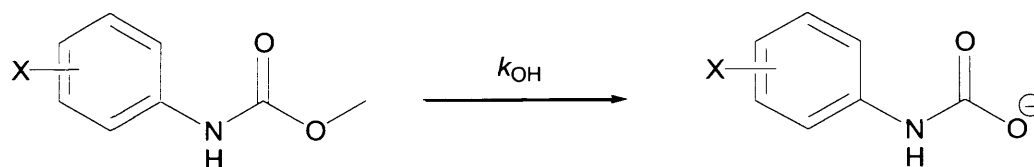
Scheme 4.9: Alkaline hydrolysis of methyl carbanilates.

A p value of 1.06 was determined for electron-withdrawing X-substituents in the reaction depicted in Scheme 4.9. This contrasts with the value of 0.65 determined for H/D exchange of **8a-e**, which also shows transmission of the electronic effect through the nitrogen atom of an anilide group. The greater value determined for the reaction in Scheme 4.9 is likely because the site of reaction is the carbonyl carbon, whereas for H/D exchange of **8a-e** the reaction site is the α-carbon.

4.4.2.3 Dual Parameter Analysis

A 3D Hammett plot of the data in Table 4.11 was constructed (Figure 4.9), with X-substituents correlated with σ^- constants and Y-substituents correlated with σ constants.
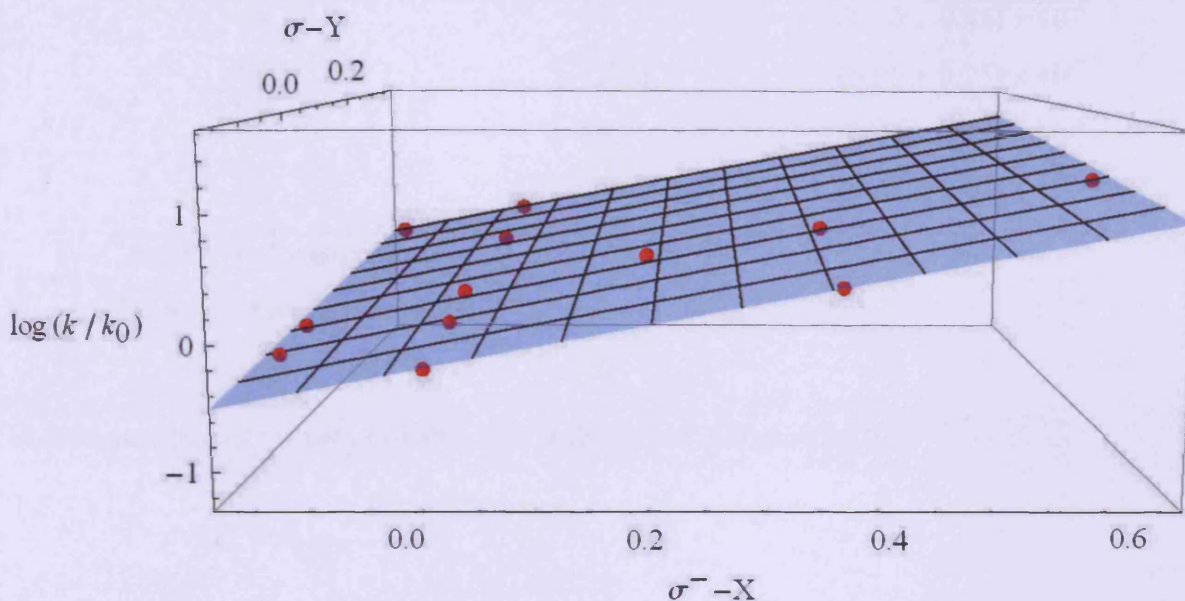
Figure 4.9: Hammett plot of k_{deut} for compounds **8a-l** determined at 0.3 M phosphate concentration, pH* 7.4, $I = 1$ M, 90 °C. X-substituents correlate with σ^- constants; Y-substituents correlate with σ constants. $\rho = (1.69 \pm 0.05)x + (0.71 \pm 0.06)y$.

Figure 4.9 shows a good correlation with the Hammett substituent constants in both the X- and Y-positions for **8a-l**. The magnitude of the slopes in both the X- and Y-directions of Figure 4.9, are similar to the ρ values determined in Figure 4.7 and Figure 4.8. The good fit to the data using a two-parameter fit suggests there is no need for a cross-interaction term (Section 1.8.2.3). We note, however, that the absence of a requirement for a cross-interaction term may be because there is not a great range in the values of the substituent constants in either the X- or Y- direction.

4.4.3 *N*-Benzoyl Phenylglycine Amides 7a-d

The LCMS method was also used to obtain rate constants for H/D exchange of **7a-d**. As with **8a-l**, each compound was only analysed at a single buffer concentration and temperature. Individual plots are displayed in the appendix. The results for each compound are displayed in Table 4.13.

Table 4.13: Rate constants of H/D exchange of **7a-d** in D_2O phosphate buffers of concentration 0.3 M, pH* 7.4, I = 1 M at 90 °C, determined by LCMS analysis.

Compound	Y-substituent [a]	k_{deut} / s^{-1} [b]
7a	-	$(6.50 \pm 0.45) \times 10^{-5}$
7b	p-OMe	$(5.06 \pm 0.25) \times 10^{-5}$
7c	p-OCF$_3$	$(8.05 \pm 0.58) \times 10^{-5}$
7d	p-CF$_3$	$(9.89 \pm 0.47) \times 10^{-5}$

[a] benzoyl ring substituent

[b] average of two experiments

A Hammett plot of the data in Table 4.13 is displayed in Figure 4.10.
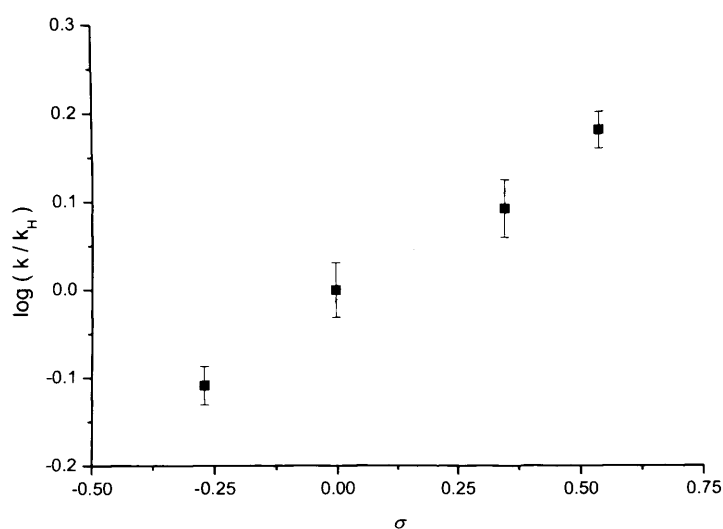
Figure 4.10: Hammett plot of k_{deut} for **7a-d** determined at 0.3 M phosphate concentration, pH* 7.4, I = 1 M, 90 °C. ρ = 0.35 ± 0.02, R^2 = 0.992.

The Hammett analysis of **7a-d** in Figure 4.10 shows a ρ value of 0.35. As with compounds **8a-e**, this value reflects the number of bonds between the negative charge and the aromatic substituent. The ρ value of 0.35 for **7a-d**, is less than the ρ value of 0.65 for **8a-e** (Figure 4.8). This suggests that a negative charge is less well transmitted through a secondary amide bond if it is orientated with the nitrogen bound to the site of negative charge build up.

4.4.4 Steric and Electronic Effects

Comparison of the rate of H/D exchange between molecular scaffolds **6** and **8** shows an interesting result. In Section 3.4.7, the rate constants of H/D exchange for **3a**, **3i** and **3j** were compared. It was found that increasing the size of the ester group markedly reduced the rate constants of H/D exchange (and hydrolysis). This was attributed to increasing steric hindrance preventing the general base from attacking the stereogenic centre. A similar effect was expected for the comparison of k_{deut} between amides **6e** and **8l**, which are the same except for the nature of the amide group (primary in **6e**, substituted with a phenyl group in **8l**). However, comparison between **6e** and **8l** shows similar rate constants under identical conditions (Table 4.14).

Table 4.14: Comparison of k_{deut} for **6e** and **8l** at 90 °C, in 0.3 M D_2O phosphate buffers of pH* 7.4, $I = 1$ M.
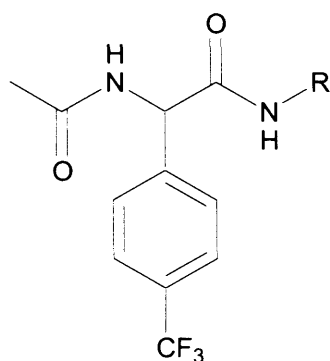
R group	$k_{deut} \times 10^4 / s^{-1}$
-H (**6e**)	6.62 ± 0.21
-C_6H_5 (**8l**)	6.00 ± 0.52

The values of k_{deut} in Table 4.14 are the same within error margins. This is somewhat surprising in light of the result mentioned earlier for the different ester compounds, as a bulky phenyl group on the amide would provide far more steric hindrance than the esters investigated. If this steric hindrance is present, it would suggest that the phenyl amide substituent present in **8l** is significantly more configurationally destabilising than the primary amide in **6e**, cancelling its rate-retarding steric effect. If this is the case, this may be due to the difference in resonance delocalisation between the two groups.

Delocalisation of the amide nitrogen lone pair onto the carbonyl oxygen will restrict any negative charge developing on the stereogenic centre during H/D exchange being delocalised onto the carbonyl oxygen (Scheme 4.2). This is a potential reason for the lower rates of racemisation seen when an ester group is replaced by an amide, and thus for the different classifications of amide and ester groups by Testa *et al.* (Table 1.1). However, for a phenyl-substituted amide the nitrogen lone-pair can be delocalised onto the phenyl ring (Scheme 4.10).
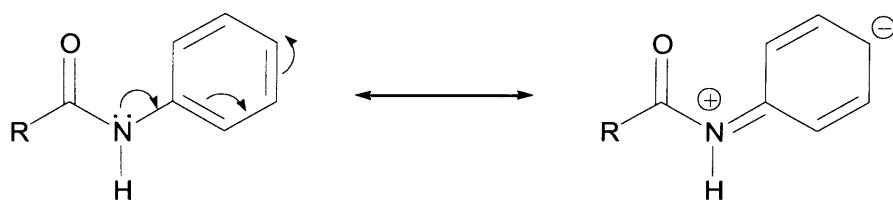
Scheme 4.10: Delocalisation of a phenyl amide nitrogen lone-pair onto aromatic ring.

The delocalisation shown in Scheme 4.10 will mean less negative charge build up on the carbonyl oxygen, allowing for greater stabilisation of any negative charge built up on the stereogenic centre during H/D exchange. It appears to be the case that the decrease in configurational stability from these electronic factors offsets the increase in configurational stability from steric hindrance. This results in similar rate constants of H/D exchange for primary amide substituted **6e** and phenyl amide substituted **8l**.

4.5 Conclusions

Rate constants for H/D exchange and hydrolysis of compounds **6b, d, e, 7a-d** and **8a-l** have been determined under aqueous conditions in phosphate buffers. Analysis of this data and comparison with the results and conclusions from Chapter 3, suggest the following conclusions.

First, rate constants of H/D exchange for compounds with an amide substituent on the stereogenic centre are much lower than those for analogous compounds with an ester substituent on the stereogenic centre. This supports the assignments of Testa *et al.* (Table 1.1), that designate an ester group as a stronger configurationally destabilising substituent than an amide. The low rate of H/D exchange for compounds **6a-e** at physiological pH and temperature suggests that stereogenic centres such as these are not at high risk of undergoing racemisation in the body under pharmacological timescales. However, the magnitude of the rate constants of H/D exchange for **6a-e** may be important in the synthesis or shelf-life of a drug based on a similar scaffold.

Second, evidence suggests that the mechanism of H/D exchange for the compounds analysed in this chapter is the S_E1 mechanism. Hammett analysis of **6b, d, e** and **8a, g, i, k, l** shows similar levels of negative charge built up on the reaction centre during H/D exchange as seen for **3a-l** in Chapter 3, for which an S_E1 mechanism was deduced. Similarly, the thermodynamic activation parameters calculated for **6e** are consistent with the S_E1 mechanism when compared to literature values.

Third, Arrhenius and Eyring plots of H/D exchange data for **6e** have shown the potential for high-temperature work to be used for rapid screening to obtain approximate information on configurational instability at lower temperatures.

Fourth, Hammett analysis of compounds **7a-d** and **8a-l** illustrates how substituents several bonds away from the stereogenic centre can still have a large influence over the rate constant for H/D exchange.

4.6 Experimental

4.6.1 General Experimental

All reagents were purchased from Acros Organics, Alfa Aesar, Fluorochem or Sigma-Aldrich. ^{1}H NMR and ^{13}C NMR spectra were recorded on a Bruker DPX 400 or DPX 500 spectrometer. HMBC and HSQC experiments were used on the same spectrometers to confirm assignments when necessary. δ values are reported in ppm downfield from trimethylsilane. LCMS experiments were performed using a Waters 2790 liquid chromatograph and a Waters ZQ mass spectrometer. Samples were loaded using a Gilson 232XL autosampler. Mass spectrometry data was processed using Waters MassLynx software and Waters QuanLynx software was used to analyse the data. Infrared spectra were obtained using a Varian 7000 FT-IR spectrometer. Samples were applied directly to the diamond tip. High-resolution mass spectra were obtained on a Waters LCT Premier XE mass spectrometer.

4.6.2 Synthesis of Compounds

4.6.2.1 Synthesis of Phenylglycine Amides 5a-e

Compounds **5a-e** were synthesised from the appropriate phenylglycine methyl ester hydrochloride salts **2a-l**, the synthesis of which was described in the experimental to Chapter 3. The method was adapted from that used by Noorduin *et al.* (Scheme 4.11).[26]
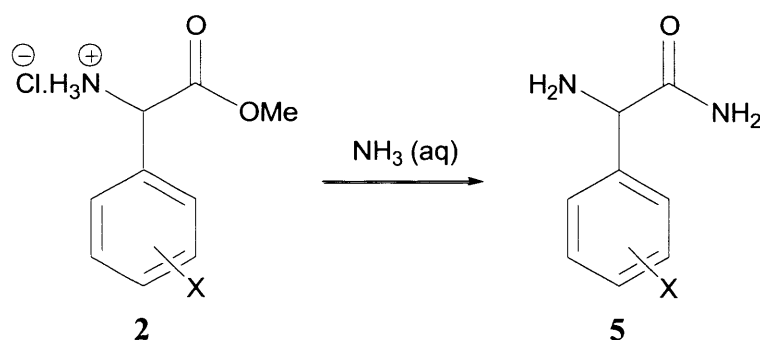
Scheme 4.11: Synthesis of phenylglycine amides **5a-e**.

The general method outlined below in the synthesis of **5a** was used for the synthesis of all compounds **5a-e**.

Phenylglycine amide (5a)

Phenylglycine methyl ester hydrochloride salt (**2a**, 10 g, 49.6 mmol), was added to a solution of concentrated aqueous ammonia (35 ml). The solution was stirred at room temperature for 5

hours. The solution was cooled to 0 °C, and the precipitate was filtered and dried under reduced pressure to give phenylglycine amide as a white solid (6.21 g, 41.4 mmol, 83 %).

^{1}H NMR (400 MHz, DMSO) δ = 7.55 (s, 1H, -C(O)NH$_a$H$_b$), 7.26-7.46 (m, 5H, -C$_6$H$_6$), 7.10 (s, 1H, -C(O)NH$_a$H$_b$), 4.37 (s, 1H, -CH(C$_6$H$_5$)-).

^{13}C NMR (100 MHz, DMSO) δ = 175.37 (1C, -C(O)NH$_2$), 142.79 (1C, ipso aromatic carbon), 128.40 (2C, meta aromatic carbon), 127.36 (1C, para aromatic carbon), 127.12 (2C, ortho aromatic carbon), 59.01 (1C, -CH(C$_6$H$_5$)-).

IR (ss) v/cm^{-1}: 3381, 3279, 1681

Found m/z (AP$^+$) = 151.0865, calculated 151.0871

M.p. = 140-141 °C

(*p*-Methyl phenyl) glycine amide (5b)

Synthesised from compound **2c**. Yield: 72 %

^{1}H NMR (400 MHz, DMSO) δ = 7.46 (s, 1H, -C(O)NH$_a$H$_b$), 7.28 (d, 2H, aromatic protons meta to methyl, $^{3}J_{H-H}$ = 7.92 Hz), 7.11 (d, 2H, aromatic protons ortho to methyl, $^{3}J_{H-H}$ = 7.84 Hz), 7.03 (s, 1H, -C(O)NH$_a$H$_b$), 4.25 (s, 1H, -CH(C$_6$H$_4$CH$_3$)-), 2.27 (s, 3H, -CH$_3$).

^{13}C NMR (100 MHz, DMSO) δ = 175.57 (1C, -C(O)NH$_2$), 139.92 (1C, aromatic carbon para to methyl), 136.36 (1C, aromatic carbon ipso to methyl), 128.92 (2C, aromatic carbon ortho to methyl), 126.98 (2C, aromatic carbon meta to methyl), 59.01 (1C, -CH(C$_6$H$_4$CH$_3$)-), 21.03 (1C, -C$_6$H$_4$CH$_3$).

IR (ss) v/cm^{-1}: 3370, 3291, 1660

Found m/z (AP$^+$) = 165.1030, calculated 165.1028

M.p. = 114-115 °C

(*p*-Fluoro phenyl) glycine amide (5c)

Synthesised from compound **2d**. Yield: 64 %

^{1}H NMR (400 MHz, DMSO) δ = 7.53 (s, 1H, -C(O)NH$_a$H$_b$), 7.44 (dd, 2H, aromatic protons meta to fluorine, $^{3}J_{H-H}$ = 8.68 Hz, $^{4}J_{H-F}$ = 5.72 Hz), 7.15 (t, 2H, aromatic protons ortho to fluorine, $^{3}J_{H-H}$ = $^{3}J_{H-F}$ = 8.92 Hz), 7.11 (s, 1H, -C(O)NH$_a$H$_b$), 4.35 (s, 1H, -CH(C$_6$H$_4$F)-).

^{13}C NMR (100 MHz, DMSO) δ = 175.57 (1C, -C(O)NH$_2$), 160.76 (d, 1C, aromatic carbon ipso to fluorine, $^{1}J_{C-F}$ = 243.52 Hz), 133.02 (d, 1C, aromatic carbon para to fluorine, $^{4}J_{C-F}$ = 3.00 Hz), 130.08 (d, 2C, aromatic carbon meta to fluorine, $^{3}J_{C-F}$ = 8.44 Hz), 114.98 (d, 2C, carbon ortho to fluorine, $^{2}J_{C-F}$ = 22.08 Hz), 58.94 (1C, -CH(C$_6$H$_4$F)-).

IR (ss) v/cm^{-1}: 3372, 3311, 1658

Found m/z (AP$^+$) = 169.0770, calculated 169.0777

M.p. = 107-108 °C

(*p*-Chloro phenyl) glycine amide (5d)

Synthesised from compound **2e**. Yield: 68 %

^{1}H NMR (400 MHz, DMSO) δ = 7.52 (s, 1H, -C(O)NH$_a$H$_b$), 7.42 (d, 2H, aromatic protons ortho to chloro, $^3J_{\text{H-H}}$ = 8.56 Hz), 7.37 (d, 2H, aromatic protons meta to chloro, $^3J_{\text{H-H}}$ = 8.52 Hz), 7.09 (s, 1H, -C(O)NH$_a$H$_b$), 4.30 (s, 1H, -CH(C$_6$H$_4$Cl)-).

^{13}C NMR (100 MHz, DMSO) δ = 175.43 (1C, -C(O)NH$_2$), 142.39 (1C, aromatic carbon para to chlorine), 131.76 (1C, aromatic carbon ipso to chlorine), 128.91 (2C, aromatic carbon ortho to chlorine), 128.27 (2C, aromatic carbon meta to chlorine), 58.54 (1C, -CH(C$_6$H$_4$Cl)-).

IR (ss) v/cm^{-1}: 3361, 3312, 3292, 1670

Found m/z (AP$^+$) = 185.0480, calculated 185.0482

M.p. = 105-106 °C

(*p*-Trifluoromethyl phenyl) glycine amide (5e)

Synthesised from compound **2h**. Yield: 73 %

^{1}H NMR (400 MHz, DMSO) δ = 7.68 (d, 2H, aromatic protons ortho to trifluoromethyl, $^3J_{\text{H-H}}$ = 8.28 Hz), 7.62 (d, 2H, aromatic protons meta to trifluoromethyl, $^3J_{\text{H-H}}$ = 8.24 Hz), 7.57 (s, 1H, -C(O)NH$_a$H$_b$), 7.13 (s, 1H, -C(O)NH$_a$H$_b$), 4.40 (s, 1H, -CH(C$_6$H$_4$CF$_3$)-).

^{13}C NMR (100 MHz, DMSO) δ = 175.07 (1C, -C(O)NH$_2$), 148.09 (s, 1C, aromatic carbon para to trifluoromethyl), 127.86 (s, 2C, aromatic carbon meta to trifluoromethyl), 127.85 (q, 1C, aromatic carbon ipso to trifluoromethyl, $^2J_{\text{C-F}}$ = 31.48 Hz), 125.22 (q, 2C, aromatic carbon ortho to trifluoromethyl, $^3J_{\text{C-F}}$ = 3.92 Hz), 124.75 (q, 1C, -CF$_3$, $^1J_{\text{C-F}}$ = 270.06 Hz), 58.88 (1C, -CH(C$_6$H$_4$CF$_3$)-).

IR (ss) v/cm^{-1}: 3349, 3315, 3285, 1686

Found m/z (AP$^+$) = 219.0744, calculated 219.0745

M.p. = 134-135 °C

4.6.2.2 Synthesis of N-Acetyl Phenylglycine Amides 6a-e

Compounds **6a-e** were synthesised from phenylglycine amides **5a-e** (Scheme 4.12).
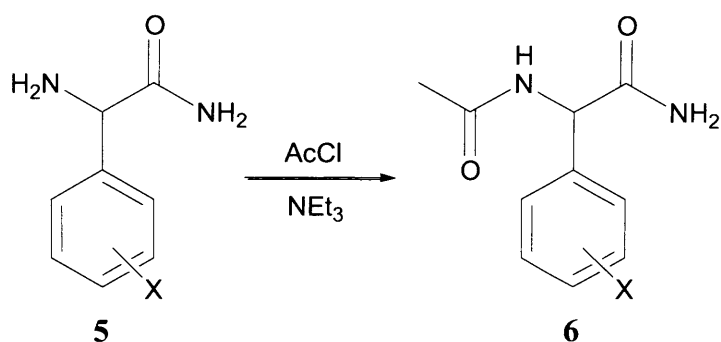
Scheme 4.12: Synthesis of *N*-acetyl phenylglycine amides **6a-e**.

The general method outlined below in the synthesis of **6a** was used for the synthesis of all compounds **6a-e**.

N-Acetyl phenylglycine amide (6a)

Phenylglycine amide (**5a**, 0.5 g, 3.33 mmol) was suspended in anhydrous DCM (30 ml) under a nitrogen atmosphere. Triethylamine (1.2 equiv., 4 mmol, 0.56 ml) was added, and the mixture stirred for 30 mins. Acetyl chloride (1.2 equivs., 4 mmol, 0.29 ml) was added and the mixture left to stir for a further three hours, before being evaporated to dryness. The residue was washed with a small quantity of ice-cold water, before being dried under reduced pressure to give *N*-acetyl phenylglycine amide as a white solid (0.49 g, 2.55 mmol, 77 %).

^{1}H NMR (400 MHz, DMSO) δ = 8.48 (d, 1H, -NH-, $^3J_{\text{H-H}}$ = 8.12 Hz), 7.68 (s, 1H, -C(O)NH$_a$H$_b$), 7.27-7.42 (m, 5H, -C$_6$H$_5$), 7.13 (s, 1H, -C(O)NH$_a$H$_b$), 5.39 (d, 1H, -CH(C$_6$H$_5$)-, $^3J_{\text{H-H}}$ = 8.12 Hz), 1.89 (s, 3H, CH$_3$C(O)-).

^{13}C NMR (100 MHz, d^6-DMSO) δ =172.17 (1C, CH$_3$C(O)-), 169.18 (1C, -C(O)NH$_2$), 139.59 (1C, aromatic), 128.56 (2C, aromatics), 127.72 (1C, aromatic), 127.45 (2C, aromatics), 56.37 (1C, - CH(C$_6$H$_5$)-), 22.81 (1C, -C(O)CH$_3$).

IR (ss) ν/cm^{-1}: 3338, 3268, 3188, 3083, 1653, 1631, 1542

Found m/z (AP$^+$) = 193.0976, calculated 193.0977

M.p. = 182-183 °C

N-Acetyl (*p*-methyl phenyl)glycine amide (6b)

Synthesised from compound **5b**. Yield: 61 %

^{1}H NMR (400 MHz, DMSO) δ = 8.42 (d, 1H, -NH-, $^3J_{\text{H-H}}$ = 8.04 Hz), 7.63 (s, 1H, - C(O)NH$_a$H$_b$), 7.29 (d, 2H, aromatic protons meta to methyl, $^3J_{\text{H-H}}$ = 7.80 Hz), 7.13 (d, 2H, aromatic protons ortho to methyl, $^3J_{\text{H-H}}$ = 7.76 Hz), 7.10 (s, 1H, -C(O)NH$_a$H$_b$), 5.34 (d, 1H, - CH(C$_6$H$_4$CH$_3$)-, $^3J_{\text{H-H}}$ = 8.08 Hz), 2.27 (s, 3H, - C$_6$H$_4$CH$_3$), 1.88 (s, 3H, -COCH$_3$).

^{13}C NMR (100 MHz, DMSO) δ = 172.36 (1C, CH$_3$C(O)-), 169.13 (1C, -C(O)NH$_2$), 136.87 (1C, aromatic carbon ipso to methyl), 136.60 (1C, aromatic carbon para to methyl), 129.07 (2C, aromatic carbon ortho to methyl), 127.41 (2C, aromatic carbon meta to methyl), 56.11 (1C, - CH(C$_6$H$_4$CH$_3$)-), 22.81 (1C, -C(O)CH$_3$), 21.03 (1C, -C$_6$H$_4$CH$_3$).

IR (ss) v/cm^{-1}: 3313, 3279, 3149, 1663, 1634, 1543

Found m/z (AP$^+$) = 207.1143, calculated 207.1134

M.p. = 224-225 °C

N-Acetyl (*p*-fluoro phenyl)glycine amide (6c)

Synthesised from compound **5c**. Yield: 49 %

^{1}H NMR (400 MHz, DMSO) δ = 8.50 (d, 1H, -NH-, $^3J_{H-H}$ = 8.04 Hz), 7.70 (s, 1H, -C(O)NH$_a$H$_b$), 7.44 (dd, 2H, -C$_6$H$_4$F (aromatic protons meta to fluorine), $^3J_{H-H}$ = 8.60 Hz, $^4J_{H-F}$ = 5.60 Hz), 7.17 (t, 2H, (aromatic protons ortho to fluorine), $^3J_{H-H}$ = $^3J_{H-F}$ = 8.92 Hz), 5.39 (d, 1H, -CH(C$_6$H$_4$F)-, $^3J_{H-H}$ = 8.08 Hz), 1.89 (s, 3H, CH$_3$C(O)-).

^{13}C NMR (100 MHz, DMSO) δ = 171.04 (1C, CH$_3$C(O)-), 169.24 (1C, -C(O)OCH$_3$), 161.88 (d, 1C, aromatic carbon ipso to fluorine, $^1J_{C-F}$ = 243.06 Hz), 132.61 (d, 1C, aromatic carbon para to fluorine, $^4J_{C-F}$ = 3.1 Hz), 129.87 (d, 2C, aromatic carbon meta to fluorine, $^3J_{C-F}$ = 8.36 Hz), 115.45 (d, 2C, carbon ortho to fluorine, $^2J_{C-F}$ = 21.59 Hz) , 55.44 (1C, - CH(C$_6$H$_4$F)-), 52.22 (1C, -OCH$_3$), 22.12 (1C, -C(O)CH$_3$).

IR (ss) v/cm^{-1}: 3322, 3254, 3158, 3061, 1652, 1628, 1551

Found m/z (AP$^+$) = 211.0879, calculated 211.0883

M.p. = 214-215 °C

N-Acetyl (*p*-chloro phenyl)glycine amide (6d)

Synthesised from compound **5d**. Yield: 71 %

^{1}H NMR (400 MHz, DMSO) δ = 8.52 (d, 1H, -NH-, $^3J_{H-H}$ = 8.00 Hz), 7.73 (s, 1H, -C(O)NH$_a$H$_b$), 7.36-7.45 (m, 4H, aromatic protons), 7.19 (s, 1H, -C(O)NH$_a$H$_b$), 5.40 (d, 1H, -CH(C$_6$H$_4$Cl)-, $^3J_{H-H}$ = 8.04 Hz).

^{13}C NMR (100 MHz, DMSO) δ = 171.78 (1C, CH$_3$C(O)-), 169.27 (1C, -C(O)NH$_2$), 138.67 (1C, aromatic carbon para to chlorine), 132.39 (1C, aromatic carbon ipso to chlorine), 129.30 (2C, aromatic carbon ortho to chlorine), 128.56 (2C, aromatic carbon meta to chlorine), 55.71 (1C, -CH(C$_6$H$_4$Cl)-), 22.77 (1C, CH$_3$C(O)-).

IR (ss) v/cm^{-1}: 3259, 3165, 3069, 1651, 1624, 1555

Found m/z (AP$^+$) = 227.0588, calculated 227.0587

M.p. = 223-224 °C

N-Acetyl (*p*-trifluoromethyl phenyl)glycine amide (6e)

Synthesised from compound **5e**. Yield: 62 %

^{1}H NMR (400 MHz, DMSO) δ = 8.63 (d, 1H, -NH-, $^3J_{\text{H-H}}$ = 8.04 Hz), 7.83 (s, 1H, -C(O)NH$_a$H$_b$), 7.73 (d, 2H, aromatic protons ortho to trifluoromethyl, $^3J_{\text{H-H}}$ = 8.12 Hz), 7.63 (d, 2H, aromatic protons meta to trifluoromethyl, $^3J_{\text{H-H}}$ = 8.04 Hz), 7.27 (s, 1H, -C(O)NH$_a$H$_b$), 5.51 (s, 1H, -CH(C$_6$H$_4$CF$_3$)-, $^3J_{\text{H-H}}$ = 8.04 Hz), 1.91 (s, 3H, -COCH$_3$).

^{13}C NMR (100 MHz, DMSO) δ = 171.39 (1C, CH$_3$C(O)-), 169.40 (1C, -C(O)NH$_2$), 144.36 (s, 1C, aromatic carbon para to trifluoromethyl), 128.23 (q, 1C, aromatic carbon ipso to trifluoromethyl, $^2J_{\text{C-F}}$ = 63.08 Hz), 128.20 (s, 2C, aromatic carbon meta to trifluoromethyl), 125.55 (q, 2C, aromatic carbon ortho to trifluoromethyl, $^3J_{\text{C-F}}$ = 3.66 Hz), 124.61 (q, 1C, -CF$_3$, $^1J_{\text{C-F}}$ = 270.40 Hz), 56.09 (1C, -CH(C$_6$H$_4$CF$_3$)-), 22.74 (1C, CH$_3$C(O)-).

IR (ss) v/cm^{-1}: 3305, 3167, 1682, 1620, 1540

Found m/z (AP$^+$) = 261.0856, calculated 261.0851

M.p. = 232-233 °C

4.6.2.3 Synthesis of N-Benzoyl Phenylglycine Amides 7a-d

Compounds **7a-d** were synthesised from phenylglycine amide **5a** (Scheme 4.13).
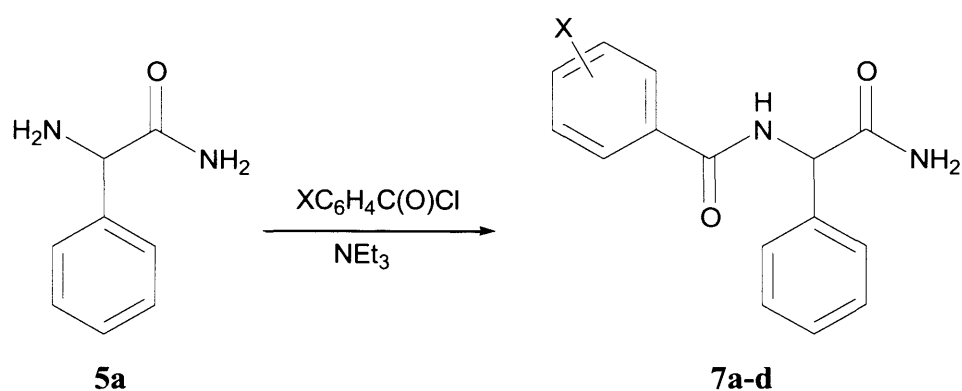
Scheme 4.13: Synthesis of *N*-benzoyl phenylglycine amides **7a-d**.

The general method outlined below in the synthesis of **7a** was used for the synthesis of all compounds **7a-d**.

N-Benzoyl phenylglycine amide (7a)

Phenylglycine amide (**5a**, 0.5 g, 3.33 mmol) was suspended in anhydrous DCM (30 ml) under a nitrogen atmosphere. Triethylamine (1.2 equiv., 4 mmol, 0.56 ml) was added, and the mixture stirred for 30 mins. Benzoyl chloride (1.2 equivs., 4 mmol, 0.29 ml) was added and the mixture left to stir for a further three hours, before being evaporated to dryness. The residue was triturated with water and filtered. The residue was washed on the filter with water, then with 1 M HCl, water, saturated $NaHCO_3$ solution, water and finally with diethyl ether before being dried under reduced pressure to give *N*-benzoyl phenylglycine amide as a white solid (0.73 g, 2.87 mmol, 86 %).

^{1}H NMR (400 MHz, DMSO) δ = 8.73 (d, 1H, -NH-, $^3J_{H-H}$ = 7.96 Hz), 7.92 (d, 2H, ortho benzoyl aromatic protons, $^3J_{H-H}$ = 7.08 Hz), 7.71 (s, 1H, -C(O)NH$_a$H$_b$), 7.28-7.56 (m, 8H, meta and para benzoyl aromatic protons and phenylglycine aromatic protons), 7.26 (s, 1H, -C(O)NH$_a$**H$_b$**), 5.63 (d, 1H, -**CH**(C$_6$H$_5$)-, $^3J_{H-H}$ = 7.96 Hz).

^{13}C NMR (125 MHz, DMSO) δ = 171.63 (1C, -**C**(O)NH$_2$), 165.89 (1C, -**C**(O)C$_6$H$_5$), 138.78 (1C, ipso phenylglycine aromatic carbon), 133.96 (1C, ipso benzoyl aromatic carbon), 131.35 (1C, para benzoyl aromatic carbon), 128.21 (2C, meta benzoyl aromatic carbon), 128.18 (2C, meta phenylglycine aromatic carbon), 127.54 (2C, ortho benzoyl aromatic carbon), 127.47 (1C, para phenylglycine aromatic carbon), 127.43 (2C, ortho phenylglycine aromatic carbon), 56.80 (1C, -**CH**(C$_6$H$_5$)-).

IR (ss) *v*/cm^{-1}: 3370, 3255, 3164, 1660, 1636, 1520

Found m/z (AP$^+$) = 255.1129, calculated 255.1134

M.p. = 224-225 °C

N-(*p*-**Methoxy benzoyl) phenylglycine amide (7b)**

Yield: 79 %

^{1}H NMR (400 MHz, DMSO) δ = 8.55 (d, 1H, -NH-, $^3J_{H-H}$ = 8.08 Hz), 7.91 (d, 2H, ortho to carbonyl benzoyl aromatic protons, $^3J_{H-H}$ = 8.84 Hz), 7.69 (s, 1H, -C(O)NH$_a$H$_b$), 7.51 (d, 2H, ortho phenylglycine aromatic protons, $^3J_{H-H}$ = 7.20 Hz), 7.35 (t, 2H, meta phenylglycine aromatic protons, $^3J_{H-H}$ = 7.56 Hz), 7.29 (t, 1H, para phenylglycine aromatic proton, $^3J_{H-H}$ = 7.16 Hz), 7.24 (s, 1H, -C(O)NH$_a$**H$_b$**), 6.99 (d, 2H, meta to carbonyl benzoyl aromatic protons, $^3J_{H-H}$ = 8.88 Hz), 5.61 (d, 1H, -**CH**(C$_6$H$_5$)-, $^3J_{H-H}$ = 8.00 Hz), 3.81 (s, 3H, -OCH$_3$).

^{13}C NMR (125 MHz, DMSO) δ = 171.79 (1C, -**C**(O)NH$_2$), 165.32 (1C, -**C**(O)C$_6$H$_4$OCH$_3$), 161.74 (1C, benzoyl aromatic carbon ipso to methoxy, para to amide), 138.96 (1C, ipso phenylglycine aromatic carbon), 129.42 (2C, benzoyl aromatic carbon meta to methoxy, ortho to amide), 128.18 (2C, meta phenylglycine aromatic carbon), 127.41 (1C, para phenylglycine

aromatic carbon), 127.41 (2C, ortho phenylglycine aromatic carbon), 126.17 (1C, benzoyl aromatic carbon para to methoxy, ipso to amide), 113.42 (2C, benzoyl aromatic carbon ortho to methoxy, meta to amide), 56.73 (1C, -CH(C$_6$H$_5$)-), 55.33 (1C, -OCH$_3$).

IR (ss) v/cm^{-1}: 3367, 3283, 3196, 1739, 1626, 1608

Found m/z (AP$^+$) = 285.1243, calculated 285.1239

M.p. = 191-192 °C

N-(*p*-Trifluoromethoxy benzoyl) phenylglycine amide (7c)

Yield: 49 %

^{1}H NMR (400 MHz, DMSO) δ = 8.93 (d, 1H, -NH-, $^3J_{H-H}$ = 7.88 Hz), 8.05 (d, 2H, ortho to carbonyl benzoyl aromatic protons, $^3J_{H-H}$ = 8.76 Hz), 7.73 (s, 1H, -C(O)NH$_a$H$_b$), 7.52 (d, 2H, ortho phenylglycine aromatic protons, $^3J_{H-H}$ = 7.20 Hz), 7.46 (d, 2H, meta to carbonyl benzoyl aromatic protons, $^3J_{H-H}$ = 8.16 Hz), 7.36 (t, 2H, meta phenylglycine aromatic protons, $^3J_{H-H}$ = 7.28 Hz), 7.30 (t, 1H, para phenylglycine aromatic proton, $^3J_{H-H}$ = 7.12 Hz), 7.26 (s, 1H, -C(O)NH$_a$H$_b$), 5.61 (d, 1H, -CH(C$_6$H$_5$)-, $^3J_{H-H}$ = 7.88 Hz).

^{13}C NMR (125 MHz, DMSO) δ = 171.52 (1C, -C(O)NH$_2$), 164.84 (1C, -C(O)C$_6$H$_4$OCF$_3$), 150.37 (1C, benzoyl aromatic carbon ipso to trifluoromethoxy, para to amide), 138.57 (1C, ipso phenylglycine aromatic carbon), 133.09 (1C, benzoyl aromatic carbon para to trifluoromethoxy, ipso to amide), 130.02 (2C, benzoyl aromatic carbon meta to trifluoromethoxy, ortho to amide), 128.19 (2C, meta phenylglycine aromatic carbon), 127.51 (1C, para phenylglycine aromatic carbon), 127.51 (2C, ortho phenylglycine aromatic carbon), 120.38 (2C, benzoyl aromatic carbon ortho to trifluoromethoxy, meta to amide), 119.96 (q, 1C, -OCF$_3$, $^1J_{C-F}$ = 255.61 Hz), 57.00 (1C, -CH(C$_6$H$_5$)-).

IR (ss) v/cm^{-1}: 3364, 3281, 3189, 1739, 1627, 1607

Found m/z (AP$^+$) = 339.0951, calculated 339.0957

M.p. = 239-240 °C

N-(*p*-Trifluoromethyl benzoyl) phenylglycine amide (7d)

Yield: 86 %

^{1}H NMR (400 MHz, DMSO) δ = 9.07 (d, 1H, -NH-, $^3J_{H-H}$ = 7.84 Hz), 8.11 (d, 2H, ortho to carbonyl benzoyl aromatic protons, $^3J_{H-H}$ = 8.12 Hz), 7.84 (d, 2H, meta to carbonyl benzoyl aromatic protons, $^3J_{H-H}$ = 8.32 Hz), 7.75 (s, 1H, -C(O)NH$_a$H$_b$), 7.53 (d, 2H, ortho phenylglycine aromatic protons, $^3J_{H-H}$ = 7.64 Hz), 7.37 (t, 2H, meta phenylglycine aromatic

protons, $^3J_{H-H}$ = 7.32 Hz), 7.31 (t, 1H, para phenylglycine aromatic proton, $^3J_{H-H}$ = 7.20 Hz), 7.27 (s, 1H, -C(O)NH$_a$H$_b$), 5.63 (d, 1H, -CH(C$_6$H$_5$)-, $^3J_{H-H}$ = 7.88 Hz).

^{13}C NMR (125 MHz, DMSO) δ = 171.42 (1C, -C(O)NH$_2$), 164.96 (1C, -C(O)C$_6$H$_4$CF$_3$), 138.46 (1C, ipso phenylglycine aromatic carbon), 137.80 (1C, benzoyl aromatic carbon para to trifluoromethyl, ipso to amide), 131.22 (q, 1C, benzoyl aromatic carbon ipso to trifluoromethyl, para to amide, $^2J_{C-F}$ = 31.64 Hz), 128.59 (2C, benzoyl aromatic carbon mate to trifluoromethyl, ortho to amide), 128.22 (2C, meta phenylglycine aromatic carbon), 127.54 (1C, para phenylglycine aromatic carbon), 127.54 (2C, ortho phenylglycine aromatic carbon), 125.10 (q, 2C, benzoyl aromatic carbon ortho to trifluoromethyl, meta to amide, $^3J_{C-F}$ = 3.42 Hz), 123.92 (q, 1C, -CF$_3$, $^1J_{C-F}$ = 270.91 Hz), 57.04 (1C, -CH(C$_6$H$_5$)-).

IR (ss) v/cm^{-1}: 3260, 3168, 1739, 1635, 1531

Found m/z (ES$^-$) = 321.0865, calculated 321.0851

M.p. = 218-220 °C

4.6.2.4 Synthesis of N-Acetyl Phenylglycine Anilides 8a-l

Compounds **8a-l** were synthesised from the corresponding *N*-acetyl phenylglycines **4a, c-e, g-h**, the synthesis of which is described in the experimental to chapter 3. The method was adapted from that used by Hyun *et al.* (Scheme 4.14).[27]
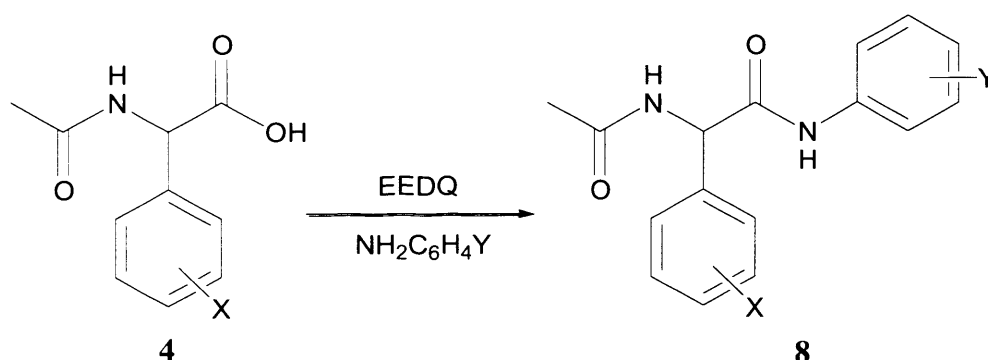
Scheme 4.14: Synthesis of *N*-acetyl phenylglycine anilides **8a-l**.

The general method outlined below in the synthesis of **8a** was used for the synthesis of all compounds **8a-l**. Assignments of ^{1}H and ^{13}C NMR spectra were made with the aid of 2D spectra (HSQC and HMBC) and the use of approximate substituent chemical shift tables by Williams and Fleming.[28]

2-Acetamido-2-phenyl acetanilide (8a)

To a stirred suspension of *N*-acetyl phenylglycine (**4a**, 0.5 g, 2.6 mmol) in DCM (35 ml) was added aniline (1.1 equiv., 0.3 ml, 3.0 mmol) and 2-ethoxy-1-ethoxycarbonyl-1,2-dihydroquinoline (EEDQ) (1.1 equiv., 0.74 g, 3.0 mmol). The mixture was stirred at room temperature overnight and then washed with 0.5 M HCl, 0.5 M NaOH and brine and then dried with magnesium sulphate. The solvent was removed and the product was washed with ethyl acetate to give 2-acetamido-2-phenyl acetanilide (0.30 g, 1.2 mmol, 43 %) as a white solid.

^{1}H NMR (500 MHz, d^6-DMSO) δ = 10.37 (s, 1H, -NH(C$_6$H$_5$)), 8.71 (d, 1H, -NHAc, $^3J_{H-H}$ = 7.85 Hz), 7.60 (d, 2H, ortho anilide aromatic protons, $^3J_{H-H}$ = 7.70 Hz), 7.50 (d, 2H, ortho phenylglycine aromatic protons, $^3J_{H-H}$ = 7.40 Hz), 7.38 (t, 2H, meta phenylglycine aromatic protons, $^3J_{H-H}$ = 7.30 Hz), 7.31 (t, 1H, para phenylglycine aromatic proton, $^3J_{H-H}$ = 7.20 Hz), 7.30 (t, 2H, meta anilide aromatic protons, $^3J_{H-H}$ = 8.00 Hz), 7.05 (t, 1H, para anilide aromatic proton, $^3J_{H-H}$ = 7.40 Hz), 5.66 (d, 1H, -C**H**(C$_6$H$_5$)-, $^3J_{H-H}$ = 7.90 Hz), 1.94 (s, 3H, -COCH$_3$).

^{13}C NMR (125 MHz d^6-DMSO) δ = 169.15 (1C, CH$_3$C(O)-), 168.87 (1C, -C(O)NHPh), 138.77 (1C, ipso anilide aromatic carbon), 138.24 (1C, ipso phenylglycine aromatic carbon), 128.75 (2C, meta anilide aromatic carbons), 128.43 (2C, meta phenylglycine aromatic carbons), 127.71 (1C, para phenylglycine aromatic carbon), 127.27 (2C, ortho phenylglycine aromatic carbons), 123.47 (1C, para anilide aromatic carbon), 119.12 (2C, ortho anilide aromatic carbons), 56.97 (1C, -CH(C$_6$H$_5$)), 22.32 (1C, -CH$_3$).

IR (ss) ν/cm^{-1}: 3254, 3136, 3081, 1739, 1647, 1598, 1541

Found m/z (EI$^+$) = 268.1206, calculated 268.1212

M.p. = 234-235 °C

2-Acetamido-2-phenyl acet(4-methyl anilide) (8b)

Synthesised from compound **4a**. Yield: 66 %

^{1}H NMR (400 MHz, d^6-DMSO) δ =10.29 (s, 1H, -NH(C$_6$H$_4$CH$_3$)), 8.70 (d, 1H, -NHAc, $^3J_{H-H}$ = 7.92 Hz), 7.49 (d, 2H, ortho phenylglycine aromatic protons, $^3J_{H-H}$ = 7.12 Hz), 7.48 (d, 2H, anilide aromatic protons meta to methyl, $^3J_{H-H}$ = 8.20 Hz), 7.37 (t, 2H, meta phenylglycine aromatic protons, $^3J_{H-H}$ = 7.12 Hz), 7.30 (tt, 1H, para phenylglycine aromatic proton, $^3J_{H-H}$ = 7.24 Hz, $^4J_{H-H}$ = 2.24 Hz), 7.10 (d, 2H, anilide aromatic protons meta to methyl, $^3J_{H-H}$ = 8.36 Hz), 5.65 (d, 1H, -C**H**(C$_6$H$_5$)-, $^3J_{H-H}$ = 7.96 Hz), 2.23 (s, 3H, -NHC$_6$H$_4$CH$_3$), 1.94 (s, 3H, -COCH$_3$).

^{13}C NMR (100 MHz d^6-DMSO) δ = 169.54 (1C, CH$_3$C(O)-), 169.00 (1C, -C(O)NHC$_6$H$_4$CH$_3$), 138.74 (1C, ipso phenylglycine aromatic carbon), 136.65 (1C, anilide

aromatic carbon para to methyl), 132.81 (1C, anilide aromatic carbon ipso to methyl), 129.52 (2C, anilide aromatic carbons ortho to methyl), 128.81 (2C, meta phenylglycine aromatic carbons), 127.08 (1C, para phenylglycine aromatic carbon), 127.64 (2C, ortho phenylglycine aromatic carbons), 119.48 (2C, anilide aromatic carbons meta to methyl), 57.27 (1C, -CH(C_6H_5)), 22.72 (1C, -COCH$_3$), 20.79 (1C, -C$_6$H$_4$CH$_3$).

IR (ss) v/cm^{-1}: 3300, 3260, 1739, 1648, 1539

Found m/z (EI$^+$) = 282.1377, calculated 282.1368

M.p. = 210-211 °C

2-Acetamido-2-phenyl acet(3-methyl anilide) (8c)

Synthesised from compound **4a**. Yield: 39 %

^{1}H NMR (400 MHz, d^6-DMSO) δ =10.27 (s, 1H, -NH($C_6H_4CH_3$)), 8.68 (d, 1H, -NHAc, $^3J_{H-H}$ = 7.80 Hz), 7.49 (d, 2H, ortho phenylglycine aromatic protons, $^3J_{H-H}$ = 7.24 Hz), 7.41 (s, 1H, anilide aromatic proton, ortho to methyl and amide), 7.35-7.39 (m, 3H, meta phenylglycine aromatic protons and anilide aromatic proton, ortho to amide, para to methyl), 7.30 (tt, 1H, para phenylglycine aromatic proton, $^3J_{H-H}$ = 7.20 Hz, $^4J_{H-H}$ = 2.20 Hz), 7.17 (t, 1H, anilide aromatic proton, meta to methyl and amide, $^3J_{H-H}$ = 7.80 Hz), 6.86 (d, 1H, anilide aromatic proton, ortho to methyl, para to amide, $^3J_{H-H}$ = 7.48 Hz), 5.63 (d, 1H, -CH(C_6H_5)-, $^3J_{H-H}$ = 7.84 Hz), 2.25 (s, 3H, -NHC$_6$H$_4$CH$_3$), 1.93 (s, 3H, -COCH$_3$).

^{13}C NMR (100 MHz d^6-DMSO) δ = 169.55 (1C, CH$_3$C(O)-), 169.19 (1C, -C(O)NHC$_6$H$_4$CH$_3$), 139.08 (1C, anilide aromatic carbon ipso to amide), 138.60 (1C, ipso phenylglycine aromatic carbon), 138.35 (1C, anilide aromatic carbon, ipso to methyl), 129.00 (1C, anilide aromatic carbon, meta to methyl and amide), 128.82 (2C, meta phenylglycine aromatic carbons), 128.11 (1C, para phenylglycine aromatic carbon), 127.67 (2C, ortho phenylglycine aromatic carbons), 124.55 (1C, anilide aromatic carbon, para to amide, ortho to methyl), 119.98 (1C, anilide aromatic carbon, ortho to methyl and amide), 116.66 (1C, anilide aromatic carbon, ortho to amide, para to methyl), 56.97 (1C, -CH(C_6H_5)), 22.32 (1C, -CH$_3$).

IR (ss) v/cm^{-1}: 3250, 1739, 1636, 1538

Found m/z (EI$^+$) = 282.1372, calculated 282.1368

M.p. = 223-224 °C

2-Acetamido-2-phenyl acet(4-chloro anilide) (8d)

Synthesised from compound **4a**. Yield: 56 %

^{1}H NMR (400 MHz, d^6-DMSO) δ = 10.57 (s, 1H, -NH(C$_6$H$_4$Cl)), 8.74 (d, 1H, -NHAc, $^3J_{H-H}$ = 7.72 Hz), 7.64 (d, 2H, anilide aromatic protons meta to chloro, $^3J_{H-H}$ = 8.76 Hz), 7.49 (d, 2H, ortho phenylglycine aromatic protons, $^3J_{H-H}$ = 7.44 Hz), 7.31-7.39 (m, 5H, meta and para phenylglycine aromatic protons and anilide aromatic protons ortho to chloro), 5.63 (d, 1H, -CH(C$_6$H$_5$)-, $^3J_{H-H}$ = 7.72 Hz), 1.93 (s, 3H, -COCH$_3$).

^{13}C NMR (100 MHz d^6-DMSO) δ = 169.62 (1C, CH$_3$C(O)-), 169.46 (1C, -C(O)NHC$_6$H$_4$Cl), 138.29 (1C, ipso phenylglycine aromatic carbon), 138.12 (1C, anilide aromatic carbon para to chloro), 129.07 (2C, anilide aromatic carbons ortho to chloro), 128.88 (2C, meta phenylglycine aromatic carbons), 128.22 (1C, anilide aromatic carbon ipso to chloro), 127.73 (2C, ortho phenylglycine aromatic carbons), 127.41 (1C, para phenylglycine aromatic carbon), 121.04 (2C, anilide aromatic carbons meta to chloro), 57.45 (1C, -CH(C$_6$H$_5$)), 22.68 (1C, -CH$_3$).

IR (ss) v/cm^{-1}: 3329, 3254, 3191, 1739, 1646, 1539

Found m/z (EI$^+$) = 302.0820, calculated 302.0822

M.p. = 221-222 °C

2-Acetamido-2-phenyl acet(3-chloro anilide) (8e)

Synthesised from compound **4a**. Yield: 42 %

^{1}H NMR (400 MHz, d^6-DMSO) δ = 10.56 (s, 1H, -NH(C$_6$H$_4$Cl)), 8.73 (d, 1H, -NHAc, $^3J_{H-H}$ = 7.60 Hz), 7.81 (t, 1H, anilide aromatic proton ortho to amide and chloro, $^4J_{H-H}$ = 1.92 Hz), 7.48 (d, 2H, ortho phenylglycine aromatic protons, $^3J_{H-H}$ = 7.24 Hz), 7.45 (d, 1H, anilide aromatic proton ortho to amide para to chloro, $^3J_{H-H}$ = 8.48 Hz), 7.38 (t, 2H, meta phenylglycine aromatic protons, $^3J_{H-H}$ = 7.04 Hz), 7.30-7.35 (m, 2H, para phenylglycine aromatic proton, meta anilide aromatic proton), 7.11 (d, 1H, anilide aromatic proton ortho to chloro para to amide, $^3J_{H-H}$ = 7.92 Hz, $^4J_{H-H}$ = 1.28 Hz), 5.60 (d, 1H, -CH(C$_6$H$_5$)-, $^3J_{H-H}$ = 7.60 Hz), 1.93 (s, 3H, -COCH$_3$).

^{13}C NMR (100 MHz d^6-DMSO) δ = 169.71 (1C, CH$_3$C(O)-), 169.69 (1C, -C(O)NHC$_6$H$_4$Cl), 140.57 (1C, anilide aromatic carbon ipso to amide), 138.05 (1C, ipso phenylglycine aromatic carbon), 133.47 (1C, anilide aromatic carbon ipso to chloro), 130.92 (1C, anilide aromatic carbon meta to amide and chloro), 128.92 (2C, meta phenylglycine aromatic carbons), 128.30 (1C, para phenylglycine aromatic carbon), 127.78 (2C, ortho phenylglycine aromatic carbons), 123.61 (1C, anilide aromatic carbon ortho to chloro para to amide), 118.90 (1C, anilide aromatic carbon ortho to amide and chloro), 117.87 (1C, anilide aromatic carbon ortho to amide para to chloro), 57.56 (1C, -CH(C$_6$H$_5$)), 22.65 (1C, -CH$_3$).

IR (ss) v/cm^{-1}: 3300, 1738, 1645, 1597

Found m/z (EI$^+$) = 302.0815, calculated 302.0822

M.p. = 211-212 °C

2-Acetamido-2-(4-methyl phenyl) acet(3-methyl anilide) (8f)

Synthesised from compound **4c**. Yield: 28 %

^{1}H NMR (500 MHz, d^6-DMSO) δ = 10.21 (s, 1H, -NH(C$_6$H$_4$CH$_3$)), 8.61 (d, 1H, -NHAc, $^3J_{H-H}$ = 7.70 Hz), 7.40 (s, 1H, anilide aromatic proton ortho to amide and methyl), 7.35-7.37 (m, 3H, phenylglycine aromatic protons meta to methyl and anilide aromatic proton ortho to amide para to methyl), 7.15-7.18 (m, 3H, phenylglycine aromatic protons ortho to methyl and anilide aromatic proton meta to amide and methyl), 6.86 (d, 1H, anilide aromatic proton para to amide ortho to methyl, $^3J_{H-H}$ = 7.30 Hz), 5.57 (d, 1H, -CH(C$_6$H$_4$CH$_3$)-, $^3J_{H-H}$ = 7.75 Hz), 2.27 (s, 3H, -CH(C$_6$H$_4$CH$_3$)-), 2.26 (s, 3H, -NHC$_6$H$_4$CH$_3$), 1.92 (s, 3H, -C(O)CH$_3$).

^{13}C NMR (125 MHz d^6-DMSO) δ = 169.08, (1C, CH$_3$C(O)-), 168.96 (1C, -C(O)NHC$_6$H$_4$CH$_3$), 138.73 (1C, anilide aromatic carbon ipso to amide), 137.91 (1C, anilide aromatic carbon ipso to methyl), 136.94 (1C, phenylglycine aromatic carbon ipso to methyl), 135.23 (1C, phenylglycine aromatic carbon para to methyl), 128.92 (2C, phenylglycine aromatic carbons ortho to methyl), 128.56 (1C, anilide aromatic carbon meta to amide and methyl), 127.19 (2C, phenylglycine aromatic carbons meta to methyl), 124.09 (1C, anilide aromatic carbon para to amide ortho to methyl), 119.60 (1C, anilide aromatic carbon ortho to amide and methyl), 116.29 (1C, anilide aromatic carbon ortho to amide para to methyl), 56.72 (1C, -CH(C$_6$H$_4$CH$_3$), 22.31 (1C, -C(O)CH$_3$), 21.12 (1C, -NHC$_6$H$_4$CH$_3$), 20.63 (1C, -CH(C$_6$H$_4$CH$_3$)-).

IR (ss) v/cm^{-1}: 3296, 2971, 1739, 1647, 1539

Found m/z (EI$^+$) = 296.1522, calculated 269.1525

M.p. = 198-200 °C

2-Acetamido-2-(4-methyl phenyl) acetanilide (8g)

Synthesised from compound **4c**. Yield: 30 %

^{1}H NMR (500 MHz, d^6-DMSO) δ = 10.28 (s, 1H, -NH(C$_6$H$_5$)), 8.60 (d, 1H, -NHAc, $^3J_{H-H}$ = 7.85 Hz), 7.58 (d, 2H, ortho anilide aromatic protons, $^3J_{H-H}$ = 7.70 Hz), 7.37 (d, 2H, phenylglycine aromatic protons meta to methyl, $^3J_{H-H}$ = 8.05 Hz), 7.29 (t, 2H, meta anilide aromatic protons, $^3J_{H-H}$ = 7.60 Hz), 7.17 (d, 2H, phenylglycine aromatic protons ortho to

methyl, $^3J_{H-H}$ = 7.95 Hz), 7.04 (t, 1H, para anilide aromatic proton, $^3J_{H-H}$ = 7.35 Hz), 5.60 (d, 1H, -CH($C_6H_4CH_3$)-, $^3J_{H-H}$ = 7.85 Hz), 2.28 (s, 3H, - C_6H_4**CH₃**), 1.93 (s, 3H, -C(O)**CH₃**).

^{13}C NMR (125 MHz d^6-DMSO) δ = 169.08, (1C, CH₃**C**(O)-), 169.02 (1C, -**C**(O)NHC₆H₅), 138.81 (1C, anilide aromatic carbon ipso to amide), 136.95 (1C, phenylglycine aromatic carbon ipso to methyl), 135.25 (1C, phenylglycine aromatic carbon para to methyl), 128.93 (2C, phenylglycine aromatic carbons ortho to methyl), 128.71 (2C, meta anilide aromatic carbons), 127.19 (2C, phenylglycine aromatic carbons meta to methyl), 123.41 (1C, para anilide aromatic carbon), 119.12 (2C, ortho anilide aromatic carbons), 56.72 (1C, -**C**H($C_6H_4CH_3$), 22.32 (1C, -C(O)**C**H₃), 20.62 (1C, -CH(C_6H_4**C**H₃)-).

IR (ss) v/cm^{-1}: 3018, 1739, 1646, 1540

Found m/z (EI$^+$) = 282.1362, calculated 282.1368

M.p. = 218-220 °C

2-Acetamido-2-(4-methyl phenyl) acet(3-chloro anilide) (8h)

Synthesised from compound **4c**. Yield: 27 %

^{1}H NMR (400 MHz, d^6-DMSO) δ =10.50 (s, 1H, -N**H**(C_6H_4Cl)), 8.66 (d, 1H, -N**H**Ac, $^3J_{H-H}$ = 7.52 Hz), 7.80 (d, 1H, anilide aromatic proton ortho to amide and chloro, $^4J_{H-H}$ = 1.96 Hz), 7.44 (td, 1H, anilide aromatic proton ortho to amide para to chloro, $^3J_{H-H}$ = 8.02 Hz, $^4J_{H-H}$ = 1.00 Hz), 7.36 (d, 2H, phenylglycine aromatic protons meta to methyl, $^3J_{H-H}$ = 8.08 Hz), 7.32 (t, 1H, anilide aromatic proton meta to amide and chloro, $^3J_{H-H}$ = 8.12 Hz), 7.18 (d, 2H, phenylglycine aromatic protons ortho to methyl, $^3J_{H-H}$ = 7.96 Hz), 7.04 (dt, 1H, anilide aromatic proton para to amide ortho to chloro, $^3J_{H-H}$ = 7.28 Hz, $^4J_{H-H}$ = 1.20 Hz), 5.53 (d, 1H, -CH($C_6H_4CH_3$)-, $^3J_{H-H}$ = 7.60 Hz), 2.28 (s, 3H, - C_6H_4**CH₃**), 1.92 (s, 3H, -C(O)**CH₃**).

^{13}C NMR (100 MHz d^6-DMSO) δ = 169.88, (1C, CH₃**C**(O)-), 169.63 (1C, -**C**(O)NHC₆H₄CH₃), 140.62 (1C, anilide aromatic carbon ipso to amide), 137.58 (1C, phenylglycine aromatic carbon ipso to methyl), 135.03 (1C, phenylglycine aromatic carbon para to methyl), 133.45 (1C, anilide aromatic carbon ipso to chloro), 130.91 (1C, anilide aromatic carbon meta to amide and chloro), 129.42 (2C, phenylglycine aromatic carbons ortho to methyl), 127.70 (2C, phenylglycine aromatic carbons meta to methyl), 123.54 (1C, anilide aromatic carbon para to amide ortho to chloro), 118.17 (1C, anilide aromatic carbon ortho to amide and chloro), 117.84 (1C, anilide aromatic carbon ortho to amide para to chloro), 57.31 (1C, -**C**H($C_6H_4CH_3$), 22.65 (1C, -C(O)**C**H₃), 21.04 (1C, -CH(C_6H_4**C**H₃)-).

IR (ss) v/cm^{-1}: 3011, 1739, 1646, 1595, 1534

Found m/z (EI$^+$) = 316.0987, calculated 316.0979

M.p. = 202-206 °C

2-Acetamido-2-(4-chloro phenyl) acetanilide (8i)

Synthesised from compound **4e**. Yield: 22 %

^{1}H NMR (400 MHz, d^6-DMSO) δ = 10.42 (s, 1H, -NH(C$_6$H$_5$)), 8.77 (d, 1H, -NHAc, $^3J_{H-H}$ = 7.88 Hz), 7.59 (d, 2H, ortho anilide aromatic protons, $^3J_{H-H}$ = 7.72 Hz), 7.52 (d, 2H, phenylglycine aromatic protons meta to chloro, $^3J_{H-H}$ = 8.56 Hz), 7.46 (d, 2H, phenylglycine aromatic protons ortho to chloro, $^3J_{H-H}$ = 8.52 Hz), 7.31 (t, 2H, meta anilide aromatic protons, $^3J_{H-H}$ = 7.68 Hz), 7.06 (t, 1H, para anilide aromatic proton, $^3J_{H-H}$ = 7.36 Hz), 5.68 (d, 1H, -CH(C$_6$H$_4$Cl)-, $^3J_{H-H}$ = 7.88 Hz), 1.94 (s, 3H, -C(O)CH$_3$).

^{13}C NMR (100 MHz d^6-DMSO) δ = 169.62, (1C, CH$_3$C(O)-), 168.84 (1C, -C(O)NHC$_6$H$_5$), 139.01 (1C, anilide aromatic carbon ipso to amide), 137.65 (1C, phenylglycine aromatic carbon para to chloro), 132.84 (1C, phenylglycine aromatic carbon ipso to chloro), 129.49 (2C, phenylglycine aromatic carbons ortho to chloro), 129.19 (2C, meta anilide aromatic carbons), 128.85 (2C, phenylglycine aromatic carbons meta to chloro), 124.01 (1C, para anilide aromatic carbon), 119.52 (2C, ortho anilide aromatic carbons), 56.66 (1C, -CH(C$_6$H$_4$Cl), 22.70 (1C, -C(O)CH$_3$).

IR (ss) v/cm^{-1}: 3290, 3260, 1739, 1643, 1536

Found m/z (EI$^+$) = 302.0814, calculated 302.0822

M.p. = 235-237 °C

2-Acetamido-2-(3-chloro phenyl) acet(4-methyl anilide) (8j)

Synthesised from compound **4g**. Yield: 39 %

^{1}H NMR (500 MHz, d^6-DMSO) δ = 10.29 (s, 1H, -NHC$_6$H$_4$CH$_3$), 8.73 (d, 1H, -NHAc, $^3J_{H-H}$ = 7.95 Hz), 7.55 (s, 1H, phenylglycine aromatic proton ortho to chloro and SC), 7.46 (d, 2H, aniline aromatic protons ortho to amide meta to methyl, $^3J_{H-H}$ = 8.30 Hz), 7.46 (obs d, 1H, phenylglycine aromatic proton ortho SC para to chloro), 7.41 (t, 1H, phenylglycine aromatic proton meta to chloro and SC), 7.38 (dt, 1H, phenylglycine aromatic proton ortho to chloro para to SC, $^3J_{H-H}$ = 7.85 Hz, $^4J_{H-H}$ = 1.75 Hz), 7.11 (d, 2H, aniline aromatic protons meta to amide ortho to methyl, $^3J_{H-H}$ = 8.30 Hz), 5.66 (d, 1H , -CH(C$_6$H$_4$Cl)-, $^3J_{H-H}$ = 7.95 Hz), 2.24 (s, 3H, -NHC$_6$H$_4$CH$_3$), 1.94 (s, 3H, -C(O)CH$_3$).

^{13}C NMR (125 MHz d^6-DMSO) δ = 169.20, (1C, CH$_3$C(O)-), 167.96 (1C, -C(O)NHC$_6$H$_5$), 140.83 (1C, phenylglycine aromatic carbon meta to chloro, ipso to SC), 136.01 (1C, anilide

aromatic carbon ipso to amide), 133.05 (1C, phenylglycine aromatic carbon ipso to chloro), 132.66 (1C, anilide aromatic carbon ipso to methyl), 130.35 (1C, phenylglycine aromatic carbon meta to chloro and SC), 129.15 (2C, anilide aromatic carbon ortho to methyl meta to amide), 127.68 (1C, phenylglycine aromatic carbon ortho to chloro, para to SC), 126.97 (1C, phenylglycine aromatic carbon ortho to chloro and SC), 125.96 (1C, phenylglycine aromatic carbon para to chloro, ortho to SC), 119.23 (2C, anilide aromatic carbon meta to methyl ortho to amide), 56.38 (1C, -CH(C_6H_4Cl), 22.31 (1C, -C(O)CH_3), 20.39 (1C, -NH$C_6H_4CH_3$).

IR (ss) v/cm^{-1}: 3270, 1738, 1640, 1533

Found m/z (EI$^+$) = 316.0984, calculated 316.0979

M.p. = 230-232 °C

2-Acetamido-2-(3-chloro phenyl) acetanilide (8k)

Synthesised from compound **4g**. Yield: 53 %

^{1}H NMR (500 MHz, d^6-DMSO) δ = 10.39 (s, 1H, -NH$C_6H_4CH_3$), 8.76 (d, 1H, -NHAc, $^3J_{H-H}$ = 7.90 Hz), 7.58 (d, 2H, ortho aniline aromatic protons, $^3J_{H-H}$ = 8.30 Hz), 7.56 (s, 1H, phenylglycine aromatic proton ortho to chloro and SC), 7.47 (d, 1H, phenylglycine aromatic proton ortho SC para to chloro), 7.41 (t, 1H, phenylglycine aromatic proton meta to chloro and SC, $^3J_{H-H}$ = 7.85 Hz), 7.38 (dt, 1H, phenylglycine aromatic proton ortho to chloro para to SC, $^3J_{H-H}$ = 7.95 Hz, $^4J_{H-H}$ = 1.55 Hz), 7.31 (t, 2H, meta aniline aromatic protons, $^3J_{H-H}$ = 8.20 Hz), 7.06 (t, 1H, para aniline aromatic protons, $^3J_{H-H}$ = 7.40 Hz), 5.68 (d, 1H , -CH(C_6H_5)-, $^3J_{H-H}$ = 7.95 Hz), 1.95 (s, 3H, -C(O)CH_3).

^{13}C NMR (125 MHz d^6-DMSO) δ = 169.23, (1C, CH_3C(O)-), 168.22 (1C, -C(O)NHC_6H_5), 140.71 (1C, phenylglycine aromatic carbon meta to chloro, ipso to SC), 138.56 (1C, ipso anilide aromatic carbon), 133.08 (1C, phenylglycine aromatic carbon ipso to chloro), 130.35 (1C, phenylglycine aromatic carbon meta to chloro and SC), 128.78 (2C, meta anilide aromatic carbon), 127.72 (1C, phenylglycine aromatic carbon ortho to chloro, para to SC), 127.02 (1C, phenylglycine aromatic carbon ortho to chloro and SC), 125.99 (1C, phenylglycine aromatic carbon para to chloro, ortho to SC), 123.68 (1C, para anilide aromatic carbon), 119.25 (2C, ortho anilide aromatic carbon), 56.47 (1C, -CH(C_6H_4Cl), 22.31 (1C, -C(O)CH_3).

IR (ss) v/cm^{-1}: 3294, 3261, 1740, 1639, 1539

Found m/z (EI$^+$) = 302.0814, 302.0822

M.p. = 205-206 °C

2-Acetamido-2-(4-trifluoromethyl phenyl) acetanilide (8l)

Synthesised from compound **4g**. Yield: 28 %

^{1}H NMR (400 MHz, d^6-DMSO) δ = 10.49 (s, 1H, -NH(C$_6$H$_5$)), 8.87 (d, 1H, -NHAc, $^3J_{H-H}$ = 7.88 Hz), 7.77 (d, 2H, phenylglycine aromatic protons ortho to trifluoromethyl, $^3J_{H-H}$ = 8.36 Hz), 7.71 (d, 2H, phenylglycine aromatic protons meta to trifluoromethyl, $^3J_{H-H}$ = 8.28 Hz), 7.58 (d, 2H, ortho anilide aromatic protons, $^3J_{H-H}$ = 7.72 Hz), 7.31 (t, 2H, meta anilide aromatic protons, $^3J_{H-H}$ = 7.68 Hz), 7.06 (t, 1H, para anilide aromatic proton, $^3J_{H-H}$ = 7.40 Hz), 5.77 (d, 1H, -CH(C$_6$H$_4$CF$_3$)-, $^3J_{H-H}$ = 7.84 Hz), 1.95 (s, 3H, -C(O)CH$_3$).

^{13}C NMR (125 MHz d^6-DMSO) δ = 169.30, (1C, CH$_3$C(O)-), 168.03 (1C, -C(O)NHC$_6$H$_5$), 142.98 (1C, phenylglycine aromatic carbon para to trifluoromethyl), 138.52 (1C, ipso anilide aromatic carbon), 128.80 (2C, meta anilide aromatic carbon), 128.35 (q, 1C, phenylglycine aromatic carbon ipso to trifluoromethyl, $^2J_{C-F}$ = 31.09 Hz), 128.01 (2C, phenylglycine aromatic carbon meta to trifluoromethyl), 125.41 (q, 2C, phenylglycine aromatic carbon ortho to trifluoromethyl, $^3J_{C-F}$ = 3.56 Hz), 124.15 (q, 1C, -CF$_3$, $^1J_{C-F}$ = 270.20 Hz), 123.72 (1C, para anilide aromatic carbon), 119.22 (2C, ortho anilide aromatic carbon), 56.61 (1C, -CH(C$_6$H$_4$CF$_3$), 22.29 (1C, -C(O)CH$_3$).

IR (ss) v/cm^{-1}: 2971, 1739, 1645, 1536

Found m/z (EI$^+$) = 336.1086 calculated 336.1086

M.p. = 244-245 °C

4.6.3 Proton-Deuterium Exchange Reactions

4.6.3.1 ^{1}H NMR Experiments at 37 °C

The H/D exchange reactions of **6e** at 37 °C, described in Section 4.4.1.1, were monitored by ^{1}H NMR spectroscopy. These experiments were carried out according to the method described in the experimental to Chapter 3, with the exception that no hydrolysis occurs for **6e**. Therefore, there is no drop in pH and hence no need to maintain the pH** with addition of NaOD solution.

4.6.3.2 LCMS Experiments at 60, 70, 80 and 90 °C

Buffers for H/D exchange experiments were made according to the following method. The appropriate quantity of NaH$_2$PO$_4$ for the desired buffer concentration was dissolved in D$_2$O. The ionic strength was made to 1 M using NaCl. As pK_a varies with temperature, the required

pH* of the solution at room temperature, was calculated so that the desired pH* at temperatures of 60, 70, 80 and 90 °C was obtained. This temperature-corrected pH* was obtained through adding portions of $NaOD/D_2O$ solution whilst monitoring with a pH probe at 25 °C. The pH* was also measured at the temperature at which the buffer was to be used in order to confirm it was at the desired value at this temperature.

H/D exchange kinetic experiments were carried out in duplicate, using a liquid chromatograph with mass spectrometer detection. Before analysis, calibration curves were produced for the mass spectrometer response of each compound for analysis. Starting with initial concentrations of 9-10 μM, these were subsequently diluted four times, each time by a dilution factor of four to produce five solutions with a range of concentrations down to < 0.1 μM. These solutions were then analysed using the mass spectrometer, with detection at the appropriate mass to find the M+1 molecular ion. A linear response was obtained for each compound **6b, d, e, 7a-d** and **8a-l**. To initiate each experiment, the autosampler injected a 10 μl portion from a stock solution of compound dissolved in acetonitrile into 1 ml of the appropriate buffer solution. The buffer solution was preheated to the appropriate temperature in a thermostatted vial tray, from where injections were made at the desired (pre-programmed) times. After each injection, the mass spectrogram was automatically analysed. The integral was converted to the concentration of compound protonated at the stereogenic centre using the calibration curve. To ensure that H/D exchange was the only process resulting in loss of the original molecular ion, in each case a control sample of the substrate in H_2O 0.3 M phosphate buffer solution was also analysed. As the mass spectrometer response for the M+1 ion of this sample did not reduce over time for any of the compounds analysed, it is safe to assume that the only process resulting in a reduction in the response of the M+1 ion is H/D exchange. For compound **6e**, a sample was left in deuterated buffers at 90 °C for 2 days to ensure all compound was deuterated at the stereogenic centre. This sample was then diluted four-fold, four times and used to produce a calibration curve with detection of the M+2 molecular ion. Formation of this species was followed at 60 °C, simultaneous with monitoring the decrease in the response for the M+1 molecular ion. These curves are plotted together in Figure 4.17.

Experiments were carried out using an XTerra column (MS C18 2.5 mm, 2.1×30 mm: part no. 186000592). Flow rate was 0.7 ml per minute. The eluents and the gradient used in the LC method are as follows:

Channel A = 5 % CH_3CN, 10 mM NH_4OAc, 0.1 % Acetic acid (pH = 4.5), Channel B = 95 % CH_3CN, 0.05 % Acetic acid.

Table 4.15: Gradient used for Chapter 4 LCMS experiments.

Time (mins)	% A	% B
0.0	100	0
6.0	0	100
10.0	0	100
10.1	100	0
14.0	100	0

The data obtained from the kinetic experiments was plotted using OriginPro 8. Observed first-order rate constants were obtained through fitting the data to eqn (3.6). Figure 4.9 was plotted using Wolfram Mathematica 8.0.

4.7 Appendix

4.7.1 Figures from ^{1}H NMR Kinetic Experiments

The graphs from which the rate constants of H/D exchange for compound **6e** in Table 4.2 were determined are displayed in Figure 4.11. All experiments were carried out at 37 °C, I = 1 M. pH** 7.4.
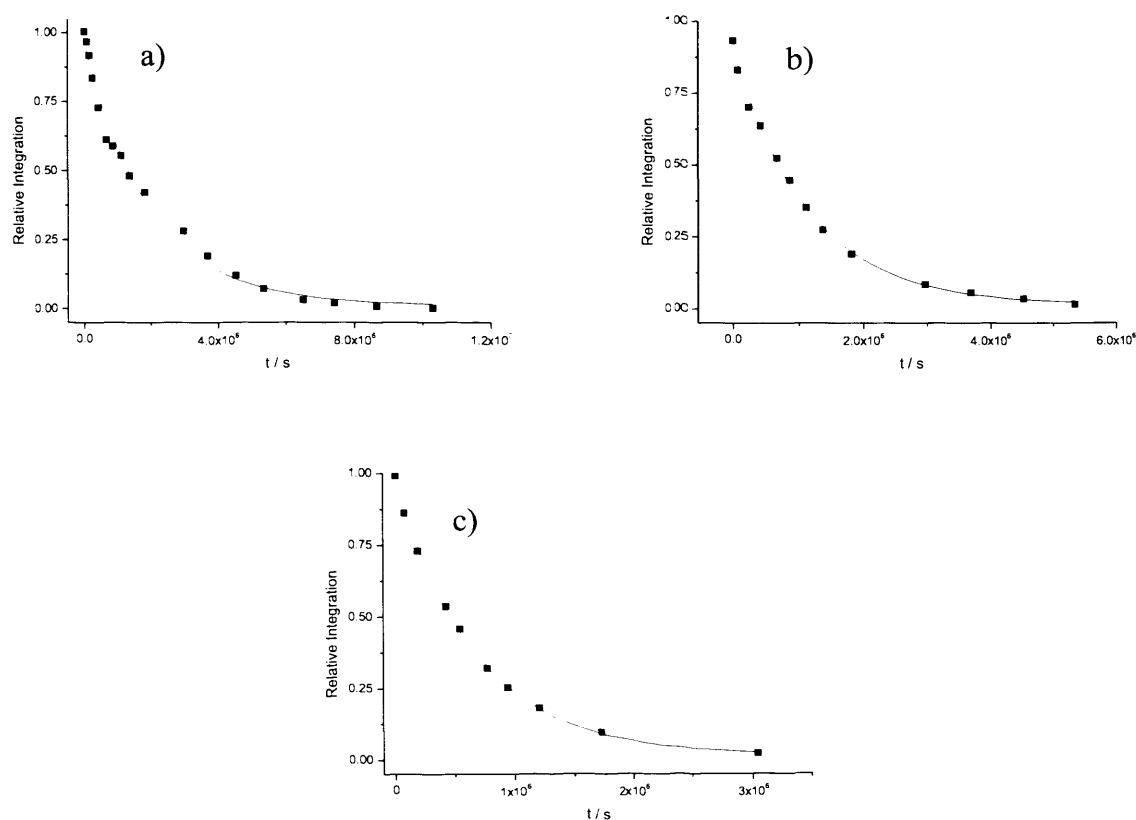
Figure 4.11: H/D exchange data for compound **6e** at 37 °C, pH** 7.4, I = 1 M. Phosphate buffer concentration a) 0.1 M, b) 0.2 M, c) 0.3 M.

4.7.2 Data Tables from LCMS Kinetic Experiments

The LCMS experimental data from which Figure 4.2 and Figure 4.4 were constructed is listed in the tables displayed in the following pages.

Table 4.16: Rate constant data for compound **6b** in D_2O buffers of pH* 7.4 at 90 °C, $I = 1$ M.

phosphate conc. / M	$[HPO_4^{2-}]$ conc. / M	k_{deut} x 10^5 / s^{-1}	k_{deut} x 10^5 / s^{-1} (duplicate)
0.100	0.061	2.31 ± 0.29	2.23 ± 0.21
0.200	0.122	2.95 ± 0.24	3.45 ± 0.35
0.300	0.182	3.62 ± 0.39	3.63 ± 0.26

$k_{gb} = (1.15 \pm 0.23) \times 10^{-4} \ s^{-1} \ M, \qquad k_0' = (1.60 \pm 0.27) \times 10^{-5} \ s^{-1}$

Table 4.17: Rate constant data for compound **6d** in D_2O buffers of pH* 7.4 at 90 °C, $I = 1$ M.

phosphate conc. / M	$[HPO_4^{2-}]$ conc. / M	k_{deut} x 10^5 / s^{-1}	k_{deut} x 10^5 / s^{-1} (duplicate)
0.150	0.091	7.20 ± 1.00	6.82 ± 0.81
0.200	0.122	10.06 ± 0.83	9.09 ± 0.98
0.300	0.182	12.06 ± 0.40	13.91 ± 0.83

$k_{gb} = (5.63 \pm 0.73) \times 10^{-4} \ s^{-1} \ M, \qquad k_0' = (2.24 \pm 1.15) \times 10^{-5} \ s^{-1}$

Table 4.18: Rate constant data for compound **6e** in D_2O buffers of pH* 7.4 at 90 °C, $I = 1$ M.

phosphate conc. / M	$[HPO_4^{2-}]$ conc. / M	k_{deut} x 10^4 / s^{-1}	k_{deut} x 10^4 / s^{-1} (duplicate)
0.100	0.061	3.36 ± 0.15	2.96 ± 0.35
0.150	0.091	4.58 ± 0.18	4.49 ± 0.29
0.200	0.122	5.40 ± 0.33	5.87 ± 0.19
0.300	0.182	6.41 ± 0.22	6.83 ± 0.20

$k_{gb} = (2.73 \pm 0.16) \times 10^{-3} \ s^{-1} \ M, \qquad k_0' = (1.91 \pm 0.19) \times 10^{-4} \ s^{-1}$

202

Table 4.19: Rate constant data for compound **6e** in D_2O buffers of pH* 7.4 at 80 °C, $I = 1$ M.

phosphate conc. / M	[HPO$_4^{2-}$] conc. / M	k_{deut} x 10^4 / s^{-1}	k_{deut} x 10^4 / s^{-1} (duplicate)
0.100	0.061	1.60 ± 0.07	1.90 ± 0.09
0.150	0.091	1.75 ± 0.06	1.91 ± 0.15
0.200	0.122	2.10 ± 0.09	1.97 ± 0.09
0.300	0.182	2.75 ± 0.07	2.89 ± 0.09

$k_{gb} = (1.04 \pm 0.07)$ x 10^{-3} s^{-1} M, $\quad k_0' = (8.61 \pm 0.88)$ x 10^{-5} s^{-1}

Table 4.20: Rate constant data for compound **6e** in D_2O buffers of pH* 7.4 at 70 °C, $I = 1$ M.

phosphate conc. / M	[HPO$_4^{2-}$] conc. / M	k_{deut} x 10^5 / s^{-1}	k_{deut} x 10^5 / s^{-1} (duplicate)
0.100	0.061	5.63 ± 0.98	6.06 ± 1.12
0.200	0.122	10.10 ± 1.89	8.16 ± 0.73
0.300	0.182	11.53 ± 0.64	13.29 ± 0.39

$k_{gb} = (6.05 \pm 0.64)$ x 10^{-4} s^{-1} M, $\quad k_0' = (1.72 \pm 1.04)$ x 10^{-5} s^{-1}

Table 4.21: Rate constant data for compound **6e** in D_2O buffers of pH* 7.4 at 60 °C, $I = 1$ M.

phosphate conc. / M	[HPO$_4^{2-}$] conc. / M	k_{deut} x 10^5 / s^{-1}	k_{deut} x 10^5 / s^{-1} (duplicate)
0.100	0.061	1.64 ± 0.33	-
0.150	0.091	3.02 ± 0.46	3.00 ± 0.45
0.200	0.122	3.76 ± 0.50	3.46 ± 0.53
0.300	0.182	4.41 ± 0.56	4.21 ± 0.54

$k_{gb} = (2.19 \pm 0.39)$ x 10^{-5} s^{-1} M, $\quad k_0' = (3.20 \pm 5.11)$ x 10^{-6} s^{-1}

The data displayed in Table 4.11 and Table 4.13 show the average rate constants of H/D exchange calculated from two kinetic experiments. Results from individual experiments are displayed in Table 4.22 and Table 4.23.

Table 4.22: Individual experiment data for H/D exchange experiments of **7a-d** in D_2O buffers pH* 7.4 with phosphate concentration 0.3 M at 90 °C, $I = 1$ M.

Compound	$k_{\text{deut}} \times 10^5 / \text{s}^{-1}$	$k_{\text{deut}} \times 10^5 / \text{s}^{-1}$ (duplicate)	Average $k_{\text{deut}} \times 10^5 / \text{s}^{-1}$
7a	6.92 ± 0.48	6.09 ± 0.41	6.50 ± 0.45
7b	5.38 ± 0.31	4.74 ± 0.18	5.06 ± 0.25
7c	8.16 ± 0.62	7.95 ± 0.55	8.05 ± 0.58
7d	10.47 ± 0.27	9.31 ± 0.66	9.89 ± 0.47

Table 4.23: Individual experiment data for H/D exchange experiments of **8a-l** in D_2O buffers pH* 7.4 with phosphate concentration 0.3 M at 90 °C, $I = 1$ M.

Compound	$k_{\text{deut}} \times 10^5 / \text{s}^{-1}$	$k_{\text{deut}} \times 10^5 / \text{s}^{-1}$ (duplicate)	Average $k_{\text{deut}} \times 10^5 / \text{s}^{-1}$
8a	5.42 ± 0.26	5.48 ± 0.28	5.45 ± 0.25
8b	3.24 ± 0.37	3.40 ± 0.33	3.32 ± 0.35
8c	4.62 ± 0.94	3.86 ± 0.55	4.24 ± 0.69
8d	6.61 ± 0.37	6.21 ± 0.50	6.41 ± 0.43
8e	8.96 ± 0.27	8.77 ± 0.24	8.86 ± 0.25
8f	2.29 ± 0.36	2.14 ± 0.55	2.22 ± 0.46
8g	2.64 ± 0.42	2.58 ± 0.45	2.61 ± 0.44
8h	4.30 ± 0.35	4.77 ± 0.16	4.54 ± 0.25
8i	11.92 ± 0.54	11.72 ± 0.55	11.82 ± 0.55
8j	14.42 ± 0.19	14.44 ± 0.64	14.43 ± 0.42
8k	21.33 ± 0.20	20.98 ± 0.62	21.15 ± 0.41
8l	51.62 ± 2.37	68.32 ± 8.12	59.97 ± 5.24

4.7.3 Figures from LCMS Kinetic Experiments

The graphs from which the data in the tables in Section 4.7.2 was obtained are displayed in the following figures. All experiments were carried out at pH* 7.4, $I = 1$ M.

4.7.3.1 Compound 6b, 90 °C
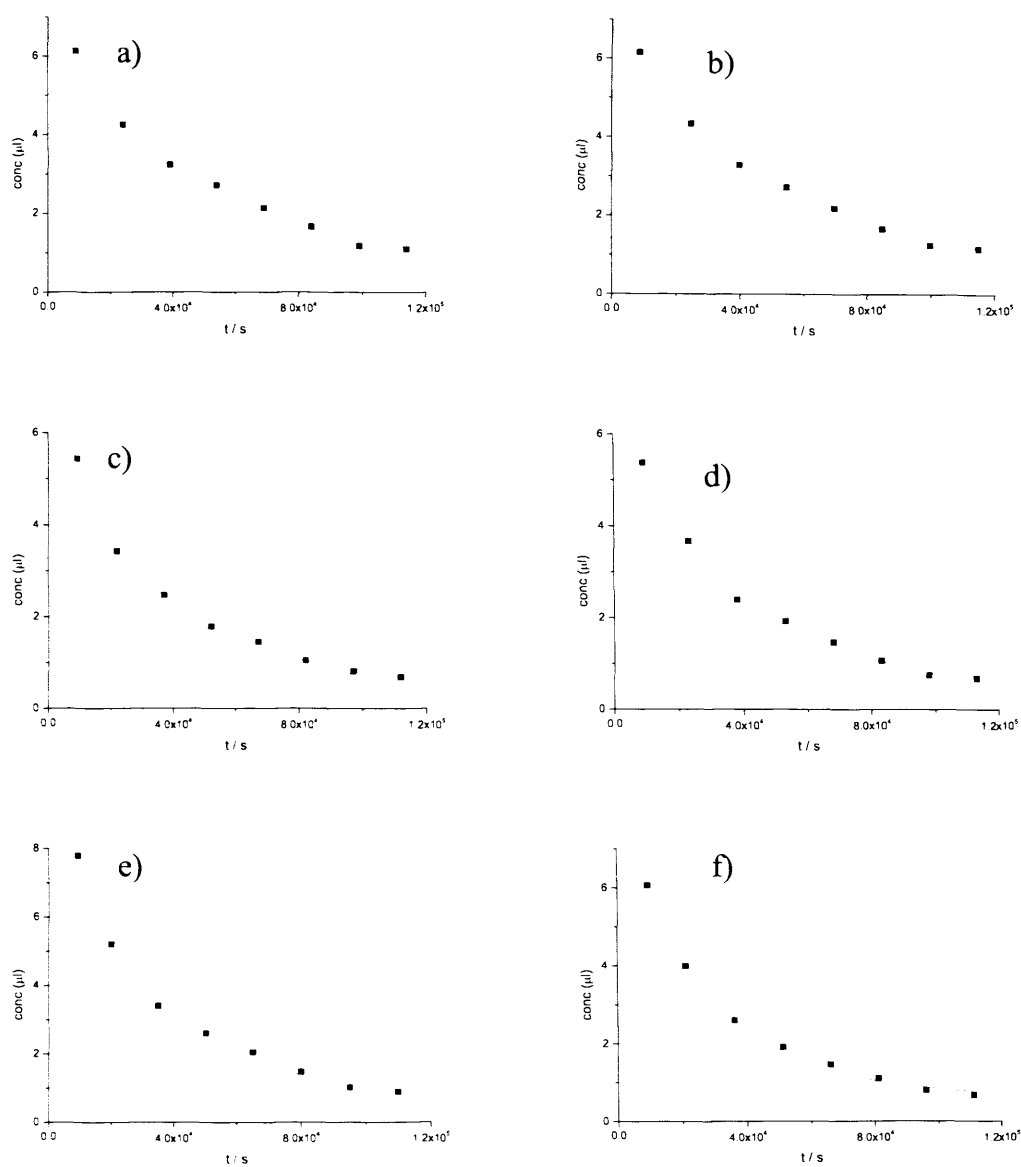
Figure 4.12: H/D exchange data for compound **6b** at 90 °C with phosphate buffer concentration a) 0.1 M, b) 0.1 M (duplicate), c) 0.2 M, d) 0.2 M (duplicate), e) 0.3 M, f) 0.3 M (duplicate).

4.7.3.2   Compound 6d, 90 °C
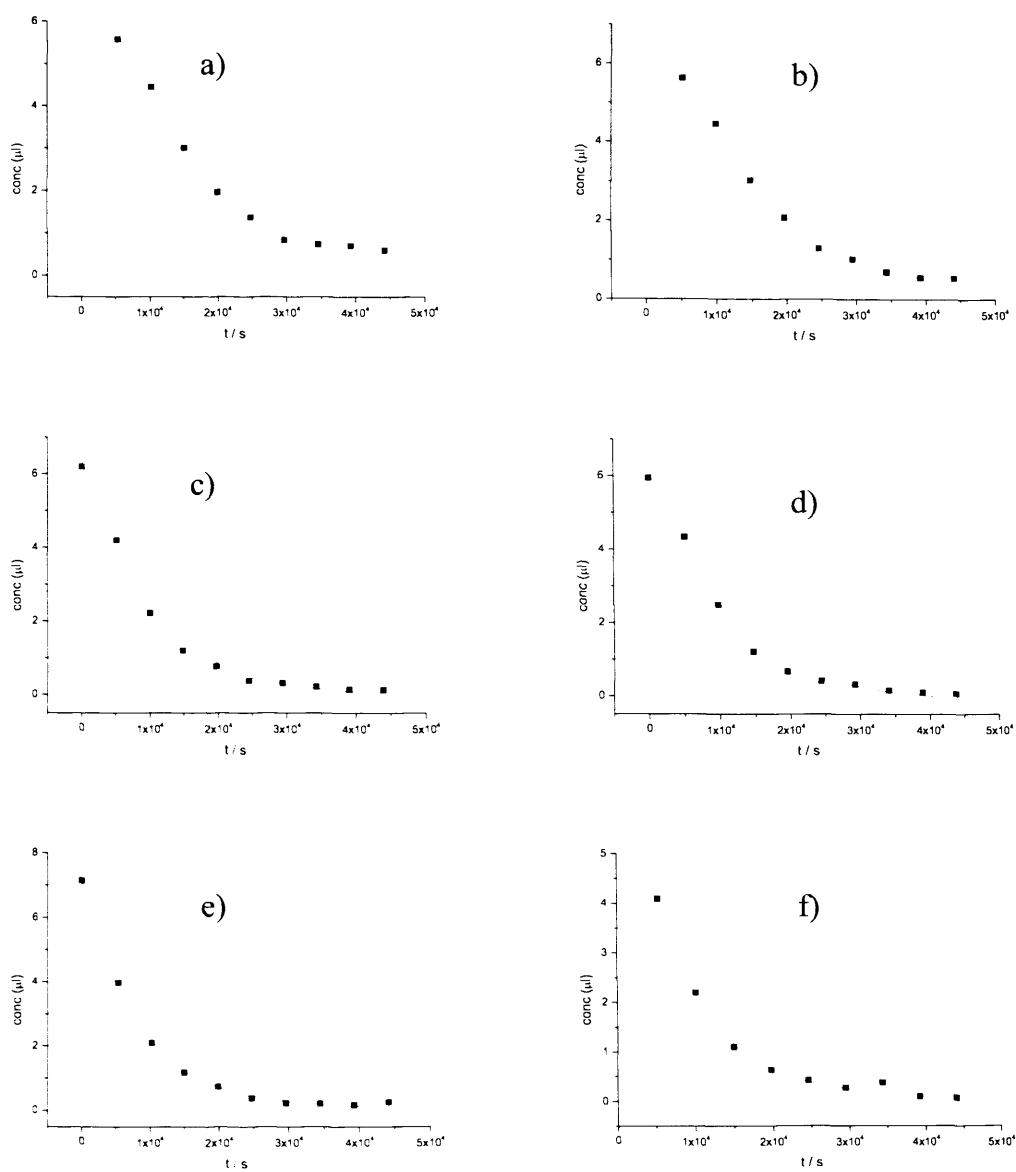
Figure 4.13: H/D exchange data for compound **6d** at 90 °C with phosphate buffer concentration a) 0.15 M, b) 0.15 M (duplicate), c) 0.2 M, d) 0.2 M (duplicate), e) 0.3 M, f) 0.3 M (duplicate).

4.7.3.3 Compound 6e, 90 °C
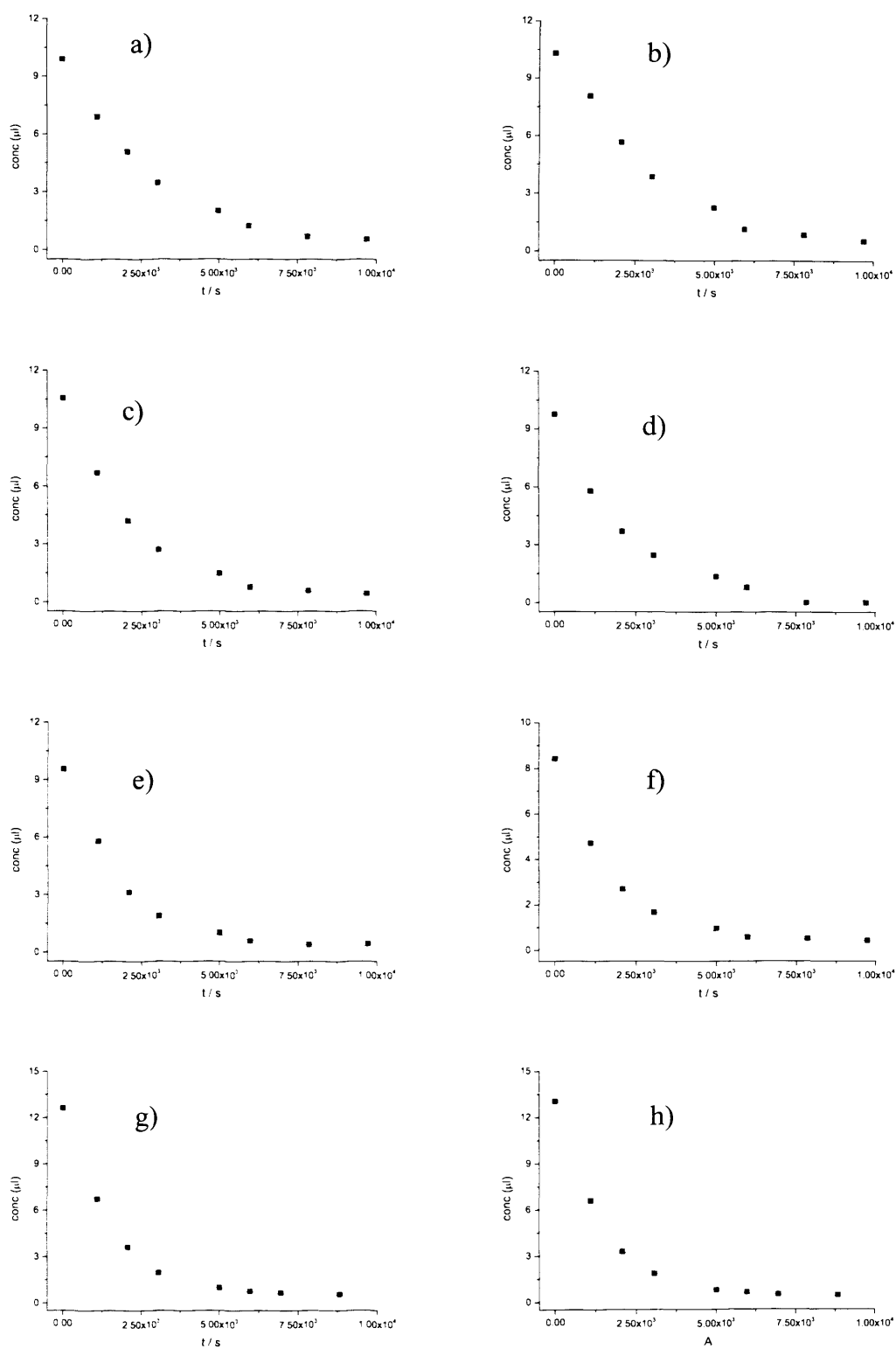
Figure 4.14: H/D exchange data for compound **6e** at 90 °C with phosphate buffer concentration a) 0.1 M, b) 0.1 M (duplicate), c) 0.15 M, d) 0.15 M (duplicate), e) 0.2 M, f) 0.2 M (duplicate), g) 0.3 M, h) 0.3 M (duplicate).

207

4.7.3.4 Compound 6e, 80 °C
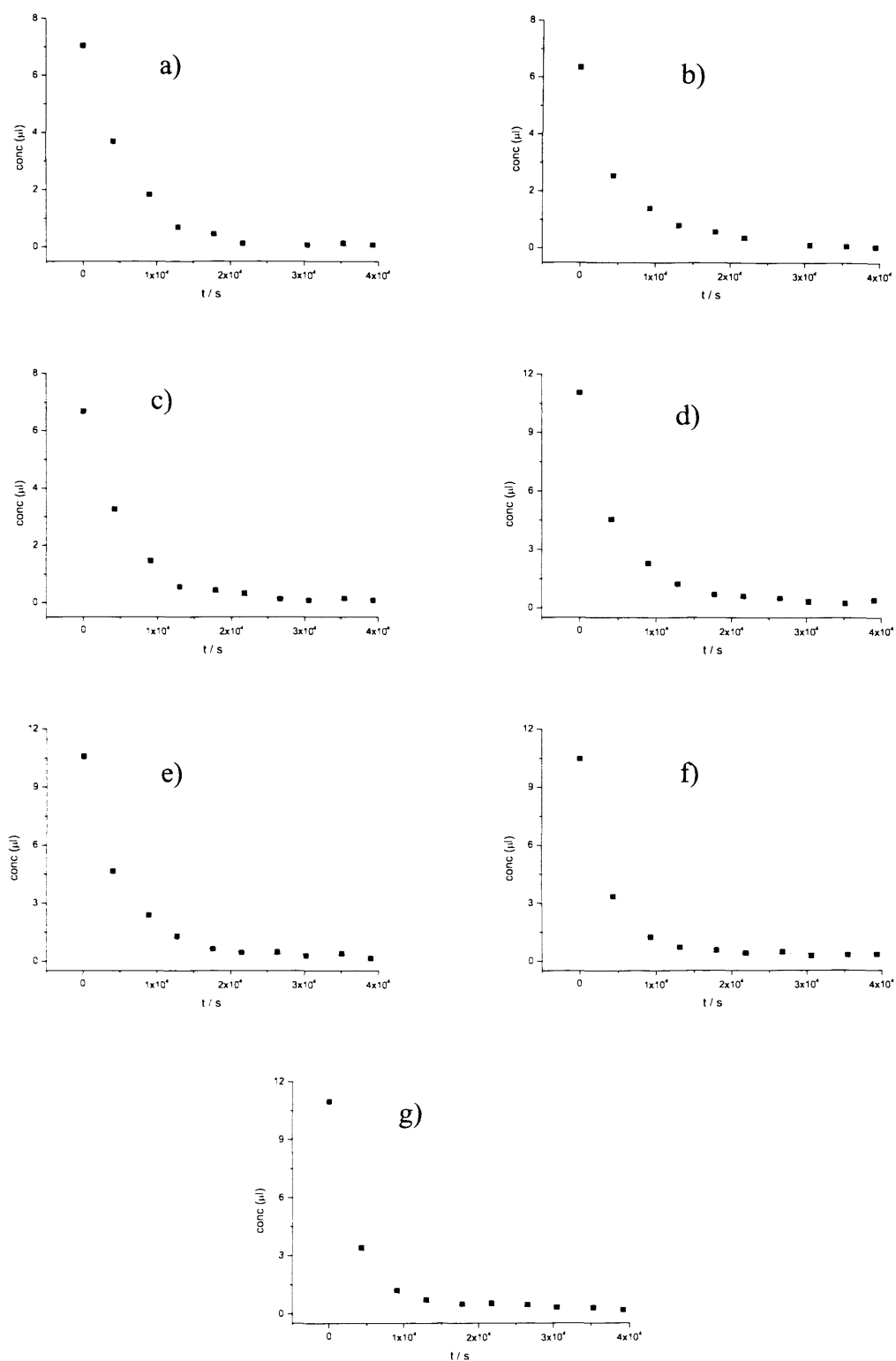
Figure 4.15: H/D exchange data for compound **6e** at 80 °C with phosphate buffer concentration a) 0.1 M, b) 0.15 M, c) 0.15 M (duplicate), d) 0.2 M, e) 0.2 M (duplicate), f) 0.3 M, g) 0.3 M (duplicate).

208

4.7.3.5 Compound 6e, 70 °C
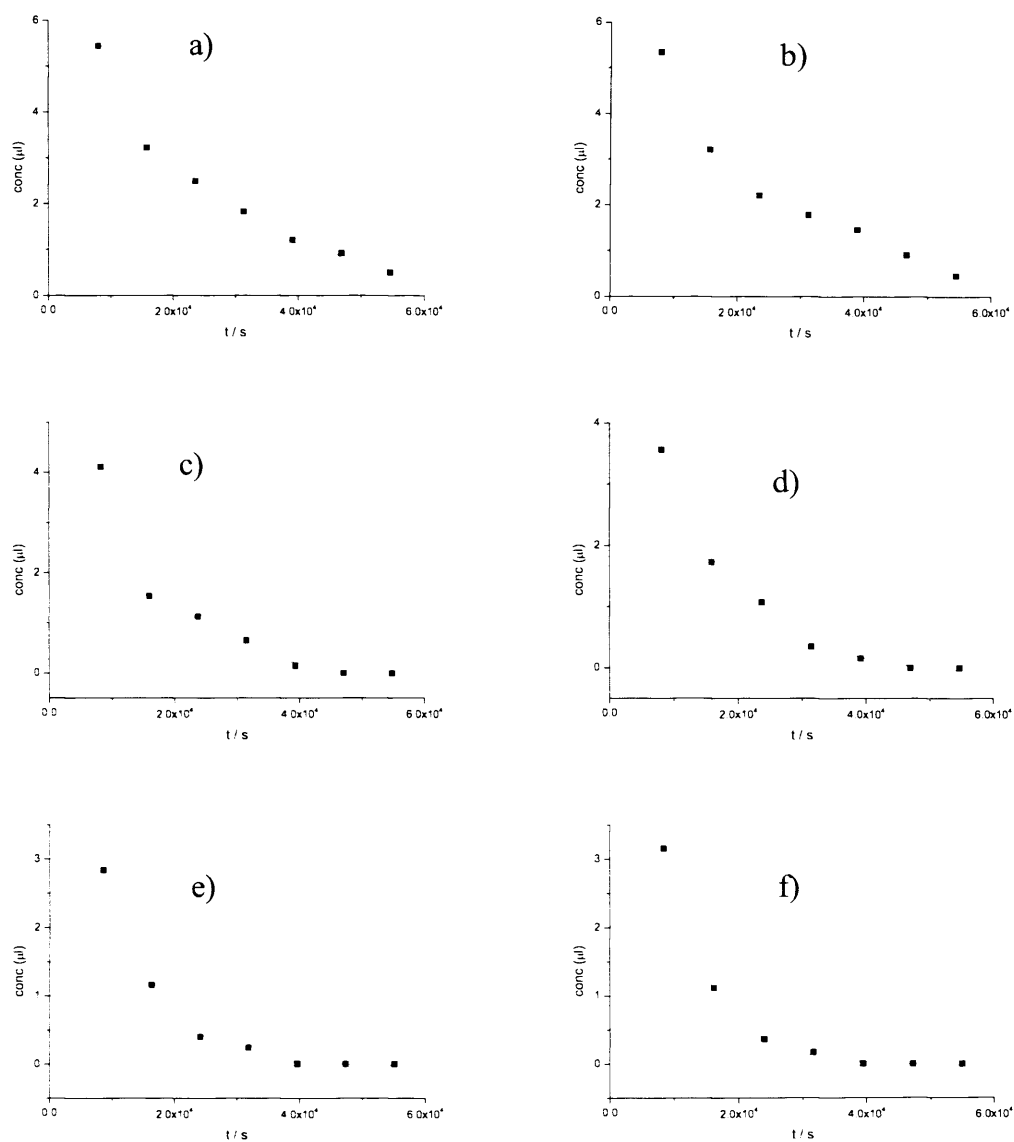
Figure 4.16: H/D exchange data for compound **6e** at 70 °C with phosphate buffer concentration a) 0.1 M, b) 0.1 M (duplicate), c) 0.2 M, d) 0.2 M (duplicate), e) 0.3 M, f) 0.3 M (duplicate).
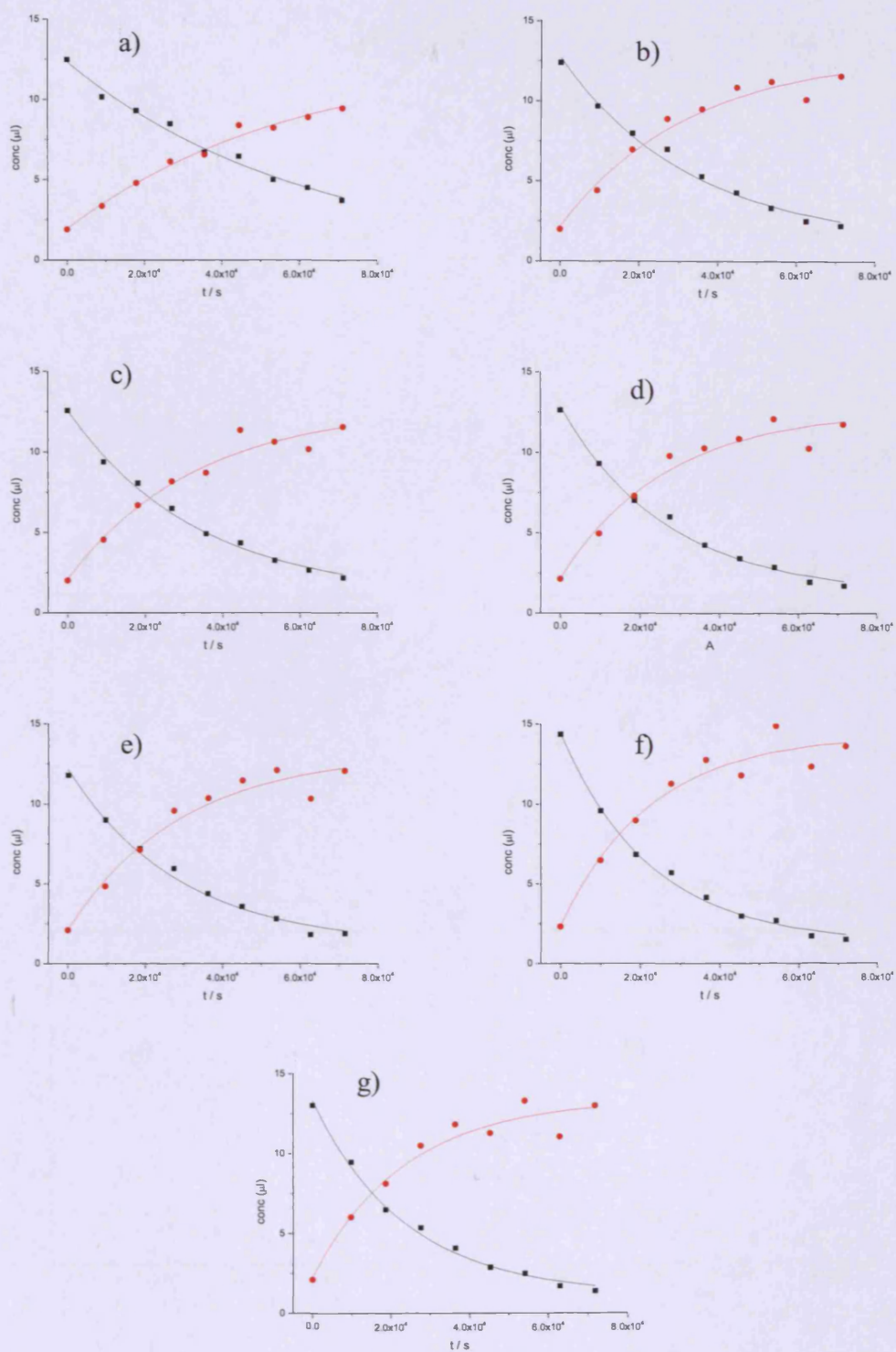
Figure 4.17: H/D exchange data for compound **6e** at 60 °C with phosphate buffer concentration a) 0.1 M, b) 0.15 M, c) 0.15 M (dup), d) 0.2 M, e) 0.2 M (dup), f) 0.3 M, g) 0.3 M (dup). (■) H species data, (●) D species data.

4.7.3.7 N-Benzoyl Phenylglycine Amides 7a-d, 90 °C
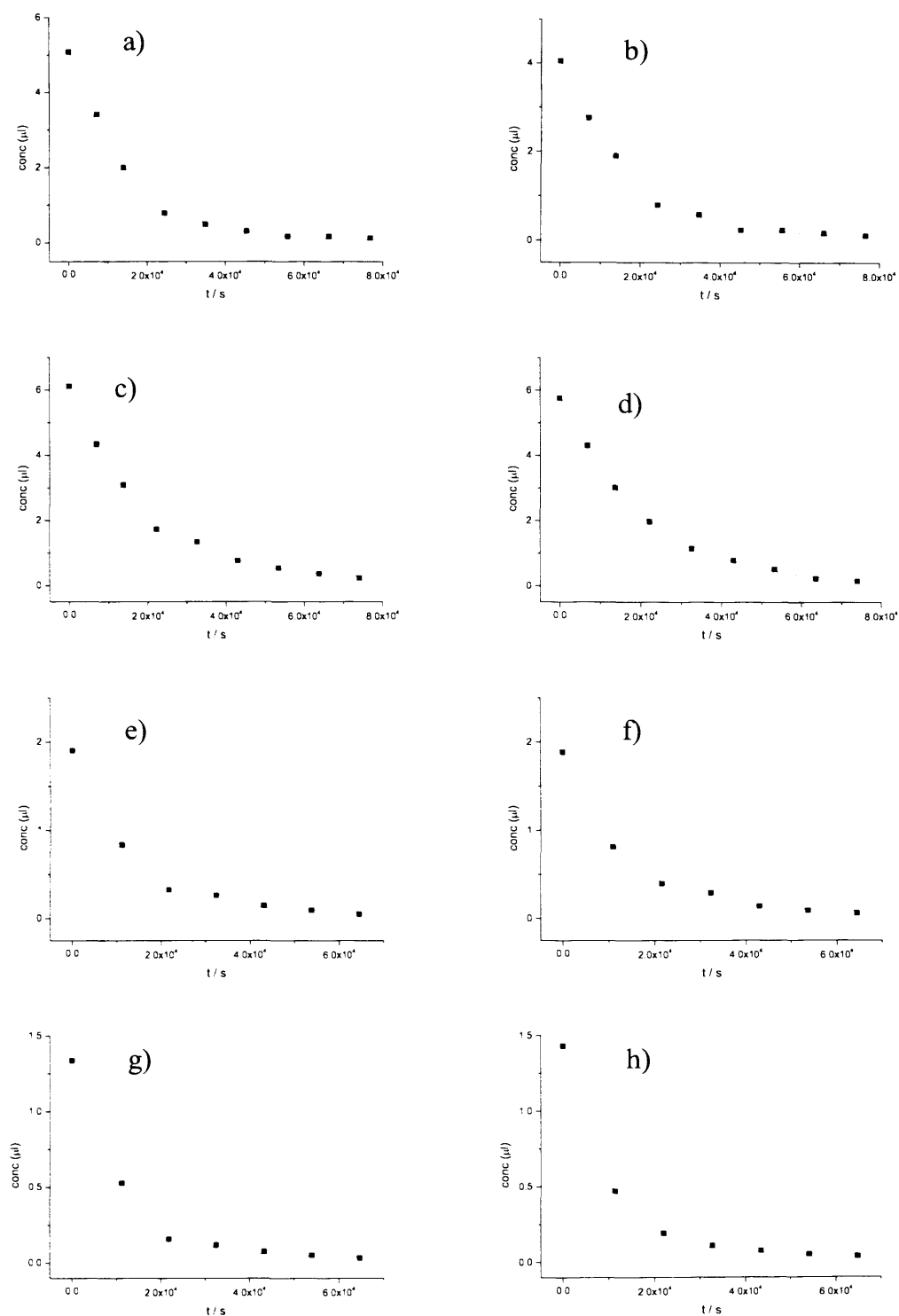
Figure 4.18: H/D exchange data for at 90 °C, 0.3 M phosphate buffer concentration for a) **7a**, b) **7a** (duplicate), c) **7b**, d) **7b** (duplicate), e) **7c**, f) **7c** (duplicate), g) **7d**, h) **7d** (duplicate).

4.7.3.8 N-Acetyl Phenylglycine Anilides 8a-l, 90 °C
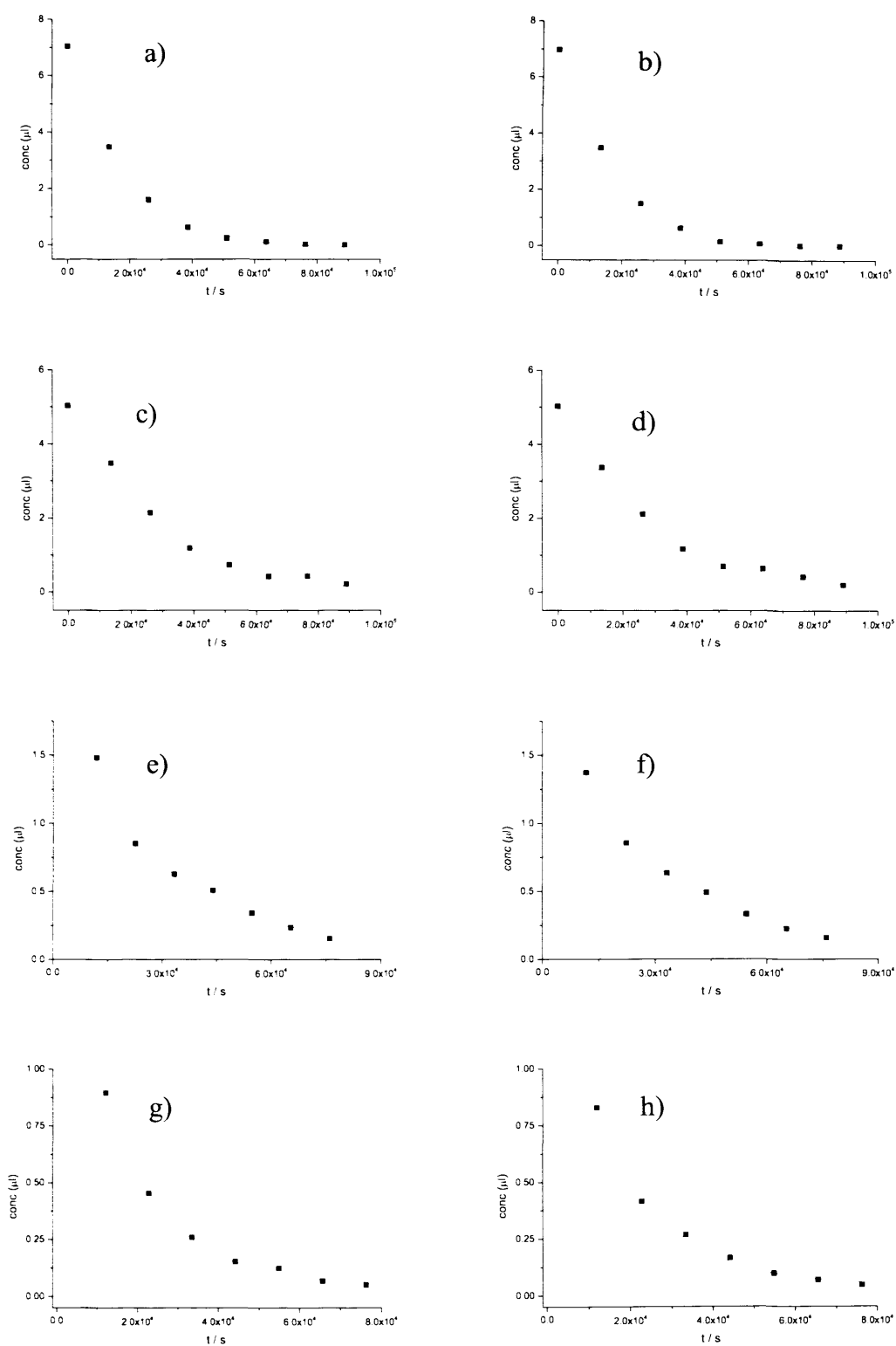
Figure 4.19: H/D exchange data for at 90 °C, 0.3 M phosphate buffer concentration for a) **8a**, b) **8a** (duplicate), c) **8b**, d) **8b** (duplicate), e) **8c**, f) **8c** (duplicate), g) **8d**, h) **8d** (duplicate).
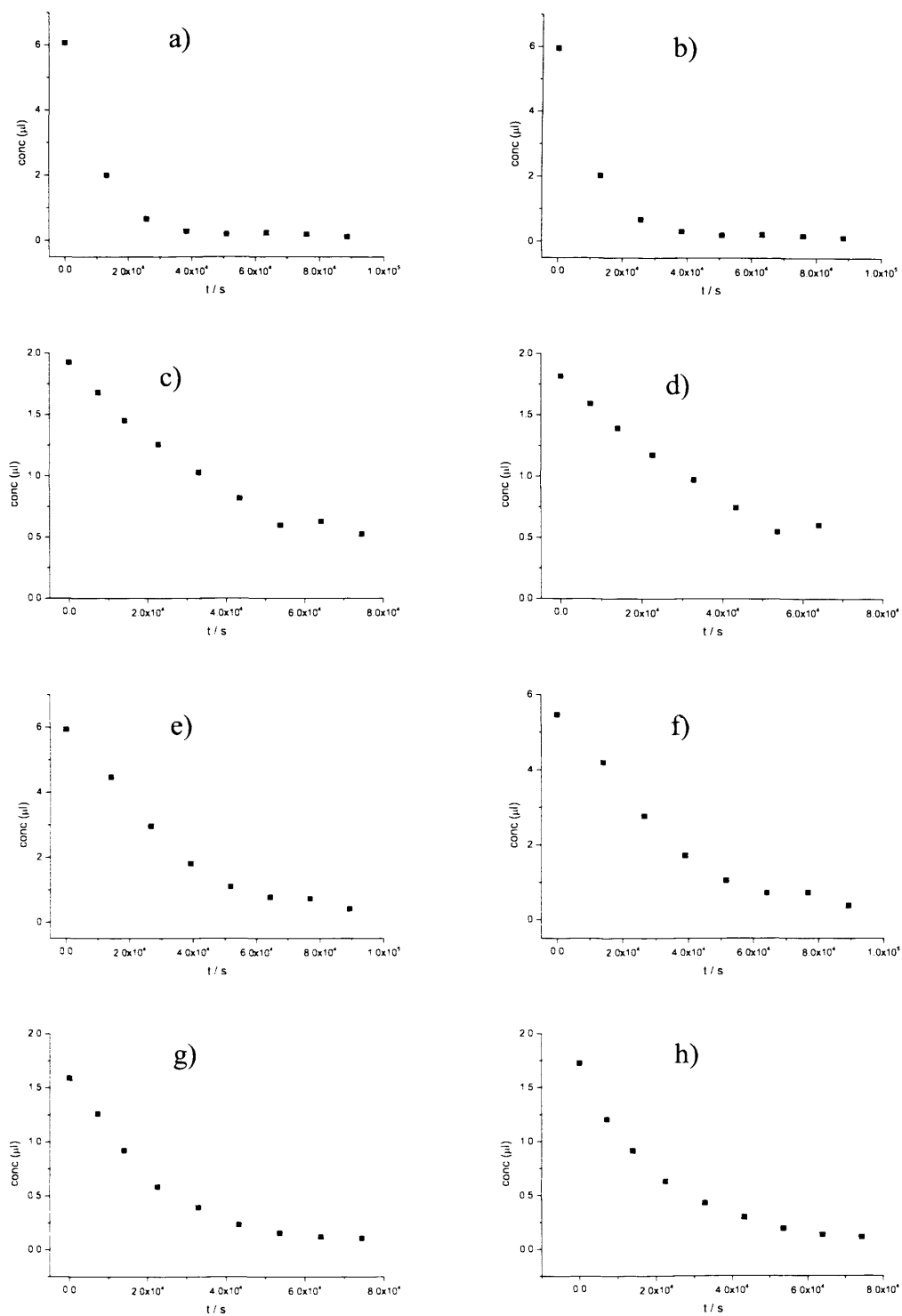
Figure 4.20: H/D exchange data for at 90 °C, 0.3 M phosphate buffer concentration for a) **8e**, b) **8e** (duplicate), c) **8f**, d) **8f** (duplicate), e) **8g**, f) **8g** (duplicate), g) **8h**, h) **8h** (duplicate).

213
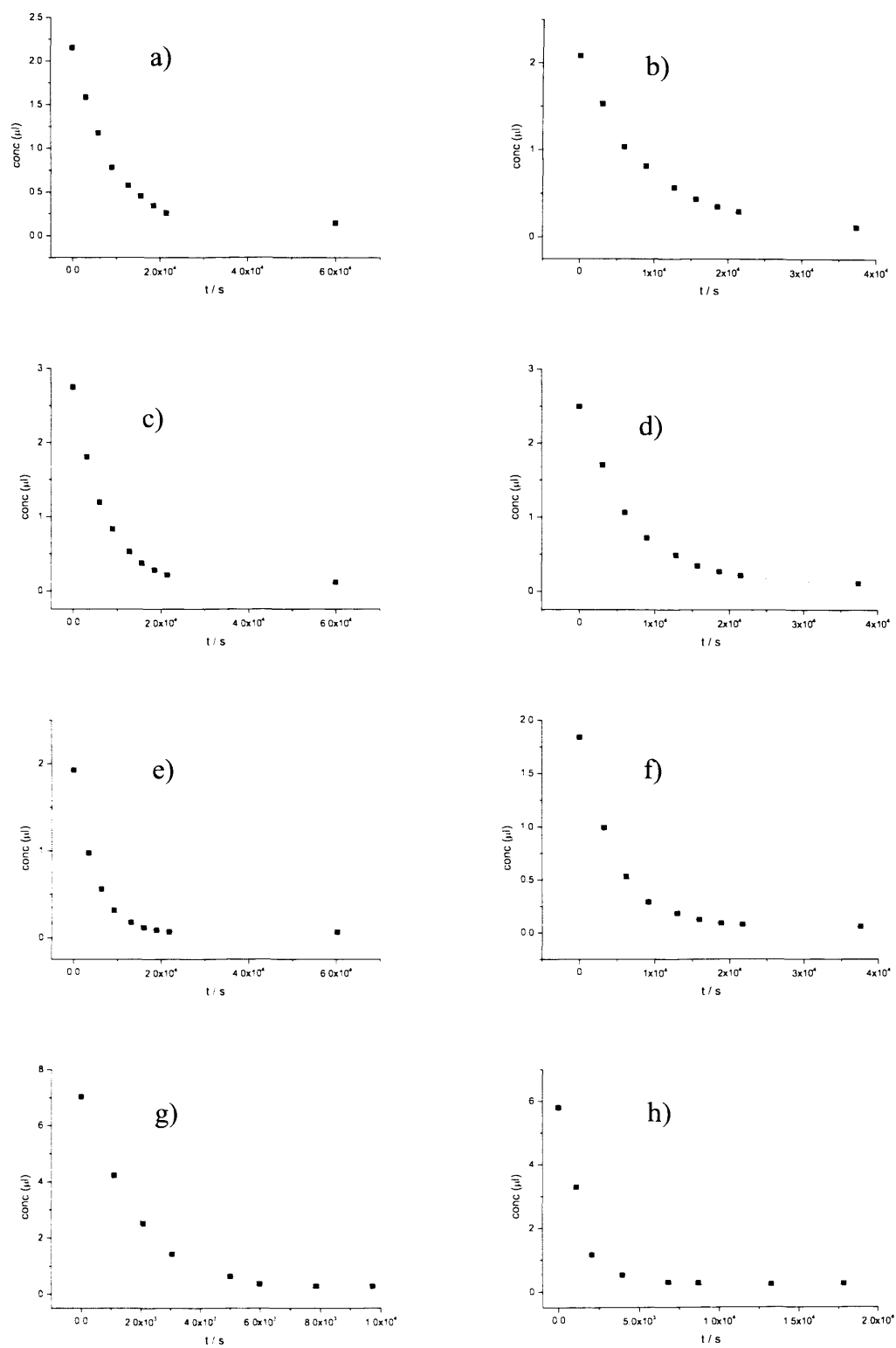
Figure 4.21: H/D exchange data for at 90 °C, 0.3 M phosphate buffer concentration for a) **8i**, b) **8i** (duplicate), c) **8j**, d) **8j** (duplicate), e) **8k**, f) **8k** (duplicate), g) **8l**, h) **8l** (duplicate).

214

4.7.3.9 Eyring Plot for Use as a Predictive Tool

As discussed in Section 4.4.1.4, an Eyring plot was constructed of using the data in Table 4.6 of rate constants of general-base catalysed H/D exchange, omitting the data point obtained using ^1H NMR spectroscopy at 37 °C. This was for the purpose of analysing the use of high-temperature work as a predictive tool for lower temperatures. The Eyring plot constructed is shown in Figure 4.22.
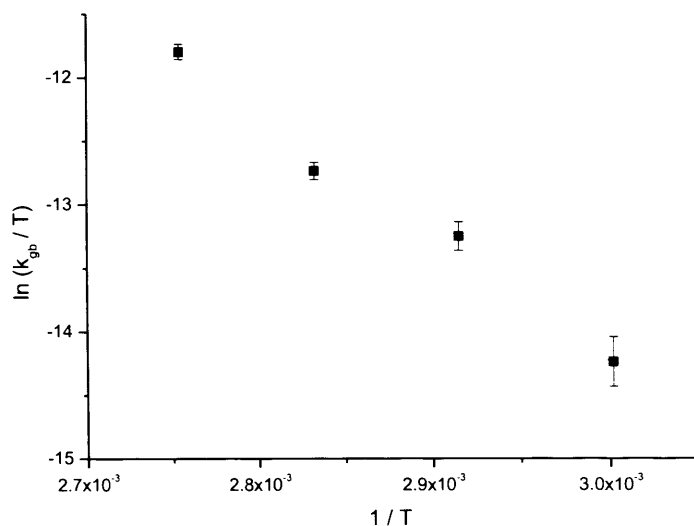
Figure 4.22: Eyring plot of general-base catalysed H/D exchange of **6e** (without data point at 37 °C), in D_2O phosphate buffers at pH* 7.4, $I = 1$ M. y-axis intercept = ln (k_B/h) + $\Delta S^{\ddagger}/R$ = 14.86 ± 3.03. Gradient = $-\Delta H^{\ddagger}/R$ = -9701.09 ± 1075.72.

The line of best fit shown in Figure 4.22 was extrapolated to 37 °C, and the expected value for k_{gb} was calculated as 2.39×10^{-5} s^{-1} M^{-1}.

4.8 References

1.   Testa, B.; Carrupt, P. A.; Gal, J., *Chirality* **1993,** *5* (3), 105-111.
2.   Reist, M.; Testa, B.; Carrupt, P. A., *Enantiomer* **1997,** *2* (3-4), 147-155.
3.   Reist, M.; Testa, B.; Carrupt, P.-A., Drug Racemization and Its Significance in Pharmaceutical Research. In *Handbook of Experimental Pharmacology*, Springer: 2003; Vol. 153, pp 91-112.
4.   Clayden, J. P.; Greeves, N.; Warren, S.; Wothers, P. D., *Organic Chemistry*. Oxford University Press: 2001; p 164-166.
5.   Bennet, A. J.; Somayaji, V.; Brown, R. S.; Santarsiero, B. D., *Journal of the American Chemical Society* **1991,** *113* (20), 7563-7571.
6.   Mujika, J. I.; Mercero, J. M.; Lopez, X., *Journal of the American Chemical Society* **2005,** *127* (12), 4445-4453.
7.   Kemnitz, C. R.; Loewen, M. J., *Journal of the American Chemical Society* **2007,** *129* (9), 2521-2528.
8.   Wang, W. H.; Cheng, C. C., *Bulletin of the Chemical Society of Japan* **1994,** *67* (4), 1054-1057.
9.   Wick, W. E., *Applied Microbiology* **1967,** *15* (4), 765-769.
10.   Abou-Khalil, B., *Neuropsychiatric Disease and Treatment* **2008,** *4* (3), 507-23.
11.   Adams, J.; Kauffman, M., *Cancer Investigation* **2004,** *22* (2), 304-311.
12.   Vallet, S.; Palumbo, A.; Raje, N.; Boccadoro, M.; Anderson, K. C., *Leukemia & Lymphoma* **2008,** *49* (7), 1238-1245.
13.   Richard, J. P.; Williams, G.; O'Donoghue, A. C.; Amyes, T. L., *Journal of the American Chemical Society* **2002,** *124* (12), 2957-2968.
14.   Fujita, T.; Hansch, C.; Iwasa, J., *Journal of the American Chemical Society* **1964,** *86* (23), 5175-5180.
15.   Leo, A.; Jow, P. Y. C.; Silipo, C.; Hansch, C., *Journal of Medicinal Chemistry* **1975,** *18* (9), 865-868.
16.   Chen, C. Y.; Chang, Y. S.; Lin, S. A.; Wen, H. I.; Cheng, Y. C.; Tsai, S. W., *Journal of Organic Chemistry* **2002,** *67* (10), 3323-3326.
17.   Smith, G. G.; Sivakua, T., *Journal of Organic Chemistry* **1983,** *48* (5), 627-634.
18.   Smith, G. G.; Williams, K. M.; Wonnacott, D. M., *Journal of Organic Chemistry* **1978,** *43* (1), 1-5.
19.   Reist, M.; Carrupt, P. A.; Testa, B.; Lehmann, S.; Hansen, J. J., *Helvetica Chimica Acta* **1996,** *79* (3), 767-778.
20.   Narduolo, S., Unpublished results.
21.   Jaffe, H. H., *Chemical Reviews* **1953,** *53* (2), 191-261.
22.   Suezawa, H.; Yuzuri, T.; Hirota, M.; Ito, Y.; Hamada, Y., *Bulletin of the Chemical Society of Japan* **1990,** *63* (2), 328-334.
23.   Yuzuri, T.; Suezawa, H.; Hirota, M., *Bulletin of the Chemical Society of Japan* **1994,** *67* (6), 1664-1673.
24.   Lee, C. K.; Yu, J. S.; Ji, Y. R., *Journal of Heterocyclic Chemistry* **2002,** *39* (6), 1219-1227.
25.   Bergon, M.; Calmon, J. P., *Tetrahedron Letters* **1981,** *22* (10), 937-940.
26.   Noorduin, W. L.; Izumi, T.; Millemaggi, A.; Leeman, M.; Meekes, H.; Van Enckevort, W. J. P.; Kellogg, R. M.; Kaptein, B.; Vlieg, E.; Blackmond, D. G., *Journal of the American Chemical Society* **2008,** *130* (4), 1158-59.
27.   Hyun, M. H.; Lee, G. S.; Han, S. C.; Cho, Y. J.; Baik, I. K., *Chirality* **2002,** *14* (6), 503-508.
28.   Williams, D. H.; Fleming, I., *Spectroscopic Methods in Organic Chemistry*. 5th ed.; McGraw-Hill: London, 1995; p 63-169.

5 Computational Studies as a Predictive Tool for Configurational Instability

5.1 Introduction

In this Chapter, the potential of computational chemistry methods to predict configurational instability in molecules (under the pharmacological conditions such as those used in Chapters 3 and 4) is investigated. The ability to obtain approximate rate constants of racemisation for molecules under investigation as a potential drug, without having to undertake the physical experimental procedures described in Chapters 3 and 4 or without synthesising a compound, would be of substantial benefit to the pharmaceutical industry. The results from computational modelling of a molecule could either eliminate or necessitate the need for further experimental analysis. If a computational model can be found that correlates with the rate constants of H/D exchange determined in Chapters 3 and 4, then application of that model to other compounds of interest could give theoretical rate constants for H/D exchange (and therefore for racemisation).

The rate constants of H/D exchange determined thus far have been for molecules of the type R''R'RC-H, and the reaction was found to take place through an S_E1 mechanism (Chapter 3). As shown in Scheme 1.7, the S_E1 mechanism takes place through loss of the labile proton bound to the stereogenic centre to leave a planar carbanion which can then be deuterated on either face (resulting in the loss of any enantiopurity). The stability of this carbanion is strongly dependent on the nature of neighbouring groups, specifically their ability to stabilise the negative charge either through delocalisation or electrostatic interactions. The results in Chapters 3 and 4 show that the stability of this carbanion is fundamental to the rate constant of H/D exchange, illustrated by the positive slope displayed in Hammett plots. Therefore, it was the stability of the carbanion, relative to the protonated state, that was investigated through computational methods. This relative stability is indicated by $\Delta G^{\ominus}$ in the reaction profile for the S_E1 mechanism (Figure 5.1).

Reaction Coordinate
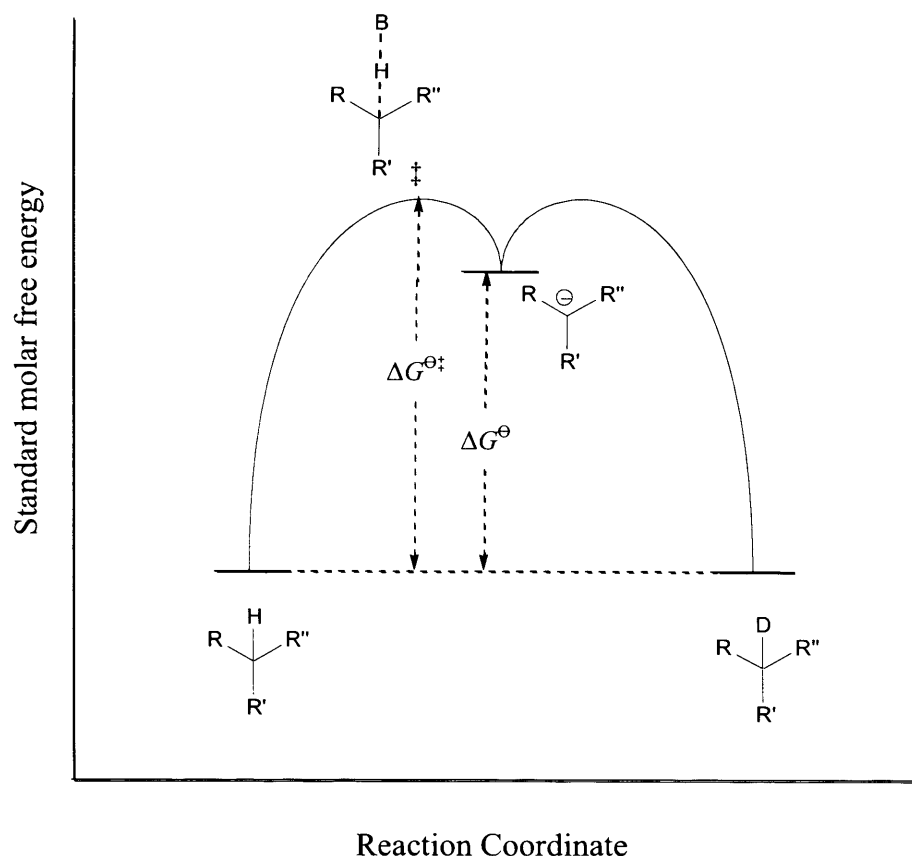
Figure 5.1: Reaction profile for H/D exchange through the S_E1 mechanism, where $\Delta G^{\ominus\ddagger}$ is the standard molar free energy of activation and $\Delta G^{\ominus}$ is the standard molar free energy of reaction.

Nakata *et al.* used computational methods to investigate the stability of benzylic anions in the gas-phase.[1] The energies and geometries of ring substituted anions and the corresponding neutral species were calculated using the B3LYP/6-311 + G(2d,p) level of theory. The substituent effects of on the relative stability of the anions was then determined through hypothetical proton transfer reactions (Scheme 5.1).

E_H (-) E_X (H) E_H (H) E_X (-)
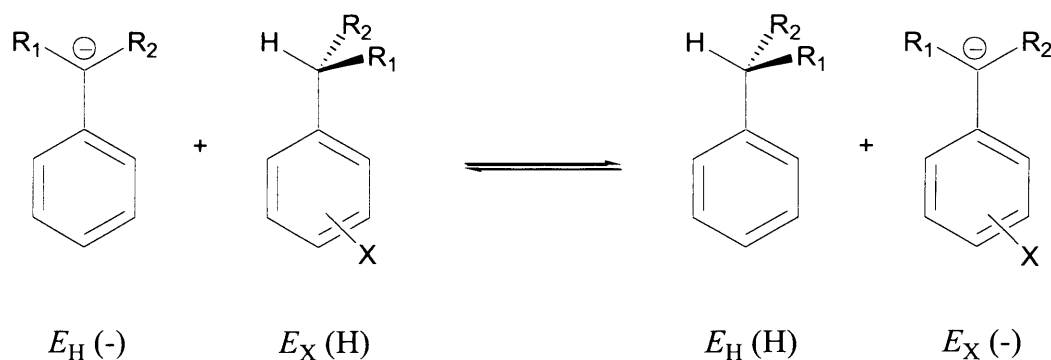
Scheme 5.1: Proton transfer reactions analysed by Nakata *et al.*

218

ΔE_X was calculated for the reaction depicted in Scheme 5.1, via equation (5.1).

$$\Delta E_X = \left[E_H(H) + E_X(-)\right] - \left[E_H(-) + E_X(H)\right] \qquad (5.1)$$

with $E_S(Y)$ the calculated energy of the species with substituent S on aromatic ring, and Y describing the protonation state at the benzylic position. ΔE_X denotes the calculated stability of the substituted benzylic anion with respect to the unsubstituted benzylic anion.

Electron-withdrawing aromatic substituents were found to stabilise a negative charge relative to the unsubstituted benzylic anion. The authors analysed their results in terms of an extended Yukawa-Tsuno equation, and found that resonance and saturation effects[2, 3] were present alongside the fundamental inductive effect.

A method of investigation similar to that of Nakata *et al.* was employed in this chapter. For all compounds under investigation, the standard molar Gibbs energy of the compound was calculated both for the protonated and deprotonated (at the stereogenic centre) form. The difference in these values for individual compounds does not mean anything in itself, as the loss of a proton from one species to the other makes direct comparison impossible. However, when compared with the values obtained in the same manner for other compounds, it can be assumed that all errors involved in the calculations cancel out (as in the example from Nakata *et al.* illustrated in Scheme 5.1). Hence, if carbanion stability is an important factor in determining H/D exchange rates and the calculations are performed at a sufficient level of accuracy, a correlation between the calculated energy difference of the two protonation states with the rate constants of H/D exchange calculated in Chapters 3 and 4 should be obtainable. If such a correlation is be found, the relationship could be used to predict rate constants of H/D exchange and racemisation from calculated energies of molecules of interest. In essence, the proposed link between anion stability and the rate constant for racemisation is a linear free energy relationship.

The rate of deprotonation at the stereogenic centre is dependent on $\Delta G^{\ominus\ddagger}$ (see Figure 5.1). However, the Hammond Postulate[4, 5] suggests that if the energy difference between protonation states is lowered by changes to the molecular scaffold, i.e. through greater stabilisation of negative charge, the energy of the activated complex should also be reduced. This is illustrated in Figure 5.2.
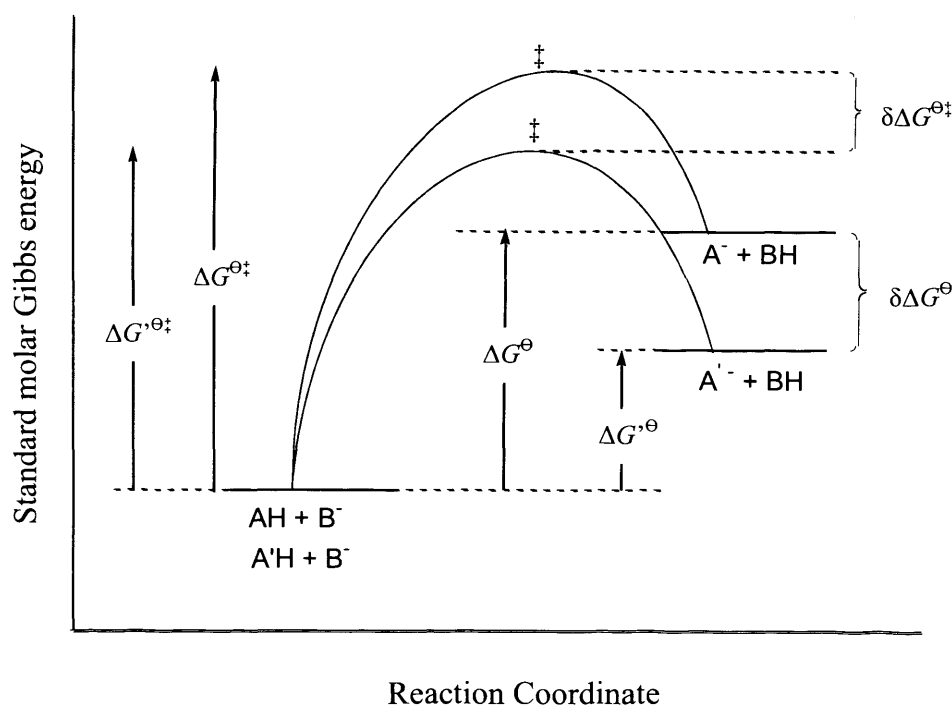
Figure 5.2: Reaction profile for proton abstraction by base. Reactants AH and A'H (in their protonated states) set at same molar free energy. The base, B⁻, is the same in both reactions.

The structural modification of A to A' results in stabilisation of the negative charge in the anionic product. According to the Hammond postulate, this structural modification will also stabilise the transition state (relative to the unmodified structure) in the same manner (although not necessarily to the same extent), by delocalisation of the negative charge built up on the transition state during proton abstraction. The relationship between $\delta\Delta G^{\ominus\ddagger}$ and $\Delta G^{\ominus}$ is typically quantified using the Brønsted relationship (Section 1.8.1).

Calculating the energy difference between the compound in its protonated and deprotonated (at the stereogenic centre) states gives a value related to $\Delta G^{\ominus}$, the real difference in energy between the two protonation states. This calculated value will include errors resultant from changes in the number of atoms in the calculation as well as limitations in the level of theory used (including solvation), and shall be referred to as '$\Delta G^{\ominus*}$'. We assume that the remaining[†] theory-specific errors in calculated energies are consistent between structures being investigated and cancel out, as illustrated in Figure 5.3.

[†] Many errors present in the calculations will have previously been cancelled when subtracting the calculated energies of the two protonation states.
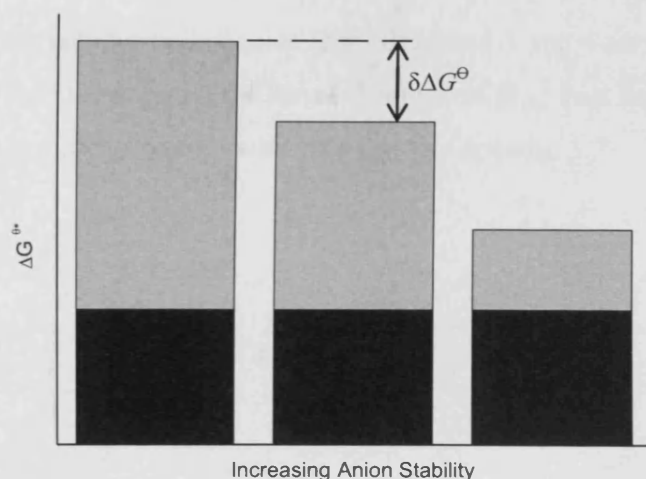
Figure 5.3: $\Delta G^{\ominus*}$ as anion stability increases with modification of molecular structure. (■) Portion of $\Delta G^{\ominus*}$ due to errors in calculation, (▪) portion of $\Delta G^{\ominus*}$ resulting from molecular structure. Contributions not to scale.

Figure 5.3 illustrates that, although the size of the errors will be unknown, these errors are anticipated to cancel out upon subtraction of $\Delta G^{\ominus*}$ for one compound from that calculated for another. This procedure should thus afford $\delta\Delta G^{\ominus}$ with acceptable residual errors (see Figure 5.2). It should then be possible to correlate this value with the rate constants of H/D exchange determined in Chapters 3 and 4.

5.2 Results

Calculations were undertaken on all species from Chapters 3 and 4 for which rate constants of H/D exchange as a function of basic buffer concentration (k_{gb}) had been determined at pH** 7.4 at 37 °C. These were compounds **3a-h**, **3k-l** and **6e** (Scheme 5.2).

3a-h

X = **a)** H, **b)** p-OH, **c)** p-Me, **d)** p-F,
  e) p-Cl, **f)** m-F, **g)** m-F, **h)** p-CF$_3$

6e

3k

3l

Scheme 5.2: Structures for which computational analysis was performed.

Calculations were performed on each structure, for both species,[‡] i.e. protonated and deprotonated at the stereogenic centre. All calculations in this chapter were performed using density functional theory (DFT, cf. Section 1.10.4) at the RB3LYP/6-31 + G(d,p) level of theory, with the geometry optimised prior to frequency calculations being performed. Each calculation was performed both in the gas-phase and with an aqueous solvent modelled using the polarisable continuum method (PCM, cf. Section 1.10.4). Calculations were performed on each species of each compound, with a range (minimum of 4) of starting geometries prior to optimisation. These starting geometries were proposed largely based on 'chemical intuition' i.e. conformations that appear to be good candidates for the most stable structure. Using several different starting geometries gives optimised structures of a range of configurations.

[‡] In this Chapter, the term 'structure' shall be used to define a general molecular scaffold, such as **3a**. The term 'species' shall be used to distinguish between the different protonation states of the stereogenic centre, for each structure.

The optimised geometry with the lowest energy in each case was used for correlation analysis.

5.2.1 Results from Calculations Employing PCM

For each structure on which calculations were performed, the calculated energy differences between the two protonation states, $\Delta G^{\Theta *}$, and the calculated energy differences between the two protonation states relative to compound **3a**, $\delta \Delta G^{\Theta}$, are displayed in Table 5.1.

Table 5.1: $\Delta G^{\Theta *}$ and $\delta \Delta G^{\Theta}$ of **3a-h**, **3k-l** and **6e**, from calculated energies of each structure in both protonation states, using the PCM.[a]

Compound	$\Delta G^{\Theta *}$ / kJ mol^{-1}	$\delta \Delta G^{\Theta}$ [b] / kJ mol^{-1}
3a	1270.253	0.000
3b	1277.833	7.580
3c	1273.848	3.594
3d	1269.718	-0.536
3e	1264.504	-5.750
3f	1259.975	-10.279
3g	1257.667	-12.587
3h	1250.814	-19.440
3k	1245.821	-24.433
3l	1263.650	-6.603
6e	1268.447	-1.806

[a] Number of decimal places carried through from Gaussian output.

[b] Relative to compound **3a**.

The calculated $\delta \Delta G^{\Theta}$ in Table 5.1 were then used for correlation analysis with the experimental rate constant data, and with Hammett substituent constants.

5.2.1.1 Correlation with Experimentally Determined k_{gb}

The rate constants for general-base catalysed H/D exchange (k_{gb}, from Tables 3.2, 3.7 and 4.3) were plotted against $\delta \Delta G^{\Theta}$ (from Table 5.1) for methyl esters **3a-h**, **3k-l** and primary amide **6e** (Figure 5.4).
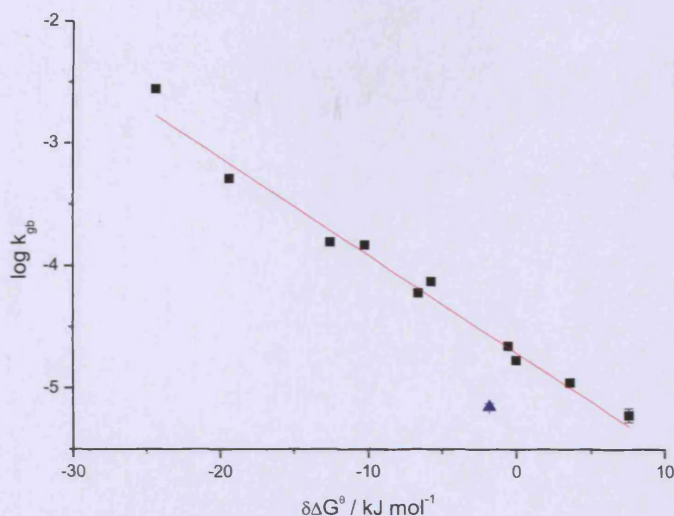
Figure 5.4: Correlation of $\delta\Delta G^{\ominus}$ (using PCM) with log k_{gb} (determined at 37 °C, I = 1 M) for (■) **3a-h, 3k-l** and (▲) **6e**. R^2 = 0.968 (fitted to (■) only).

Figure 5.4 shows a clear correlation for log k_{gb} with $\delta\Delta G^{\ominus}$ for methyl esters **3a-h, k-l**. As $\delta\Delta G^{\ominus}$ increases, the rate constant of H/D exchange becomes smaller accordingly. The straight line displayed in Figure 5.4 is compatible with a common mechanism of H/D exchange for methyl ester compounds **3a-h, k-l**, with proton abstraction as the rate-determining step. The correlation between $\delta\Delta G^{\ominus}$ and log k_{gb} therefore supports the proposed S_E1 mechanism for H/D exchange in compounds **3a-h, k-l**.

The calculated $\delta\Delta G^{\ominus}$ for primary amide **6e** does not quite fit the trend displayed by methyl esters **3a-h, k-l**. The $\delta\Delta G^{\ominus}$ value obtained for this compound suggests a slightly faster rate constant of general-base catalysed H/D exchange than that obtained experimentally in Chapter 4. However, the rate constant 'predicted' through computations is not too far off that obtained experimentally, less than an order of magnitude. This suggests that the general correlation between calculated $\delta\Delta G^{\ominus}$ and k_{gb} can be extended to a range of 'scaffolds', and hence suggests its potential for use as a predictive tool. Limitations to its applicability will be discussed later.

5.2.1.2 Hammett Analysis of Computational Data

The data displayed in Table 5.1 was plotted (Figure 5.5) as a function of the Hammett σ^--values for **3a-h** (from Table 1.5) and σ-values for **3k-l** (from Table 1.8).
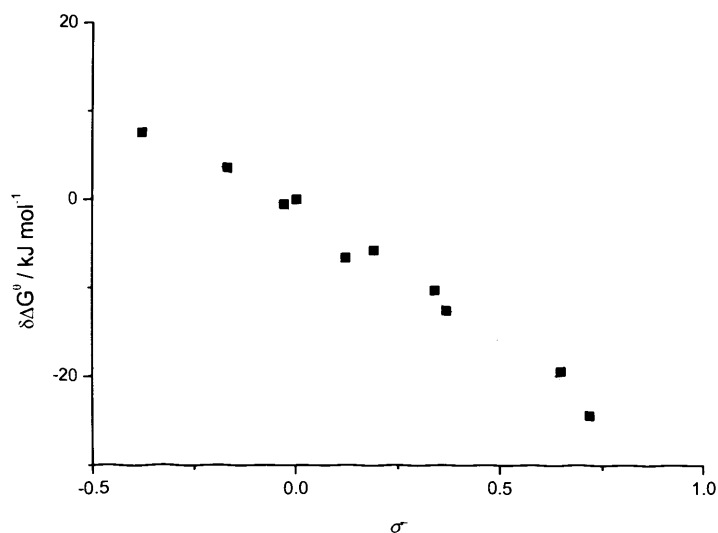
Figure 5.5: Hammett analysis of calculated $\delta\Delta G^{\ominus}$ for **3a-h** and **3k-l** correlated with σ^--constants. $R^2 = 0.979$.

Figure 5.5 shows a good correlation between $\delta\Delta G^{\ominus}$ and the Hammett σ^--constants. These results also support the heterocyclic Hammett constants of 0.72 and 0.12 for the thiophene derivatives **3k** and **3l** respectively. This suggested that the computational data could be used to analyse proposed Hammett substituent constants for other heterocycles.

5.2.1.3 Analysis of Heterocyclic Substituent Constants

As discussed in Section 1.8.2.4, there have been a range of different Hammett constants suggested for individual heterocyclic groups, many of which are contradictory. Inspired by the good correlation between σ^- and $\delta\Delta G^{\ominus}$ (Figure 5.5), calculations were performed on the furan-, pyrrole- and pyridine-containing compounds **3m-o** (Scheme 5.3), to assess the accuracy of the Hammett constants proposed for these structures (Table 1.8).
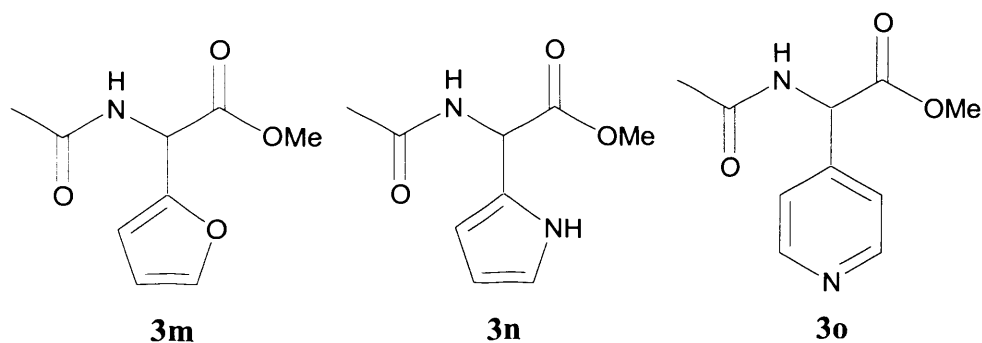
Scheme 5.3: Structures **3m-o**.

The lowest calculated energy for each species of each structure and the calculated $\delta\Delta G^\ominus$ for compounds **3m-o** are given in Table 5.2.

Table 5.2: $\Delta G^{\ominus*}$ and $\delta\Delta G^\ominus$ of **3m-o**, from calculated energies of each structure in both protonation states, using the PCM.[a]

Compound	$\Delta G^{\ominus*}$ / kJ mol^{-1}	$\delta\Delta G^{\ominus\,b}$ / kJ mol^{-1}
3m	1262.193	-8.060
3n	1268.158	-2.095
3o	1238.947	-31.306

[a] Number of decimal places carried through from Gaussian output.

[b] Relative to compound **3a**.

The correlation between $\delta\Delta G^\ominus$ and σ (Figure 5.5) was used to calculate σ-values for furan, pyrrole and pyridine heterocycles, from the values calculated for $\delta\Delta G^\ominus$ of **3m-o** displayed in Table 5.2. These 'predicted' heterocyclic σ-values are compared with those from literature (Table 1.8) in Table 5.3.

Table 5.3: Comparison of σ-values calculated from $\delta\Delta G^\ominus$ with proposed σ-values from Table 1.8.

Heterocycle	Calculated σ-value	σ-value from Table 1.6
2-Furan	0.22	1.08
2-Pyrrole	0.02	-0.24
4-Pyridine	1.03	0.76

Table 5.3 shows that the proposed σ-values from Table 1.8 do not correlate with the calculated $\delta\Delta G^\ominus$ data from **3m-o**. The successful fitting of our experimental data to calculated $\delta\Delta G^\ominus$ values for compounds **3a-h**, and the subsequent fitting of this computational data to σ-values of known reliability, suggests that the proposed σ-values for heterocyclic compounds displayed in Table 1.8 are at the very least not applicable to the system under investigation here.

The calculated energy gap of the pyridine-containing compound **3o** (Table 5.3) suggests that such a compound would undergo rapid H/D exchange (and presumably racemisation) under the experimental conditions used in Chapter 3. This strong anion stabilisation by the 4-pyridine moiety is of particular interest. Database mining studies showed that pyridine was

the second most frequently occurring aromatic group (after benzene) adjacent to a stereogenic centre in the AstraZeneca ISAC database (Section 2.3.2). Literature studies also show that pyridine is the most commonly found heterocycle in drug molecules.[6, 7] The results in Table 5.3 suggest that a drug molecule with a 4-pyridine substituent adjacent to a stereogenic centre of type R''R'RC-H, could be at particular risk of configurational instability under physiological conditions, even if other substituents are not stabilising towards an anion.

5.2.2 Computational Analysis Without PCM

Computational analysis in the gas-phase is less expensive than analysis using a solvent model such as PCM. Although PCM is a relatively cheap solvent model, it still requires the use of far greater computing resources than gas-phase calculations. As a result, gas-phase calculations would be preferable to calculations performed using the PCM if they could be shown to produce results of comparable predictive power. We therefore carried out gas-phase calculations on **3a-h**, **3k-l** and **6e** (Table 5.4).

Table 5.4: $\Delta G^{\ominus*}$ and $\delta\Delta G^{\ominus}$ for **3a-h**, **3k-l** and **6e**, from calculated energies of each structure in both protonation states calculated in the gas-phase.[a]

Compound	$\Delta G^{\ominus*}$ / kJ mol^{-1}	$\delta\Delta G^{\ominus}$ [a] / kJ mol^{-1}
3a	1449.163	0.000
3b	1456.394	7.231
3c	1458.116	8.953
3d	1440.226	-8.937
3e	1436.366	-12.797
3f	1429.802	-19.360
3g	1425.688	-23.475
3h	1406.583	-42.580
3k	1414.002	-35.161
3l	1431.078	-18.084
6e	1433.420	-15.742

[a] Number of decimal places carried through from Gaussian output.

[b] Relative to compound **3a**.

The rate constants for general-base catalysed H/D exchange (k_{gb}, from Tables 3.2, 3.7 and 4.3) were plotted against $\delta\Delta G^{\ominus}$ (from Table 5.4) for compounds **3a-h**, **3k-l** and **6e** (Figure 5.6).
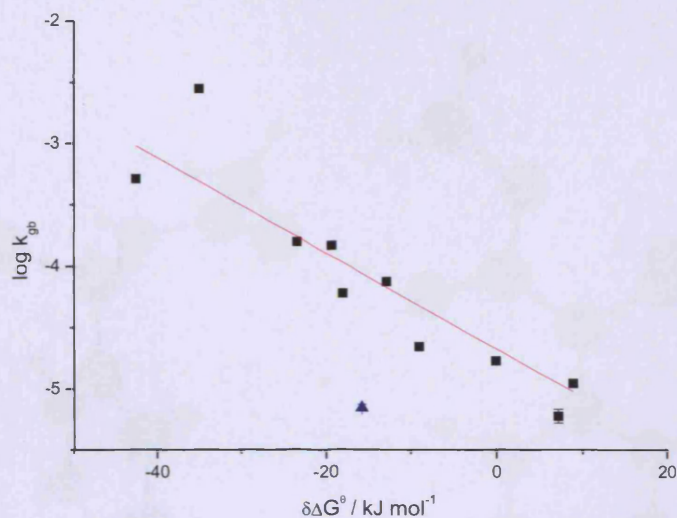
Figure 5.6: Correlation of $\delta\Delta G^{\ominus}$ from gas-phase with log k_{gb} (determined at 37 °C, I = 1 M) for (■) **3a-h**, **3k-l** and (▲) **6e**. R^2 = 0.755 (fitted to (■) only).

Figure 5.6 shows only a very loose correlation between the experimentally-determined rate constants for H/D exchange of **3a-h**, **3k-l** and **6e** with the values of $\delta\Delta G^{\ominus}$ calculated in the gas-phase. A greater rate constant for H/D exchange broadly correlates with a smaller value of $\delta\Delta G^{\ominus}$, although the relationship is far less consistent than that shown in Figure 5.4 when the PCM was employed. This is reflected in the R^2 values determined for the data in the two graphs; R^2 = 0.968 and 0.755 for the PCM and gas-phase calculations, respectively. These results suggest that employment of the PCM is necessary if computational chemistry is to be used to predict rate-constants of H/D exchange or racemisation for stereogenic centres of type R''R'RC-H.

5.2.3 Geometry of Computational Structures

The lowest energy geometries of both neutral and anionic states of **3a** when PCM is applied are displayed in Figure 5.7.
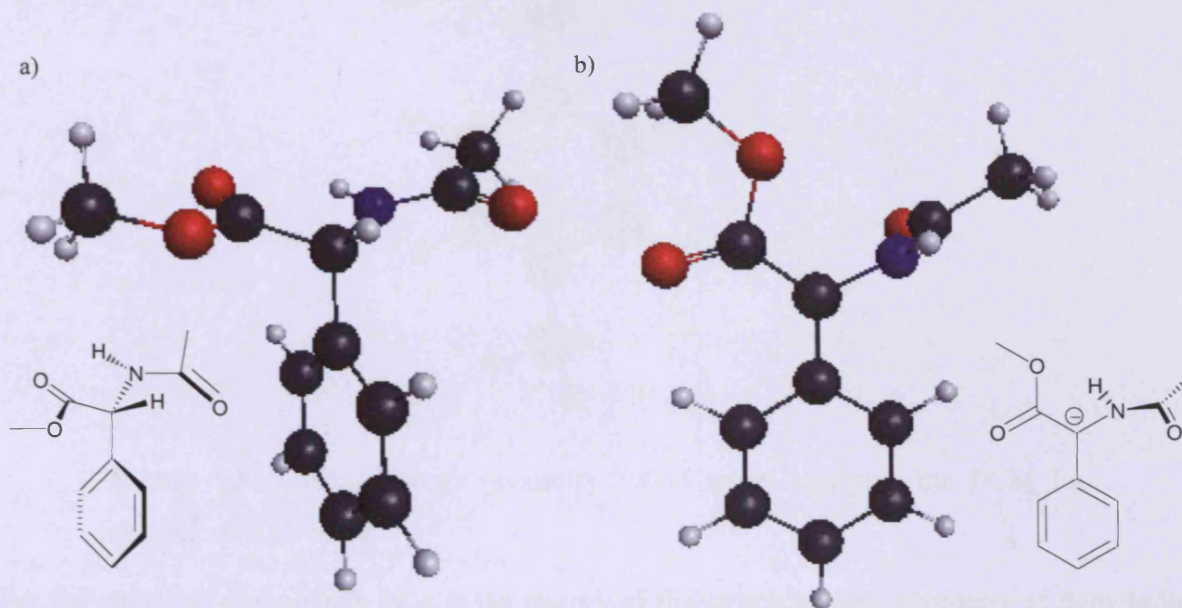
Figure 5.7: Lowest energy geometries found when applying the PCM for **3a**, a) protonated at stereogenic centre, b) deprotonated at stereogenic centre.

The geometries of the lowest energy structures found are quite consistent for the set of compounds **3a-h**. For each compound **3a-h**, the neutral species has the configuration as seen in Figure 5.7a for **3a**, with the phenyl ring perpendicular to the main chain of the molecule. Generally, the lowest energy configurations found for the anionic species of **3a-h** are as depicted for **3a** in Figure 5.7b, with the planar carbanion in the same plane as the phenyl ring and the amide group perpendicular to this. The only difference from the geometry depicted in Figure 5.7b found for the anions of the set **3a-h**, is the orientation of the ester group. For compounds **3a-b, f-g** the orientation is as shown in Figure 5.7b, with the methoxy group of the ester pointing away from the phenyl ring. For compounds **3c-e, h** the orientation is reversed, with the carbonyl group of the ester pointing away from the phenyl ring. This alternative configuration is illustrated in Figure 5.8, for the anionic species of **3c**.
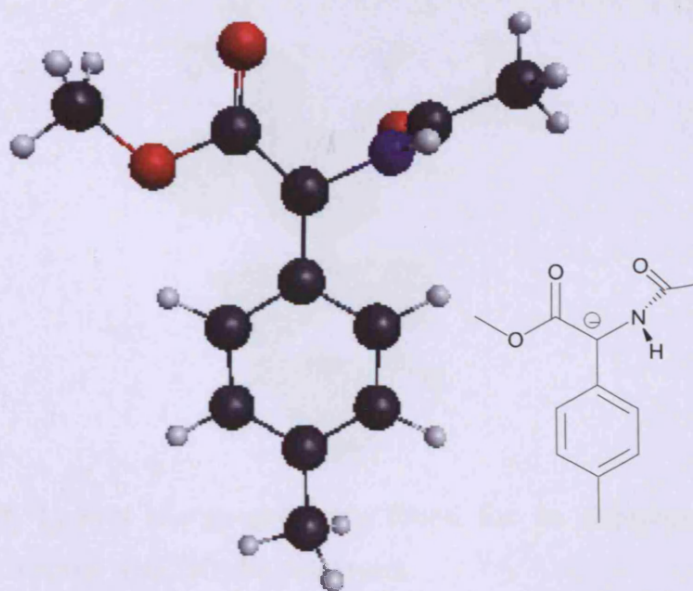
Figure 5.8: Lowest energy geometry found when applying the PCM for anionic species of **3c**.

For the anions of compounds **3c-e, h** the energy of the structure with geometry as depicted in Figure 5.7b was found to be slightly higher (0.228 kJ mol^{-1} for **3c**, number of decimal places carried through from Gaussian output) than that for the orientation with the carbonyl pointing away from the phenyl group (Figure 5.8). For the anionic species of each compound **3c-e, h**, the lowest energy structure found when not using the PCM solvent model was with the methoxy group of the ester away from the phenyl ring. This suggests that the interactions of the phenyl ring substituents in **3c-e, h** with the continuum solvent model, somehow causes the geometry of the anionic species to differ from that displayed by **3a-b, f-g**. For each compound **3a-h**, the anionic structure was also investigated with the carbonyl orientated in the opposite direction to ensure the lowest energy structure was taken in each case.

To further understand the anion-stabilising effect of the different substituents, the HOMO of **3a** deprotonated at the stereogenic centre was visualised (Figure 5.9).
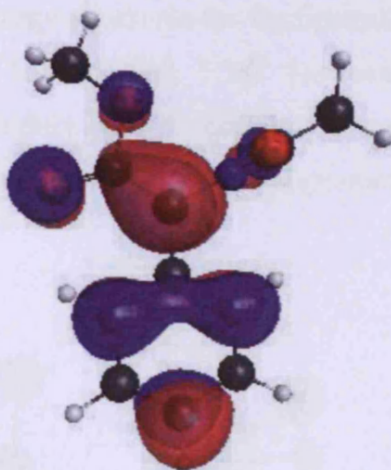
Figure 5.9: Lowest energy geometry found for **3a** deprotonated at the stereogenic centre, with HOMO displayed.

The HOMO of the deprotonated species of **3a** displayed in Figure 5.9 formally corresponds to the negative charge formed by removal of the proton bound to the stereogenic centre. Figure 5.9 shows that the orbital is delocalised over the entire molecule, suggesting all substituents on the stereogenic centre play a role in anion stabilisation. This observation is consistent with the presumed additivity of substituent effects.

The geometry of the lowest energy structure found for both species of amide **6e** is similar to those found for **3a** (Figure 5.7). The protonated species has the main chain of the molecule perpendicular to the aromatic group. The anionic species is planar at the location of the carbanion, with the primary amide group in the plane of the aromatic group. The secondary amide is perpendicular to the plane of the rest of the molecule (Figure 5.10).
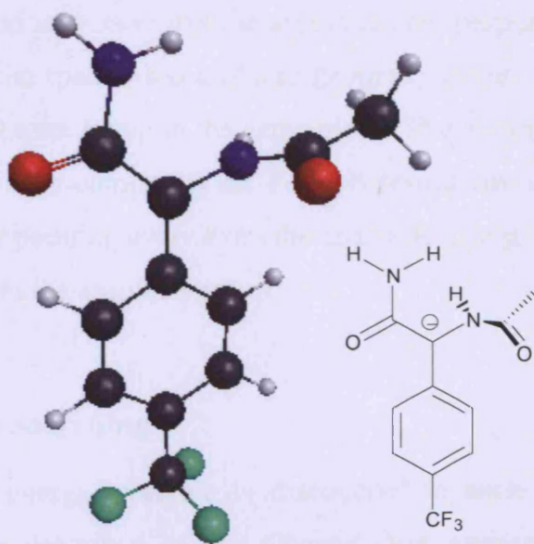
Figure 5.10: Lowest energy geometry found when applying the PCM for anionic species of **6e**.

The geometry of the lowest energy structures for the neutral species of compounds **3k, l** was the same as that found for **3a-h** (Figure 5.7a). However, the deprotonated species of compounds **3k, l** displayed a slightly different configuration compared to that found for **3a-h**. This is depicted for **3k** in Figure 5.11 (**3l** has the same geometrical arrangement).
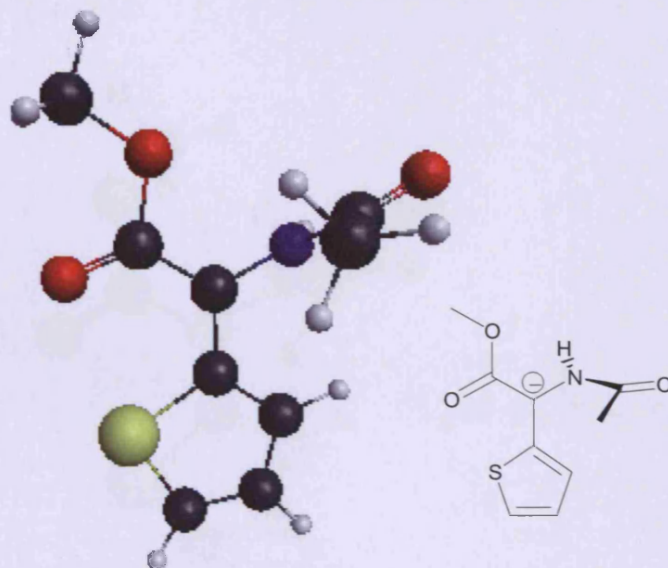
Figure 5.11: Lowest energy geometry found for deprotonated species of **3k**.

As Figure 5.11 shows, the lowest energy geometrical structure of the deprotonated species of **3k** (and **3l**) has the amide group twisted round in front of the molecule. This orientation is displayed by the lowest energy conformation of the anionic species of both **3k-l** whether the calculation is performed in the gas-phase or with the PCM employed.

The heterocyclic compounds **3m-o** were found to display similar geometries to compounds **3a-h**. The neutral species in each case has the aromatic ring perpendicular to the main chain of the molecule. The anionic species has a planar geometry at the site of deprotonation, with the heterocycle and methyl ester group in the same plane. The amide group is perpendicular to this plane, as in Figure 5.7b for compound **3a**. For compound **3m**, the anionic species has the carbonyl group of the ester pointing away from the aromatic group. For **3n-o**, the methyl ester group is pointing away from the aromatic group.

5.2.3.1 Conformational Searching

Ensuring that the lowest energy structure is discovered in each case is of importance in undertaking work such as described in this Chapter. For every species of each structure analysed here, at least 4 different starting geometries were investigated. Such a process is required to ensure the molecular geometry of lowest energy is discovered in each case. Failure

to discover the lowest energy configuration could result in large errors in $\delta\Delta G^{\ominus}$, and several examples of this initially occurred whilst undertaking the work in this Chapter. One such case was when trying to calculate $\delta\Delta G^{\ominus}$ for **3k**. After analysing 4 different optimised molecular geometries for the anionic species of **3k**, the conformation found to have the lowest energy was that depicted in Figure 5.12.
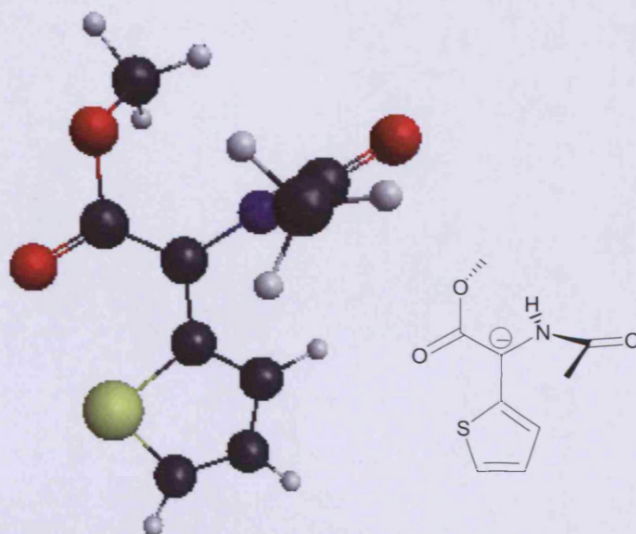
Figure 5.12: Initial lowest energy geometry found for the deprotonated species of **3k**.

Using this particular geometry, the plot of $\delta\Delta G^{\ominus}$ against log k_{gb} for methyl ester compounds **3a-h, k-l** is depicted in Figure 5.13.
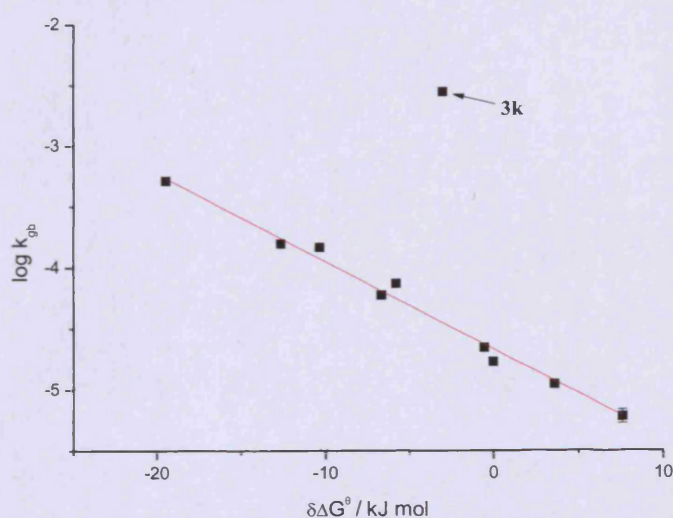
Figure 5.13: Correlation of $\delta\Delta G^{\ominus}$ with log k_{gb} (determined at 37 °C, $I = 1$ M) for **3a-h, k-l**, using original value of $\delta\Delta G^{\ominus}$ obtained for **3k**.

233

As Figure 5.13 shows, using the value of $\delta\Delta G^{\ominus}$ calculated for **3k** from the geometry displayed in Figure 5.12 gives an erroneous result. Because of the incompatibility of this value of $\delta\Delta G^{\ominus}$ with the experimental data from Chapter 3, and the different geometry displayed by the structure shown in Figure 5.12 from the geometry of the other anionic species of **3a-h, l**, it seemed likely that further conformational searching would find a structure lower in energy than that displayed in Figure 5.12. Such analysis yielded the geometry displayed in Figure 5.11, which gave a value of $\delta\Delta G^{\ominus}$ much more compatible with the experimental data (Figure 5.4). However, if computational analysis were to be used as a tool to investigate configurational stability of compounds not yet synthesised or for which no experimental racemisation data is available, it would not be as apparent that further investigation was required. As a result, it is imperative that a thorough investigation of many different molecular geometries be undertaken, before any conclusions are drawn from computational data.

5.2.4 Extension of Computational Analysis

5.2.4.1 Analysis of Functional Group Dependence

Calculations were also performed on several other compounds to further examine the computational method of analysis used in this Chapter for the prediction of configurational instability. According to Testa et al.[8] (Table 1.1), methyl and ethyl groups are classified as neutral in the assignment of substituents as configurationally stabilising, destabilising or neutral, for stereogenic centres of type R''R'RC-H. To investigate this assignment, calculations were performed on compounds **9-11** (Scheme 5.4).
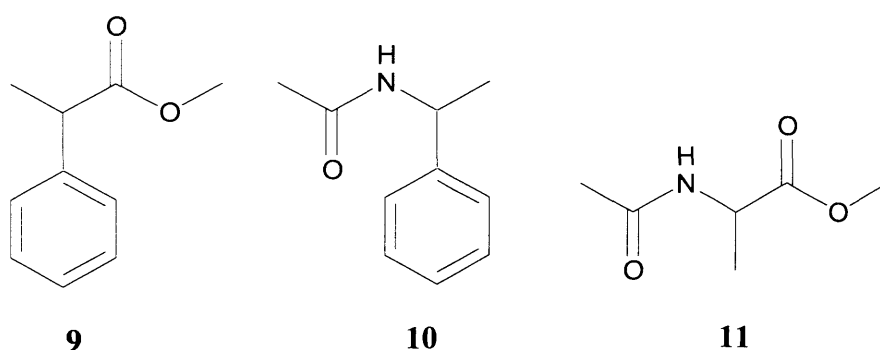
Scheme 5.4: Compounds **9-11**.

Each compound **9-11** is based on the same framework as **3a**, but with one of the substituents replaced by a methyl group. The value of $\delta\Delta G^{\ominus}$ for each compound **9-11** with respect to **3a** should therefore inform as to the ability of a methyl group to stabilise a negative charge in

comparison with the substituent replaced from **3a**. The results of these calculations are summarised in Table 5.5.

Table 5.5: $\Delta G^{\ominus *}$ and $\delta \Delta G^{\ominus}$ for **9-11**, from calculated energies of each structure in both protonation states, using the PCM.[a]

Compound	$\Delta G^{\ominus *}$ / kJ mol^{-1}	$\delta \Delta G^{\ominus\,b}$ / kJ mol^{-1}
9	1294.642	24.388
10	1385.610	115.357
11	1312.521	42.268

[a] Number of decimal places carried through from Gaussian output.

[b] Relative to compound **3a**.

The values of $\delta \Delta G^{\ominus}$ displayed in Table 5.5 for compounds **9-11** strongly support the classification in Table 1.1 of a methyl group as neutral towards configurational instability, within the guidelines set out by Testa *et al*. Exchange of any one of the substituents of **3a** for a methyl group causes a substantial increase in $\Delta G^{\ominus *}$, suggesting a decrease in negative charge stabilisation. This suggests all substituents present in **3a** help stabilise negative charge during H/D exchange, in line with observations from Figure 5.9 where the HOMO of the anion of **3a** was shown to be delocalised onto all three substituents.

If the relationship in Figure 5.4 were to be extended to compounds **9-11**, they would be expected to have k_{gb} and $t_{1/2}$ of H/D exchange as displayed in Table 5.6.

Table 5.6: Estimated values of k_{gb} at 37 °C, pH** 7.4, $I = 1$ M for **9-11** and resultant half-lives of H/D exchange at 0.3 M phosphate concentration, based on $\delta \Delta G^{\ominus}$ from Figure 5.5 and relationship between $\delta \Delta G^{\ominus}$ and log k_{gb} from Figure 5.4.

Compound	'Predicted' k_{gb} / s^{-1} M^{-1}	$t_{1/2}$ / days
9	$(2.24 \pm 0.14) \times 10^{-7}$	120
10	$(1.31 \pm 0.30) \times 10^{-15}$	2.04×10^{9}
11	$(8.48 \pm 0.80) \times 10^{-10}$	3154

The predicted half-lives of H/D exchange of **9-11** displayed in Table 5.6 suggest that none of the three compounds would be at risk of *in vivo* configurational instability. This is in line with the guidelines and substituent classifications outlined by Testa *et al.*, as none of the compounds **9-11** would be expected to undergo pharmacologically significant H/D exchange by these designations.

The greatest value of $\delta\Delta G^{\ominus}$ is displayed by compound **10**, for which the methyl ester substituent of **3a** was replaced by a methyl group. This implies that the methyl ester group of **3a** provides the greatest degree of negative charge stabilisation, in line with the classification in Table 1.1 of a methyl ester group as 'strongly configurationally destabilising' (compared to the classification of amido and aryl groups as 'configurationally destabilising'). The comparative values of $\delta\Delta G^{\ominus}$ for **9** and **11** suggest that a phenyl substituent provides more stabilisation of an adjacent negative charge than an amide (bonded through nitrogen) moiety.

5.2.4.2 Analysis of Experimental Data from Literature

Attempts were also made to compare computational results with experimental data from the literature. The relationship between $\delta\Delta G^{\ominus}$ and rate constants of general-base catalysed H/D exchange displayed in Figure 5.4 is based on data obtained in aqueous conditions at pH 7.4, 37 °C using phosphate buffers. Only comparison with experimental data obtained under the same (or very similar) conditions will be meaningful. As such data is sparse, the only direct comparison that could be made is with the data collected by Reist *et al.*[9] for the amphetamines amfepramone and cathinone (Scheme 5.5). They determined rate constants of H/D exchange for both compounds at a range of phosphate concentrations, under near identical conditions and using the same method of analysis (^{1}H NMR spectroscopy) employed in Chapters 3 and 4. As discussed in Section 1.5.1, the amine functional group present in both amfepramone and cathinone will be protonated at the pH under which the experiments were performed. As a result, calculations were carried out on the structures depicted in Scheme 5.5, both protonated and deprotonated at the stereogenic centre.

Amfepramone   Cathinone
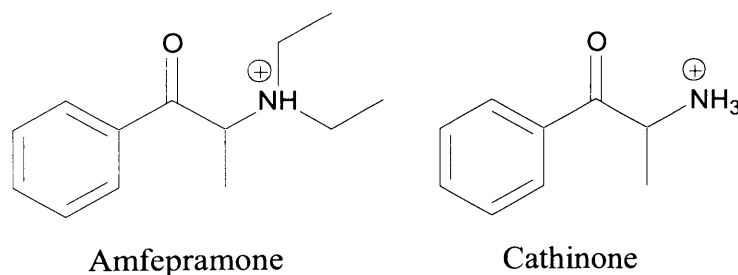
Scheme 5.5: Amfepramone and cathinone, protonated at amine moiety.

The k_{gb} values displayed in Table 5.7 were not explicitly stated, and thus were determined from the reported kinetic data (see Experimental Section 5.4.2).

Table 5.7: Rate constants of general-base catalysed H/D exchange of amfepramone and cathinone from reference 9, determined at 37 °C, pD 7.4, $I = 0.43$ M.

Compound	k_{gb} / s^{-1} M^{-1}
Amfepramone	(5.09 ± 0.27) x 10^{-3}
Cathinone	(9.80 ± 0.87) x 10^{-4}

The calculated values of $\delta\Delta G^{\ominus}$ for amfepramone and cathinone are given in Table 5.8.

Table 5.8: $\Delta G^{\ominus*}$ and $\delta\Delta G^{\ominus}$ of amfepramone and cathinone (both protonated at the amine), from calculated energies of each structure in both protonation states (at the stereogenic centre), using the PCM.[a]

Compound	$\Delta G^{\ominus*}$ / kJ mol^{-1}	$\delta\Delta G^{\ominus\,b}$ / kJ mol^{-1}
Amfepramone	1226.715	-43.539
Cathinone	1233.381	-36.873

[a] Number of decimal places carried through from Gaussian output.

[b] Relative to compound **3a**.

The data from Table 5.7 and Table 5.8 was plotted alongside those for compounds **3a-h**, **3k-l** (Figure 5.14).
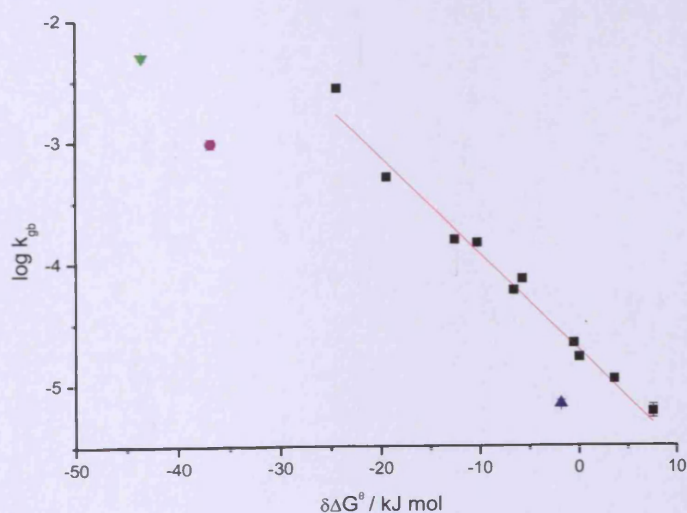
Figure 5.14: Correlation of $\delta\Delta G^{\ominus}$ (using PCM) with log k_{gb} for (■) **3a-h, k-l**, (▲) **6e**, (▼) amfepramone, (●) cathinone.

Figure 5.14 shows that the data for amfepramone and cathinone does not correlate particularly well with that obtained for methyl esters **3a-h, k-l**. A partial explanation for the lack of correlation of the data for amfepramone and cathinone is the positive charge on the amine. This will result in a different set of errors in the computational analysis than those present in the comparison between the methyl ester species.

Figure 5.14 reveals an important limitation of the method of analysis employed in this chapter. Major changes in molecular structure will change the set of errors to the point that any correlation will break down. However, Figure 5.14 also suggests a gradient between the data points found for amfepramone and cathinone which is similar to the gradient found for **3a-h, k-l**. This suggests that the introduction of a positive charge on the amine in amfepramone and cathinone adds (or removes) a consistent error to $\Delta G^{\ominus*}$, compared to the error found in $\Delta G^{\ominus*}$ for **3a-h, k-l**. Further experimental work would be required to confirm and quantify such a standard 'offset' for calculations performed on a compound containing a protonated amine. Hypothetically, it may also prove possible to discover standard 'offsets' for other major structural changes.

5.3 Conclusion

Comparison of computationally determined values for $\delta\Delta G^{\ominus}$ with experimentally determined rate constants for general-base catalysed H/D exchange has produced the following conclusions.

First, correlation analysis shows that for minor changes in molecular structure, computationally determined values of $\delta\Delta G^{\ominus}$ could be used to predict k_{gb}.

Second, major changes to the molecular structure will introduce additional errors that make the relationship between computationally determined $\delta\Delta G^{\ominus}$ and k_{gb} break down at this level of theory.

Third, employment of the Polarisable Continuum Model leads to increased accuracy in correlation analysis.

Fourth, determination of $\delta\Delta G^{\ominus}$ for compounds **9-11** broadly supports the assignments of functional groups ability to stabilise an anion by Testa *et al.* (Table 1.1).

5.4 Experimental

5.4.1 Computational Details

All computations were performed at the RB3LYP/6-31 + G(d,p) level of theory, using the Gaussian03 suite of programs.[10] Geometry optimisation was performed prior to frequency calculations. A range of starting geometries (> 4) was tested in each case; the lowest energy optimised geometry is reported for each compound. Energies are reported in Hartrees. All compounds were analysed with the PCM model, using the Gaussian default parameters for water. Compounds **3a-h, k-l** and **6e** were also analysed in the gas-phase. Molecular orbitals were calculated using GAMESS.[11] Visualisations were created using the MacMolPlot program.[12]

5.4.1.1 Calculations Performed Using Polarisable Continuum Model

Energies are given in units of Hartrees.

Geometry and energy of **3a**, protonated at stereogenic centre

1	6	0	1.211986	-0.819877	1.191912
2	6	0	2.412138	-1.513168	1.371850
3	6	0	3.205154	-1.845368	0.267050
4	6	0	2.791216	-1.481604	-1.018306
5	6	0	1.589447	-0.788219	-1.197947
6	6	0	0.792229	-0.455094	-0.095838
7	6	0	-0.517644	0.311889	-0.304961
8	7	0	-1.660967	-0.296588	0.357456
9	6	0	-0.362732	1.751328	0.190271
10	8	0	0.348536	2.483537	-0.672156
11	8	0	-0.802761	2.171910	1.246299
12	6	0	0.633172	3.851133	-0.288425
13	6	0	-2.487739	-1.164946	-0.277508
14	6	0	-3.609913	-1.752318	0.553580
15	8	0	-2.339732	-1.472636	-1.471035
16	1	0	0.601679	-0.569615	2.059580
17	1	0	2.728147	-1.793157	2.375857
18	1	0	4.139315	-2.387166	0.408305
19	1	0	3.399681	-1.740677	-1.883747
20	1	0	1.266740	-0.509779	-2.200964
21	1	0	-0.730814	0.345522	-1.378440
22	1	0	-1.813378	-0.079170	1.344848
23	1	0	1.227871	4.258644	-1.104729
24	1	0	1.196556	3.868393	0.647111
25	1	0	-0.298669	4.408880	-0.173082
26	1	0	-4.553833	-1.617767	0.018106
27	1	0	-3.689576	-1.304501	1.547521
28	1	0	-3.439172	-2.828514	0.662507

Sum of electronic and thermal Free Energies=   -707.342232

Geometry and energy of **3a**, deprotonated at stereogenic centre

1	6	0	1.885641	1.046461	-0.375006

240

2	6	0	3.276652	1.121728	-0.302905
3	6	0	4.045737	-0.004363	0.020180
4	6	0	3.374698	-1.209346	0.268598
5	6	0	1.983279	-1.296113	0.198602
6	6	0	1.177838	-0.165752	-0.129169
7	6	0	-0.271563	-0.206409	-0.228680
8	7	0	-0.944227	1.015114	-0.579911
9	6	0	-1.065308	-1.359983	-0.070862
10	8	0	-2.424605	-1.132850	-0.305750
11	8	0	-0.694690	-2.523093	0.233478
12	6	0	-3.285583	-2.259809	-0.131436
13	6	0	-1.432421	1.914476	0.302521
14	6	0	-2.165730	3.105816	-0.291085
15	8	0	-1.308186	1.809538	1.537617
16	1	0	1.327468	1.942432	-0.628437
17	1	0	3.765047	2.076004	-0.502018
18	1	0	5.131151	0.055420	0.076492
19	1	0	3.944144	-2.103831	0.523253
20	1	0	1.493251	-2.241251	0.395154
21	1	0	-1.128524	1.196227	-1.569474
22	1	0	-4.291903	-1.895756	-0.349655
23	1	0	-3.244508	-2.641300	0.894195
24	1	0	-3.028848	-3.073365	-0.817741
25	1	0	-1.743875	4.027097	0.121009
26	1	0	-3.217072	3.059150	0.012236
27	1	0	-2.116319	3.144374	-1.382931

Sum of electronic and thermal Free Energies=   -706.858418

Geometry and energy of 3b, protonated at stereogenic centre

1	6	0	-1.177957	-0.123066	-1.132616
2	6	0	-2.550984	-0.318592	-1.270047
3	6	0	-3.350410	-0.474076	-0.128236
4	6	0	-2.765917	-0.434805	1.143515
5	6	0	-1.387661	-0.239490	1.266362
6	6	0	-0.577346	-0.084193	0.135950
7	8	0	-4.690878	-0.661670	-0.320113
8	6	0	0.928579	0.128890	0.291050
9	7	0	1.732103	-0.861985	-0.411985
10	6	0	1.315988	1.526505	-0.197000
11	8	0	0.976155	2.461479	0.697025
12	8	0	1.837632	1.767512	-1.272247
13	6	0	1.219757	3.839666	0.323740
14	6	0	2.283638	-1.931081	0.213916
15	8	0	2.163580	-2.125970	1.434510
16	6	0	3.065339	-2.890478	-0.660113
17	1	0	-0.572778	-0.004413	-2.031600
18	1	0	-3.013894	-0.350172	-2.254940
19	1	0	-3.386688	-0.559376	2.031150
20	1	0	-0.941505	-0.211365	2.260207
21	1	0	-5.159792	-0.759348	0.542695
22	1	0	1.181445	0.061916	1.353981
23	1	0	1.850506	-0.749611	-1.421638
24	1	0	0.873972	4.430499	1.170792
25	1	0	0.655709	4.089026	-0.577812
26	1	0	2.286424	3.998505	0.151297
27	1	0	2.592731	-3.876477	-0.609041
28	1	0	4.078466	-2.986882	-0.258619
29	1	0	3.120609	-2.574897	-1.705104

Sum of electronic and thermal Free Energies=   -782.576559

Geometry and energy of **3b**, deprotonated at stereogenic centre

1	6	0	-1.517258	1.047008	-0.363065
2	6	0	-2.908777	1.129587	-0.293539
3	6	0	-3.671017	-0.004596	0.001029
4	6	0	-3.012423	-1.217316	0.223883
5	6	0	-1.618273	-1.297758	0.153386
6	6	0	-0.809938	-0.166934	-0.144957
7	8	0	-5.046885	0.130906	0.059272
8	6	0	0.646772	-0.208216	-0.243605
9	7	0	1.315105	1.017822	-0.586627
10	6	0	1.437194	-1.356917	-0.083560
11	8	0	2.802027	-1.129995	-0.309259
12	8	0	1.065131	-2.523678	0.218826
13	6	0	3.665748	-2.245519	-0.091772
14	6	0	1.828914	1.898035	0.299988
15	8	0	1.741050	1.767016	1.536467
16	6	0	2.542295	3.104064	-0.288594
17	1	0	-0.962760	1.951178	-0.595608
18	1	0	-3.409777	2.081212	-0.468614
19	1	0	-3.592502	-2.112161	0.455817
20	1	0	-1.135045	-2.250614	0.329139
21	1	0	-5.465196	-0.736467	0.261962
22	1	0	1.470093	1.221653	-1.576944
23	1	0	4.673518	-1.882635	-0.306311
24	1	0	3.424505	-3.080999	-0.757289
25	1	0	3.613822	-2.598535	0.943905
26	1	0	2.088300	4.016828	0.108974
27	1	0	2.511109	3.135080	-1.381338
28	1	0	3.588181	3.088085	0.035085

```
Sum of electronic and thermal Free Energies=        -782.089858
```

Geometry and energy of **3c**, protonated at stereogenic centre

1	6	0	-1.093291	-0.312379	-1.108608
2	6	0	-2.473824	-0.491126	-1.239686
3	6	0	-3.322968	-0.429538	-0.124567
4	6	0	-2.744640	-0.182233	1.131178
5	6	0	-1.366279	-0.004792	1.267076
6	6	0	-0.525895	-0.069757	0.148250
7	6	0	0.982491	0.144482	0.308309
8	7	0	1.793053	-0.859569	-0.364759
9	6	0	1.368074	1.527808	-0.220051
10	8	0	1.010563	2.489277	0.636882
11	8	0	1.903715	1.735122	-1.295291
12	6	0	1.250047	3.855999	0.219828
13	6	0	2.212218	-1.987221	0.261879
14	6	0	3.027062	-2.956600	-0.569486
15	8	0	1.949935	-2.222933	1.452224
16	6	0	-4.814417	-0.634185	-0.261489
17	1	0	-0.462377	-0.370194	-1.995391
18	1	0	-2.894934	-0.681078	-2.226830
19	1	0	-3.378538	-0.132532	2.016857
20	1	0	-0.939889	0.181032	2.252767
21	1	0	1.224004	0.113267	1.376313
22	1	0	2.018045	-0.711226	-1.350754
23	1	0	0.890743	4.472640	1.042467
24	1	0	0.694728	4.070675	-0.695920
25	1	0	2.317676	4.015402	0.054442
26	1	0	3.986155	-3.128421	-0.071768
27	1	0	3.208257	-2.604648	-1.588280
28	1	0	2.498370	-3.914137	-0.610676

29	1	0	-5.372307	0.196488	0.185774
30	1	0	-5.136452	-1.549756	0.249436
31	1	0	-5.110025	-0.715008	-1.311441

Sum of electronic and thermal Free Energies=   -746.636470

Geometry and energy of 3c, deprotonated at stereogenic centre

1	6	0	1.468523	1.181120	0.122338
2	6	0	0.631509	0.068670	-0.175070
3	6	0	1.321259	-1.164456	-0.364784
4	6	0	2.707959	-1.271449	-0.269175
5	6	0	3.519694	-0.163210	0.023808
6	6	0	2.857429	1.057839	0.216271
7	6	0	-0.822192	0.114122	-0.297123
8	7	0	-1.480707	-1.128986	-0.603056
9	6	0	-2.002669	-1.974892	0.310933
10	8	0	-1.943858	-1.785713	1.541450
11	6	0	5.024127	-0.284429	0.119839
12	1	0	5.472771	-0.567714	-0.841436
13	1	0	5.477367	0.663642	0.427293
14	1	0	5.325102	-1.048094	0.848144
15	6	0	-1.700177	1.214301	-0.210069
16	8	0	-1.095770	2.436686	0.074727
17	8	0	-2.949526	1.187553	-0.368841
18	6	0	-2.668715	-3.227102	-0.235369
19	1	0	0.751222	-2.059541	-0.592159
20	1	0	3.168392	-2.248312	-0.427015
21	1	0	3.441705	1.949690	0.448915
22	1	0	1.021183	2.152352	0.283367
23	1	0	-1.623726	-1.369625	-1.587047
24	1	0	-3.692610	-3.281296	0.146575
25	1	0	-2.690886	-3.265165	-1.328014
26	1	0	-2.130624	-4.104086	0.139109
27	6	0	-1.960948	3.574066	0.135301
28	1	0	-1.312159	4.422535	0.363177
29	1	0	-2.469013	3.741013	-0.819710
30	1	0	-2.715340	3.461818	0.920109

Sum of electronic and thermal Free Energies=   -746.151287

Geometry and energy of 3c, deprotonated at stereogenic centre (with alternate geometry, see Section 5.2.3)

1	6	0	-2.942080	-1.253854	0.276105
2	6	0	-1.547078	-1.320506	0.217244
3	6	0	-0.758896	-0.192349	-0.142626
4	6	0	-1.487876	0.993311	-0.436300
5	6	0	-2.879808	1.044335	-0.373590
6	6	0	-3.647775	-0.077010	-0.014387
7	6	0	0.694631	-0.210780	-0.234367
8	6	0	1.501981	-1.351616	-0.075360
9	8	0	2.862028	-1.105777	-0.299776
10	6	0	3.728946	-2.223864	-0.118207
11	6	0	-5.153449	-0.010265	0.061319
12	7	0	1.356882	1.021909	-0.568054
13	6	0	1.761489	1.955960	0.323108
14	6	0	2.407933	3.194698	-0.268635
15	8	0	1.594868	1.854150	1.552410
16	8	0	1.143763	-2.520904	0.219282
17	1	0	-5.592522	0.325721	-0.886306
18	1	0	-5.579150	-0.991024	0.296352

243

19	1	0	-5.490072	0.691047	0.835668
20	1	0	-0.948377	1.891492	-0.721335
21	1	0	-3.380926	1.983872	-0.612458
22	1	0	-3.495678	-2.150979	0.557844
23	1	0	-1.044260	-2.253989	0.441875
24	1	0	1.592169	1.192278	-1.548193
25	1	0	3.102528	3.620809	0.457297
26	1	0	2.934140	2.989019	-1.205752
27	1	0	1.631022	3.940674	-0.473884
28	1	0	4.735880	-1.855500	-0.326611
29	1	0	3.680365	-2.605675	0.907109
30	1	0	3.483324	-3.039225	-0.806376

Sum of electronic and thermal Free Energies=   -746.151200

Geometry and energy of 3d, protonated at stereogenic centre

1	6	0	-1.134387	-0.227109	-1.131816
2	6	0	-2.508051	-0.432955	-1.279422
3	6	0	-3.288649	-0.486753	-0.131144
4	6	0	-2.764692	-0.347967	1.146414
5	6	0	-1.386898	-0.143812	1.272512
6	6	0	-0.563444	-0.083221	0.141569
7	9	0	-4.635455	-0.689704	-0.267325
8	6	0	0.941664	0.147291	0.303154
9	7	0	1.759430	-0.842252	-0.380370
10	6	0	1.317490	1.544279	-0.198000
11	8	0	0.905230	2.487313	0.654731
12	8	0	1.893811	1.773449	-1.246876
13	6	0	1.137641	3.864308	0.268432
14	6	0	2.236331	-1.948378	0.248006
15	6	0	3.049463	-2.893694	-0.615775
16	8	0	2.024362	-2.170606	1.449664
17	1	0	-0.510273	-0.185615	-2.024311
18	1	0	-2.964840	-0.547944	-2.260780
19	1	0	-3.414762	-0.402770	2.017809
20	1	0	-0.952872	-0.035123	2.265896
21	1	0	1.183857	0.100683	1.370389
22	1	0	1.944973	-0.704663	-1.376951
23	1	0	0.730011	4.461751	1.082668
24	1	0	0.620310	4.082876	-0.668446
25	1	0	2.208591	4.045498	0.154342
26	1	0	3.391181	-3.730208	-0.005731
27	1	0	3.916688	-2.379603	-1.044468
28	1	0	2.444189	-3.274957	-1.445635

Sum of electronic and thermal Free Energies=   -806.591982

Geometry and energy of 3d, deprotonated at stereogenic centre

1	6	0	-1.333545	-1.195580	-0.348789
2	6	0	-2.720070	-1.330048	-0.254961
3	6	0	-3.482310	-0.205749	0.025244
4	6	0	-2.898497	1.038532	0.213624
5	6	0	-1.510597	1.163024	0.116547
6	6	0	-0.664663	0.051253	-0.171437
7	6	0	0.786216	0.116496	-0.297456
8	7	0	1.461739	-1.115758	-0.606785
9	6	0	1.648752	1.229711	-0.208434
10	8	0	1.027825	2.440896	0.082394
11	8	0	2.896425	1.219383	-0.369519
12	6	0	1.873729	3.594031	0.131720
13	6	0	2.007398	-1.948333	0.306850

14	6	0	2.720351	-3.173777	-0.239982
15	8	0	1.940644	-1.762082	1.537100
16	9	0	-4.857608	-0.328498	0.120461
17	1	0	-0.752604	-2.084019	-0.570140
18	1	0	-3.197661	-2.298212	-0.398086
19	1	0	-3.517865	1.906592	0.435148
20	1	0	-1.070349	2.138597	0.265420
21	1	0	1.609040	-1.350576	-1.591818
22	1	0	1.211563	4.431264	0.362130
23	1	0	2.370342	3.765435	-0.828363
24	1	0	2.636104	3.497138	0.910664
25	1	0	3.766629	-3.146991	0.080822
26	1	0	2.685483	-3.244222	-1.330766
27	1	0	2.265874	-4.071153	0.190957

Sum of electronic and thermal Free Energies=   -806.108372

Geometry and energy of 3e, protonated at stereogenic centre

1	6	0	-0.788792	-0.185997	-1.084995
2	6	0	-2.175871	-0.293958	-1.209245
3	6	0	-2.962693	-0.222782	-0.059096
4	6	0	-2.397202	-0.048700	1.203325
5	6	0	-1.007373	0.055885	1.308806
6	6	0	-0.193630	-0.013201	0.172186
7	6	0	1.326802	0.115324	0.311978
8	7	0	2.068834	-0.931582	-0.370685
9	6	0	1.785167	1.479248	-0.211666
10	8	0	1.411385	2.460562	0.613953
11	8	0	2.389972	1.654107	-1.254952
12	6	0	1.729091	3.814369	0.205702
13	6	0	2.415005	-2.091460	0.247154
14	6	0	3.155373	-3.098124	-0.611942
15	8	0	2.138585	-2.314688	1.435325
16	17	0	-4.718050	-0.359769	-0.206330
17	1	0	-0.176683	-0.242757	-1.984986
18	1	0	-2.634572	-0.429019	-2.186724
19	1	0	-3.025215	0.000187	2.090595
20	1	0	-0.555610	0.191588	2.290981
21	1	0	1.578170	0.068648	1.377743
22	1	0	2.308092	-0.786351	-1.354438
23	1	0	1.336140	4.450562	0.997460
24	1	0	1.246989	4.040494	-0.747887
25	1	0	2.810906	3.933365	0.114894
26	1	0	3.503906	-3.917041	0.017945
27	1	0	4.009832	-2.636272	-1.117815
28	1	0	2.488273	-3.499727	-1.383202

Sum of electronic and thermal Free Energies=   -1166.947320

Geometry and energy of 3e, deprotonated at stereogenic centre

1	6	0	-0.976617	-1.088292	-0.455350
2	6	0	-2.366324	-1.163127	-0.384436
3	6	0	-3.097676	-0.030690	-0.026614
4	6	0	-2.440542	1.166429	0.257457
5	6	0	-1.049459	1.233050	0.181906
6	6	0	-0.251062	0.108069	-0.180681
7	6	0	1.198074	0.110346	-0.276010
8	7	0	1.832528	-1.144770	-0.576363
9	6	0	2.102885	1.191602	-0.189073
10	8	0	1.526357	2.433601	0.048604
11	8	0	3.351247	1.122531	-0.320989

245

12	6	0	2.424532	3.544716	0.134801
13	6	0	2.172830	-2.082920	0.336526
14	6	0	2.842800	-3.330719	-0.218406
15	8	0	1.926761	-1.980206	1.552772
16	17	0	-4.871037	-0.114841	0.071381
17	1	0	-0.434173	-1.984229	-0.737181
18	1	0	-2.871785	-2.101131	-0.607800
19	1	0	-3.007233	2.051856	0.540980
20	1	0	-0.569192	2.174413	0.409720
21	1	0	2.161517	-1.294140	-1.533596
22	1	0	1.793443	4.414252	0.329289
23	1	0	2.975384	3.685491	-0.800157
24	1	0	3.141811	3.414454	0.950817
25	1	0	3.408938	-3.818745	0.576940
26	1	0	3.510903	-3.104186	-1.055444
27	1	0	2.078759	-4.030529	-0.576325

Sum of electronic and thermal Free Energies=   -1166.465696

Geometry and energy of **3f**, protonated at stereogenic centre

1	6	0	0.916530	-0.205895	1.492373
2	6	0	2.231989	-0.461193	1.888972
3	6	0	3.244153	-0.626140	0.936614
4	6	0	2.891431	-0.525606	-0.401723
5	6	0	1.595532	-0.273007	-0.833096
6	6	0	0.593349	-0.111553	0.130931
7	6	0	-0.844348	0.176592	-0.315438
8	7	0	-1.821383	-0.738200	0.250782
9	6	0	-1.230402	1.608903	0.060318
10	8	0	-0.627975	2.493324	-0.738343
11	8	0	-1.970720	1.906248	0.981596
12	6	0	-0.852425	3.895163	-0.447544
13	6	0	-2.141966	-1.910557	-0.352201
14	6	0	-3.141691	-2.787116	0.373498
15	8	0	-1.641256	-2.257269	-1.433244
16	9	0	3.866622	-0.689697	-1.349561
17	1	0	0.141644	-0.085956	2.248301
18	1	0	2.475383	-0.533160	2.947826
19	1	0	4.275125	-0.828312	1.221092
20	1	0	1.376965	-0.208960	-1.897991
21	1	0	-0.889870	0.091032	-1.407154
22	1	0	-2.244912	-0.492319	1.148266
23	1	0	-0.281037	4.437101	-1.199691
24	1	0	-0.492363	4.130830	0.556452
25	1	0	-1.916382	4.128320	-0.527048
26	1	0	-3.893516	-3.132410	-0.340947
27	1	0	-3.635555	-2.278574	1.205614
28	1	0	-2.618708	-3.668888	0.759552

Sum of electronic and thermal Free Energies=   -806.593491

Geometry and energy of **3f**, deprotonated at stereogenic centre

1	6	0	-1.321684	-1.504931	-0.420349
2	6	0	-2.671598	-1.843040	-0.374107
3	6	0	-3.660996	-0.885430	-0.100964
4	6	0	-3.202597	0.407487	0.117120
5	6	0	-1.875895	0.795303	0.082585
6	6	0	-0.864472	-0.171161	-0.195940
7	6	0	0.544850	0.148993	-0.263835
8	7	0	1.454984	-0.920651	-0.566533
9	6	0	1.087333	1.443405	-0.111356

246

10	8	0	2.467133	1.489236	-0.304849
11	8	0	0.478038	2.509363	0.155165
12	6	0	3.082897	2.766616	-0.119538
13	6	0	2.062352	-1.704792	0.352514
14	6	0	3.026123	-2.747278	-0.187971
15	8	0	1.858620	-1.616863	1.577870
16	9	0	-4.141709	1.386547	0.391181
17	1	0	-0.596719	-2.282121	-0.636473
18	1	0	-2.966676	-2.876437	-0.554058
19	1	0	-4.719987	-1.126857	-0.059695
20	1	0	-1.608218	1.827720	0.265034
21	1	0	1.719669	-1.065152	-1.543849
22	1	0	4.147129	2.607759	-0.304958
23	1	0	2.935452	3.136732	0.900182
24	1	0	2.689796	3.507668	-0.822626
25	1	0	4.021990	-2.553857	0.223265
26	1	0	3.086994	-2.759200	-1.279448
27	1	0	2.712859	-3.735542	0.163282

Sum of electronic and thermal Free Energies=   -806.113592

Geometry and energy of 3g, protonated at stereogenic centre

1	6	0	-0.736439	0.404691	1.883148
2	6	0	-2.109139	0.404030	2.146451
3	6	0	-3.026994	0.107309	1.135034
4	6	0	-2.538546	-0.187538	-0.138289
5	6	0	-1.174735	-0.191896	-0.423585
6	6	0	-0.264743	0.106357	0.599940
7	6	0	1.240591	0.126574	0.310147
8	7	0	1.709412	-1.033176	-0.429407
9	6	0	1.600412	1.391595	-0.474148
10	8	0	1.563497	2.470681	0.310662
11	8	0	1.859328	1.414978	-1.664560
12	6	0	1.814729	3.749444	-0.324096
13	6	0	2.105599	-2.171144	0.195526
14	6	0	2.548254	-3.310570	-0.698622
15	8	0	2.104880	-2.281436	1.431348
16	17	0	-3.682303	-0.566644	-1.432194
17	1	0	-0.029158	0.631272	2.679963
18	1	0	-2.471011	0.629947	3.148428
19	1	0	-4.096835	0.101238	1.333202
20	1	0	-0.829763	-0.431144	-1.428145
21	1	0	1.771968	0.161415	1.268161
22	1	0	1.719679	-0.980074	-1.450005
23	1	0	1.734314	4.484727	0.475155
24	1	0	1.067043	3.935310	-1.098268
25	1	0	2.815560	3.759951	-0.760817
26	1	0	3.538503	-3.646512	-0.378114
27	1	0	2.582541	-3.040005	-1.757041
28	1	0	1.854858	-4.147844	-0.568021

Sum of electronic and thermal Free Energies=   -1166.948348

Geometry and energy of 3g, deprotonated at stereogenic centre

1	6	0	0.813758	-2.027680	0.287015
2	6	0	2.147815	-2.402527	0.424274
3	6	0	3.198987	-1.491730	0.240475
4	6	0	2.834126	-0.186766	-0.088580
5	6	0	1.517366	0.227726	-0.233435
6	6	0	0.442212	-0.691438	-0.050018
7	6	0	-0.925662	-0.248603	-0.214730

8	7	0	-1.144367	1.138430	-0.521994
9	6	0	-2.061903	-1.084822	-0.141683
10	8	0	-3.254600	-0.411515	-0.400544
11	8	0	-2.103506	-2.314498	0.108832
12	6	0	-4.446671	-1.197378	-0.322693
13	6	0	-1.327749	2.112093	0.399035
14	6	0	-1.611746	3.502542	-0.142948
15	8	0	-1.266866	1.918122	1.627577
16	17	0	4.127706	1.018195	-0.338706
17	1	0	0.031031	-2.759591	0.436085
18	1	0	2.383247	-3.434649	0.684138
19	1	0	4.239866	-1.783756	0.348352
20	1	0	1.310367	1.258699	-0.494766
21	1	0	-1.259782	1.402847	-1.503203
22	1	0	-5.264915	-0.509652	-0.545894
23	1	0	-4.437356	-2.013008	-1.052871
24	1	0	-4.580762	-1.622054	0.677331
25	1	0	-0.879003	4.203444	0.268160
26	1	0	-1.585078	3.554995	-1.234886
27	1	0	-2.601462	3.819022	0.202317

Sum of electronic and thermal Free Energies=   -1166.469328

Geometry and energy of **3h**, protonated at stereogenic centre

1	6	0	-0.403622	0.298796	1.328671
2	6	0	-1.797188	0.253761	1.241768
3	6	0	-2.400766	-0.061895	0.021474
4	6	0	-1.616506	-0.337515	-1.107155
5	6	0	-0.227099	-0.291679	-1.010538
6	6	0	0.388897	0.027355	0.208510
7	6	0	1.916018	0.100579	0.319014
8	7	0	2.603922	-0.986673	-0.355084
9	6	0	2.413326	1.431224	-0.254967
10	8	0	2.140446	2.442717	0.571428
11	8	0	2.962992	1.552810	-1.335407
12	6	0	2.497177	3.772752	0.117689
13	6	0	2.861011	-2.165554	0.267218
14	6	0	3.577184	-3.218197	-0.553017
15	8	0	2.527538	-2.376944	1.443433
16	6	0	-3.895107	-0.146056	-0.100720
17	9	0	-4.547178	0.304494	0.998651
18	9	0	-4.369026	0.573806	-1.157347
19	9	0	-4.324678	-1.427361	-0.305394
20	1	0	0.066647	0.541283	2.280886
21	1	0	-2.401055	0.459916	2.122415
22	1	0	-2.085609	-0.585104	-2.058714
23	1	0	0.374991	-0.511358	-1.891200
24	1	0	2.184793	0.071567	1.381652
25	1	0	2.891223	-0.845255	-1.325800
26	1	0	2.182208	4.440482	0.918339
27	1	0	1.970141	4.004594	-0.810511
28	1	0	3.576224	3.837136	-0.038309
29	1	0	4.436752	-3.582808	0.016475
30	1	0	3.917207	-2.849075	-1.524141
31	1	0	2.899212	-4.063225	-0.711995

Sum of electronic and thermal Free Energies=   -1044.403854

Geometry and energy of **3h**, deprotonated at stereogenic centre

| 1 | 6 | 0 | 0.543874 | 1.008850 | -0.408134 |
| 2 | 6 | 0 | 1.927553 | 1.059466 | -0.354317 |

248

3	6	0	2.678036	-0.091397	-0.049198
4	6	0	1.991259	-1.290449	0.200826
5	6	0	0.603834	-1.345859	0.145819
6	6	0	-0.187461	-0.196120	-0.163436
7	6	0	-1.624233	-0.203806	-0.242751
8	6	0	4.157031	-0.003646	0.022636
9	9	0	4.604640	0.842210	1.013977
10	9	0	4.763249	-1.198067	0.256436
11	9	0	4.729196	0.492407	-1.125452
12	7	0	-2.282541	1.027320	-0.583047
13	6	0	-2.441982	-1.349218	-0.067589
14	8	0	-3.791885	-1.090080	-0.273488
15	8	0	-2.084528	-2.512979	0.228876
16	6	0	-4.677537	-2.198463	-0.091211
17	6	0	-2.752789	1.925480	0.314032
18	6	0	-3.524552	3.095771	-0.275702
19	8	0	-2.585706	1.820097	1.542379
20	1	0	0.001443	1.916949	-0.648729
21	1	0	2.433118	2.004791	-0.550845
22	1	0	2.545312	-2.195474	0.442031
23	1	0	0.102623	-2.284605	0.340927
24	1	0	-2.504140	1.197264	-1.567566
25	1	0	-5.677497	-1.809375	-0.292598
26	1	0	-4.627398	-2.583633	0.932190
27	1	0	-4.447403	-3.012338	-0.785874
28	1	0	-3.628697	3.877529	0.477860
29	1	0	-4.525147	2.763201	-0.576559
30	1	0	-3.029434	3.505543	-1.162134

Sum of electronic and thermal Free Energies=   -1043.927444

Geometry and energy of 3k, protonated at stereogenic centre

1	6	0	-0.440341	0.281831	0.332374
2	6	0	-0.119460	1.698660	-0.163944
3	7	0	-1.578695	-0.246087	-0.405194
4	6	0	0.786983	-0.603259	0.279280
5	6	0	1.391710	-1.232558	1.338514
6	6	0	2.530483	-2.011432	0.958561
7	6	0	2.778422	-1.961614	-0.388184
8	16	0	1.626256	-0.960005	-1.216939
9	8	0	0.562580	2.387447	0.754788
10	8	0	-0.423716	2.130221	-1.261760
11	6	0	-2.649737	-0.809816	0.211120
12	6	0	-3.740369	-1.339843	-0.696741
13	8	0	-2.738391	-0.898391	1.445659
14	6	0	0.989945	3.722624	0.386580
15	1	0	-0.736738	0.353386	1.384728
16	1	0	-1.552952	-0.186209	-1.426995
17	1	0	1.029613	-1.140741	2.360661
18	1	0	3.134749	-2.584669	1.657737
19	1	0	3.564499	-2.452548	-0.954264
20	1	0	-4.695467	-0.904220	-0.390510
21	1	0	-3.810943	-2.424164	-0.562406
22	1	0	-3.565464	-1.124373	-1.753720
23	1	0	1.526264	4.100082	1.255830
24	1	0	0.121050	4.346298	0.166397
25	1	0	1.646571	3.678066	-0.484947

Sum of electronic and thermal Free Energies=   -1028.124167

Geometry and energy of 3k, deprotonated at stereogenic centre

1	6	0	1.181587	0.167321	-0.189614
2	6	0	1.903215	1.348184	-0.360438
3	6	0	3.311055	1.202291	-0.170335
4	6	0	3.692678	-0.074468	0.147561
5	16	0	2.302929	-1.144287	0.222769
6	6	0	-0.237139	-0.023735	-0.325109
7	7	0	-0.994025	1.121790	-0.730897
8	6	0	-0.871416	-1.262472	-0.132978
9	8	0	-0.312271	-2.333021	0.216921
10	8	0	-2.243777	-1.242565	-0.359894
11	6	0	-2.935154	-2.473768	-0.128798
12	6	0	-1.734654	1.924759	0.065138
13	8	0	-2.391904	2.877560	-0.408752
14	6	0	-1.760304	1.615311	1.546900
15	1	0	1.424692	2.288566	-0.616417
16	1	0	4.014147	2.027847	-0.266874
17	1	0	4.685721	-0.460821	0.351799
18	1	0	-1.008590	1.382830	-1.724891
19	1	0	-3.981703	-2.270427	-0.364000
20	1	0	-2.844132	-2.791629	0.914828
21	1	0	-2.556733	-3.271984	-0.774944
22	1	0	-2.144073	2.485426	2.082078
23	1	0	-0.768867	1.345935	1.919433
24	1	0	-2.424734	0.763993	1.730794

Sum of electronic and thermal Free Energies=   -1027.649659

Geometry and energy of **3k**, deprotonated at stereogenic centre (not lowest energy, from Section 5.2.3.1)

1	6	0	1.136441	0.184020	-0.188868
2	6	0	1.667612	1.423286	-0.535576
3	6	0	3.092365	1.487100	-0.457391
4	6	0	3.668367	0.312966	-0.049469
5	16	0	2.453128	-0.910571	0.262303
6	6	0	-0.253619	-0.210663	-0.200881
7	7	0	-1.178288	0.807810	-0.596183
8	6	0	-0.682028	-1.489992	0.174064
9	8	0	0.054299	-2.376647	0.684308
10	8	0	-2.030532	-1.850311	0.052958
11	6	0	-2.750471	-1.568125	-1.156466
12	6	0	-1.932406	1.577615	0.225710
13	6	0	-1.863560	1.300827	1.712385
14	8	0	-2.684387	2.461755	-0.235085
15	1	0	1.045463	2.258096	-0.843974
16	1	0	3.664181	2.381775	-0.697019
17	1	0	4.718291	0.085163	0.103297
18	1	0	-1.230011	1.080125	-1.586009
19	1	0	-3.468168	-2.383393	-1.284024
20	1	0	-2.074467	-1.544510	-2.017681
21	1	0	-3.289738	-0.618810	-1.095034
22	1	0	-2.271155	2.159548	2.248143
23	1	0	-0.840705	1.098274	2.038929
24	1	0	-2.466966	0.417611	1.951313

Sum of electronic and thermal Free Energies=   -1027.641464

Geometry and energy of **3l**, protonated at stereogenic centre

1	6	0	-3.359185	-0.973851	0.655789
2	6	0	-2.069851	-1.026610	1.113006
3	6	0	-1.157729	-0.276146	0.298152

4	6	0	-1.784958	0.332191	-0.763776
5	16	0	-3.483135	-0.005323	-0.779792
6	6	0	0.331341	-0.208693	0.583338
7	7	0	1.071549	-1.085691	-0.315843
8	6	0	0.818901	1.248564	0.563959
9	8	0	1.312708	1.624483	-0.619241
10	8	0	0.727666	1.984948	1.531835
11	6	0	1.776489	2.992905	-0.724580
12	6	0	2.342706	-1.470523	-0.044745
13	6	0	3.008587	-2.376874	-1.058176
14	8	0	2.928866	-1.102510	0.986520
15	1	0	-4.245299	-1.440591	1.075230
16	1	0	-1.766491	-1.576969	2.001346
17	1	0	-1.355027	0.951048	-1.544745
18	1	0	0.506568	-0.545253	1.611827
19	1	0	0.634987	-1.343115	-1.204940
20	1	0	2.145691	3.092159	-1.744396
21	1	0	2.577184	3.171973	-0.003904
22	1	0	0.950620	3.684103	-0.542276
23	1	0	3.321865	-3.297111	-0.555719
24	1	0	3.908781	-1.882182	-1.436095
25	1	0	2.358706	-2.630186	-1.899477

Sum of electronic and thermal Free Energies=   -1028.124896

Geometry and energy of **3l**, deprotonated at stereogenic centre

1	6	0	-1.996790	-1.073063	0.154851
2	6	0	-1.124621	-0.042548	-0.178563
3	6	0	-1.865823	1.188847	-0.389805
4	6	0	-3.217182	1.071167	-0.221514
5	16	0	-3.664968	-0.551121	0.207688
6	6	0	0.321410	-0.108833	-0.323137
7	7	0	0.999463	1.091310	-0.725112
8	6	0	1.060568	-1.283100	-0.123268
9	8	0	0.617911	-2.407156	0.232509
10	8	0	2.433945	-1.137249	-0.354173
11	6	0	3.236697	-2.290789	-0.095694
12	6	0	1.703252	1.927234	0.068128
13	8	0	2.334717	2.897528	-0.409413
14	6	0	1.719595	1.642702	1.555096
15	1	0	-1.748909	-2.101383	0.372194
16	1	0	-1.389955	2.127225	-0.659811
17	1	0	-3.975113	1.841683	-0.322744
18	1	0	1.049751	1.328775	-1.723327
19	1	0	4.262378	-1.991783	-0.322334
20	1	0	2.947702	-3.133658	-0.731919
21	1	0	3.165236	-2.602309	0.951726
22	1	0	2.028319	2.546205	2.083853
23	1	0	2.442915	0.846438	1.762450
24	1	0	0.745695	1.302879	1.914728

Sum of electronic and thermal Free Energies=   -1027.643597

Geometry and energy of **3m**, protonated at stereogenic centre

1	6	0	-0.674286	-0.970699	0.196892
2	6	0	-1.088794	-1.911235	1.092995
3	6	0	-1.921388	-2.828704	0.364262
4	6	0	-1.952904	-2.379746	-0.921931
5	8	0	-1.196862	-1.242846	-1.043719
6	6	0	0.218108	0.229183	0.305842
7	7	0	1.468112	0.076928	-0.422174

8	6	0	-0.503478	1.509317	-0.149110
9	8	0	-0.183997	2.181661	-1.111361
10	8	0	-1.536536	1.781933	0.653808
11	6	0	-2.326598	2.951900	0.327643
12	6	0	2.662908	-0.080194	0.203736
13	6	0	3.870086	-0.253936	-0.693743
14	8	0	2.771600	-0.091504	1.439859
15	1	0	-0.831531	-1.945843	2.146219
16	1	0	-2.427345	-3.706252	0.751601
17	1	0	-2.434812	-2.725735	-1.828442
18	1	0	0.468457	0.351614	1.366715
19	1	0	1.425798	0.088453	-1.444904
20	1	0	-3.106908	2.989807	1.086434
21	1	0	-2.760423	2.844218	-0.668837
22	1	0	-1.703151	3.847704	0.368641
23	1	0	4.631373	0.476613	-0.405731
24	1	0	3.638131	-0.135911	-1.755262
25	1	0	4.288057	-1.252440	-0.529429

Sum of electronic and thermal Free Energies=   -705.145688

Geometry and energy of **3m**, deprotonated at stereogenic centre

1	6	0	1.131204	-0.568871	-0.149344
2	6	0	1.509969	-1.905159	-0.155244
3	6	0	2.926599	-1.940344	0.068983
4	6	0	3.337686	-0.648839	0.200382
5	8	0	2.253794	0.201569	0.067932
6	6	0	-0.159828	0.034043	-0.354891
7	7	0	-1.174989	-0.905081	-0.730103
8	6	0	-0.543517	1.388498	-0.285654
9	8	0	-1.689631	1.844688	-0.528873
10	8	0	0.462689	2.260627	0.108224
11	6	0	0.093086	3.641169	0.196437
12	6	0	-2.172976	-1.368381	0.053389
13	8	0	-3.049319	-2.137893	-0.401520
14	6	0	-2.204398	-0.908406	1.494891
15	1	0	0.849676	-2.750283	-0.299272
16	1	0	3.557963	-2.820827	0.128156
17	1	0	4.289939	-0.169274	0.385772
18	1	0	-1.198800	-1.254423	-1.696241
19	1	0	-0.705948	3.795661	0.928113
20	1	0	-0.236151	4.030034	-0.772289
21	1	0	0.996482	4.163853	0.517581
22	1	0	-2.903948	-1.534735	2.050659
23	1	0	-2.540009	0.133466	1.538185
24	1	0	-1.211506	-0.952097	1.950266

Sum of electronic and thermal Free Energies=   -704.664424

Geometry and energy of **3n**, protonated at stereogenic centre

1	6	0	-0.218764	0.213796	0.277677
2	6	0	0.433951	1.514610	-0.205070
3	7	0	-1.476635	0.006798	-0.433555
4	6	0	0.748416	-0.934870	0.156024
5	8	0	1.216745	2.044709	0.740359
6	8	0	0.290186	1.987105	-1.319744
7	6	0	1.962918	3.233352	0.380429
8	6	0	-2.647919	-0.236659	0.207210
9	6	0	-3.861748	-0.449646	-0.673852
10	8	0	-2.737371	-0.283052	1.444707
11	6	0	1.236591	-1.782241	1.137626

252

12	6	0	2.120259	-2.706054	0.506488
13	6	0	2.144922	-2.392313	-0.841636
14	7	0	1.316240	-1.315776	-1.042177
15	1	0	-0.460166	0.325691	1.338781
16	1	0	-1.454433	0.031573	-1.456613
17	1	0	2.530603	3.495134	1.272251
18	1	0	1.276880	4.038390	0.108421
19	1	0	2.632526	3.015892	-0.454675
20	1	0	-4.291463	-1.430566	-0.449016
21	1	0	-3.635732	-0.392781	-1.741677
22	1	0	-4.612940	0.306395	-0.425149
23	1	0	0.979771	-1.733408	2.190487
24	1	0	2.673378	-3.507585	0.983433
25	1	0	2.679097	-2.843314	-1.669888
26	1	0	1.137006	-0.892521	-1.958181

Sum of electronic and thermal Free Energies=   -685.287175

Geometry and energy of **3n**, deprotonated at stereogenic centre

1	6	0	1.386380	0.026917	-0.138576
2	6	0	2.187446	1.163361	-0.322278
3	6	0	3.549890	0.774609	-0.123007
4	6	0	3.560290	-0.575044	0.175629
5	7	0	2.246488	-1.012332	0.162122
6	6	0	-0.051844	-0.139689	-0.239174
7	7	0	-0.801181	1.023760	-0.608451
8	6	0	-0.685875	-1.370234	-0.065291
9	8	0	-0.128908	-2.466336	0.250170
10	8	0	-2.065565	-1.351800	-0.280692
11	6	0	-2.746306	-2.592883	-0.083368
12	6	0	-1.375019	1.888979	0.258955
13	6	0	-2.128080	3.054655	-0.360702
14	8	0	-1.320944	1.767351	1.496745
15	1	0	1.824899	2.153725	-0.568245
16	1	0	4.422481	1.416131	-0.190136
17	1	0	4.373302	-1.255917	0.396485
18	1	0	1.908638	-1.953770	0.339407
19	1	0	-0.904435	1.233117	-1.604639
20	1	0	-3.798546	-2.385889	-0.290619
21	1	0	-2.636384	-2.952551	0.945081
22	1	0	-2.380316	-3.366736	-0.766056
23	1	0	-1.791421	3.984585	0.106215
24	1	0	-3.195465	2.942519	-0.141981
25	1	0	-1.997865	3.127040	-1.444110

Sum of electronic and thermal Free Energies=   -684.804159

Geometry and energy of **3o**, protonated at stereogenic centre

1	7	0	-3.856704	-0.873289	0.175635
2	6	0	-3.041670	-0.658545	1.222186
3	6	0	-1.676936	-0.392647	1.095954
4	6	0	-1.112745	-0.352452	-0.185088
5	6	0	-1.953883	-0.574173	-1.279049
6	6	0	-3.308093	-0.828135	-1.049477
7	1	0	-3.500735	-0.697167	2.210646
8	1	0	-1.077170	-0.224133	1.990268
9	6	0	0.371208	-0.079079	-0.393502
10	1	0	-1.567601	-0.550462	-2.297176
11	1	0	-3.981082	-1.003274	-1.889571
12	1	0	0.570005	-0.003272	-1.469281
13	6	0	0.755129	1.278812	0.225597

14	7	0	1.178811	-1.156937	0.152129
15	6	0	2.477174	-1.314913	-0.211713
16	1	0	0.775762	-1.756811	0.876962
17	6	0	3.233978	-2.444614	0.453188
18	8	0	3.015998	-0.565744	-1.041140
19	1	0	3.793765	-2.992989	-0.308703
20	1	0	3.957655	-2.015092	1.154761
21	1	0	2.583779	-3.134200	0.997372
22	8	0	1.338761	1.428098	1.281742
23	8	0	0.330411	2.281971	-0.552557
24	6	0	0.566223	3.627909	-0.071055
25	1	0	0.152828	4.282493	-0.837146
26	1	0	0.056188	3.778826	0.883093
27	1	0	1.638187	3.800084	0.047820

Sum of electronic and thermal Free Energies=   -723.391632

Geometry and energy of 3o, deprotonated at stereogenic centre

1	7	0	4.045273	-0.025536	0.035984
2	6	0	3.280535	1.040837	-0.289250
3	6	0	1.897725	1.022849	-0.387953
4	6	0	1.159295	-0.174506	-0.143274
5	6	0	1.976402	-1.295305	0.199200
6	6	0	3.356299	-1.164703	0.270268
7	1	0	3.816732	1.971719	-0.483117
8	1	0	1.382384	1.938720	-0.657839
9	6	0	-0.269810	-0.201633	-0.250542
10	1	0	1.518684	-2.253985	0.405405
11	1	0	3.957225	-2.036939	0.535252
12	6	0	-1.071533	-1.359717	-0.075297
13	7	0	-0.938425	1.022060	-0.597105
14	1	0	-1.168746	1.183398	-1.580521
15	6	0	-1.402991	1.922845	0.299405
16	6	0	-2.111333	3.136575	-0.276793
17	8	0	-1.252169	1.807529	1.529701
18	1	0	-3.057046	3.280998	0.253120
19	1	0	-1.494496	4.024368	-0.100801
20	1	0	-2.307095	3.052859	-1.349450
21	8	0	-2.423215	-1.123646	-0.288559
22	8	0	-0.694363	-2.514309	0.226178
23	6	0	-3.291097	-2.248305	-0.114218
24	1	0	-4.296140	-1.876286	-0.322627
25	1	0	-3.041131	-3.056676	-0.808430
26	1	0	-3.241276	-2.634056	0.909015

Sum of electronic and thermal Free Energies=   -722.919742

Geometry and energy of 6e, protonated at stereogenic centre

1	6	0	0.061389	-0.086942	1.004426
2	6	0	1.441435	-0.257862	1.116796
3	6	0	2.261161	-0.030038	0.005161
4	6	0	1.701008	0.358304	-1.217256
5	6	0	0.319741	0.525509	-1.319422
6	6	0	-0.510702	0.306857	-0.212609
7	6	0	3.742040	-0.258482	0.101314
8	9	0	4.215823	-0.126711	1.366554
9	9	0	4.098871	-1.515423	-0.306286
10	9	0	4.456266	0.599109	-0.675270
11	6	0	-2.020383	0.529269	-0.338083
12	7	0	-2.813250	-0.483601	0.340475
13	6	0	-2.390915	1.904933	0.257616

14	7	0	-2.338607	2.940429	-0.595876
15	8	0	-2.678984	2.019156	1.456106
16	6	0	-3.172530	-1.644256	-0.260901
17	6	0	-4.014051	-2.597468	0.562474
18	8	0	-2.840070	-1.918038	-1.425397
19	1	0	-0.568259	-0.265721	1.873940
20	1	0	1.872419	-0.562585	2.068238
21	1	0	2.332717	0.526815	-2.087628
22	1	0	-0.113566	0.821367	-2.274733
23	1	0	-2.285247	0.511652	-1.401786
24	1	0	-3.097549	-0.292101	1.303294
25	1	0	-2.167692	2.815701	-1.592083
26	1	0	-2.528826	3.881975	-0.252859
27	1	0	-4.961980	-2.768953	0.042959
28	1	0	-4.220176	-2.228724	1.570578
29	1	0	-3.494213	-3.557899	0.630125

Sum of electronic and thermal Free Energies=   -985.258608

Geometry and energy of 6e, deprotonated at stereogenic centre

1	6	0	-2.367262	0.027264	-0.055091
2	6	0	-1.512974	-1.040984	-0.385987
3	6	0	-0.140126	-0.860220	-0.441411
4	6	0	0.478964	0.402353	-0.172342
5	6	0	-0.417950	1.465945	0.161659
6	6	0	-1.793141	1.279836	0.219587
7	1	0	-1.928231	-2.024738	-0.604162
8	1	0	0.477645	-1.710855	-0.707781
9	6	0	1.907001	0.552326	-0.249825
10	1	0	-0.001581	2.441625	0.372310
11	1	0	-2.427934	2.124222	0.481250
12	6	0	-3.829915	-0.200076	0.024976
13	9	0	-4.549627	0.939330	0.210853
14	9	0	-4.350064	-0.797991	-1.098395
15	9	0	-4.199565	-1.042064	1.054252
16	6	0	2.626912	1.772588	-0.096704
17	7	0	2.679372	-0.619974	-0.579831
18	1	0	2.870872	-0.810163	-1.568444
19	6	0	3.087601	-1.556293	0.315335
20	6	0	3.804450	-2.766392	-0.257674
21	8	0	2.896704	-1.459029	1.539834
22	1	0	4.759263	-2.893408	0.260863
23	1	0	3.200935	-3.658769	-0.061217
24	1	0	3.985550	-2.692680	-1.333527
25	7	0	4.010425	1.749094	-0.319013
26	8	0	2.111754	2.903345	0.173832
27	1	0	4.497932	2.545510	0.084794
28	1	0	4.501249	0.869338	-0.217031

Sum of electronic and thermal Free Energies=   -984.775482

Geometry and energy of 9, protonated at stereogenic centre

1	6	0	-1.202928	0.408133	1.027234
2	6	0	-2.456083	-0.102264	1.379366
3	6	0	-3.261862	-0.720685	0.416289
4	6	0	-2.804119	-0.826607	-0.900786
5	6	0	-1.547649	-0.319401	-1.250072
6	6	0	-0.735366	0.306199	-0.293179
7	6	0	0.625641	0.876835	-0.699651
8	6	0	0.711578	2.400455	-0.508377
9	6	0	1.723444	0.162272	0.080107

10	8	0	2.100617	-0.977181	-0.527795
11	8	0	2.199838	0.540256	1.138476
12	6	0	3.093385	-1.780632	0.150836
13	1	0	-0.587568	0.885370	1.788673
14	1	0	-2.803057	-0.016459	2.408445
15	1	0	-4.238635	-1.116399	0.691262
16	1	0	-3.422462	-1.305598	-1.659037
17	1	0	-1.195248	-0.407557	-2.277700
18	1	0	0.780445	0.636031	-1.758503
19	1	0	1.677815	2.781900	-0.854559
20	1	0	0.593693	2.676080	0.542767
21	1	0	-0.079422	2.887947	-1.086005
22	1	0	3.261878	-2.639183	-0.498524
23	1	0	2.716856	-2.102395	1.124883
24	1	0	4.015828	-1.210167	0.282247

Sum of electronic and thermal Free Energies=   -538.642453

Geometry and energy of 9, deprotonated at stereogenic centre

1	6	0	1.882371	1.166928	-0.018170
2	6	0	3.231306	0.806567	-0.023892
3	6	0	3.621596	-0.538453	-0.006068
4	6	0	2.611500	-1.512000	0.015139
5	6	0	1.261139	-1.162884	0.020422
6	6	0	0.827714	0.200629	0.006118
7	6	0	-0.561000	0.635471	0.014931
8	6	0	-0.830824	2.129091	0.028923
9	6	0	-1.638678	-0.270700	-0.002975
10	8	0	-2.905426	0.349240	-0.017263
11	8	0	-1.620541	-1.534534	-0.009622
12	6	0	-4.033098	-0.523156	-0.008235
13	1	0	1.641460	2.224663	-0.036148
14	1	0	3.986949	1.592582	-0.043454
15	1	0	4.673354	-0.818940	-0.009871
16	1	0	2.879897	-2.569140	0.028218
17	1	0	0.508498	-1.940244	0.035399
18	1	0	-1.899169	2.332757	0.093305
19	1	0	-0.455171	2.637820	-0.873955
20	1	0	-0.348562	2.631626	0.882163
21	1	0	-4.909652	0.129289	-0.020849
22	1	0	-4.054008	-1.150057	0.889986
23	1	0	-4.048009	-1.176959	-0.886875

Sum of electronic and thermal Free Energies=   -538.149350

Geometry and energy of 10, protonated at stereogenic centre

1	6	0	-0.800593	0.343194	0.062719
2	6	0	-1.213006	-0.265065	-1.132815
3	6	0	-2.462163	-0.887318	-1.221870
4	6	0	-3.320240	-0.906617	-0.115871
5	6	0	-2.918481	-0.301300	1.079177
6	6	0	-1.666008	0.317368	1.165193
7	1	0	-0.555698	-0.261200	-2.002009
8	1	0	-2.765538	-1.357690	-2.156449
9	1	0	-4.292467	-1.392579	-0.185081
10	1	0	-3.575630	-0.315121	1.947876
11	1	0	-1.355568	0.781085	2.101962
12	6	0	0.536391	1.075086	0.167589
13	1	0	0.777155	1.183244	1.230346
14	7	0	1.643664	0.321182	-0.430825
15	6	0	0.469503	2.471619	-0.472059

16	1	0	1.413249	3.007299	-0.325949
17	1	0	0.269684	2.401207	-1.547693
18	1	0	-0.337302	3.054099	-0.018031
19	1	0	1.813162	0.437006	-1.432780
20	6	0	2.428597	-0.534517	0.263341
21	6	0	3.522735	-1.233767	-0.520395
22	8	0	2.279646	-0.748459	1.479940
23	1	0	4.482240	-1.051385	-0.027471
24	1	0	3.337868	-2.312522	-0.497060
25	1	0	3.585623	-0.906139	-1.561466

Sum of electronic and thermal Free Energies=   -518.783181

Geometry and energy of **10**, deprotonated at stereogenic centre

1	6	0	-0.885958	0.230689	-0.027515
2	6	0	-2.037652	1.111504	-0.051288
3	6	0	-3.339512	0.632747	0.034150
4	6	0	-3.624645	-0.744931	0.126316
5	6	0	-2.529339	-1.630873	0.124470
6	6	0	-1.216462	-1.178909	0.048674
7	1	0	-1.882487	2.184397	-0.133287
8	1	0	-4.161036	1.351358	0.018383
9	1	0	-4.647805	-1.108869	0.187308
10	1	0	-2.707050	-2.705921	0.190364
11	1	0	-0.410902	-1.909671	0.083415
12	6	0	0.429721	0.712601	-0.090464
13	7	0	1.465038	-0.232675	-0.394765
14	6	0	0.770224	2.160790	-0.327347
15	1	0	1.826728	2.347799	-0.111506
16	1	0	0.583013	2.500154	-1.367381
17	1	0	0.193868	2.830909	0.323184
18	1	0	1.291123	-0.899877	-1.154639
19	6	0	2.688455	-0.297535	0.170960
20	6	0	3.659176	-1.298967	-0.430344
21	8	0	3.050987	0.435034	1.122341
22	1	0	4.134737	-1.863273	0.377413
23	1	0	3.181332	-1.996151	-1.125911
24	1	0	4.451270	-0.765099	-0.968387

Sum of electronic and thermal Free Energies=   -518.255430

Geometry and energy of **11**, protonated at stereogenic centre

1	6	0	-0.386072	2.173101	-0.297560
2	6	0	-0.071343	0.727913	0.136536
3	6	0	-1.231246	-0.202649	-0.228904
4	8	0	-1.237788	-0.985091	-1.162913
5	7	0	1.167404	0.254898	-0.453589
6	6	0	2.197115	-0.246273	0.273612
7	6	0	3.405998	-0.711062	-0.513076
8	8	0	2.172603	-0.317511	1.513652
9	8	0	-2.268255	-0.019929	0.600458
10	1	0	1.227342	0.237309	-1.475344
11	1	0	0.049382	0.693298	1.224206
12	1	0	-1.317231	2.516032	0.161019
13	1	0	0.426584	2.831190	0.021524
14	1	0	-0.485020	2.242084	-1.386275
15	1	0	3.296292	-0.576445	-1.592136
16	1	0	4.284373	-0.155817	-0.170125
17	1	0	3.578811	-1.770172	-0.298492
18	6	0	-3.463948	-0.792630	0.334610
19	1	0	-4.172794	-0.498290	1.107408
20	1	0	-3.852692	-0.553509	-0.657744

21	1	0	-3.242377	-1.860114	0.400194

Sum of electronic and thermal Free Energies=   -515.641260

Geometry and energy of **11**, deprotonated at stereogenic centre

1	6	0	0.074676	1.899561	-0.483017
2	6	0	0.133305	0.419940	-0.213678
3	6	0	1.281899	-0.339007	-0.085709
4	8	0	2.480839	0.405630	-0.130468
5	7	0	-1.078427	-0.328573	-0.386936
6	6	0	-2.266889	-0.077166	0.197712
7	6	0	-3.429976	-0.953522	-0.239175
8	8	0	-2.447444	0.837552	1.035306
9	8	0	1.365811	-1.607369	0.027009
10	1	0	-1.020866	-1.162186	-0.976392
11	1	0	1.058998	2.347152	-0.329064
12	1	0	-0.233667	2.121199	-1.519698
13	1	0	-0.640998	2.410397	0.173485
14	1	0	-3.119541	-1.818139	-0.833301
15	1	0	-3.969163	-1.298214	0.648103
16	1	0	-4.128471	-0.356475	-0.836635
17	6	0	3.635889	-0.252293	0.385810
18	1	0	4.462830	0.450741	0.258260
19	1	0	3.519918	-0.487162	1.451849
20	1	0	3.852871	-1.178884	-0.154489

Sum of electronic and thermal Free Energies=   -515.141347

Geometry and energy of Amfepramone (protonated at amine), protonated at stereogenic centre

1	6	0	4.150926	0.723576	0.282224
2	6	0	4.450917	-0.291236	-0.636780
3	6	0	3.425807	-1.070583	-1.182794
4	6	0	2.100284	-0.844129	-0.809841
5	6	0	1.790083	0.174381	0.112365
6	6	0	2.829912	0.958513	0.652599
7	6	0	0.403722	0.470066	0.538204
8	6	0	-0.716520	-0.561132	0.268598
9	8	0	0.111372	1.482113	1.172068
10	7	0	-2.036815	0.199000	0.277272
11	6	0	-0.632713	-1.642068	1.357986
12	6	0	-3.269419	-0.648171	0.555157
13	6	0	-2.161805	1.027069	-0.996382
14	6	0	-3.361133	1.964248	-1.003263
15	6	0	-3.604008	-1.656623	-0.534164
16	1	0	4.949751	1.328254	0.708823
17	1	0	5.485021	-0.473228	-0.927322
18	1	0	3.657159	-1.854687	-1.901762
19	1	0	1.320531	-1.455769	-1.259930
20	1	0	2.588537	1.742259	1.367050
21	1	0	-0.621450	-1.012497	-0.725066
22	1	0	-1.962311	0.873577	1.072536
23	1	0	-1.326621	-2.464273	1.173057
24	1	0	-0.822202	-1.221500	2.350867
25	1	0	0.376819	-2.060502	1.357042
26	1	0	-4.086599	0.061170	0.701761
27	1	0	-3.099510	-1.134519	1.516349
28	1	0	-2.191184	0.320138	-1.828956
29	1	0	-1.237017	1.602022	-1.072497
30	1	0	-3.283311	2.600895	-1.889708

31	1	0	-3.367834	2.617234	-0.123730
32	1	0	-4.315928	1.435358	-1.060006
33	1	0	-4.456243	-2.249714	-0.188936
34	1	0	-2.781379	-2.348785	-0.737303
35	1	0	-3.895805	-1.178800	-1.473176

Sum of electronic and thermal Free Energies=   -637.047397

Geometry and energy of Amfepramone (protonated at amine), deprotonated at stereogenic centre

1	6	0	-3.732934	1.294354	-0.120478
2	6	0	-4.577073	0.218302	0.171305
3	6	0	-4.039912	-1.070773	0.281196
4	6	0	-2.670532	-1.278738	0.100405
5	6	0	-1.809092	-0.201904	-0.175183
6	6	0	-2.359328	1.085483	-0.290041
7	6	0	-0.348432	-0.467493	-0.393437
8	6	0	0.624081	0.280847	0.236815
9	8	0	-0.025356	-1.446621	-1.200982
10	7	0	1.970087	-0.206115	-0.177409
11	6	0	0.506017	1.341269	1.290328
12	6	0	2.761439	-0.839958	0.941285
13	6	0	2.764002	0.731768	-1.066294
14	6	0	3.469991	1.874396	-0.346608
15	6	0	3.972934	-1.627119	0.452216
16	1	0	-4.142465	2.298637	-0.222742
17	1	0	-5.645748	0.380193	0.305823
18	1	0	-4.690211	-1.915430	0.506136
19	1	0	-2.257443	-2.282987	0.174641
20	1	0	-1.715570	1.927874	-0.534366
21	1	0	1.636394	-0.985843	-0.804246
22	1	0	0.678986	2.363053	0.923474
23	1	0	1.204185	1.178248	2.121865
24	1	0	-0.500148	1.322539	1.715676
25	1	0	2.053842	-1.497168	1.453883
26	1	0	3.055607	-0.052889	1.639118
27	1	0	2.042099	1.112155	-1.793366
28	1	0	3.489278	0.115501	-1.606521
29	1	0	3.993093	2.474712	-1.097792
30	1	0	4.219814	1.520510	0.367330
31	1	0	2.772520	2.530830	0.176980
32	1	0	4.415835	-2.149975	1.305549
33	1	0	4.746549	-0.986120	0.019898
34	1	0	3.688656	-2.380670	-0.290676

Sum of electronic and thermal Free Energies=   -636.580166

Geometry and energy of Cathinone (protonated at amine), protonated at stereogenic centre

1	6	0	2.845091	0.926591	0.299515
2	6	0	3.292948	-0.360714	-0.026363
3	6	0	2.375480	-1.353922	-0.384834
4	6	0	1.010012	-1.067570	-0.413915
5	6	0	0.551747	0.223770	-0.088413
6	6	0	1.484374	1.219213	0.265907
7	6	0	-0.883109	0.588098	-0.111080
8	6	0	-1.943606	-0.524469	-0.179061
9	8	0	-1.274523	1.750750	-0.031857
10	7	0	-3.236354	0.123090	-0.594982
11	6	0	-2.126076	-1.219430	1.175602
12	1	0	3.559304	1.699029	0.580430

13	1	0	4.358001	-0.588509	-0.001682
14	1	0	2.722552	-2.352525	-0.644912
15	1	0	0.320054	-1.854440	-0.711757
16	1	0	1.127826	2.214849	0.520077
17	1	0	-1.708965	-1.252812	-0.965225
18	1	0	-4.015686	-0.555967	-0.595694
19	1	0	-3.170294	0.515559	-1.549985
20	1	0	-3.483372	0.907817	0.032016
21	1	0	-2.905848	-1.984655	1.108755
22	1	0	-2.398623	-0.497171	1.952548
23	1	0	-1.195448	-1.708203	1.471006

Sum of electronic and thermal Free Energies=   -479.905944

Geometry and energy of Cathinone (protonated at amine), deprotonated at stereogenic centre

1	6	0	-2.704372	-0.864843	0.656872
2	6	0	-3.243325	0.282748	0.061084
3	6	0	-2.401020	1.164591	-0.623439
4	6	0	-1.027456	0.906402	-0.704119
5	6	0	-0.475713	-0.237715	-0.104641
6	6	0	-1.334906	-1.125423	0.566365
7	6	0	0.986357	-0.569548	-0.212754
8	6	0	1.945694	0.352795	0.138758
9	8	0	1.307553	-1.759681	-0.645111
10	7	0	3.307732	-0.190257	-0.068621
11	6	0	1.876900	1.709926	0.762145
12	1	0	-3.353078	-1.558342	1.190873
13	1	0	-4.311871	0.483687	0.125733
14	1	0	-2.812151	2.053017	-1.101484
15	1	0	-0.383599	1.591109	-1.252940
16	1	0	-0.920357	-2.023699	1.020661
17	1	0	3.872719	0.338935	-0.751396
18	1	0	3.132540	-1.149644	-0.440400
19	1	0	3.864582	-0.265578	0.797655
20	1	0	2.282300	2.502324	0.114146
21	1	0	2.439856	1.752808	1.707795
22	1	0	0.841556	1.971036	0.988963

Sum of electronic and thermal Free Energies=   -479.436174

5.4.1.2 Calculations Performed in the Gas-Phase

Geometry and energy of 3a, protonated at stereogenic centre

1	6	0	1.450945	-1.044862	-1.166920
2	6	0	2.648054	-1.732771	-0.949942
3	6	0	3.190492	-1.808288	0.334887
4	6	0	2.529194	-1.195185	1.403900
5	6	0	1.333493	-0.508606	1.186130
6	6	0	0.786513	-0.428496	-0.102070
7	6	0	-0.528000	0.318089	-0.347574
8	7	0	-1.663193	-0.257827	0.355089
9	6	0	-0.397462	1.775239	0.092400
10	8	0	0.333131	2.487265	-0.774974
11	8	0	-0.877145	2.225063	1.116538
12	6	0	0.585133	3.863757	-0.418799
13	6	0	-2.416513	-1.256818	-0.195109
14	6	0	-3.587807	-1.737909	0.643099
15	8	0	-2.156875	-1.742822	-1.293878
16	1	0	1.021154	-1.001228	-2.163357

17	1	0	3.151065	-2.214098	-1.783642
18	1	0	4.119910	-2.344251	0.504237
19	1	0	2.944435	-1.250799	2.406139
20	1	0	0.823897	-0.036159	2.022141
21	1	0	-0.741168	0.290170	-1.419684
22	1	0	-1.943325	0.192814	1.216342
23	1	0	1.184035	4.265535	-1.234798
24	1	0	-0.356901	4.408044	-0.323432
25	1	0	1.132417	3.914160	0.525127
26	1	0	-3.745412	-1.151150	1.552386
27	1	0	-4.492902	-1.707563	0.030968
28	1	0	-3.412000	-2.781636	0.920443

Sum of electronic and thermal Free Energies=   -707.317933

Geometry and energy of **3a**, deprotonated at stereogenic centre

1	6	0	-1.884334	1.115982	-0.313033
2	6	0	-3.272664	1.216587	-0.254758
3	6	0	-4.069823	0.095815	0.010954
4	6	0	-3.422536	-1.130824	0.221688
5	6	0	-2.036077	-1.246688	0.166090
6	6	0	-1.204373	-0.120271	-0.111791
7	6	0	0.234471	-0.200012	-0.207145
8	7	0	0.950372	0.993078	-0.561904
9	6	0	0.988378	-1.386769	-0.059801
10	8	0	2.366285	-1.184767	-0.309543
11	8	0	0.604092	-2.534820	0.228657
12	6	0	3.176917	-2.330104	-0.104041
13	6	0	1.541976	1.865142	0.300314
14	8	0	1.442545	1.832721	1.526480
15	6	0	2.381149	2.958438	-0.367998
16	1	0	-1.298579	2.008774	-0.507134
17	1	0	-3.738146	2.188799	-0.413433
18	1	0	-5.153268	0.175704	0.058740
19	1	0	-4.012647	-2.021186	0.436503
20	1	0	-1.558845	-2.203834	0.334505
21	1	0	1.195484	1.121709	-1.537134
22	1	0	4.200634	-2.015001	-0.330749
23	1	0	2.886809	-3.159031	-0.760948
24	1	0	3.119205	-2.685392	0.931847
25	1	0	3.429244	2.808232	-0.088729
26	1	0	2.068628	3.930881	0.023278
27	1	0	2.306993	2.969953	-1.461051

Sum of electronic and thermal Free Energies=   -706.765983

Geometry and energy of **3b**, protonated at stereogenic centre

1	6	0	-1.357280	-0.349804	1.261219
2	6	0	-2.735410	-0.500750	1.119026
3	6	0	-3.321784	-0.343712	-0.140296
4	6	0	-2.524960	-0.038648	-1.250010
5	6	0	-1.146811	0.111091	-1.092810
6	6	0	-0.545910	-0.041904	0.162557
7	8	0	-4.680144	-0.502197	-0.228197
8	6	0	0.965252	0.115534	0.338450
9	7	0	1.747973	-0.870235	-0.392002
10	6	0	1.407751	1.499963	-0.130431
11	8	0	1.102108	2.446224	0.766909
12	8	0	1.946233	1.718672	-1.200254
13	6	0	1.403737	3.806583	0.389044
14	6	0	2.075523	-2.077629	0.157458

261

15	6	0	2.916469	-2.993489	-0.714500
16	8	0	1.705840	-2.407108	1.282643
17	1	0	-0.904217	-0.489546	2.238189
18	1	0	-3.364190	-0.746829	1.968253
19	1	0	-2.977755	0.083354	-2.231707
20	1	0	-0.539502	0.348183	-1.962521
21	1	0	-4.968890	-0.384481	-1.142676
22	1	0	1.197398	0.010387	1.401570
23	1	0	2.131201	-0.581285	-1.282307
24	1	0	1.087109	4.415554	1.234587
25	1	0	0.850931	4.078518	-0.512960
26	1	0	2.474744	3.920220	0.207784
27	1	0	3.240203	-2.530732	-1.651078
28	1	0	2.331352	-3.888888	-0.944858
29	1	0	3.794044	-3.310937	-0.145313

Sum of electronic and thermal Free Energies=   -782.541245

Geometry and energy of 3b, deprotonated at stereogenic centre

1	6	0	-1.502925	1.058162	-0.349156
2	6	0	-2.894939	1.142142	-0.302226
3	6	0	-3.656576	0.008464	-0.023535
4	6	0	-3.001938	-1.202833	0.209384
5	6	0	-1.609536	-1.290014	0.162833
6	6	0	-0.799353	-0.156712	-0.126115
7	8	0	-5.048896	0.130714	0.013879
8	6	0	0.647775	-0.213407	-0.206481
9	7	0	1.350314	0.987405	-0.561959
10	6	0	1.411608	-1.386279	-0.049497
11	8	0	2.794956	-1.166046	-0.275731
12	8	0	1.037934	-2.543589	0.227366
13	6	0	3.614014	-2.304565	-0.069436
14	6	0	1.815978	1.934780	0.298109
15	6	0	2.668008	3.030081	-0.350653
16	8	0	1.585322	1.974124	1.506646
17	1	0	-0.937051	1.960844	-0.553869
18	1	0	-3.396128	2.091760	-0.473379
19	1	0	-3.583351	-2.099286	0.432450
20	1	0	-1.118912	-2.237551	0.347092
21	1	0	-5.414739	-0.726527	0.264271
22	1	0	1.707441	1.056826	-1.507916
23	1	0	4.637403	-1.978507	-0.282757
24	1	0	3.339512	-3.132197	-0.734775
25	1	0	3.549335	-2.668407	0.963324
26	1	0	3.655444	3.022526	0.121434
27	1	0	2.210232	4.002800	-0.145679
28	1	0	2.791383	2.915353	-1.433142

Sum of electronic and thermal Free Energies=   -781.986873

Geometry and energy of 3c, protonated at stereogenic centre

1	6	0	-1.113641	0.072741	-1.098606
2	6	0	-2.493702	-0.062133	-1.249548
3	6	0	-3.323891	-0.307285	-0.144910
4	6	0	-2.723281	-0.407475	1.117163
5	6	0	-1.341832	-0.273906	1.273048
6	6	0	-0.522292	-0.033398	0.167064
7	6	0	0.991059	0.112210	0.343618
8	7	0	1.762491	-0.885168	-0.381221
9	6	0	1.445911	1.489625	-0.135538
10	8	0	1.119693	2.448704	0.740721

262

11	8	0	2.011375	1.692341	-1.194183
12	6	0	1.432207	3.803156	0.350690
13	6	0	2.074053	-2.094902	0.172529
14	6	0	2.908562	-3.021688	-0.694167
15	8	0	1.695684	-2.418090	1.296557
16	6	0	-4.814291	-0.488687	-0.316832
17	1	0	-0.496227	0.262523	-1.973117
18	1	0	-2.932868	0.026961	-2.240358
19	1	0	-3.341438	-0.598508	1.991012
20	1	0	-0.897696	-0.370508	2.259584
21	1	0	1.222033	0.013149	1.407814
22	1	0	2.158016	-0.600384	-1.267554
23	1	0	1.094076	4.424791	1.178520
24	1	0	0.903370	4.061731	-0.569406
25	1	0	2.507697	3.913661	0.195891
26	1	0	3.778911	-3.349700	-0.119917
27	1	0	3.243086	-2.563612	-1.629241
28	1	0	2.313508	-3.909746	-0.927492
29	1	0	-5.359962	-0.187072	0.582526
30	1	0	-5.062558	-1.539423	-0.513342
31	1	0	-5.194568	0.099120	-1.158202

Sum of electronic and thermal Free Energies=   -746.614771

Geometry and energy of **3c**, deprotonated at stereogenic centre

1	6	0	3.689004	0.014415	-0.011937
2	6	0	3.003097	-1.195041	0.199963
3	6	0	1.615763	-1.287287	0.149735
4	6	0	0.800561	-0.148783	-0.125792
5	6	0	1.505168	1.069002	-0.331379
6	6	0	2.897306	1.140014	-0.276623
7	1	0	3.574809	-2.099141	0.414328
8	1	0	1.125063	-2.237214	0.321195
9	6	0	-0.641144	-0.204140	-0.212338
10	1	0	0.940893	1.975555	-0.525559
11	1	0	3.379544	2.104682	-0.439053
12	6	0	5.197667	0.092844	0.054512
13	7	0	-1.337256	1.001517	-0.563381
14	6	0	-1.413126	-1.377068	-0.059376
15	8	0	-2.790177	-1.152285	-0.298462
16	8	0	-1.045845	-2.532129	0.226066
17	6	0	-3.617804	-2.283821	-0.085645
18	1	0	-4.637646	-1.953024	-0.307730
19	1	0	-3.344612	-3.119190	-0.741659
20	1	0	-3.560606	-2.637378	0.950969
21	1	0	-1.591217	1.131702	-1.536194
22	6	0	-1.900161	1.889129	0.302037
23	6	0	-2.725013	2.996644	-0.360897
24	8	0	-1.786681	1.859997	1.527147
25	1	0	-2.391238	3.963860	0.025716
26	1	0	-2.660488	3.004797	-1.454610
27	1	0	-3.773206	2.866175	-0.072124
28	1	0	5.547761	1.111200	-0.152578
29	1	0	5.584700	-0.189418	1.044510
30	1	0	5.680740	-0.573328	-0.675122

Sum of electronic and thermal Free Energies=   -746.059404

Geometry and energy of **3d**, protonated at stereogenic centre

| 1 | 6 | 0 | -1.135278 | 0.122371 | -1.103428 |
| 2 | 6 | 0 | -2.512355 | -0.024030 | -1.275083 |

263

3	6	0	-3.286633	-0.332317	-0.162215
4	6	0	-2.739764	-0.502455	1.102489
5	6	0	-1.358994	-0.352446	1.254007
6	6	0	-0.547082	-0.038491	0.159099
7	9	0	-4.629579	-0.475930	-0.321211
8	6	0	0.964427	0.116387	0.344167
9	7	0	1.744215	-0.871539	-0.384023
10	6	0	1.414986	1.500900	-0.119129
11	8	0	1.076409	2.448981	0.763148
12	8	0	1.987418	1.714661	-1.171673
13	6	0	1.387666	3.809710	0.391175
14	6	0	2.038081	-2.091048	0.159575
15	6	0	2.889207	-3.009888	-0.698193
16	8	0	1.630182	-2.425115	1.269982
17	1	0	-0.517520	0.361877	-1.964761
18	1	0	-2.982736	0.097621	-2.244773
19	1	0	-3.380647	-0.753008	1.940751
20	1	0	-0.909531	-0.498939	2.231234
21	1	0	1.189198	0.010023	1.408988
22	1	0	2.160030	-0.573311	-1.256702
23	1	0	1.039012	4.420334	1.222668
24	1	0	0.866771	4.076232	-0.531074
25	1	0	2.464188	3.925161	0.248408
26	1	0	3.751707	-3.337417	-0.111834
27	1	0	3.236897	-2.545598	-1.625248
28	1	0	2.301703	-3.899199	-0.945040

Sum of electronic and thermal Free Energies=   -806.568383

Geometry and energy of 3d, deprotonated at stereogenic centre

1	6	0	3.631304	-0.017528	-0.020319
2	6	0	3.000013	-1.231841	0.216467
3	6	0	1.607698	-1.305759	0.166055
4	6	0	0.803906	-0.164376	-0.126106
5	6	0	1.509056	1.051342	-0.349305
6	6	0	2.902060	1.128812	-0.300872
7	1	0	3.593885	-2.114248	0.439777
8	1	0	1.108700	-2.248728	0.349989
9	6	0	-0.639870	-0.213811	-0.208576
1C	1	0	0.945952	1.955056	-0.554639
11	1	0	3.415870	2.071044	-0.471255
12	9	0	5.014542	0.052938	0.030373
13	7	0	-1.338276	0.989194	-0.565557
14	6	0	-1.411833	-1.383748	-0.047030
15	8	0	-2.791403	-1.154643	-0.272068
16	8	0	-1.044230	-2.540818	0.232174
17	6	0	-3.618364	-2.289104	-0.068756
18	1	0	-4.639500	-1.954834	-0.278849
19	1	0	-3.350083	-3.115050	-0.738390
20	1	0	-3.553334	-2.657005	0.962239
21	1	0	-1.713223	1.048080	-1.505062
22	6	0	-1.791166	1.943083	0.295190
23	6	0	-2.650354	3.035373	-0.348170
24	8	0	-1.541507	1.988634	1.499430
25	1	0	-2.189588	4.008874	-0.154125
26	1	0	-2.787506	2.915052	-1.428319
27	1	0	-3.631698	3.030912	0.136417

Sum of electronic and thermal Free Energies=   -806.019830

Geometry and energy of 3e, protonated at stereogenic centre

1	6	0	-0.793828	0.207665	-1.053262
2	6	0	-2.179683	0.135255	-1.193495
3	6	0	-2.961826	-0.137582	-0.069845
4	6	0	-2.379655	-0.341285	1.180265
5	6	0	-0.990458	-0.265149	1.303508
6	6	0	-0.186272	0.010327	0.193899
7	6	0	1.335028	0.084037	0.344934
8	7	0	2.041362	-0.946599	-0.398245
9	6	0	1.848747	1.441221	-0.133924
10	8	0	1.568637	2.410084	0.745828
11	8	0	2.418433	1.618768	-1.194513
12	6	0	1.942058	3.751777	0.361434
13	6	0	2.262592	-2.185479	0.136226
14	6	0	3.045746	-3.152024	-0.733496
15	8	0	1.846091	-2.497626	1.249741
16	17	0	-4.710201	-0.230075	-0.237629
17	1	0	-0.185389	0.418311	-1.928844
18	1	0	-2.647799	0.289711	-2.159464
19	1	0	-2.999801	-0.562427	2.041928
20	1	0	-0.530301	-0.440923	2.271030
21	1	0	1.577661	-0.030962	1.405042
22	1	0	2.463259	-0.670009	-1.275218
23	1	0	1.637077	4.383097	1.194603
24	1	0	1.420701	4.039332	-0.554207
25	1	0	3.020654	3.812367	0.201769
26	1	0	3.904599	-3.518022	-0.164613
27	1	0	3.394515	-2.712864	-1.672271
28	1	0	2.408741	-4.012514	-0.958246

Sum of electronic and thermal Free Energies=   -1166.924404

Geometry and energy of 3e, deprotonated at stereogenic centre

1	6	0	-0.931686	-1.053752	-0.451011
2	6	0	-2.322432	-1.109093	-0.453424
3	6	0	-3.060352	0.005538	-0.057382
4	6	0	-2.402748	1.167449	0.345380
5	6	0	-1.010673	1.218173	0.344647
6	6	0	-0.208519	0.112428	-0.065016
7	6	0	1.234317	0.130138	-0.106482
8	7	0	1.944207	-1.076769	-0.437073
9	6	0	2.118988	1.233991	-0.104114
10	8	0	1.545917	2.482516	0.143734
11	8	0	3.347789	1.173568	-0.342833
12	6	0	2.443709	3.582261	0.066009
13	6	0	2.011444	-2.224170	0.292994
14	6	0	3.031225	-3.244569	-0.217273
15	8	0	1.286506	-2.499388	1.253455
16	17	0	-4.842044	-0.059112	-0.052846
17	1	0	-0.384962	-1.939091	-0.749209
18	1	0	-2.828473	-2.020659	-0.757907
19	1	0	-2.974093	2.034298	0.665494
20	1	0	-0.526062	2.129351	0.665681
21	1	0	2.745038	-0.899895	-1.033187
22	1	0	1.843265	4.468160	0.293057
23	1	0	2.882947	3.674353	-0.933828
24	1	0	3.260845	3.486050	0.789177
25	1	0	3.605980	-3.612404	0.637576
26	1	0	3.718530	-2.841855	-0.968726
27	1	0	2.500957	-4.099957	-0.651050

Sum of electronic and thermal Free Energies=   -1166.377321

Geometry and energy of **3f**, protonated at stereogenic centre

1	6	0	0.955283	0.355784	1.434563
2	6	0	2.292267	0.330131	1.835196
3	6	0	3.300981	-0.001191	0.925495
4	6	0	2.928599	-0.303459	-0.377599
5	6	0	1.606849	-0.287988	-0.806678
6	6	0	0.607572	0.048057	0.111456
7	6	0	-0.857003	0.063013	-0.337517
8	7	0	-1.665993	-0.960003	0.303383
9	6	0	-1.490643	1.420500	-0.035788
10	8	0	-1.057820	2.361885	-0.882681
11	8	0	-2.272362	1.620909	0.874904
12	6	0	-1.536547	3.704340	-0.646956
13	6	0	-1.749008	-2.226183	-0.206370
14	6	0	-2.654880	-3.184616	0.544970
15	8	0	-1.120239	-2.567633	-1.205690
16	9	0	3.896790	-0.632962	-1.273404
17	1	0	0.182639	0.613297	2.153442
18	1	0	2.554534	0.570884	2.860970
19	1	0	4.346872	-0.029254	1.210790
20	1	0	1.368103	-0.554442	-1.830457
21	1	0	-0.884493	-0.106303	-1.417472
22	1	0	-2.250596	-0.664324	1.074222
23	1	0	-1.078406	4.312008	-1.425788
24	1	0	-1.227290	4.045317	0.343523
25	1	0	-2.625741	3.735081	-0.719839
26	1	0	-3.357006	-3.631050	-0.163929
27	1	0	-3.212664	-2.713172	1.358887
28	1	0	-2.042557	-3.992979	0.955708

```
Sum of electronic and thermal Free Energies=          -806.568007
```

Geometry and energy of **3f**, deprotonated at stereogenic centre

1	6	0	1.458304	-1.730214	0.212815
2	6	0	2.836993	-1.882767	0.302712
3	6	0	3.724032	-0.807422	0.120621
4	6	0	3.135194	0.421604	-0.150590
5	6	0	1.772737	0.626849	-0.248295
6	6	0	0.866235	-0.460330	-0.072937
7	6	0	-0.553056	-0.255306	-0.202239
8	7	0	-1.012932	1.062427	-0.536059
9	6	0	-1.527694	-1.277014	-0.091973
10	8	0	-2.830614	-0.806916	-0.362170
11	8	0	-1.377152	-2.480702	0.180209
12	6	0	-3.854175	-1.776233	-0.198881
13	6	0	-1.451997	2.004647	0.345620
14	6	0	-2.042849	3.261416	-0.298669
15	8	0	-1.396685	1.909573	1.570626
16	9	0	3.966296	1.512258	-0.333263
17	1	0	0.801554	-2.577452	0.359950
18	1	0	3.242211	-2.869006	0.522671
19	1	0	4.801440	-0.910501	0.189044
20	1	0	1.404390	1.625763	-0.448749
21	1	0	-1.205173	1.262447	-1.510911
22	1	0	-4.790748	-1.262959	-0.438380
23	1	0	-3.890312	-2.154435	0.829566
24	1	0	-3.714559	-2.632738	-0.869084
25	1	0	-1.556743	4.140263	0.134374
26	1	0	-3.107200	3.310842	-0.046436
27	1	0	-1.937729	3.293438	-1.388688

Sum of electronic and thermal Free Energies=   -806.023424

Geometry and energy of 3g, protonated at stereogenic centre

1	6	0	-0.654411	-0.574914	1.871906
2	6	0	-1.992098	-0.903114	2.105201
3	6	0	-2.937471	-0.804127	1.083028
4	6	0	-2.519002	-0.372950	-0.176790
5	6	0	-1.189311	-0.042018	-0.427369
6	6	0	-0.248231	-0.142829	0.606277
7	6	0	1.221076	0.205413	0.347695
8	7	0	1.871356	-0.696226	-0.588054
9	6	0	1.341982	1.624721	-0.205363
10	8	0	1.143353	2.541330	0.749333
11	8	0	1.566328	1.883917	-1.372691
12	6	0	1.161892	3.922176	0.324062
13	6	0	2.457287	-1.859047	-0.170033
14	6	0	3.123376	-2.690104	-1.251364
15	8	0	2.435657	-2.212588	1.007006
16	17	0	-3.696748	-0.241564	-1.478900
17	1	0	0.078534	-0.672740	2.666300
18	1	0	-2.301899	-1.245165	3.088073
19	1	0	-3.977369	-1.058671	1.254967
20	1	0	-0.893964	0.287589	-1.418583
21	1	0	1.753577	0.150754	1.301040
22	1	0	1.966580	-0.374849	-1.542607
23	1	0	0.995200	4.502504	1.230245
24	1	0	0.367254	4.101874	-0.403367
25	1	0	2.128043	4.166415	-0.122437
26	1	0	4.145029	-2.919095	-0.937576
27	1	0	3.145283	-2.200231	-2.228764
28	1	0	2.585720	-3.638728	-1.342302

Sum of electronic and thermal Free Energies=   -1166.923944

Geometry and energy of 3g, deprotonated at stereogenic centre

1	6	0	0.895200	-2.020205	0.222173
2	6	0	2.236058	-2.367434	0.332081
3	6	0	3.269485	-1.427049	0.188517
4	6	0	2.874944	-0.114488	-0.066373
5	6	0	1.550463	0.276698	-0.180913
6	6	0	0.495337	-0.675185	-0.046436
7	6	0	-0.876575	-0.267016	-0.197543
8	7	0	-1.137290	1.107696	-0.514184
9	6	0	-1.987963	-1.142904	-0.120962
10	8	0	-3.204967	-0.492120	-0.406130
11	8	0	-2.011121	-2.359002	0.136081
12	6	0	-4.358806	-1.306814	-0.266366
13	6	0	-1.493899	2.078618	0.374594
14	6	0	-1.885907	3.415561	-0.258857
15	8	0	-1.513710	1.946165	1.596925
16	17	0	4.146153	1.131454	-0.253876
17	1	0	0.121876	-2.767888	0.339818
18	1	0	2.495029	-3.404801	0.537654
19	1	0	4.315510	-1.697801	0.274561
20	1	0	1.313376	1.316741	-0.365801
21	1	0	-1.250448	1.354548	-1.490779
22	1	0	-5.208920	-0.661598	-0.508710
23	1	0	-4.335110	-2.166377	-0.946665
24	1	0	-4.460785	-1.687530	0.756581
25	1	0	-1.337509	4.216831	0.244077
26	1	0	-1.694020	3.469205	-1.336085

27	1	0	-2.954218	3.581050	-0.083974

Sum of electronic and thermal Free Energies=   -1166.380928

Geometry and energy of **3h**, protonated at stereogenic centre

1	6	0	-0.391865	-0.221373	1.355034
2	6	0	-1.783202	-0.280174	1.251748
3	6	0	-2.394065	-0.097146	0.009601
4	6	0	-1.614058	0.142495	-1.128669
5	6	0	-0.227509	0.199065	-1.017390
6	6	0	0.394956	0.021194	0.226579
7	6	0	1.920160	0.078155	0.349691
8	7	0	2.596427	-0.964049	-0.403214
9	6	0	2.441107	1.427868	-0.144815
10	8	0	2.165823	2.406363	0.724651
11	8	0	3.012816	1.589185	-1.206491
12	6	0	2.549960	3.742532	0.329116
13	6	0	2.790006	-2.210598	0.126343
14	6	0	3.551646	-3.190954	-0.746342
15	8	0	2.365116	-2.515675	1.238317
16	6	0	-3.893471	-0.113804	-0.120636
17	9	0	-4.505060	-0.672337	0.950648
18	9	0	-4.403030	1.143633	-0.249234
19	9	0	-4.302468	-0.802100	-1.218119
20	1	0	0.083788	-0.385160	2.316788
21	1	0	-2.385638	-0.478337	2.131123
22	1	0	-2.088877	0.280204	-2.094623
23	1	0	0.372176	0.378918	-1.905372
24	1	0	2.180294	-0.033768	1.406202
25	1	0	3.027753	-0.690196	-1.276637
26	1	0	2.246905	4.383158	1.155742
27	1	0	2.033094	4.024975	-0.590560
28	1	0	3.629395	3.793473	0.172364
29	1	0	4.405724	-3.572771	-0.180628
30	1	0	3.905190	-2.757919	-1.686109
31	1	0	2.898197	-4.039529	-0.968819

Sum of electronic and thermal Free Energies=   -1044.379636

Geometry and energy of **3h**, deprotonated at stereogenic centre

1	6	0	0.547249	1.048923	-0.370259
2	6	0	1.931275	1.109372	-0.334374
3	6	0	2.697784	-0.041587	-0.081326
4	6	0	2.015399	-1.251230	0.153510
5	6	0	0.632440	-1.320276	0.119578
6	6	0	-0.171569	-0.167381	-0.154104
7	6	0	-1.601336	-0.200221	-0.232601
8	6	0	4.172422	0.027277	0.017195
9	9	0	4.647701	0.191764	1.306016
10	9	0	4.801573	-1.104516	-0.432139
11	9	0	4.715788	1.068975	-0.685094
12	7	0	-2.288189	1.013542	-0.573097
13	6	0	-2.393422	-1.368154	-0.060059
14	8	0	-3.759706	-1.124590	-0.284647
15	8	0	-2.032975	-2.519525	0.230455
16	6	0	-4.605489	-2.245184	-0.066882
17	6	0	-2.844864	1.890012	0.311325
18	6	0	-3.677665	3.004206	-0.326181
19	8	0	-2.713380	1.838809	1.532628
20	1	0	-0.011780	1.957783	-0.563338
21	1	0	2.427670	2.060308	-0.507159

22	1	0	2.583124	-2.154904	0.360119
23	1	0	0.131208	-2.262507	0.298029
24	1	0	-2.562382	1.142065	-1.539981
25	1	0	-5.620966	-1.894662	-0.274015
26	1	0	-4.538196	-2.603307	0.966694
27	1	0	-4.352884	-3.078792	-0.732291
28	1	0	-3.349129	3.965145	0.079410
29	1	0	-4.724272	2.861177	-0.037852
30	1	0	-3.615480	3.034792	-1.419395

Sum of electronic and thermal Free Energies=   -1043.843897

Geometry and energy of **3k**, protonated at stereogenic centre

1	6	0	-0.373009	0.428139	0.378542
2	6	0	0.288222	1.732077	-0.076278
3	7	0	-1.601431	0.256373	-0.380743
4	6	0	0.585213	-0.739908	0.270683
5	6	0	0.886547	-1.646192	1.254314
6	6	0	1.804269	-2.655270	0.829343
7	6	0	2.187941	-2.503006	-0.476031
8	16	0	1.435043	-1.123351	-1.210626
9	8	0	1.137321	2.200693	0.845834
10	8	0	0.079616	2.258332	-1.152457
11	6	0	-2.714786	-0.311505	0.174851
12	6	0	-3.922993	-0.421493	-0.737442
13	8	0	-2.732959	-0.716991	1.334966
14	6	0	1.876128	3.388977	0.487168
15	1	0	-0.643997	0.515769	1.434454
16	1	0	-1.625292	0.650289	-1.312016
17	1	0	0.448266	-1.597731	2.244768
18	1	0	2.157783	-3.458587	1.465508
19	1	0	2.865772	-3.116632	-1.053689
20	1	0	-4.792933	-0.012880	-0.217329
21	1	0	-4.119596	-1.480949	-0.928510
22	1	0	-3.796807	0.092630	-1.694290
23	1	0	2.507228	3.604088	1.348163
24	1	0	1.189612	4.215645	0.292033
25	1	0	2.482270	3.200166	-0.401519

Sum of electronic and thermal Free Energies=   -1028.100759

Geometry and energy of **3k**, deprotonated at stereogenic centre

1	6	0	1.177318	0.175442	-0.188346
2	6	0	1.892950	1.362209	-0.366327
3	6	0	3.298243	1.223267	-0.179895
4	6	0	3.683496	-0.052782	0.142075
5	16	0	2.301069	-1.130712	0.224247
6	6	0	-0.237809	-0.020898	-0.314407
7	7	0	-1.008174	1.111880	-0.726662
8	6	0	-0.850086	-1.275194	-0.117474
9	8	0	-0.289854	-2.337405	0.211853
10	8	0	-2.240889	-1.259747	-0.316820
11	6	0	-2.878718	-2.516670	-0.143867
12	6	0	-1.761840	1.929959	0.055188
13	8	0	-2.431984	2.857178	-0.424414
14	6	0	-1.755661	1.640221	1.545870
15	1	0	1.404254	2.295372	-0.621111
16	1	0	3.996325	2.050505	-0.280609
17	1	0	4.678899	-0.427465	0.342122
18	1	0	-1.071721	1.340053	-1.715107
19	1	0	-3.941456	-2.338195	-0.333044

20	1	0	-2.739064	-2.905852	0.871511
21	1	0	-2.494387	-3.264926	-0.847179
22	1	0	-2.171959	2.505610	2.065076
23	1	0	-0.748148	1.417939	1.907791
24	1	0	-2.378173	0.761660	1.747380

Sum of electronic and thermal Free Energies=   -1027.562194

Geometry and energy of **3l**, protonated at stereogenic centre

1	16	0	3.168649	-0.909137	-0.625978
2	6	0	2.527243	-1.789594	0.725275
3	6	0	1.262915	-1.375424	1.043016
4	6	0	0.790889	-0.326723	0.186052
5	6	0	1.717134	0.025183	-0.764850
6	1	0	1.626666	0.772530	-1.541819
7	6	0	-0.606441	0.267815	0.317015
8	1	0	0.666143	-1.799540	1.842210
9	1	0	3.120099	-2.557486	1.203040
10	1	0	-0.907462	0.211439	1.365578
11	6	0	-0.616895	1.726210	-0.129045
12	7	0	-1.608607	-0.454817	-0.456404
13	8	0	-0.894326	2.090250	-1.256471
14	8	0	-0.254778	2.550016	0.863627
15	6	0	-0.153421	3.950645	0.527170
16	1	0	0.141731	4.446261	1.450849
17	1	0	0.600562	4.098262	-0.249386
18	1	0	-1.116810	4.325579	0.175133
19	1	0	-1.731163	-0.177271	-1.420959
20	6	0	-2.330072	-1.483641	0.078484
21	6	0	-3.327870	-2.146676	-0.853833
22	8	0	-2.184378	-1.850695	1.243768
23	1	0	-4.319801	-2.096114	-0.396531
24	1	0	-3.366947	-1.693471	-1.848232
25	1	0	-3.064189	-3.203603	-0.952508

Sum of electronic and thermal Free Energies=   -1028.101708

Geometry and energy of **3l**, deprotonated at stereogenic centre

1	6	0	-1.982848	-1.060032	0.162976
2	6	0	-1.112218	-0.030536	-0.177086
3	6	0	-1.856212	1.194568	-0.403463
4	6	0	-3.208462	1.075626	-0.240735
5	16	0	-3.652878	-0.544202	0.202786
6	6	0	0.330539	-0.102919	-0.307363
7	7	0	1.023463	1.082155	-0.723225
8	6	0	1.042804	-1.298094	-0.099247
9	8	0	0.592760	-2.411530	0.238089
10	8	0	2.434725	-1.159625	-0.301109
11	6	0	3.181772	-2.351380	-0.119422
12	6	0	1.720431	1.950127	0.057301
13	8	0	2.356356	2.900269	-0.425877
14	6	0	1.692062	1.694918	1.554428
15	1	0	-1.715063	-2.080976	0.386116
16	1	0	-1.374652	2.126632	-0.677804
17	1	0	-3.962426	1.843890	-0.352682
18	1	0	1.148762	1.270386	-1.714587
19	1	0	4.225651	-2.079257	-0.304517
20	1	0	2.871862	-3.136118	-0.820544
21	1	0	3.074128	-2.749275	0.896933
22	1	0	2.054488	2.590552	2.062925
23	1	0	2.350874	0.851455	1.787665

| 24 | 1 | 0 | 0.690249 | 1.428284 | 1.901328 |

Sum of electronic and thermal Free Energies=   -1027.556639

Geometry and energy of **6e**, protonated at stereogenic centre

1	6	0	-0.106941	0.527701	-0.963152
2	6	0	-1.479871	0.344762	-1.101242
3	6	0	-2.237525	-0.094162	-0.007648
4	6	0	-1.616836	-0.352882	1.215852
5	6	0	-0.238083	-0.167973	1.345595
6	6	0	0.526322	0.279251	0.263822
7	6	0	-3.728765	-0.240498	-0.153606
8	9	0	-4.077612	-0.741360	-1.365722
9	9	0	-4.265459	-1.055605	0.785712
10	9	0	-4.366864	0.958644	-0.037793
11	6	0	2.033017	0.486624	0.418260
12	7	0	2.820497	-0.422048	-0.391973
13	6	0	2.446739	1.924816	0.034407
14	7	0	1.921310	2.906708	0.810983
15	8	0	3.210342	2.148019	-0.900069
16	6	0	3.099796	-1.688422	0.041474
17	6	0	4.021741	-2.504999	-0.844738
18	8	0	2.618673	-2.139580	1.079588
19	1	0	0.476939	0.861952	-1.816354
20	1	0	-1.961877	0.537861	-2.053884
21	1	0	-2.199289	-0.711820	2.057140
22	1	0	0.250434	-0.406589	2.285530
23	1	0	2.289127	0.319957	1.471949
24	1	0	3.350837	0.010263	-1.140546
25	1	0	1.198297	2.716192	1.488464
26	1	0	2.101598	3.866544	0.553410
27	1	0	4.866918	-2.853702	-0.245065
28	1	0	4.395494	-1.952765	-1.711104
29	1	0	3.478599	-3.388466	-1.192683

Sum of electronic and thermal Free Energies=   -985.225524

Geometry and energy of **6e**, deprotonated at stereogenic centre

1	6	0	-0.046912	-0.803961	-0.530645
2	6	0	-1.416219	-0.990034	-0.544435
3	6	0	-2.288260	-0.040084	0.026805
4	6	0	-1.720975	1.096437	0.626877
5	6	0	-0.347293	1.290936	0.638300
6	6	0	0.560738	0.367978	0.025283
7	6	0	-3.754536	-0.212544	-0.056808
8	9	0	-4.155456	-1.519593	0.017171
9	9	0	-4.438734	0.454737	0.921849
10	9	0	-4.308909	0.246602	-1.241329
11	6	0	1.974075	0.575408	-0.034213
12	7	0	2.850604	-0.510361	-0.357214
13	6	0	2.676540	1.820198	-0.105221
14	7	0	1.987765	3.047469	0.015878
15	8	0	3.919460	1.880071	-0.320096
16	6	0	2.964482	-1.711101	0.273949
17	6	0	4.152984	-2.558006	-0.182623
18	8	0	2.167667	-2.155188	1.107000
19	1	0	0.588260	-1.568180	-0.960185
20	1	0	-1.824575	-1.889507	-0.997080
21	1	0	-2.362675	1.822032	1.118992
22	1	0	0.046976	2.133329	1.194824
23	1	0	3.689639	-0.169602	-0.817908

271

24	1	0	1.028399	3.051917	-0.312403
25	1	0	2.549427	3.788005	-0.387888
26	1	0	4.674391	-2.927666	0.705306
27	1	0	4.860708	-2.015936	-0.818332
28	1	0	3.783979	-3.430272	-0.734038

```
Sum of electronic and thermal Free Energies=        -984.679563
```

5.4.2 Determination of k_{gb} for Amfepramone and Cathinone

The rate constants for general-base catalysed H/D exchange of amfepramone and cathinone (Section 5.2.4.2) were obtained from the data reported by Reist et al.[9] This data is reproduced in Table 5.9.

Table 5.9: Rate constants of H/D exchange for amfepramone and cathinone from reference 9, in D_2O phosphate buffers of pD 7.4, $I = 0.43$, at 37 °C.

phosphate conc. / M	[HPO$_4^{2-}$] conc. / M	k_{deut} / s^{-1} Amfepramone	k_{deut} / s^{-1} Cathinone
0.00067	0.00041	1.50×10^{-7}	-
0.0013	0.00079	2.72×10^{-6}	-
0.0020	0.0012	3.33×10^{-6}	-
0.013	0.008	3.06×10^{-5}	-
0.067	0.041	1.61×10^{-4}	4.95×10^{-5}
0.100	0.061	-	6.50×10^{-5}
0.133	0.081	3.56×10^{-4}	8.11×10^{-5}
0.167	0.102	-	9.78×10^{-5}
0.200	0.122	6.47×10^{-4}	1.30×10^{-4}

From the data displayed in Table 5.9, the rate constant of H/D exchange was plotted as a function of basic buffer component (Figure 5.15 and Figure 5.16). From these plots, k_{gb} and k_0' were obtained for amfepramone and cathinone.
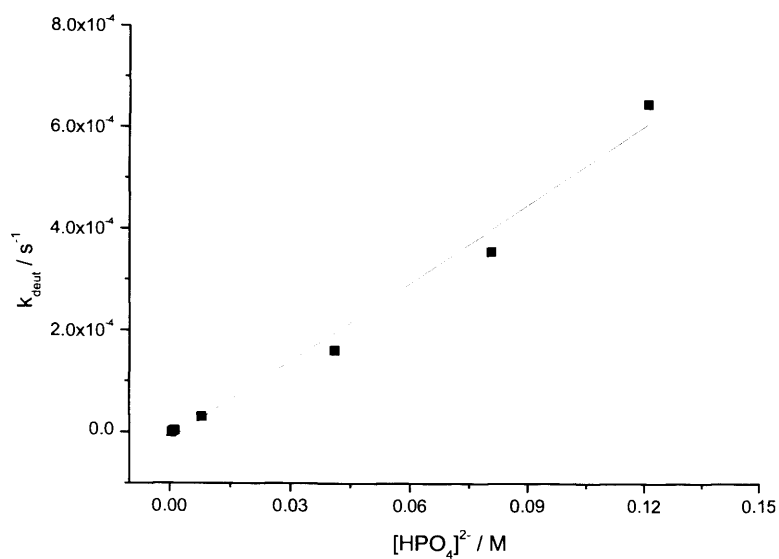
Figure 5.15: Variation of k_{deut} of amfepramone with [HPO_4^{2-}] at 37 °C, pD 7.4, $I = 0.43$. $k_{gb} = (5.09 \pm 0.27) \times 10^{-3}$, $k_0' = (-1.34 \pm 1.54) \times 10^{-5}$.
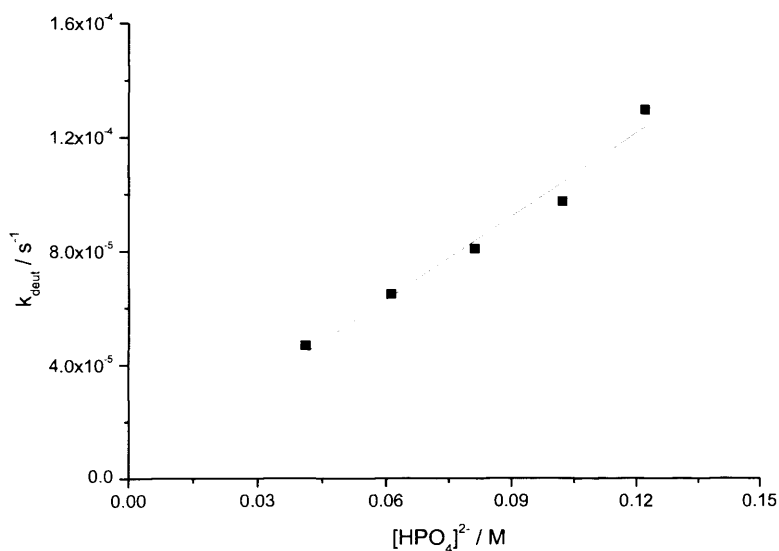
Figure 5.16: Variation of k_{deut} of cathinone with [HPO_4^{2-}] at 37 °C, pD 7.4, $I = 0.43$. $k_{gb} = (9.80 \pm 0.87) \times 10^{-4}$, $k_0' = (4.37 \pm 7.48) \times 10^{-6}$.

5.5 References

1. Nakata, K.; Fujio, M.; Nishimoto, K.; Tsuno, Y., *Journal of Physical Organic Chemistry* **2010**, *23* (11), 1057-1065.
2. Hoefnagel, A. J.; Hoefnagel, M. A.; Wepster, B. M., *Journal of the American Chemical Society* **1976**, *98* (20), 6194-6197.
3. Taagepera, M.; Summerhays, K. D.; Hehre, W. J.; Topsom, R. D.; Pross, A.; Radom, L.; Taft, R. W., *Journal of Organic Chemistry* **1981**, *46* (5), 891-903.
4. Maskill, H., *The Physical Basis of Organic Chemistry*. Oxford Science Publications: Oxford, 1985; p 261-263.
5. Hammond, G. S., *Journal of the American Chemical Society* **1955**, *77* (2), 334-338.
6. Xu, J.; Stevenson, J., *Journal of Chemical Information and Computer Sciences* **2000**, *40* (5), 1177-1187.
7. Lameijer, E. W.; Kok, J. N.; Back, T.; IJzerman, A. P., *Journal of Chemical Information and Modeling* **2006**, *46* (2), 553-562.
8. Testa, B.; Carrupt, P. A.; Gal, J., *Chirality* **1993**, *5* (3), 105-111.
9. Reist, M.; Christiansen, L. H.; Christoffersen, P.; Carrupt, P. A.; Testa, B., *Chirality* **1995**, *7* (6), 469-473.
10. Frisch, M. J.; Trucks, G. W.; Schlegel, H. B.; Scuseria, G. E.; Robb, M. A.; Cheeseman, J. R.; Montgomery, J., J.A.; Vreven, T.; Kudin, K. N.; Burant, J. C.; Millam, J. M.; Iyengar, S. S.; Tomasi, J.; Barone, V.; Mennucci, B.; Cossi, M.; Scalmani, G.; Rega, N.; Petersson, G. A.; Nakatsuji, H.; Hada, M.; Ehara, M.; Toyota, K.; Fukuda, R.; Hasegawa, J.; Ishida, M.; Nakajima, T.; Honda, Y.; Kitao, O.; Nakai, H.; Klene, M.; Li, X.; Knox, J. E.; Hratchian, H. P.; Cross, J. B.; Bakken, V.; Adamo, C.; Jaramillo, J.; Gomperts, R.; Stratmann, R. E.; Yazyev, O.; Austin, A. J.; Cammi, R.; Pomelli, C.; Ochterski, J. W.; Ayala, P. Y.; Morokuma, K.; Voth, G. A.; Salvador, P.; Dannenburg, J. J.; Zakrzewski, V. G.; Dapprich, S.; Daniels, A. D.; Strain, M. C.; Farkas, O.; Malick, D. K.; Rabuck, A. D.; Raghavachari, K.; Foresman, J. B.; Ortiz, J. V.; Cui, Q.; Baboul, A. G.; Clifford, S.; Cioslowski, J.; Stefanov, B. B.; Liu, G.; Liashenko, A.; Piskorz, P.; Komaromi, I.; Martin, R. L.; Fox, D. J.; Keith, T.; Al-Laham, M. A.; Peng, C. Y.; Nanayakkara, A.; Challacombe, M.; Gill, P. M. W.; Johnson, B.; Chen, W.; Wong, M. W.; Gonzalez, C.; Pople, J. A. *03. Gaussian, E01. Revision*, Gaussian, Inc.: Wallingford CT, 2004.
11. Schmidt, M. W.; Baldridge, K. K.; Boatz, J. A.; Elbert, S. T.; Gordon, M. S.; Jensen, J. H.; Koseki, S.; Matsunaga, N.; Nguyen, K. A.; Su, S. J.; Windus, T. L.; Dupuis, M.; Montgomery, J. A., *Journal of Computational Chemistry* **1993**, *14* (11), 1347-1363.
12. Bode, B. M.; Gordon, M. S., *Journal of Molecular Graphics & Modelling* **1998**, *16* (3), 133-138.

6 Epilogue

6.1 General Conclusions

This thesis describes our endeavours to improve our understanding of the many factors affecting configurational instability, specifically addressing the potential problem of enantiopure compounds undergoing racemisation after being administered as a drug.

Literature studies suggested that the threat of racemisation under aqueous conditions is greatest for compounds with a stereogenic centre of the type R''R'RC-H. If adjacent R groups can stabilise a negative charge, then an anion may be formed by deprotonation at the stereogenic centre and any enantiopurity will be lost as a result. Research by the Testa group classified specific groups as increasing or decreasing configurational stability. A wealth of literature from the Richard group into how adjacent functional groups influence the pK_a of carbon acids also provided insight into how functional groups bound to a stereogenic centre will affect the lability of the proton.

The goal of this project was thus to test the conclusions from these studies as well as to expand on them, through determining rate constants for the H/D exchange reactions of selected compounds. From these rate constants, it was hoped that mechanisms and substituent effects for the process could be elucidated. To do so, a range of experimental techniques and methods in physical organic chemistry were used.

The database mining studies outlined in Chapter 2 were undertaken with the intent of exploring and categorising the structure of stereogenic centres most commonly found in pharmacologically-active compounds. To this end, the wealth of compounds found in the databases under analysis (ISAC and IBEX databases, containing over 1 million and over half a million compounds respectively) comprises a great resource. Specifically, the goal of this part of our research was to assess which combinations of functional groups are frequently found together around stereogenic centres and to identify frequently found combinations thought to be at risk of racemisation for further analysis. It became apparent that when so many compounds containing stereogenic centres were under analysis, it would be possible to find almost any combination of substituents that could be imagined. As a result it was decided to narrow down the analysis to the top 250 most frequently appearing combinations in each database. In this selection, the majority of stereogenic centres were not deemed to be susceptible to *in vivo* racemisation. However, there were many regularly-appearing combinations that did appear to be at risk of configurational instability under the conditions

under investigation. In particular, the combination of adjacent carbonyl, nitrogen and aromatic groups on a stereogenic was commonly found. As a result, this particular combination was targeted for further investigation through physical experimentation.

In Chapter 3, specific rate constants for proton-deuterium exchange (as a model for configurational instability of stereogenic centres carrying a relatively labile proton) were determined for a series of N-acetyl arylglycine methyl esters. The magnitude of these rate constants showed that compounds containing stereogenic centres of this type are at risk of undergoing racemisation under physiological conditions. The linear relationship between rate constants for proton-deuterium exchange with basic buffer component showed that the process under analysis is general-base catalysed. These results also broadly fit with the assignments by Testa et $al.$ of functional groups as promoting or retarding configurational stability when adjacent a stereogenic centre. Hammett correlations showed that electron-withdrawing groups increased rate constants of racemisation, through stabilisation of a (developing) negative charge. Comparison of the rate constants for racemisation with rate constants for proton-deuterium exchange allowed us to conclude that these two processes take place via an S_E1 mechanism, consistent with the mechanism determined for similar structures. For H/D exchange of N-acetyl phenylglycine methyl esters the best Hammett relationship was found with σ^- values. Rate constants for proton-deuterium exchange were also determined for thiophene-substituted analogues, and were of a magnitude that suggests that such compounds are at risk of racemisation under physiological conditions. The rate constants for one of the thiophene-containing compounds also suggests that a 2-thiophene moiety is more electron-withdrawing than any of the substituted-phenyl groups also analysed in Chapter 3. Attempts to fit these heterocycle-containing analogues into the previously-mentioned Hammett analysis using σ values found in the literature proved successful.

Rate constants for proton-deuterium exchange for a set of N-substituted phenylglycine amides were determined in Chapter 4, for the purpose of comparison with those determined for N-acetyl phenylglycine methyl esters in Chapter 3. The rate constants determined in Chapter 4 suggest that the N-substituted phenylglycine amides investigated are not at risk of configurational instability under physiological conditions. This dataset, in combination with the data collected in Chapter 3, allowed for a direct comparison of the effects of an ester and of an amide on configurational instability, and showed that an adjacent ester group will destabilise a stereogenic centre of type R''R'RC-H more than an amide group in the same position. These findings are consistent with the assignments made by Testa et $al.$ As with the ester compounds analysed in Chapter 3, the amides investigated in Chapter 4 undergo

proton-deuterium exchange through general-base catalysis and via an S_E1 mechanism. Variable-temperature work in Chapter 4 allowed for the determination of thermodynamic activation parameters. The large positive enthalpy and negative entropy of activation found were consistent with the S_E1 mechanism. The variable-temperature work also showed that high-temperature kinetics could potentially be used for rapid screening, providing approximate information on configurational instability at lower temperatures.

Chapter 5 used computational chemistry to relate experimental data with theoretical calculations. Because the proton-deuterium exchange reactions examined in Chapters 3 and 4 were found to proceed through an S_E1 mechanism, it was suspected that the stability of the anion formed upon deprotonation at the stereogenic centre relative to the compound prior to deprotonation could provide a good correlation with the rate at which proton-deuterium exchange occurs. It was found that this calculated energy difference correlated well with the rate constants of proton-deuterium exchange experimentally determined in Chapters 3 and 4, when the PCM solvent model is applied. This relationship holds well for minor structural changes, such as the modification of Hammett substituents, but less well for major structural changes.

6.2 Outlook

It is hoped that the correlation between the computationally-calculated energy differences and the experimentally-determined rate constants could be of significant use to the pharmaceutical industry, by enabling the prediction of configurational instability in a compound only from calculations. In order for this to become reality a great deal of further work would have to be done. Foremost, the number of compounds for which rate constants of proton-deuterium exchange has been determined under conditions analogous to those used in Chapters 3 and 4 would need to be greatly expanded. Correlation with a greater number and a wider range of structures would allow for increased confidence in the relationship. An increase in the range of structures may also allow for the discovery of a standard 'offset' for functional groups which significantly change the electronic properties of the compound, such as the cation found in the quaternary amines amfepramone and cathinone analysed in Chapter 5.